UNIVERSITAT DE BARCELONA

Application of chemotaxonomy to the study of the phytoplankton community structure in the Mediterranean Sea and in the Atlantic and Southern Oceans

Aplicación de la quimiotaxonomía al estudio de la estructura de la comunidad fitoplanctónica en el Mar Mediterráneo y en los oceános Atlántico y Antártico

Sdena Oliveira Nunes

Application of chemotaxonomy to the study of the phytoplankton community structure in the Mediterranean Sea and in the Atlantic and Southern Oceans

Sdena Oliveira Nunes

Tesis Doctoral

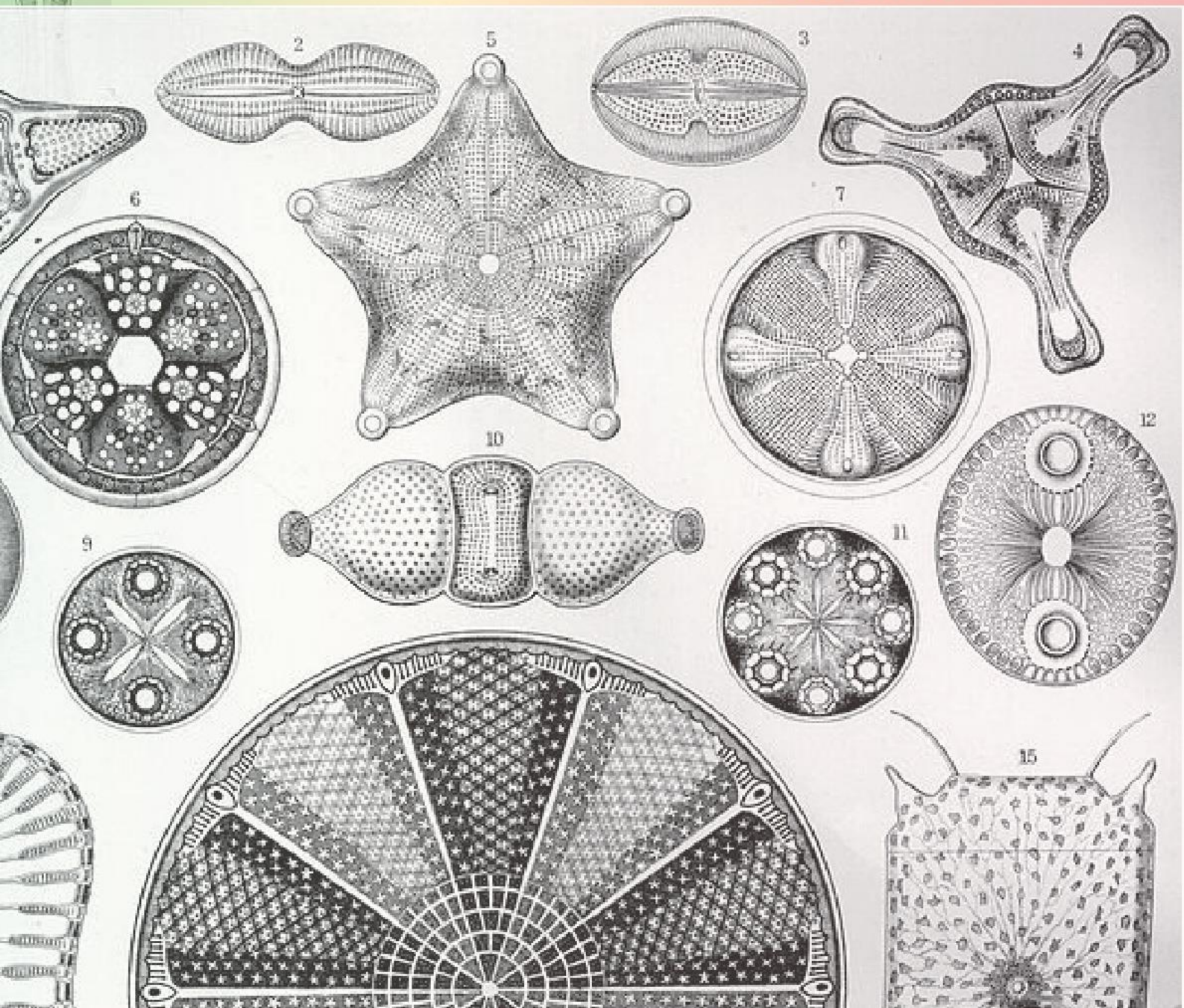

Application of chemotaxonomy to the study of the phytoplankton community structure in the Mediterranean Sea and in the Atlantic and Southern Oceans

Aplicación de la quimiotaxonomia al estudio de la estructura de la comunidad fitoplanctónica en el Mar Mediterráneo y en los océanos Atlántico y Antártico.

Sdena Oliveira Nunes

Memoria presentada por Sdena Oliveira Nunes para optar al grau de doctor por la Universitat de Barcelona.

Programa de Doctorat en Ciències del Mar

Sdena Oliveira Nunes
La doctoranda

Dra. Marta Estrada
El Director

Dr. Mikel Latasa
El Co-director

Dr. Jordi Flos
El tutor

En Barcelona, a 26 de Septiembre de 2018

INFORME DEL DIRECTOR

La doctoranda **Sdena Oliveira Nunes** presenta su tesis doctoral titulada "***Application of chemotaxonomy to the study of the phytoplankton community structure in the Mediterranean Sea and in the Atlantic and Southern Oceans*****"**. El director de tesis, la Dra. Marta Estrada Miyares, el co-director Dr. Mikel Latasa y el tutor Jordi Flos, informan que la presente tesis doctoral consta de tres trabajos científicos a modo de capítulos. Los capítulos están publicados, aceptados y enviados a revistas científicas internacionales reconocidas en el Science Citation Index (SCI). A continuación se detalla la contribución del doctorando en cada uno de ellos, así como el factor de impacto según el Thomson Institute for Scientific Information:

CAPITULO 2

Nunes, S.**;** Latasa, M.; Gasol, J.M.; Estrada, M. (2018) **Seasonal and interannual variability of the phytoplankton community structure in a Mediterranean coastal site.** Marine Ecology Progress Series. 592: 57–75. doi: https://doi.org/10.3354/meps12493.

Factor de impacto (2016): 2.29

El doctorando ha participado en el trabajo de laboratorio para la obtención de los datos, el análisis de los datos y la redacción científica.

CAPITULO 3

Nunes, S.; Peréz, G. L.; Latasa, M.; Zamanillo, M.; Delgado, M.; Ortega-Retuerta, E.; Marrasé, C.; Simó, R.; Estrada, M. (2018) **Size fractionation, chemotaxonomic groups and bio-optical properties of phytoplankton along a transect across the Atlantic Ocean.** Scientia Marine. *Aceptado.*

Factor de impacto (2017): 1.183

El doctorando ha participado en el trabajo de campo, en el trabajo de laboratorio para la obtención de los datos, en el análisis de los datos y en la redacción científica.

CAPITULO 4

Nunes, S.; Latasa, M.; Delgado, M.; Emelianov, M.; Simó, R.; Estrada, M. (2018) **Phytoplankton community structure in contrasting ecosystems of the Southern Ocean: South Georgia, South Orkneys and Western Antarctic Peninsula.** Deep Sea Research I. *Enviado.*

Factor de impacto (2017): 2.653

El doctorando ha participado en el trabajo de campo, en el trabajo de laboratorio para la obtención de los datos, en el análisis de los datos y en la redacción científica.

Los coautores participantes en los artículos que componen esta tesis no han utilizado ni implícita ni explícitamente ninguno de estos trabajos para la elaboración de otras tesis doctorales.

Dra. Marta Estrada Dr. Mikel Latasa Dr. Jordi Flos

Barcelona, 26 Septiembre de 2018

Esta tesis está encuadrada dentro del Programa de Doctorat de Ciencias de Mar de la Universidad de Barcelona y ha sido realzada en el Instituto de Ciencias del Mar – ICM dentro de Grups Consolidats de Recerca 2014 SGR/761 y 2014 SGR/1179 de la Generalitat de Catalunya y el proyecto PEGASO (CTM2012-37615) financiado por el Ministerio de la Economia y competitividad de España. Durante el periodo de elaboración de la tesis, la doctoranda ha disfrutado de una Beca Brasileña concedida por Council of Technological and Scientific Development (CNPq) of Brazil.

Portada principal y de cada capitulo:
Diatoms – Ernst Haeckel: Kunstformen der Natur – Kunstformen aus dem Meer

A mi mejor puerto afectivo, Abel Cortada

Al meu gran port professional, Marta Estrada

E aos meus eternos portos seguros, Maria José e Heleno.

Tudo no mundo começou com um sim. Uma molécula disse sim a outra molécula e nasceu a vida. Mas antes da pré-história havia a pré-história da pré-história e já havia o nunca e já havia o sim. E como começar pelo início, se as coisas acontecem antes de acontecer?

(...)

...Então, começaremos no presente...

...porque a ***eternidade*** é o estado das coisas nesse momento.

Clarice Lispector

Contents

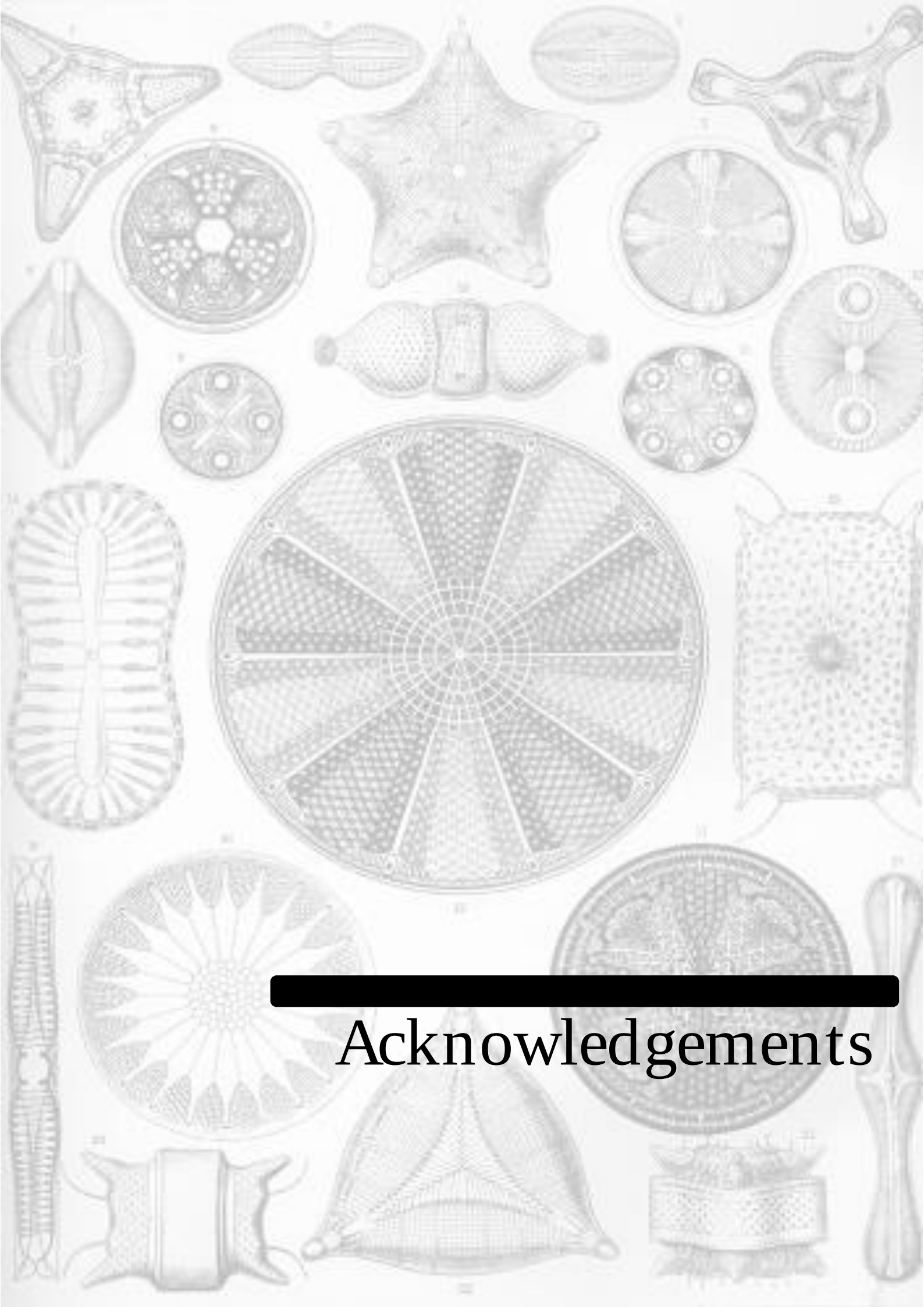

Acknowledgements

ACKNOWLEDGEMENTS

"...Coisa que gosto é poder partir sem ter planos,
melhor ainda é poder voltar quando quero..."
Maria Rita – Encontros e despedidas

Llegado a este momento, miro hacia atrás y veo los grandes cambios que hice en los últimos 5 años no sólo de ciudad, de país, de continente, de mares, de océano, pero sobretodo de vida… Y me di cuenta que la vida es un viaje de dos lados: los billetes de partida también son los mismos billetes de llegada. Muchas personas dejamos en los "puertos" de salimos. No obstante, muchas vamos conocer en los "puertos" de llegada. Y no importa se es un océano que nos separa o una calle: en esta jornada doctoral fueron muchos "puertos" dónde pude anclarme el tiempo necesario para luego seguir hacia delante más completa. Y sobre todo, fueron (son) mucho los "puertos" que hicieron de esta jornada posible y agradable. Ahora, me gustaría de sinceramente agradece a todos y todas que compartirán esa maravillosa aventura, mismo que estén en puertos distintos.

Mi puerto profesional

Seguramente, este trabajo no seria posible si yo "pasase por otra Estrada". Muchas gracias, Marta por todo lo que me aportaste. Muchas gracias por la comprensión de mis limitaciones y apoyar mis ideas (o por hacerme entender que no eran taaan buenas así). Gracias por los ánimos súper directos y sinceros, por la orientación desde el inicio al final, por arreglar de la forma más justa las cosas que parecían incomprensibles a mí, por compartir las historias de tu vida académica en la época de Margalef y por la oportunidad de ser tu ultima becaria. Eres una de las personas más humanas que conocí y que intenta hacer las cosas más justas y más moralmente posible. Siempre tendré mucho orgullo de haber sido tu alumna. Gracias por guiarme hasta aquí, incluso en este momento final de la tesis. Ojalá un día consiga hacer 10% de la Ciencia que haces.

Mikel Latasa, muchas gracias por abrir el fantástico, increíble (y al mismo tiempo martirizante) mundo del HPLC con todas sus inyecciones, logros de datos, cromatogramas y dolores de cabeza (pero sólo cuando se rompen). Gracias por recibirme en el IEO – Gijón, por tu buen humor mismo en las horas de mucho trabajo, por ayudarme a crecer profesionalmente y principalmente, gracias por apoyarme en el momento que la investigación no se adelantaba.

Gràcies en Jordi Flos, el meu tutor, per rebran dins la UB i permetre el desenvolupament d'aquesta tesi.

Rafel Simó, tu tenacidad ligera, tu profesionalismo y tu filosofía de vida siempre me acompañarán. Gracias por demostrarme que siempre es posible oír y ser oído, por ser este grande profesional sin dejar de ser tú. Muchas gracias por extenderme la mano en las vueltas confusas de mi vida. Célia Marrasé, gracias por todo lo que me aportaste en el laboratorio, tus preocupaciones de madre hacia nosotros becarios y por enseñarme la importancia de los blancos, los negros, los azules, los guantes, de los apuntes de todo lo que hace y de que cada gota de agua puede convertirse en un articulo. Muchas gracias Dolors, por llevarme alegría y optimismo todos los días que te encontraba, por hacer los duros días de laboratorio más positivos. Muchisimas gracias por el "empujón" de ánimo en el final de la tesis. Elisa Berdalet, gracias por la amabilidad que siempre me has tratado. Ojalá un día consigamos poner ese UPLC en marcha!

Obviamente, este trabajo no habría sido posible sin el apoyo que recebí en los laboratorios: Laura Arin, gracias por las mañanas de enseñanza de microscopía y por compartir las historias de inmigrantes, vecinas de ciudad y fans de Marta Estrada. Laia, que sería de mi vida en laboratorio sin ti? Gracias por ser lo que eres y por preocuparte tanto, has sido un apoyo impar a lo largo de estos años. Aún tenemos que zarpar juntas por aguas mediterráneas… Carolina Antequera, eres un sol. Muchas gracias no sólo por las ayudas en el laboratorio, pero por las buenas conversas y momentos de risa. La dupla Vanessa Balagué y Clara Cardelús, la alegría y el bueno humor que nunca falta. Como me alegro de haber compartido parte de mi historia profesional con vosotras. A Raquel Guitierre por llevar mis muestras en los meses que estuve en Gijón.

Los investigadores del ICM: Montse Sala, Gonzalo Luis Pérez, Eva Ortega-Retuerta, Magda Villa, Pep Gasol, Lluïsa Cros, Francesc Peter, mis sinceros agradecimientos por todo lo que habéis aportado para mi crecimiento profesional. A Conchita, nuestra eterna secretaria, por la atención y amabilidad que siempre atendía a nosotros becarios. Gracias a todos que compartimos campaña en el Hespérides: Dall'Osto, Encarna, Isabel Ferrera, Pau Cortés, Pablo Rodriguez-Ros, Alicia y a los chicos de UTM: Alberto, Gustavo, Cris, Dulce y Iago.

El tiempo que pasé en Gijón ha sido de mucho trabajo, pero con el equipo técnico que me ha acompañado, mis días eran mucho mejores. Gracias a todos del IEO- Gijón: Carmen Cabeza por enseñarme toda la parte técnicas del HPLC, tricot y como

escaquearse de Mikel en la hora del café. A Carmen, Pili, Ale, Floren, Paloma, Eva Velasco, Virginia, Dani, Paqui, Juan, Eva Pietro, Sofia, Felipe, Renate, Cristobon, Lucie mis sinceros agradecimientos. Estoy segura que si no fuera por todos vosotros esta tesis no habría llegado en buen puerto.
Gracias al profesor Antonio Calafat (UB), que con disposición y profesionalidad estubo muy presente en los años de mi tesis. Siempre dispuesto a ayudarme.

Mi Puerto Amistad/Meu Porto Amizade

Este puerto es lleno de colores y buenos recuerdos. Nos hemos unido por amor al mar y hoy es el mar el que nos separa. Pero me siento muy afortunada por un día haber estado en el mismo puerto, compartiendo alegrías, aprendizajes, esperanzas, logros y principalmente, mucho, mucho estrés.

Daffne, mi hermana del alma, eres intesidad. En mi camino a lo largo de la tesis has sido la mano que me levantó en todos los momentos que he caído. Te agradezco todos los consejos, los apoyos y principalmente, por hacerte presente en los momentos más duros. Gracias, lo siento, te amo y perdoname. Tú y Francisco Aparicio habéis sido el lado bueno de los días duros en mi jornada "tesisciana". Franzius, mi Pheebo, mi compañero de aventuras y del amor por Mercadona, si estamos al lado o distante, no importa, siempre compartimos las aventuras. Como siempre reímos de todo lo que nos pasa! Muchas gracias por hacer la vida y los días más bonitos (aunque parezcan feos) y por los regalitos llenos de cariño. En mi "generalife" yo sé que estaremos juntos forever. Isabel! Isabé! Tronca! Isa! Muchas gracias por todo que me enseñastes, no sólo mejorando mi castellano - ahora ya no pido más una *borracha* en el lab, ya sé diferenciar enfadado de aburrido y ya consigo usar el verbo "pillar" sin problemas – pero también por haber puesto un poco más de velocidad y energía en mi vida, por las carcajadas con "bromas de ultima hora" sobre nosotras y por principalmente, por enseñarme que con determinación y foco todo es posible. Y que siempre podemos sacar el mejor de nosotros en los momentos críticos de tensión. Hemos compartido la parte más duras del estrés en el laboratorio y hemos sobrevivido unidas. Somos unas campeonas. Mireia, Mireshita para shaaaaa: "Deve ser legal ser Negão no Senegal". Has sido un gran regalo en mis 5 años de doctorado, principalmente en los últimos 3 años.

Eres ese espíritu libre, con ganas de aprender siempre que me gusta hablar desde ideas-tontas-para-sacar-fotos hasta debates socio-antro-filo-políticos. Cuantas buenas conversas hemos tenido! Me encanta tenerte como amiga. Gracias por enseñarme a ver que hay distintas maneras de ver el mismo punto. Gracias por poner la leveza y creatividad en los momentos que hemos pasado juntas. Caterina R. Giner! Cuando llegué en ICM miraba a ti hablando con todos en el pasillo y pensaba: ¿quien es esta chica tan *pop* en el instituto? En los últimos años nos hemos aproximado y la verdad es que hoy comprendo porque eres *pop*. ¡Que capacidad de organización y de solucionar problemas tienes! Cuando no sé más que hacer, te cojo a ti y en 1 minuto me presentas 5 soluciones y otra posibilidad "por si acaso". Gracias por todos los mensajitos de ánimos, mismo cuando estabas cansada con tus cosas. Gracias por preocuparte y querer siempre ayudarme. Eres la *frick* más *pop star* que conozco y me alegro mucho por ser tu amiga. Gracias a todos vosotros. No hace falta decir cuanto os echo de menos por aquí. Que la vida permita que nuestros caminos sigan juntos aunque en puertos distantes.

Y no sólo lo que estáis físicamente distantes, pero la gente que sigue en puerto catalan el cual he compartido buenos momentos: Dorle! Mi amiga Vasca. Gracias por escucharme todas las veces que necesité oídos, por la atención y todo el cariño. Siempre recordaré de la buena amiga que eres, honesta y prudente. Cuenta conmigo siempre! Estela, la mujer cosmopolita. Que visión genial del mundo tienes. Con tus pensamientos e ideas, has conquistado mi amistad aunque no convivíamos mucho. Gracias por enseñarme que los cambios no son tan duros si podemos hacer una broma. Carmen Herrero, eres la amiga virtual más real que tengo. Gracias por todo el apoyo ahora en la parte final. Gracias por los momentos "interneticos" de risa. Ramiro ¿una brasileña puede ser amiga de un Argentino? Desde que no sea durante el mundial, off course! Hemos compartido momentos muy divertidos en las fiestas de Gracia, de Sants, de la Mercè y de las que inventamos entre todos. Y Xavi, el siempre espíritu joven, la enciclopedia ambulante. A los dos, gracias por los momentos de risas, por las compañías en los *Fridays beers* y barbacoas. Meu amigo catalao que fala portugués, Jordi Grinyo, muito obrigada por todos os momentos de conselhos na hora do estresse e por compartilhar as boas surpresas da vida. Te desejo o melhor sempre. Carol, Lisandra, Yaiza, Mariri, Marta, Pablo Sanchez con sus super pantallas matrix y Clara Ruiz: aunque casi no voy al ICM, gracias por recibirme siempre con una sorrisa cada vez que aparezco. Muchas gracias a todos los que habéis pasado de manera positiva en

mi vida: Idaira, Maria Pascual, Maria de la Fuente, Teresa Morganti, Fran Cornejo (vamos a las Caipirinhaaaas), Ana Mari, Guillerm, Marina Zamanillo, Lucia Quirós, Paola Castellanos que siempre se sacan una buena sonrisa cuando me ven. Y gracias a Margarita y Hector por la buena compañía fuera de ICM. Gracias a los amigos CEMyD por todo el cariño y respecto que me dispensais.

El puerto Gijón también me ha regalado mi mejor (y única) cuadrilla. Nestor! Mi mejor amigo Vasco. Cuantos momentazos pasamos. Gracias por enseñarme que las danzas, las comidas y los deportes Vascos son todas cosas muy ligeras, y por comprender rapidamente que un partido de futbol se hace con por lo menos 21 gols ficticios. Gracias por cuidarme, por darme apoyo en los momentos que el HPLC no funcionaba, por compartir la comida, las alegrías, las idas en bici al IEO, los desayunos en portugués y las "arengas" con Tamara. ¡Megan! que *crack* eres. ¡Aún me impresiona la cantidad de cosas que consigues hacer a la vez y planear otras cuantas más! Gracias por todo lo que me has hecho reir y pasar bien en situaciones que parecían desastre. Has sido la buena amiga que ha conseguido mi confianza de manera muy sensilla, por ser como eres. Gracias por enseñarme que hay siempre algo muy bueno y divertido para hacer, ni que sea las Estrellas Galicias con Fuet Espetec y azeitunas compartidas delante de la tele un viernes por la noche (que pereza de juventud!). Aitor, te incluyo aquí porque eres mi amigo catalá más asturiano que conozco. Que bueno amigo eres, una persona con un corazón increíble, siempre listo para ayudar. Gracias por todo lo que compartimos en nuestros desayunos de sabados en Gijón, por los consejos de deporte, consejos de vida y por hacer de aquellos momentos duros mucho más ligeros. Me siento muy afortunada por conoceros, chicos. Rosa y Laustin! Gran pareja de amigos. Muchas gracias por todo el cariño y hacer sentirme siempre muy importante. Sara y Maria, muchísimas gracias por todos los buenos momentos que hemos pasado. Paloma, muchas gracias por la compañía en los paseos por las playas y consejos de vida saludable.

También quiero agradecer de manera muy especial aquellos mis amigos que están en otros puertos. Pero cuando estábamos juntos, los momentos han sido inolvidables. Karlita, Nico, Yuli, Roy, Rodrigo!!! Mi vida en Barna no habría sido la misma sin vosotros. Gracias por todo lo que habéis hecho por mí aquí. Me habéis recibido como si fuera vuestra nueva amiga de infancia. Gracias por absolutamente todo. ¡Habéis sido increíble en mi vida! El mundo necesita de más amistad sincera, así como la vuestra. Os

echo muchísimo de menos. Rosana Arizmendi, amiga! Muchas gracias por toda la ayuda que me has dado en los momentos que tanto necesité. Gracias por oírme, por apoyarme, por preocuparte, por compartir consejos sobre espiritualidad y de como ser mejores personas. Recuerdo de muchas de nuestras conversas en la hora del té. Te deseo el mejor en tu vida, siempre. Cuenta eternamente comigo para lo que necesites. Sarah-Jeanne! You are amazing. I will always remember the good energy you transmit to everyone. I miss you, baby! Denisse, la mejicana francesa. Muchas gracias por nuestras salidas por Barcelona, por enseñarme a hacer crepes (y no guacamole jejejeje) y por los buenos momentos que hemos compartido. Me alegra saber que estás bien. Eres la prueba que hay vida después de la tesis.

E por fim, meu porto brasileiro. Meus muitos amigos que deixei em terras amadas para hoje está onde estou. Esses meus amigos que mesmo distante continuam me apoiando em todos os momentos. Estão ao meu lado por pelo menos 15 anos e me sinto uma sortuda, porque a distancia e o tempo deixaram intacto o sentimento de carinho e amizade que sentimos.

Kuka e Lili, minhas forças nos momentos que estou triste. Obrigada por sempre estarem ahí me apoiando e me enviando os melhores pensamentos do mundo para vencer. Obrigada por nossas conversas quase que diárias, sempre divertindo meus dias. Vcs faxceis do coração - Sandra, Emilia, Danile, aMari, Erikáo, Taty e Tate – mesmo estando longe posso sentir o carinho que vcs me enviam. Que bom é estar de volta a minha terra Natal e ver vocês me recebendo com a mesma alegria de sempre! E que as nossas conquistas são conjuntas. Lorena, tipo Gioconda!!! Obrigada por se preocupar comigo en todos os momentos. Sandra e Analu, minha representação familiar aqui na Europa e que seguem continuamente minha historia de vida, que alegria saber que seguimos celebrando muitas conquistas juntas. E 2018 será um ano que ficará marcado em nossas vidas. Contem sempre comigo. Recy e Debys, minhas primas adotadas que me ajudam em qualquer situação. As Betáo, Betoa e Lula, muito bom saber que posso contar com o apoio de vocês. Dani e Manu, obrigada por sempre estarem ao meu lado. Tantos anos juntas habitando esse maravilhoso “poço da sinceridade” e continuamos desejando sempre o melhor uma para a vida da outra. Obrigada por tudo que vocês representam.

Meu porto seguro: Familia

E agoro agradço ao pilar da minha vida: Minha família. Aos meus pais, Heleno Nunes y Maria José. A pessoa que sou hoje devo a vocês. Me ensinaram a alcançar meus objetivos e nunca cortaram minhas asas. Obrigada pelo o incentivo e força de sempre, pelas chamadas enviando otimismo e tranquilidade, por me animar me mostrando que tudo de bom do que plantamos hoje renderá bons frutos. Obrigada por aguentar a saudade para ver meu florescer desde longe. Minha vitoria devo a vocês. E nesse conjunto coloco a minha irmá Francinete. Franeteeee, obrigada por me enviar as melhores energias do mundo, por compartilhar os momentos de besteirol online que me faz desopilar um pouco (e bolar de rir toda vez que vc me pergunta: Serio? Vc achou isso engraçado?) e principalmente, obrigada pela senha do Netflix (rsrsrsrsrs). Obrigada por todos esses anos ao meu lado, Franete. Você é um pilar forte na minha vida. A meio-irma/meio tia: Silvinha (e extendo os agradecimentos a toda família Cruz), obrigada pelo carinho que sempre me recebe de volta a casa, fazendo todas as comidas tipicas, buscando sempre fazer o melhor. A Pino, meu sobrinho do coração. O carinho que você me transmite quando a gente se fala, faz reiniciar meu otimismo. Neguinha Anna Iris, torço muito por você! Muita musica na sua vida. Vovó Sebastiana, como me emociono cada vez que falo com a senhora! Se herdei de alguém essa vontade de "viver no mundo" certamente foi da senhora. Obrigada tia Nega, minha "bixa feia" preferida pelas bonitas frases que me envia pelo whats. Sei que vem repleta de carinho. A Luzia, porque sei que vc me ama (rsrsrsrs) e torcemos muito uma pela outra. Ainda espero sua visita pra gente cozinhar juntas fideus e paella. Agradeço Ivam, por todo o incentivo e apoio que me deu na hora de decidir sair do Brasil. Ainda que nos últimos anos eu sinto você mais "distante" em relação a nossa amizade, sua presença nos conselhos e exemplo de vida me acompanham. E como você uma vez me disse: "talvez não vamos acompanhar nossos familiares nas pequenas coisas do cotidiano, mas a gente conquista outras coisas também e temos que estar agradecidos". E vc tem razão.

A todos da família Oliveira, que me recebe com tanta alegria quando estou de passagem em minha terra Natal (e vem de Joao Pessoa, das Aroeiras, de Floripa) com a mala repleta de saudades. Arroxa o foli, sanfoneiro! A todos da família Nunes, que sei que

torcem por mim sempre, não importa onde eu esteja. Meu agradecimento em especial a meus primos Cleia, Gleik e Aglacy que, por alguma forma, se mostram presente nos dias que aqui se fazen muito frios.

Ao meu núcleo familiar da Espanha, os Cortada-Galvao, por me aceitarem como membro da família, me recebendo com alegria em todos os momentos que passamos juntos e deixando a minha saudade de casa mais amena. Nunca deixaram eu me sentir só. Com vocês vivi muitos momentos cheios de emoção e carinho aqui na Espanha. Vocês põem muito mais sabor no meu cotidiano (com tempero brasileiro – de norte a sul, catalão e japonês!). Em especial, agradeço a D. Elza e Seu Joaquim por verdadeiramente me "adotarem" como uma filha, sempre me dando mimos, atenção e muito otimismo. También, de manera muy cariñosa agradezco a Maria Cortada y Eduard Oliveras, por estar siempre atentos a mi trabajo. Muchas gracias por el tiempo que pasé en vuestra casa, por haber hecho lo posible para asistenciarme de la mejor forma posible. Muchas gracias a vosotros. Gracias a Lori y Pepa por las palabras tiernas y de optimismo hacia mí y mi trabajo en los momentos que nos juntamos.

And… *at last but not least*: A você meu apoio diario, o meu "gestionador de emoções" (se é que isso existe) nos momentos que eu já não sabia que fazer, meu companheiro de viagens, melhor amigo nessa jornada, Abel Cortada. Obrigada pela paciência e por manter a serenidade nos momento das noticias inesperadas que me fazia pensar que teria que desistir. Você sempre acreditou que isso era possível. Investiu o melhor de você para eu poder concluir esse trabalho. Obrigada por colocar esse objetivo também como prioritário na sua vida. Obrigada pelos carinhos nos momentos de choro e por *always* ter razão quando me dizia: "tudo vai ficar bem". Obrigada por fazer a comida quando eu nem tinha tempo de comer e por me levar para ver o horizonte quando passava mais de 5 dias diante do computador. Finalmente, conseguimos. Agora podemos visitar os amigos e seus pais sem que eu precise levar um *paper* para ler durante a viagem. Agora já podemos fazer a nossa desejada lua-de-mel. Agora já podemos fazer planos de *fim-de-semana-de-sexta-a-domingo* inteiros. Agora juntos outra vez vamos unir forças para outra nova grande feliz mudança em nossa vida.

A todos vocês, meu muito obrigado! Aquesta tesis és per tots vosaltres! Gracies à tots!

Summary

Despite their small size, phytoplankton represents up to 50% of the global primary production of the Earth and serves as a connector between oceanic and atmospheric processes. Therefore, phytoplankton constitutes a central pillar in the comprehension of the cycles of mass and energy in the oceans. Their different attributes like size, abundance, community composition, functions, pigment complex and taxonomy provide relevant information to understand the processes of global change. In the past decades, the use of HPLC chromatography (High-Performance Liquid Chromatography) has proven as a very effective methodology to study marine phytoplankton. This technique, combined with the use of the statistic program CHEMTAX, allows to identify efficiently the contribution of certain taxonomic classes. This thesis is centered around the use of HPLC-CHEMTAX to identify the phytoplanktonic communities of three regions: the Mediterranean Sea, the Atlantic Ocean and the Antarctic Ocean, each characterized by different trophic conditions (from oligotrophic to eutrophic). With the results obtained, we expect to contribute to the comprehension of the local biochemical responses in a context of global change, as well as to improve future models of ecosystems and algorithms for remote sensing. To validate the data obtained, the results originated from the HPLC-CHEMOTAX were compared to other techniques used for identification and quantification, such as microscopy, flow cytometry and bio-optics. First, we focused on a temporal series (14 years) where we analyzed the seasonal and inter-annual dynamics of the phytoplanktonic community. We have verified that the phytoplanktonic community follows a seasonal pattern, just as had been observed in previous studies: diatoms dominated the blooms of late winter/early spring, while *Synechococcus* showed maximum abundances during the months of April and August. The cryptophytes and dinoflagellates showed a positive response to sporadic fertilization events, associated mainly to stormy events. In the next study of this thesis, we analyzed the size fractions obtained from sequential filtrations by HPLC-CHEMTAX (total, n+m>3 µm and pico<3 µm) and we compared the results obtained with the algorithms proposed by Vidussi et al. (2001), Uitz et al. (2006) and Hirata et al. (2011). We also measured the specific absorption coefficient of phytoplankton and we compared it with size indicators. Our observations suggest that studies using size fractionation can inform about the sturcture of sizes of a community and that the absorption coefficient of phytoplankton is mainly associated with the pigment composition of the cells and the photoacclimation processes in different phytoplanktonic communities. Finally, with the aim of describing the diversity, abundance and physiologic characteristics of the phytoplanktonic community associated with the formation of marine aerosols, we have used the HPLC-CHEMOTAX in the Antarctic Ocean. Our study highlighted the association of cryptophytes in stratified surface waters influenced by ice fusion, the bloom of diatoms in South Georgia, an area rich in iron, as well as the substantial contributions of less studied groups such as the pelagophytes. In summary, this thesis shows the effectiveness of the HPLC-CHEMOTAX to study phytoplanktonic

communities in varying ecological processes and environmental conditions. And in addition, the results obtained demonstrate that the HPLC-CHEMOTAX is also appropriate to quantify simultaneously different size classes of phytoplankton.

Resumen

A pesar de su microscópico tamaño, el fitoplancton representa hasta el 50% de toda la producción primaria de la Tierra y ejerce de conector entre los procesos oceánicos y atmosféricos. Por lo tanto, el fitoplancton constituye un pilar central necesario para la comprensión de los ciclos de materia y energía de los océanos. Sus atributos como el tamaño, abundancia, comunidades, funciones, conjunto pigmentario y taxonomía proporcionan información relevante para entender los procesos de cambio global. En las últimas décadas, el uso de la cromatografía por HPLC (High-performance Liquid Chromatography) se ha revelado como una metodología muy efectiva para el estudio del fitoplancton marino. Dicha técnica combinada con la utilización del programa estadístico CHEMTAX permite identificar de forma eficiente la contribución de diversas clases taxonómicas. Esta tesis se ha centrado en el uso del HPLC-CHEMTAX para identificar las comunidades fitoplanctónicas en tres regiones: el Mar Mediterráneo, el Océano Atlántico y el Océano Antártico, caracterizados por distintos estados tróficos (desde oligotróficos a eutróficos). Con los resultados obtenidos esperamos contribuir a la comprensión de las respuestas biogeoquímicas locales en un contexto de cambios globales, así como mejorar futuros modelos de ecosistemas y algoritmos para sensores remotos. Para validar los datos obtenidos, los resultados provenientes del HPLC-CHEMTAX fueron comparados con otras técnicas de identificación y cuantificación, tales como microscopía, citometría de flujo y bio-óptica. Primeramente, nos centramos en una serie temporal (14 años) donde se analizaron las dinámicas estacionales e interanuales de las comunidades fitoplanctónicas. Hemos verificado que el conjunto de la comunidad fitoplanctónica sigue un patrón estacional, tal y como se había visto en estudios anteriores: las diatomeas dominaron las proliferaciones de final de invierno/inicio de primavera, mientras que *Synechococcus* presentó su máximo en los meses de Abril y Agosto. Los criptofitos y los dinoflagelados respondieron de forma positiva a fenómenos esporádicos de fertilización, principalmente a los asociados con eventos de precipitación. En el siguiente estudio de esta tesis hemos analizados las fracciones de tamaño obtenidas por filtraciones seriadas con HPLC-CHEMTAX (total, n+m>3 µm y pico<3 µm) y comparamos los resultados obtenidos con los algoritmos propuestos por Vidussi et al. (2001), Uitz et al. (2006) e Hirata et al. (2011). También medimos el coeficiente específico de absorción del fitoplancton y se comparó con indicadores de tamaño. Nuestras observaciones sugieren que los análisis mediante fraccionamientos pueden informar sobre la estructura de tamaños de la comunidad, y que la variación del coeficiente de absorción del fitoplancton está relacionada principalmente con la composición pigmentaria de las células y los procesos de fotoaclimatación en las diferentes comunidades de fitoplancton. Finalmente, con la finalidad de describir la diversidad, abundancia y características fisiológicas de la comunidad fitoplanctónica en relación con la formación de aerosoles marinos, se ha utilizado el HPLC-CHEMTAX en el Océano Antártico. Nuestro análisis destacó la asociación de criptofitas con aguas superficiales estratificadas influenciadas por la fusión del hielo, la floración de diatomeas en Georgia del Sur, una región rica en hierro,

así como la contribución sustancial de formas menos estudiadas como las pelagofitas. En resumen, esta tesis prueba la eficacia del uso del HPLC-CHEMTAX para el estudio de las comunidades fitoplanctónicas en distintos procesos ecológicos y condiciones ambientales. Además, los resultados obtenidos demuestran que el HPLC-CHEMTAX es adecuado para cuantificar e identificar simultáneamente distintas clases de tamaño de fitoplancton.

Resum

Tot i la seva mida microscòpica, el fitoplàncton contribueix fins al 50% de tota la producció primària de la Terra i fa de 'connector' entre els processos oceànics i atmosfèrics. Això fa que el fitoplàncton sigui un pilar fonamental per a la comprensió dels cicles de matèria i energia dels oceans. Les seves característiques, tals com la mida, abundància, comunitats, funcions, conjunt pigmentari i taxonomia, proporcionen informació rellevant per entendre els processos de canvi global. Durant les últimes dècades, l'ús de la cromatografia per HPLC (*High-performance Liquid Chromatography*) ha esdevingut una metodologia molt efectiva per a l'estudi del fitoplàncton marí. Combinat amb la utilització del programa estadístic CHEMTAX permet identificar de manera efectiva la contribució de diverses classes taxonòmiques. Aquesta tesis s'emmarca en l'ús del HPLC-CHEMTAX per tal d'identificar les comunitats de fitoplàncton en tres regions: el Mar Mediterrani, l'Oceà Atlàntic i l'Oceà Antàrtic, aquestes tres regions es caracteritzen per tenir diferents condicions de fertilitat (des de oligotròfiques fins a eutròfiques). Amb els resultats obtinguts en aquesta tesi esperem a millorar la comprensió de les respostes biogeoquímiques locals en un context de canvis globals, així com també millorar futurs models d'ecosistemes i algoritmes per a sensors remots. Per tal de validar les dades obtingudes, els resultats provinents del HPLC-CHEMTAX van ser comparats amb altres tècniques de identificació i quantificació, tals com microscopia, citometria i bio-òptica. Primerament, vam analitzar una sèrie temporal (14 anys) on es van analitzar les dinàmiques estacionals i interanuals de les comunitats fitoplantòniques. S'ha comprovat que el conjunt de tota la comunitat de fitoplàncton segueix un patró estacional i, tal com s'havia observat en estudis anteriors, les diatomees van dominar les proliferacions al final de l'hivern/inici de primavera, mentre que *Synechococcus* va presentar el seu màxim durant els mesos d'abril i agost. Les criptofites i els dinoflagel·lats van respondre de manera positiva a fenòmens esporàdics de fertilització, principalment associats a events de precipitació. Posteriorment, durant el següent estudi d'aquesta tesis, hem analitzat les fraccions de mida obtingudes per filtracions amb els resultats obtinguts per HPLC-CHEMTAX (total, n+m>3 µm i pico<3 µm) i es van comparar els resultats obtinguts amb els algoritmes proposats per Vidussi et al. (2001), Uitz et al. (2006) i Hirata et al. (2011). També es va medir el coeficient específic d'absorció del fitoplàncton i es va comparar amb indicadors de tamany. Les nostres observacions suggereixen que els anàlisis de fraccionament poden informar sobre la estructura de mides de la comunitat, i que la variació del coeficient d'absorció del fitoplàncton està relacionat principalment amb la composició pigmentaria de les cèl·lules i amb els processos de fotoaclimatació en les diferents comunitats de fitoplàncton. Finalment, amb la finalitat de descriure la diversitat, abundància i característiques fisiològiques de la comunitat fitoplanctònica en relació amb la formació d'aerosols marins s'ha utilitzat el HPLC-CHEMTAX a l'Oceà Antàrtic. El nostre anàlisis destaca la associació de criptofites amb aigües superficials estratificades influenciades per la fusió del gel, la floració de diatomees a Georgia del Sud, una regió rica en ferro, així com la contribució substancial de formes menys

estudiades de pelagophytes. En resum, aquesta tesis prova la eficàcia de l'ús del HPLC-CHEMTAX per a l'estudi de les comunitats fitoplanctòniques en diferents processos ecològics i condicions ambientals. A més, els resultats obtinguts demostren que el HPLC-CHEMTAX es adequat per quantificar i identificar simultàniament diferents classes de mides de fitoplàncton.

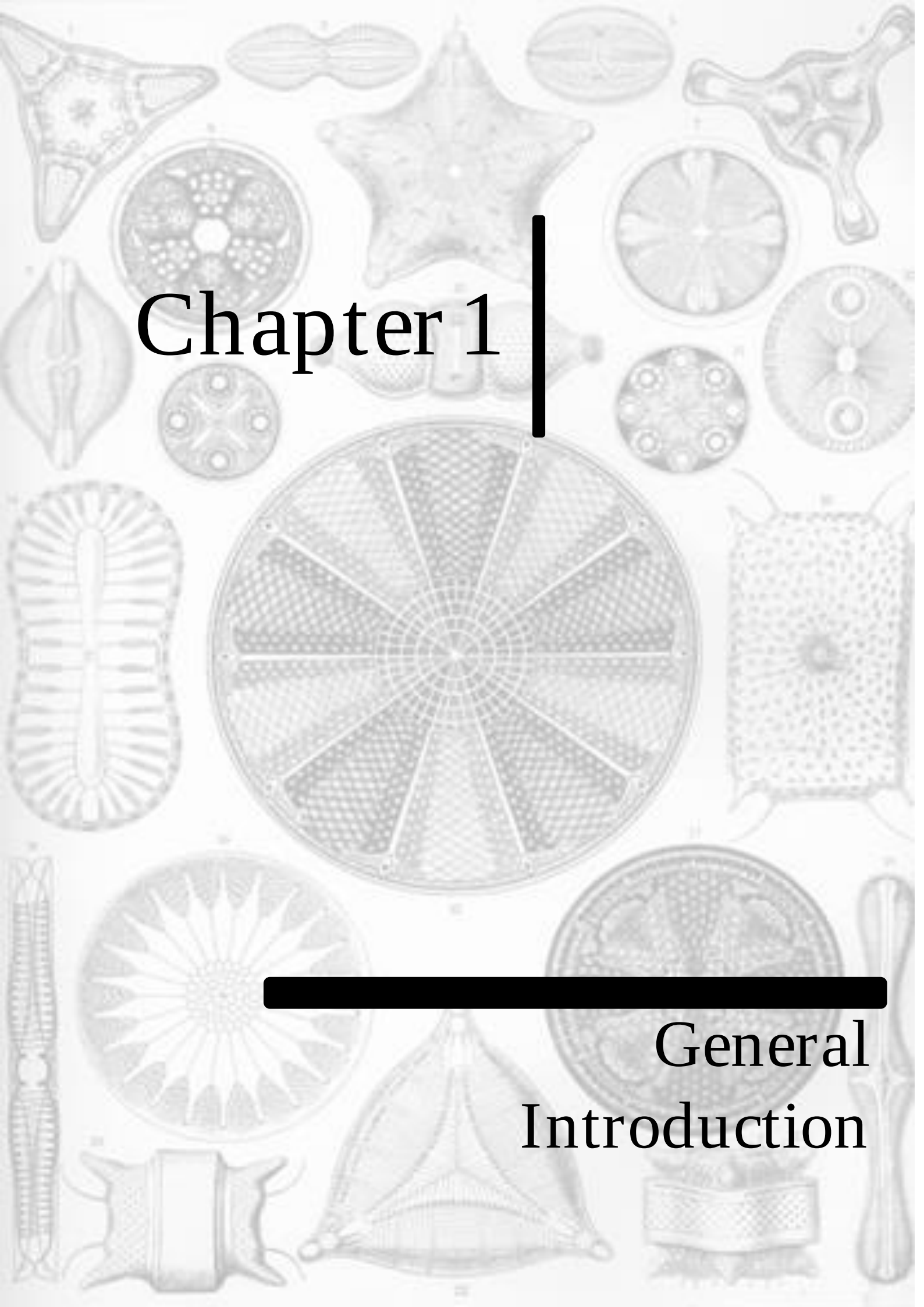

Chapter 1

General Introduction

CHAPTER 1

GENERAL INTRODUCTION

1.1. THE GRANDEUR OF THE TINY

They are not usually popular, neither well known yet. Their sizes are so small that they can only be seen under the light of a microscope (and sometimes not even that). They are at the mercy of the currents due to its nonexistent or very limited swimming capacity. Nevertheless, their relevance for marine and freshwater ecosystems and for the whole planet is exceptional (Falkowski et al., 2004). They work as "connecting bridge" between the atmosphere and the ocean since the origin of the oxygenation history of Earth when they modified the biochemistry of both environments. It is estimated that approximately 95% of total productivity in marine environments is dominated by them (Kennish, 2001). Furthermore, their diversity seems to be crucial for the stability and functioning of oceanic ecosystems and biogeochemical cycles (Roy et al., 2011; Ptacnik et al. 2008). Nevertheless, without them half of Earth's oxygen would not exist (Field et al., 1998; Falkowski, 2002).

These tiny powerful organisms are called PHYTOPLANKTON (from Greek: phyton = plant; plankton = wanderer). And about them, we are just getting started.

1.1.1. The role of phytoplankton in the biogeochemical cycles

The distribution of phytoplankton biomass and net primary production is defined by the bio-availability of light and nutrients, and these growth limiting factors are, in turn, regulated by physical processes (Kennish, 2001; Roy et al., 2011). Through the photosynthesis process, the phytoplankton represents the entry of solar energy into the

marine ecosystem playing a vital role in the energy flow and biogeochemical cycles of elements such as carbon, nitrogen, phosphorus, oxygen and sulfur (Margalef, 1978; Falkowski and Woodhead, 1992). Regarding the carbon biogeochemical cycle, the flux of CO_2 that is absorbed every year by phytoplankton is approximately of 10 GT (Tréguer et al., 2003). Phytoplankton primary producers use sunlight and inorganic nutrients to produce organic matter from dissolved CO_2. This organic matter can be consumed by zooplankton or processed by bacteria, which in turn can be eaten by larger organisms. As a result, a part of this surface biomass ends up as dead cells, detritus or fecal pellets and sinks into the deep ocean. Most of the organic matter produced at surface is respired, but a small fraction (0.1 to 1%) reaches the bottom of the mesopelagic zone, where it can remain sequestered for a long time. Therefore, photosynthetic microorganisms contribute to reduce the rate at which inorganic carbon currently accumulates in the atmosphere and help to 'pump' this excess of dioxide carbon to the deep layers of the ocean were it can be trapped for hundreds of years (Jiao et al., 2010). This process is so important that if these aquatic microorganisms stopped sending carbon to the deep sea in our current days, atmospheric levels of carbon dioxide would eventually rise by another 200 ppm and global warming would be accelerated (Falkowski, 2012).

Phytoplankton plays an important role not only in the cycle of carbon, but also in those of other elements such as nitrogen, phosphorus, silicon and sulphur. Cloud formation is one of the processes in which phytoplankton may take part in an active way. In 1972, Lovelock suggested that phytoplankton could regulate the Earth's climate through the production on DMS, which is oxidized in the atmosphere to form a sulphate aerosol, a major source of cloud condensation nuclei (lovelock, 1972). In what became known as the 'CLAW hypothesis', an acronym that includes the names of its four coauthors:

Charlson, Lovelock, Andreae and Warren. Charlson et al. (1987) proposed that because an increased cloud cover increases albedo, climate regulation by phytoplankton could be possible because of the enhancing effects of higher temperature and sunlight on phytoplankton growth and DMS production. In other words, this is a feedback mechanism involving in a global scale the marine phytoplankton and the Earth's climate. Yet, the climate effects of DMS and the underlying atmospheric processes remain highly controversial (Quinn and Bates, 2011). Despite numerous contributions on the role of phytoplankton in aerosol production (Asher et al., 2011; Galí et al., 2015) and on the influence of aerosols in the optical properties of the atmosphere and the radioactive budget (Simó, 2001), the biological processes governing the ocean-atmosphere exchange need to be better understood.

1.2. MARINE PHYTOPLANKTON TAXA COMPOSITION

Within the tree of life, the marine phytoplankton previously described is distributed across many clades in two life domains: eukaryotic algae and the prokaryotic organisms (Sournia et al., 1991). Some years before, in 1978, Sieburth and collaborators classified the phytoplankton in microphytoplankton (20-200 µm), nanophytoplankton (2-20 µm) and picophytoplankton (<2 µm). The nano- and microphytoplankton are mostly composed of eukaryotes algae, whereas the picoplankton is composed of prokaryotes and an abundance of small eukaryotes that fits this class size (Johnson and Sieburth, 1982). The principal phytoplankton clades are Bacillariophyceae (diatoms), Dinophyceae (dinoflagellates), Prymnesiophyceae (coccolithophorids) and Chrysophyceae (silicoflagellates) – eukaryotes - and Cyanophyceae (*Synechococcus* spp. and *Prochlorococcus* spp.) – prokaryotes. Diatoms, dinoflagellates, haptophytes

and green algae are the most identified groups – being known 40, 40, 10 and 6% of the total of the phytoplankton species describe respectively, while the cryptophytes, chlorarachniophytes and euglenophytes appear far less than 2% for each group (Simon et al., 2004).

Another peculiar characteristic in the identification of phytoplankton organisms is to distinguish them by the combination of their pigment composition. Basically, pigments are present in all photosynthetic organisms and function as light harvesting agents for photosynthesis and photoprotection to the cell (Porra et al., 1997). Alternatively, these pigments serve as biomarkers for particular classes or even genera of phytoplankton (Zapata et al., 2004; Wright and Jeffrey, 2006). The automated measurements of pigment concentrations are obtained from high-performance liquid chromatography (HPLC) methods and to date, it has been possible to quantify until over 50 phytoplankton pigments (Aneeshkumar and Sujatha, 2012). Some photosynthetic pigments (19'-butanofucoxanthin, 19'hexanofucoxanthin, alloxanthin, chlorophyll *b*, fucoxanthin, peridinin, zeaxanthin,) are considered diagnostic pigments (DP) of specific phytoplankton groups -pelagophytes, haptophytes, cryptophytes, chlorophytes, diatoms, dinoflagellates and cyanobacteria, respectively; Vidussi et al., 2001; Le Quéré et al., 2005; Chai et al., 2016). In general, Chlorophyll *a* and Chlorophyll *c* are indicators of total algal biomass, even if divinyl chlorophyll *a* is *Prochlorococcus* biomarker pigment (Table 1). This approach has been termed phytoplankton chemotaxonomy and it has contributed in the last fifteen years to a much better understanding of the distribution and composition of oceanic phytoplankton populations in different ocean zones (Gibb et al., 2001).

Table 1. Summary of pigments recovered in the water column and their taxonomic. Compiled for Jeffrey et al. (1997) and Roy et al. (2011). * Biomarkers unambiguous Pigments

Pigment	**Phytoplankton Groups**
Chlorophylls	
Chl *a*	All photosynthetic algae
Chl *b*	Green algae, euglenophytes
Chl *c* (all)	Dinoflagellates, Diatoms, Chrysophytes
Dv chl *a**	Prochlorophytes
Carotenoids	
19'-hex	Haptophytes, some dinoflagellates
19'-but	Pelagophytes, haptophytes
α – car	Cryptophytes, prochlorophytes
β - car	Most algae
Alloxanthin*	Cryptophytes
Fucoxanthin	Diatoms, prymnesiophytes, chrysophytes, several dinoflagellates, Parmales
Diadinoxanthin	Diatoms, dinoflagellates, chrysophytes, prymnesiophytes, cryptophytes
Peridinin*	Dinoflagellates
Zeaxanthin	Cyanobacteria, chrysophytes, pelagophytes
Lutein	Green algae, prasinophytes
Neoxanthin	Green algae, prasinophytes, some dinoflagellates
Prasinoxanthin*	Prasinophytes
Violaxanthin	Chrysophytes, chlorophytes, prasinophytes and dinoflagellates
Chlorophyll *a*	**(degradation products)**
Pheophytin *a*	Chl *a* derivative (general)
Pheophorbide *a*	Grazing, senescent diatoms

1.2.1. Structural and functional description of phytoplankton the community

Species with similar biogeochemical roles or physiological traits can be grouped into the so-called phytoplankton life-forms (Margalef, 1978) or functional types (PFTs; Kostadinov et al., 2010). For example, *Synechococcus* and *Prochlorococcus*, have a high surface area to volume ratio, which is very efficient to nutrient uptake. This allows them to thrive in oligotrophic regions, whereas diatoms, which have high growth rates, need to keep a high intake of nutrients for maintaining growth (Zubkov et al., 2003). On

the other hand, the dominance of different types of phytoplankton may affect the efficiency of the biological pump (Eppley and Peterson, 1979; Falkowski et al., 1998). Eventually, the taxonomic classifications and PFTs have a correspondence (see Lé Quére et al, 2005): for example the diatoms and some coccolithophores (Prymnesiophyte class) produce mineral-phase shells: Prymnesiophyte is mostly known by phytoplankton calcifying while diatoms are associated with silica (Klaas and Archer, 2002; Zeng et al., 2018) and both also contribute to vertical carbon fluxes and influence phytoplankton sinking rates, important information to evaluate and study global warming and climate change. This way, the PFTs associated with the phytoplankton size structure (PSC) studies, could provide responses face to change biochemical, ecology, physiological and behavior. This relationship between PSC and PFT is already recognized in some studies (Peters, 1983; Brewin et al., 2015; Zeng et al., 2018) and has helped to characterize both the energy flow and biogeochemical cycling on a global scale and determine the capacity of the aquatic environment to recycle carbon.

1.3. PHYTOPLANKTON IDENTIFICATION METHODOLOGIES: AN OVERVIEW

Phytoplankton organisms span a wide range of genetic, morphological and functional diversity. To gain knowledge into this diversity is crucial for understanding the functioning not only of aquatic ecosystems but also of biogeochemical and climate processes affecting the whole planet. However, characterizing phytoplankton is not a straightforward task and many techniques to describe and monitor the abundance, composition and diversity of the phytoplankton community have been developed,

especially over the last 80 years. Some traditional techniques, of global focus or genetic are briefly described below.

1.3.1. The Microscopy method

The most traditional and the most widely used technique for the identification and quantification of the phytoplankton community structure, is the inverted microscope technique (Utermöhl, 1958). It consists on sedimenting the water sample on a composite chamber and lately performing a phytoplankton counting. The great advantage of this technique is the identification of phytoplankton species by a morphology criterion (Alvarez, 2014). Nevertheless, is necessary a big effort to process each sample, it becomes a high-time consuming and a specialized task. The time required to both, preparing a high-quality taxonomist and identifying the organisms in the sample is excessive. Moreover, it is only adequate for the larger forms (> 10 µm) and there are fragile forms that degrade easily in fixed samples (Rodriguez, 2001). In addition, there are genetically diverse forms that, at least in practice, cannot be distinguished using morphological characteristics (cryptic diversity) and many species are present only in exceptionally low abundances (Uusitalo et al., 2013). It is believed that less than 5,000 species of marine phytoplankton in fourteen genera have been described by morphological criteria at the end of the 1980s (Sournia et al., 1991). Thus, using only microscopy to study phytoplankton diversity would be a utopian challenge.

1.3.2. Flow cytometry and molecular techniques

Conventional light microscopy is the main tool for the identification and enumeration of phytoplankton, but it has limitations, particularly for the differentiation of small-sized phytoplankton groups (nanophytoplankton and picophytoplankton). Epifluorescence microscopy of cells retained on filters (Porter and Feig, 1980), based on

the natural fluorescence of phytoplankton pigments and on the use of colorants like DAPI (4,6-diamidino-2-phenylindole), which stains the cells DNA, gives an idea of the size, broad morphology and general features of the organisms, as for instance the presence of flagella or chloroplasts (Giner, 2017). Another example is Flow Cytometry (FC). The FC, technique developed initially for medical science, allows the enumeration of isolated cells (Yentsch et al., 1983; Sieracki et al., 1998) and the estimation of biomass from cell biovolume (Gasol and Giorgio, 2000), permitting to differentiate size and shape (Jochem, 2001). However, both methods are unable to obtain high resolution in the classification of the organisms.

With the advancement of the modern molecular techniques, the ability to characterize and quantify the phytoplankton biodiversity has improved very quickly. The recent development of molecular approaches, particularly analyses of DNA from genes encoding rRNA and RuBPC, has revolutionized analysis of phytoplankton populations (Díez et al, 2001), allowing characterization even of unculturable organisms to beyond the species level (Roy et al., 2011). In fact, many new strains have been discovered in the last decades, especially in the fraction of picophytoplankton size (Guillou et al., 1999; Not et al., 2009). These techniques also improved our understanding in relation to the evolution and diversity of phytoplankton and the need to connect genomics, phylogenies and physiology (Johnson and Martiny, 2015). These molecular surveys give us a lot of information that increases our knowledge about diversity, but many of the detected sequences correspond to organisms never seen before, and we end up without the knowledge about their morphology, ecology or even their function (Giner, 2017).

1.3.3. Writing Colors by phytoplankton - the Chromatography analysis

Chlorophyll *a* is the biochemical parameter most studied since the mid-1950s (Richards and Thompson, 1952). Since then, the study of phytoplankton pigments has become of relevant importance in oceanographic studies. This parameter can be analyzed using spectrophotometry methods (Yentsch and Menzel, 1963), using fluorometry methods *in vitro* (Lorenzen, 1966) and also *in vivo* in the water column (Rodriguez, 2001).

Phytoplankton species differ in the combination of their pigment composition (Table 1). This approach has been termed phytoplankton chemotaxonomy, and it has contributed in the last fifteen years to a much better understanding of the distribution and composition of oceanic phytoplankton populations (Gibb et al., 2001). The analysis of phytoplankton pigments by high-performance liquid chromatography (HPLC - Writing Colors) has proved to be an important instrument for the taxonomic classification based on the specificity of the pigments photosynthetic. This technique, also known as chromatography, was employed for the first time in 1903 by the Russian botanist M. Tswett, who used it to separate plant pigments such as chlorophyll, carotenes and xanthophylls (Ettre, 2003).

The base of modern study of phytoplankton pigments and, consequently of chromatography, begun with Jeffrey (1968; 1974) who verified that could relate pigments as markers of taxonomic groups (Jeffrey, 1976). Then, it was possible to separate and quantify different pigments (Wright and Shearer, 1984). In 1978, the SCOR-78 (Scientific Committee on Oceanic Research) working group reviewed modern analytical techniques and their application to biological oceanography and released “The Phytoplankton Manual”, divided into two volumes. The results include

the "ICO manuals and guides" series and the UNESCO "Monographs on oceanographic methodology" publications (Jeffrey et al., 1997).

In the last 30 years the use of HPLC has been improved and has shown to be an important tool in many biomass quantification studies and also for unveiling the composition of taxonomic phytoplankton classes (Rodriguez, 2001). The HPLC methodology has also been used to estimate the contribution of different phytoplankton size fractions - micro, nano- and picophytoplankton (Vidussi et al., 2001; Uitz et al., 2006, Hirata et al., 2011), characterizing the physiology of phytoplankton by pigments results (Gieskes and Kraay, 1986; Araujo et al, 2017), photopigment indices (Vega-Moreno et al., 2012; Araujo et al, 2017) and Phytoplankton Size Class/Phytoplankton Functional Types (Brewin et al, 2015; Zeng et al., 2018; Nunes et al, 2018a). In addition, the HPLC is presented as a technique that allows to analyze a relatively large number of samples, that can be collected and analyzed rapidly with low cost (Wright et al., 1996), and also to identify all phytoplankton types of smaller and larger size (Hirata et al., 2011).

Taking into account the existence of different pigments that are present in different groups of phytoplankton and the multiple combination of that can be detected, Mackey et al. (1996) developed a statistical toolbox for MATLAB called CHEMTAX (CHEMical-TAXonomic). An output matrix with the percentage contribution of each taxonomic group in relation to Chlorophyll *a* in the sample is used. The key is to prepare the initial matrices that represent the reality of each environment, i.e., different regions will have different matrices. It is also possible to differentiate any algal class despite of whether or not the marker pigments correspond to a single class (Latasa, 2007). Nevertheless, it is recommended to develop specific matrices for different study

areas, comparing analyses in microscope with the analyses of pigment composition by HPLC and a different technique (Latasa, 2014).

The HPLC pigment analysis and subsequent CHEMTAX application have proven to be successful techniques to process the high number of samples needed to study large-scale phytoplankton distributions (Roy et al, 2011) and to track the composition of the communities in long-term time series (Marty et al., 2002; Armbrecht et al., 2015; Nunes et al., 2018b). With due caution about limitations and minimal knowledge about the populations of the study regions (Irigoien et al., 2004), the combination of HPLC and CHEMTAX may result in a fairly feasible and reliable method for the determination of composition and fluctuation of phytoplankton communities (Mendes, 2011).

There is no technique that is best fitted in all circumstances and for all purposes. The particular strength of these techniques is that they can be compared with other methodologies in order to achieve an improved conclusion to the data that has been demonstrated. This overlap is useful for the broader goal of characterizing the biodiversity of the phytoplankton community in order to understand what is out there, how they are related and what they are doing.

1.3.4. Phytoplankton estimation from the space

In the 1970s and 1980s, a large number of researches were conducted to estimate marine primary productivity in the oceans (Nunes-Neto, 2009). One of the advances in this line of research was the advent of remote sensors specially developed to monitor the color of the ocean and phytoplankton began to be observed from space. The Moderate Resolution Imaging Spectroradiometer (MODIS) instrument aboard NASA's Earth and Aqua satellites measure the color of the ocean every day from the Chlorophyll a concentrations detected in the oceans (NASA, 2018). Changes in the amount of

phytoplankton can indicate the change in ocean productivity, providing an important ocean link for monitoring global climate change. From the absorption of sunlight by photosynthetic pigments in different species of phytoplankton, the absorption coefficient of phytoplankton is obtained and applied to the use of satellite observations of the color of the ocean (Sathyendranath et al., 2001). Moreover, through the use of this coefficient, is possible calculate the propagation of light (Sathyendranath and Platt, 1988), primary production (Morel, 1991; Marra et al, 2007) and even phytoplankton physiology (Stramski and Reynolds 1993; Bouman et al., 2003). Although remote sensing has the great advantage of instantly covering an area of hundreds of kilometers for repeated times, it does not replace sampling in situ. The data obtained by satellite does not get the profiles below the surface layer, and in the ocean often the maximum primary production occurs at greater depths (McClain et al., 2003). In addition, for the calculation of satellite algorithms it is required to know in advance the bio-optical data (pigment concentration and its oscillations in the cellular pigment composition and package effect), the composition of pigments (Jeffrey et al., 1999), the phytoplankton identification and biodiversity, the biomass and the phytoplankton community (Bricaud et al, 1995; Brewin et al, 2010). These data can only be made available with previous sampling in situ and hence these data must be generated with resolute methods for the most diverse oceanic zones.

1.4. BIO-OPTICAL DESCRIPTION OF THE PHYTOPLANKTON COMMUNITY

Cell size and pigment content obtained on a single cell basis allow the exploration of the size-scaling of pigment content. These pigments composition also

could determine the spectral dependence of the absorption coefficients, that is the effect of the interactions between the physical states diagnose and the diverse pigment combinations expression through the changes in phytoplankton physiology (Hoepffner and Sathyendranath, 1991). Thus, also influences the relative absorbed energy that excites chlorophyll fluorescence (Yentsch and Phinney, 1985). For example, when phytoplankton responses to the spectral quality of light at a given time, the photoacclimation. This can be reflected in changes both in: (1) the pigment cellular composition and; (2) the concentration of intracellular pigment (package effect; Bricaud et al., 1995; Lohrenz et al., 2003; Babin et al., 2003; Wang et al., 2014). Essentially, if the irradiance increases, photoprotector pigments also increase while the content of chlorophyll *a* and accessory light-harvesting pigments decreases (Falkowski and Ravem, 1997). Basically, the package effect increases because of the lowered efficiency of light absorption (Kirk, 1994). In turn, the packing effect could be partitioned into changes in cell size or changes in the intracellular concentration of pigments, which can be determined by changes in the community structure and by photoacclimation (Morel and Bricaud, 1981). These changes deeply influence the specific absorption of chlorophyll *a* in the blue region of the spectrum and consequently, the phytoplankton spectral absorption will be different.

In the last years, many studies of phytoplankton spectral absorption coefficients (aph*(λ)) and their variations at different spatial and temporal scales have been developed (Babin et al., 2003; Perez et al., 2016). These interactions require an accurate understanding of environmental factors, which in turn regulate phytoplankton growth. Therefore, knowing the phytoplankton light absorption coefficient is fundamental to understand the optical variability of ocean waters, and consequently, to improve bio-optical analytical models, in particular for the interpretation of ocean color. Hence, cell

size and elemental composition appear as fundamental traits in phytoplankton growth models. The analysis of the structural and physiological aspects allows us to make inferences of energetic nature, relative to such questions as the maximum photosynthetic rate, the efficiency in the energy transfer across the food-web or the fate of primary production (Alvarez, 2014).

1.5. AIMS OF THIS THESIS

This thesis used High Performance Liquid Chromatography (HPLC) analysis of phytoplankton pigments (Jeffrey et al, 1997; Roy et al, 2011; Latasa, 2014) and CHEMTAX algorithm (Mackey et al., 1996; Latasa, 2007) to identify the phytoplankton communities in three different regions of the globe: a) the Mediterranean Sea, b) the Atlantic Ocean and c) the Southern Ocean. In each chapter, we combined the HPLC results with microscopic observations to obtain information and validate our results. We expect that the results obtained in this study will contribute to a better understanding of phytoplankton distribution and its response to environmental forcing in a context of global change, and that they will help to improve future ecosystem models and remote sensing algorithms.

The thesis is structured in three main objectives:

- To identify the temporal variability of the phytoplankton community structure in a coastal station and to ascertain the occurrence of trends that could be associated with global change - ***Chapter 2***
- To describe the chemotaxonomic composition and size structure of the phytoplankton of surface waters and relate these results with bio-optical properties across a variety of marine environments - ***Chapter** 3*

- To document the links between phytoplankton community structure and aerosol composition in Southern Ocean - ***Chapter 4***

Chapters 2 and **3** are presented in the form of scientific papers, one already published, one accepted and one submitted to an international journal. A brief presentation of each chapter and its specific objectives is given below.

Chapter 2: **Seasonal and interannual variability of phytoplankton community structure in a Mediterranean coastal site**

This chapter studies the seasonal and multiannual variability of the phytoplankton community during a long temporal series (14 years) sampled in the Blanes Bay Microbial Observatory (Northwestern Mediterranean Sea).

The seasonal dynamics of the phytoplankton assemblages and the multiannual trends in total biomass are related to environmental parameters and long-term changes in anthropogenic forcing.

Chapter 3: **Size fractionation, chemotaxonomic groups and bio-optical properties of phytoplankton along a transect from the Mediterranean Sea to the Southwestern Atlantic Ocean**

This chapter uses HPLC pigment analysis followed by the CHEMTAX algorithm to identify the variability of three size fractions (whole water, nano+microplankton and picoplancton) of the phytoplankton community across several biogeochemical provinces of different fertility characteristics. Experimental results for size-fractionated Chl *a* are compared with the size class estimates derived from the diagnostic pigment approach of Vidussi et. al (2001) and Uitz et al. (2006), and the Chl *a*-based expressions

of Hirata et al. (2011). Bio-optical properties of surface waters are interpreted in the context of the phytoplankton characteristics.

Chapter 4: **Phytoplankton community structure in contrasting ecosystems of the Southern Ocean: South Georgia, South Orkneys and Western Antarctic Peninsula**

HPLC-CHEMTAX results are combined with microscopic observations of nano- and microphytoplankton to report the quantitative distribution and taxonomic composition of the phytoplankton community in each study region, as a function of environmental variables. The work is part of an effort to document the links between the structure of the planktonic ecosystem and marine aerosol composition.

.

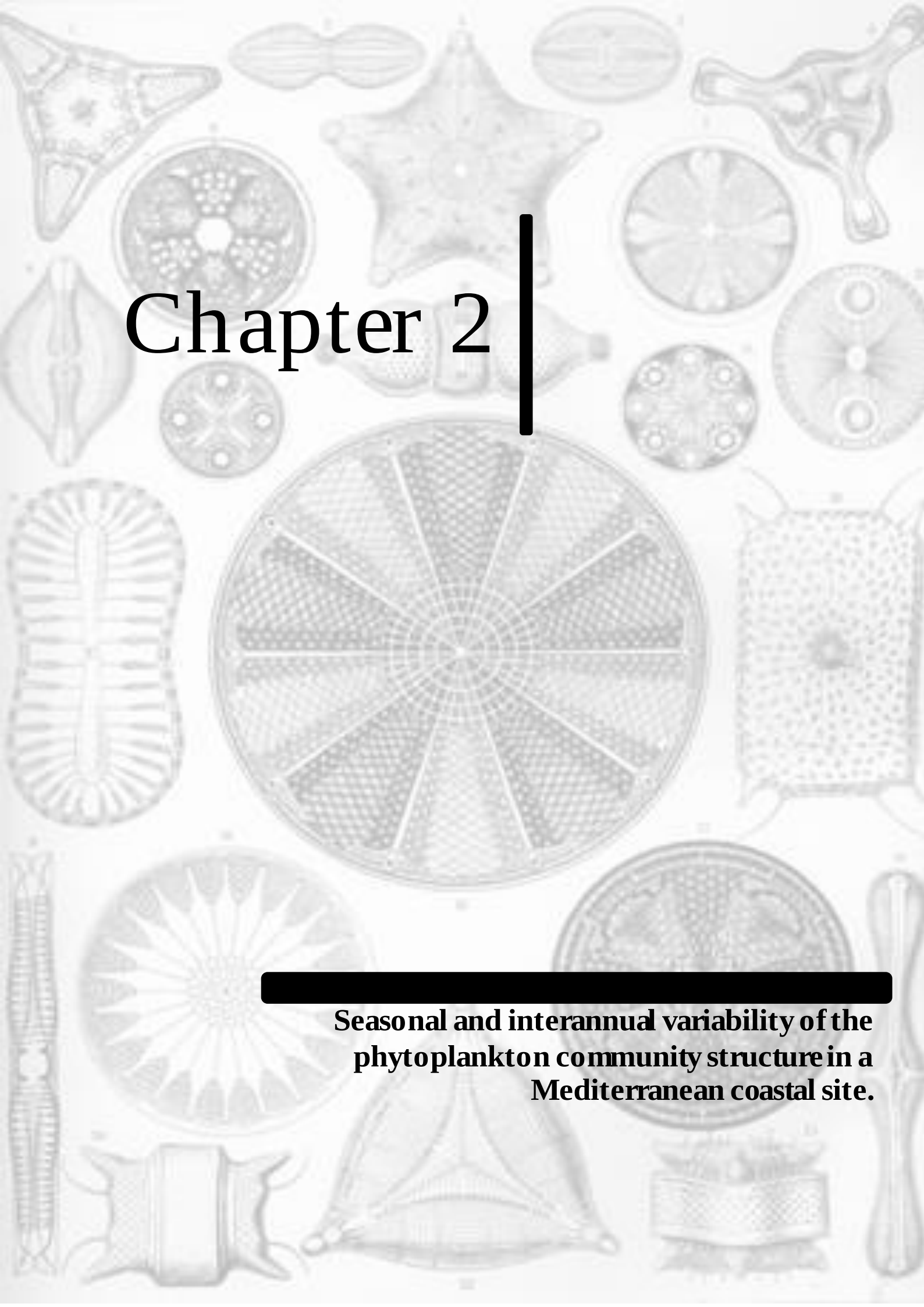

Chapter 2

Seasonal and interannual variability of the phytoplankton community structure in a Mediterranean coastal site.

The scientific contribution of this work has resulted in the publication of this chapter as a manuscript entitled: Nunes, S.**;** Latasa, M.; Gasol, J.M.; Estrada, M. (2018) **Seasonal and interannual variability of the phytoplankton community structure in a Mediterranean coastal.** Marine Ecology Progress Series. 592: 57–75. doi: https://doi.org/10.3354/meps12493.

CHAPTER 2

Seasonal and interannual variability of phytoplankton community structure in a Mediterranean coastal site

ABSTRACT: We studied phytoplankton community structure in surface waters of the fixed coastal station of the Blanes Bay Microbial Observatory (NW Mediterranean Sea). A chemotaxonomic approach based on HPLC analysis of phytoplankton pigments, followed by CHEMTAX algorithm implementation, was applied to a set of monthly samples taken during a 14-year period (2000-2014). Additional samples were taken for nutrient analyses, flow cytometric measurements and during part of the period for phytoplankton cell counts by optical microscopy. Overall, the most abundant groups in terms of chlorophyll *a* (Chl *a*) were haptophytes, diatoms and prasinophytes. In general, diatoms were the most important components of the total Chl *a* maxima (T_Chl *a*). We observed a merked seasonality of T_Chl *a* and several phytoplankton groups (prasinophytes, diatoms, haptophytes, cryptophytes and pelagophytes) with autumn-winter or winter-spring maxima and summer minima, coinciding with similar variation in major nutrient concentrations. *Prochlorococcus* presented a fall-winter maximum and a spring-summer minimum, while *Synechococcus* peaked in April and August, and dinoflagellates were relatively important in summer. Superimposed to this general pattern, prasinophytes and diatoms responded positively to episodic fertilization events associated with freshwater runoff caused by rain storms. Most phytoplankton groups presented a decreasing linear interannual trend that could be associated with a reduction in nutrient availability. A possible driver for this oligotrophication is the improvement of wastewater treatment in the region.

KEYWORDS: Mediterranean, Blanes Bay, phytoplankton, community structure, HPLC, pigments, time series

2.1. INTRODUCTION

Phytoplankton organisms constitute a crucial link in marine ecosystems dynamics. They contribute about half of total primary production of the world, are the main base of the food web of ocean communities and represent a key component of nutrient cycling and particle fluxes from surface to deep waters (Ryther 1969, Eppley and Peterson, 1979). Furthermore, phytoplankton plays a key role in climate processes, contributing to the biological carbon pump and helping to remove the anthropogenic carbon liberated to the atmosphere (Sabine and Feely 2007).

Phytoplankton distributions are strongly influenced by abiotic factors such as turbulence, temperature, irradiance and nutrient availability (Margalef 1978), and by interactions with other biological components of the food web. Classically, most studies on the composition of phytoplankton have been conducted by means of microscopic examination, which is time-consuming, requires a high level of taxonomic skill and is only adequate for the larger forms (>10 μm). For groups in the picoplankton (< 2 μm) and small nanoplankton (< 5 μm) size fractions, techniques such as flow cytometry (FC) and epifluorescence microscopy (Porter and Feig 1980, Marie et al. 2001) have enhanced knowledge and understanding of phytoplankton morphotypes, although with low taxonomic specificity. Recently, molecular techniques have provided new possibilities for the assessment of microbial biodiversity, but molecular information still needs to be related with the morphological counterpart (e. g. Amato et al. 2007).

Another alternative, the application of chemical taxonomy methods has been implemented and progressively improved over the past 20 years. Accurate and relatively fast determination of chlorophyll *a* (Chl *a*) and other phytoplankton pigments can be carried out by means of High Performance Liquid Chromatography (HPLC), even for

samples collected from very oligotrophic areas. In a given sample, Chl *a* concentration provides an estimate of total phytoplankton biomass while pigment composition patterns can be used to derive quantitative information on the spatio-temporal variability of the coarse taxonomic structure of the phytoplankton communities, including the contribution of small-sized cells that cannot be reliably identified by microscopy.

The presence and relative contribution of the different phytoplankton pigments depends on the composition of the community. Some pigments are unambiguous markers of certain phytoplankton groups; for example, prasinoxantin is only found in prasinophytes, peridinin in dinoflagellates, divinyl-chlorophyll *a* in *Prochlorococcus* and alloxantin in cryptophytes (Jeffrey et al. 1997, Mackey et al. 1996, Roy et al. 2011). Other pigments, however, occur in several classes of phytoplankton, as for example fucoxanthin, found in diatoms, haptophytes and pelagophytes, among others (Roy et al. 2011).

The lack of unique markers for some groups and the presence of shared pigments in others makes it difficult estimating the abundance of all algal groups using pigment composition. A useful approach to this problem is based on the implementation of the CHEMTAX software program (CHEMical TAXonomy: CHEMTAX), developed by Mackey et al. (1996) to estimate the contribution of different algal classes to the total Chl *a*, based on the pigment data. The calculations start with one or several initial Chl *a*: pigment ratio matrices for the selected phytoplankton groups (Latasa 2007). Next, the program performs iterations to optimize the proportion of Chl *a* accounted for by the phytoplankton groups considered.

Phytoplankton varies in response to seasonal and other sources of environmental variability and tracking community composition in space or along a temporal series provides crucial information on potential ecological effects of natural and anthropogenic

perturbations, including climate change. HPLC pigment analysis and subsequent application of CHEMTAX allow the processing of the high number of samples needed in these studies (Millie et al. 1993). Although this approach estimates phytoplankton biomass in terms of pigments rather than carbon content, which may be the desired variable for some applications, a number of studies have shown the usefulness of Chl *a* concentration as a predictor of phytoplankton carbon biomass estimated from cell counts and biovolume measurements (Schlüter et al. 2000, Lionard et al. 2008, Mendes et al. 2016).

In this work, we use HPLC to determine the concentration of phytoplankton pigments in samples collected at the time-series station of Blanes Bay (NW Mediterranean) between 2000 and 2014 (Gasol et al. 2012), and we apply CHEMTAX to derive the contribution of major phytoplankton chemotaxonomic groups to total Chl *a*. Blanes Bay is a temperate, coastal environment with a typical Mediterranean seasonality and strong physico-chemical and biological variability (Mura et al. 1996, Calbet et al. 2001, Schauer et al. 2003, Lucea et al. 2005, Alonso-Sáez et al. 2007, Guadayol et al. 2009, Gutiérrez-Rodríguez et al. 2011). The site is oligotrophic with an estimated annual integrated primary production of 48 g C m^{-2} yr^{-1} (Gasol et al. 2016). Nutrient availability is driven mainly by the mixing –stratification cycle of the water column (Estrada and Vaqué 2014), but is also influenced by terrestrial runoff from episodic rains that occur predominantly in spring and fall and from the contribution of treated wastewater that rises in the summer due to increased tourist activity (Guadayol et al. 2009). Nutrient concentrations may also be enhanced by advection of oceanic water (Arin et al. 2013) and, during strong wind events, by sediment resuspension and augmented nutrient diffusion from the sediments (Guadayol et al. 2009). Another factor that could play a role in supplying nutrients to the surface waters is aerosol deposition

(Gallisai et al. 2014). In a context of marked vulnerability to climate change of the Mediterranean Sea (UNEP-MAP-RAC/SPA 2010, Martin-Vide 2016), these characteristics heighten the interest of gathering information on the temporal evolution of the Blanes Bay phytoplankton communities. Although previous studies have assessed different aspects of phytoplankton variability, mainly in relation to the seasonal cycle, an integrated view of the long-term (14 years) seasonal and multiannual variability of phytoplankton composition using comparable methodology is still lacking. Specifically, our investigation aimed to:

1) Identify seasonal and interannual patterns in the variability of phytoplankton community structure of Blanes Bay, and 2) Investigate the relation between the environmental parameters of the study area and the variability of the phytoplankton groups.

2.2. MATERIALS AND METHODS

2.2.1. Study area and sampling.

Sampling was conducted over a period of 14 years (2000 to 2014) at the Blanes Bay Microbial Observatory (BBMO) station, located in the Bay of Blanes, in the Northwestern Mediterranean Coast (Fig. 1), approximately 60 km North of Barcelona. The BBMO station is a shallow site (about 20 m depth) approximately 800 m offshore from the town of Blanes (41°40'N, 2°48'E). A total of 162 surface water samples were considered for analysis. The first one was taken in September 2000; from 2001 to 2014, samples were in general collected monthly, with some exceptions (see Table S1). Until 2007, water temperature and salinity were measured, respectively, with a mercury thermometer at surface and with an YSI 556 MPS Multi Probe system. After 2007,

vertical profiles of these variables were obtained with a CTD model SAIV A/S SD204. Due to problems in the calibration of the sensors, only salinities determined in 2007-2008 and 2010-2014 with the CTD were used to calculate monthly averages. Water samples for pigment determinations were collected by gently sinking 20 L polycarbonate acid-cleaned carboys with a 200 µm mesh net in the mouth into the water. This step is generally adopted to avoid the capture of larger zooplankton. Immediately after collection, the carboys were covered with black plastic bags and transferred to the laboratory within 2 hours. Additional samples were taken for classic fluorometric determination of extracted total chlorophyll *a* (Fl_Chl *a*), for nutrient analyses and for flow cytometric counts, and during some periods (June 2006 - June 2014) also for phytoplankton enumeration by inverted microscopy. Records of 24-hour precipitation (Fig. 2B) and wind velocity and direction were obtained from meteorological measurements (41.65° N, 2.76° E) at Malgrat de Mar, about 6 km southwards from the sampling site). Wind data were taken at 2 m from the ground between 2000 and 4 May 2005 (data set 2000 - 2005) and at 10 m afterwards (data set (2005 – 2014). Because of the biass introduced by this change, we dealt separately with the two sets of wind data and used only the second, longest period for statistical analyses. A precipitation index (PI7) consisting on the total amount of precipitation during the 7 days ending two days before each sampling date was used to test the potential relationship between precipitation and Chl *a* concentration anomalies. The reason for the 2-day gap between the precipitation index and the sampling day is the observation that while phytoplankton response to nutrient discharges takes some time, the likely short-term effect of heavy rains is the dilution of the coastal phytoplankton communities (Estrada et al. 2008).

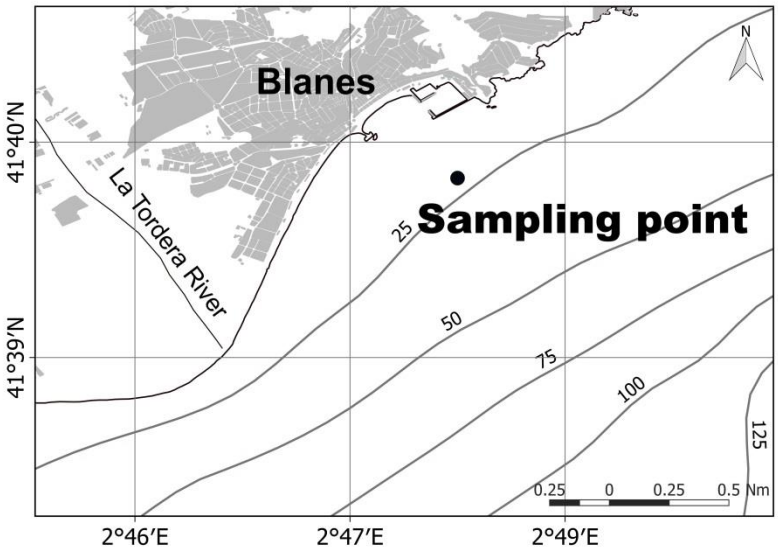

Figure 1. Position of the Blanes Bay Microbial Observatory station in Blanes Bay (NW Mediterranean Sea). The isobaths of 25, 50, 75, 100 and 125 m are shown.

2.2.2 - Dissolved inorganic nutrient and fluorometric chlorophyll a (Fl_Chl *a*) concentrations.

Water for nitrate (NO3), nitrite (NO2), ammonium (NH4), silicate (SiO4) and phosphate (PO4) determination was stored in 100 mL polyethylene bottles and kept frozen (−20 °C) until analysis in the laboratory. Nutrient concentrations were measured colorimetrically with an Alliance Evolution II autoanalyser, following the procedures described in Hansen & Koroleff (1999). Precision was ± 0.015 µmol kg^{-1} for NO2, ± 0.02 µmol kg^{-1} for NO3, ± 0.016 µmol kg^{-1} for NH4, ± 0.0015 µmol kg^{-1} for SiO4 and ± 0.02 µmol kg^{-1} for PO4.

For fluorometric Chl *a* **(**Fl_Chl *a*) determination, 150 ml of water were filtered onto Whatman 25 mm diameter GF/F filters that were subsequently frozen at −20 °C. For analysis, the filters were ground in 90% acetone and left in the dark at 4°C for at least

24 h. The fluorescence of the extract was measured with a Turner Designs fluorometer as described in Yentsch & Menzel (1963). No phaeophytin "correction" was applied.

2.2.3. Phytoplankton abundance

Immediately after collection, 100 ml of water were placed in glass bottles and preserved with formaldehyde-hexamine solution (4%). The samples were kept in dark and cool (4°C) conditions until examination following the Uthermöhl (1958) method. For this purpose, 50 ml of sample were left to settle for 24 h in a composite chamber, and the phytoplankton cells were enumerated using an inverted microscope, as described in Estrada et al. (2016). At least two transects of the chamber bottom were observed at 312 X magnification to enumerate the most frequent phytoplankton forms (note that the method is not adequate for cells in the picoplankton size range). Additionally, the whole chamber bottom was examined at 125 X magnification to count the larger, less frequent cells. When possible, classification was done at the genus or species level, but many taxa could not be properly identified and were pooled in categories such as "small flagellates" or "small dinoflagellates.

2.2.4. Abundance of cyanobacteria by flow cytometry.

Water subsamples of 1.8 ml were fixed with 0.18 ml of a 10% paraformaldehyde and 0.5% glutaraldehyde mixture and stored at −80 °C until analysis. The abundance of *Synechococcus* spp. and *Prochlorococcus* spp. was estimated by flow cytometry using a Becton Dickinson FACSCalibur flow cytometer with a laser emitting at 488 nm (Marie et al. 2001).

2.2.5. Determination of phytoplankton pigments and total Chlorophyll *a* (T_Chl *a*) by HPLC.

The pigment data set consisted of 162 samples (Table S1). A volume of water varying from 0.7 L to 1 L (depending on the sampling season) was filtered onto Whatman GF/F (nominal pore size 0.7 μm; 25 mm diameter) glass fiber filters with low vacuum (0.4 bars) to prevent cells from breaking. Subsequently, the filters were folded, dried, wrapped in aluminum foil and stored frozen at -80°C until analysis. The method of Wright and Jeffrey (1997) was chosen for pigment extraction. The filters were introduced in tubes with 2.5 mL of 90% acetone submerged in ice and the pigments were extracted by sonication during 30 seconds. Subsequently, the filters were stored at - 20 °C. After 24h, the samples were vortexed and filtered through Whatman GF/F glass fiber filters. Prior to 2008, the samples were analyzed at the Institute of Marine Sciences (CSIC) of Barcelona according to the method of Zapata et al. (2000), using a ThermoQuest chromatograph (hereafter System 1), which included a P2000 solvent module, an A/S 3000 autosampler, a UV-3000 absorbance detector (440 nm), a FL2000 fluorescence detector (Ex = 430 nm, Em = 662 nm), and an SN 4000 controller. After 2008, analyses were carried out at the Centro Oceanográfico de Gijón (IEO, Instituto Español de Oceanografía) following the procedure of Latasa (2014, hereafter System 2), which increased the sensibility and lowered the detection limit, using an Agilent (Waldbronn, Germany) series 1200 chromatographic system consisting of a G1311A quaternary pump, a G1367C autosampler with a 100 μL capillary loop, a G1316B column thermostat, and a G1315C diode array detector. A significant change added to the System 2 analyses was the use of trans-β-apo-8'-carotenal, as internal standard, dissolved in the acetone used for sample extraction. In total, 28 pigments (Table S2)

were detected at 440 and 665 nm (System 1) or 474 and 664 nm (System 2), and identified by retention time and online diode array detector. Total monovinyl-chlorophyll *a* (TMV_Chl *a*) concentration was estimated as the sum of monovinyl-chlorophyll *a* (MV_Chl *a*), chlorophyllide *a*, and chlorophyll *a* allomers and epimers. The total Chl *a* concentration (T_Chl *a*) was calculated as TMV_Chl *a* + divinyl-chlorophyll *a* (DV_Chl *a*).

2.2.6. CHEMTAX analysis.

The CHEMTAX computer program version 1.95 (Mackey et al. 1996, Latasa 2007) was used to calculate the relative contribution of different phytoplankton groups to total chlorophyll *a* biomass, based on marker pigments. Essentially, the program uses an initial matrix of pigment:Chl *a* ratios for all the algal groups considered and optimizes the ratio matrix to generate the fraction of the total Chl *a* accounted for by each phytoplankton group. Before running CHEMTAX, the samples were clustered according to the contribution of the pigments 19'-butanoyloxyfucoxanthin, 19'-hexanoyloxyfucoxanthin, alloxanthin, chlorophyll *b*, chlorophyll c_2, chlorophyll c_2-MGDG [14:0/14:0], divinyl-chlorophyll *a*, fucoxanthin, neoxanthin, peridinin, prasinoxanthin, violaxanthin, uriolide and zeaxanthin. The statistical similarity matrix among samples was calculated using the Manhattan distances and the samples were clustered according to Ward's method using the Statistica 5.5 software. Following the procedures of Latasa (2007) and Latasa et al. (2010), 29 random initial pigment ratio matrices were created considering 8 phytoplankton pigment groups: cryptophytes (Crypto), diatoms (Diat), dinoflagellates (Dino), haptophytes (Hapto), pelagophytes (Pelago), prasinophytes (Pras), *Prochlorococcus* (Prochl) and *Synechococcus* (Syn). The Hapto group combined haptophytes types 6 + 7, which include *Chrysochromulina* and

the cosmopolitan coccolithophore *Emiliana huxleyi*, and haptophytes type 8, which comprise *Phaeocystis* (Zapata et al. 2004). Prasinophytes contain prasinoxanthin as major carotenoid and share chlorophyll *b*, neoxanthin, violaxanthin and zeaxanthin with other chlorophytes, which in turn present lutein instead of prasinoxanthin as their dominant carotenoid. As lutein was almost always below detection limits, we assumed that chlorophytes in Blanes Bay were basically represented by prasinophytes. Eight successive CHEMTAX runs were performed with the 29 matrices. A single average matrix was obtained from the eighth run of the 29 matrices. This average matrix was run again to estimate the contribution of each phytoplankton pigment group to the T_Chl *a* in the sample. This procedure was performed independently with each cluster of samples.

2.2.7. Statistical analyses

The significance of the regressions between phytoplankton cell abundances and HPLC pigment concentrations was tested by means of the *t* test. Linear correlations were calculated among the monthly anomalies of the variables (the difference between the variable value for a particular month in a given year and the mean of the values corresponding to that month in all the years of the series); Chl *a* concentrations were previously subjected to a square root transformation to improve the normality and homoscedasticity of the data. Some analyses were also carried out separately for "winter" and "summer"; in this context, winter comprised the months of January, February and March, and summer July, August and September. Temporal trends were examined by means of linear regression of the monthly anomalies of the dependent variable with respect to sampling date. Bivariate linear regression equations with Chl *a* concentrations as dependent variables and time and PI7 as predictor variables were also

calculated. The significance of the slopes was determined by the *t* statistic and the standardized slopes (equal in absolute value to the correlation coefficient), which indicate how much a dependent variable increases (in terms of standard deviations) when the independent valuable increases one standard deviation, were used to compare interannual trends among Chl *a* variables. Figures 6 and S1 were produced using the Ocean Data View software (Schlitzer, 2016).

2.3. RESULTS

2.3.1. Hydrography

The highest surface water temperature, 26.2 °C, was recorded on 12 September 2007 and the lowest (11.0 °C) on 26 March 2003. Monthly-averaged values showed a clear seasonality (Figs. 2A and 3A), with summer maxima [mean ± standard error of the mean (SE) of 24.2 ± 0.3 ºC in August] and winter minima (12.8 ± 0.2 ºC in February). Monthly averages of salinity (after 2007) ranged in general between 38 and 38.1 and were lowest (37.7 ± 0.1) in June (Fig. 3A). In general, the water column presented a vertically homogeneous distribution of temperature in autumn and winter; stratification of the upper waters started around May and a 5-10 m mixed layer became established between June and September. Vertical homogenization took place again in October (Fig. S1). The record of 24-hour precipitation (Fig. 2B) observed at Malgrat, taken here as a proxy for freshwater runoff, showed a typical Mediterranean pattern of high episodic events superimposed to a regime driven by dry summer periods and rains in spring and autumn. As expected (Stull, 1988), mean daily wind speed was lower for the 2000-2005 data set, measured 2 m above the ground, than for the 2005-2014 one, measured at 10 m. Few daily means exceeded 5 m s^{-1} (Fig. S2); strong winds were

generally from the north (data not shown). There was a weak but significant correlation between daily 24-hour precipitation and mean wind speed (2000-2005 data set, N = 1925, $R^2 = 0.015$, $p < 0.0001$; 2005-2014 data set, N = 3275, $R^2 = 0.04$, $p < 0.0001$). Nutrient concentrations were generally low and increased during winter (Figs. 3B, C and D). Average (± SE) monthly values peaked in March (Fig. 3B) for nitrate (2.52 ± 0.52 µM) and silicate (2.26 ± 0.44 µM), nitrite showed a summer minimum and ammonium did not present a clear seasonal cycle (Fig. 3C). Phosphate (Fig. 3D) presented relatively low seasonal variability, with a maximum monthly mean of 0.16 ± 0.22 µM in March (a value of 0.94 µM recorded on 19 April 2001 was not included in the calculations) and a minimum of 0.083 ± 0.014 µM in September. The N:P ratio was mostly affected by the nitrate variability and, except in March, was lower than the Redfield value of 16 (Fig. 3D).

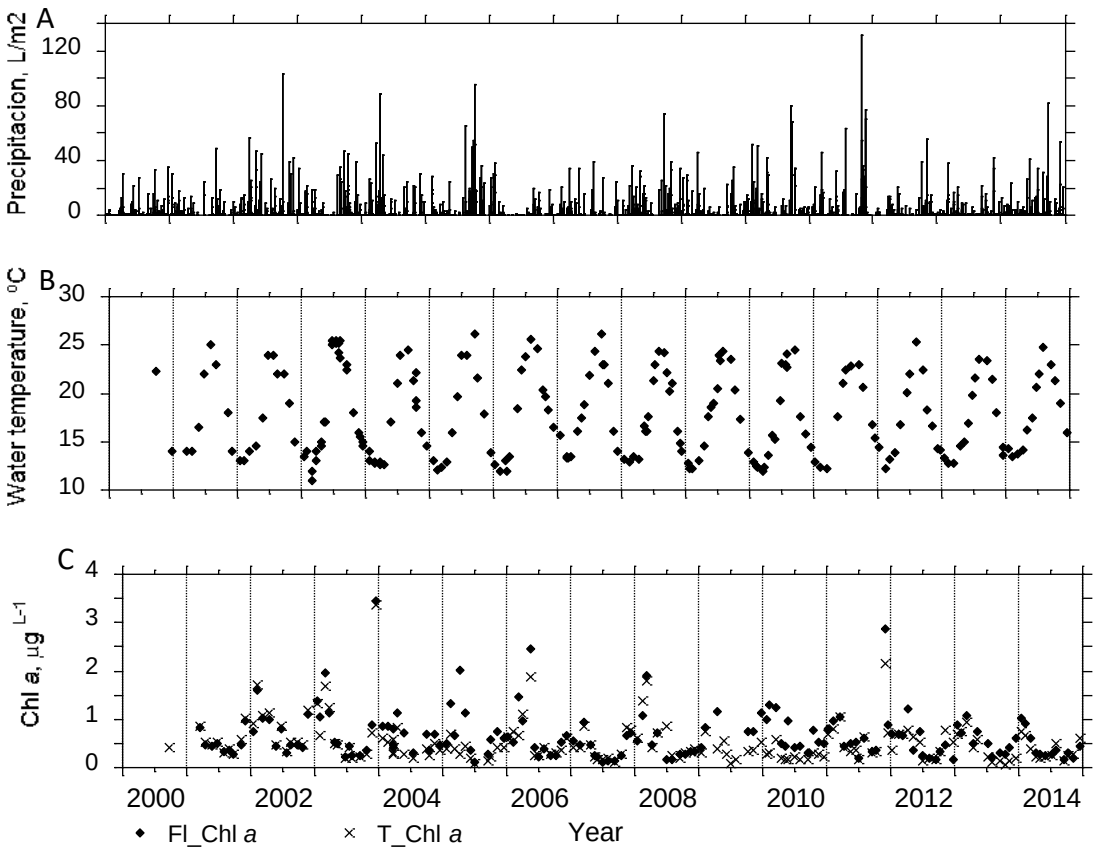

Fig. 2. Temporal variation of surface water temperature (A), daily precipitation at the Malgrat meteorological station, 5 km south of Blanes (B) and temporal variation of Classic (fluorimetric) Chlorophyll *a* (Cl_Chl *a*) and Total Chlorophyll *a* (T_Chl *a*) concentrations (C).

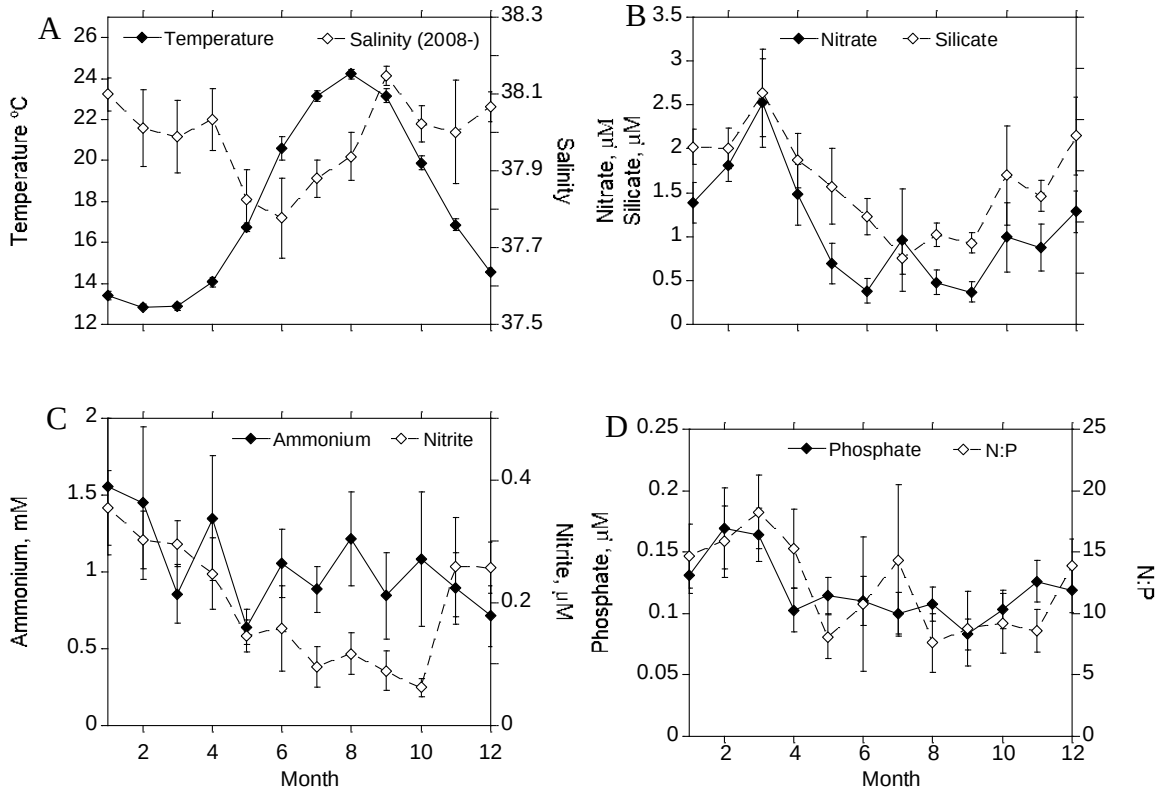

Fig. 3. Monthly climatology of water temperature (ºC) and salinity (A), nitrate and silicate concentration (B), ammonium and nitrite concentration (C) and phosphate concentration and N:P ratio (D). Error bars indicate the standard error of the mean.

2.3.2. Chl *a* distribution and HPLC pigment composition

There was a good agreement between fluorometric and HPLC Chl *a* measurements (Fl_Chl *a* = 0.84*T_Chl*a* + 0.152, N = 157, R^2 = 0.70, p<0.0001). Fluoromeric Chl *a* (Fl_Chl *a*) and total Chl *a* (T_Chl *a*) presented a parallel seasonal evolution, with a main maximum in March and a minimum between July and September (Figs. 2C, 4). Chl *a* concentrations were generally lower than 1 µg L^{-1} but there were several samples with T_Chl *a* values exceeding 1.5 µg L^{-1}, as noted, for example, on 7 February 2002, 4

March 2003, 16 December 2003, which registered the highest T_Chl *a* concentration of the series (3.37 µg L^{-1}), 16 May 2006, 12 March 2008 and 29 November 2011 (Fig. 2C). Among the 28 pigments detected by the HPLC analyses (Table S2, Fig. S3), the most abundant ones were MV_Chl *a*, fucoxanthin, 19'-hexanoyloxyfucoxanthin, chlorophyll b, chlorophyll *c2*, chlorophyll *c3*, diadinoxanthin and 19'-butanoyloxyfucoxanthin. Most pigments presented their highest monthly average concentrations between mid-autumn and mid-spring, and their lowest ones in summer. Among the exceptions were peridinin and chlorophyll c_2 MGDG [14:|14], which did not have a clear seasonal cycle, and zeaxanthin, which had maxima in April and August.

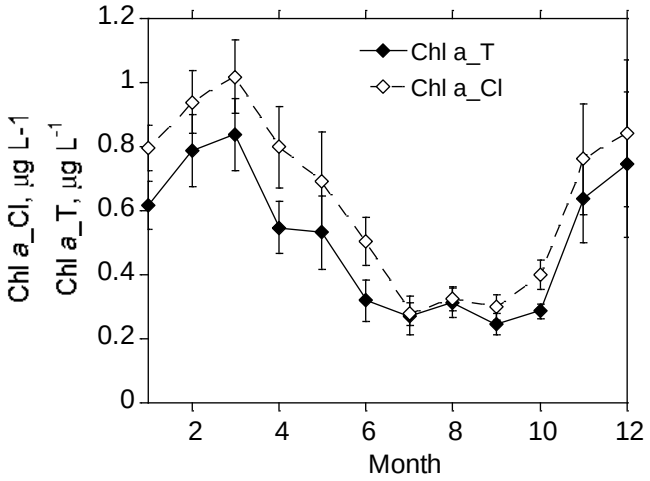

Figure 4. Monthly climatology of Classic (fluorimetric) Chlorophyll a (Cl_Chl *a*) and Total Chlorophyll a (T_Chl *a*) concentration.

2.3.3. Seasonal variability of the phytoplankton community

Among the phytoplankton groups characterized by CHEMTAX, the main global contributors to T_Chl *a* (Fig. 5A) were haptophytes, diatoms, prasinophytes and cryptophytes, followed by *Synechococcus*, pelagophytes, dinoflagellates and *Prochlorococcus* (in the following, unless otherwise stated, the group name will be used to indicate the CHEMTAX-derived contribution to T_Chl *a* of the group). In general,

there was a marked seasonality (Table 1, Figs. 5B, 6, 7), but interannual variability of the timing of population maxima was high. On average, diatoms peaked in March (40.5%), May (39%), and November (37%) and were the prevailing group in the high T_Chl *a* episodes, contributing 44%-83% of T_Chl *a* in these cases. The exception was represented by the 16 December 2003 event, in which the dominant groups were prasinophytes, cryptophytes and haptophytes. According to available phytoplankton counts, the most abundant diatom taxa in the proliferations, particularly those of autumn-winter, were *Chaetoceros* spp., *Pseudo-nitzschia* spp., *Asterionellopsis glacialis* (e. g. in December 2009), *Lioloma pacificum* (e. g. in November 2009) and *Thalassionema nitzschioides* (e. g. in December 2013 and May 2014). However, other taxa, like *Proboscia alata*, were dominant on some occasions (e. g., May-June 2007). The contribution of prasinophytes, cryptophytes and pelagophytes tended to be more important from December to March, although cryptophytes presented also a marked peak in August. The haptophytes followed a comparable pattern but varied relatively little throughout the year, while dinoflagellates were particularly important from winter to summer, with a minimum between September and November. It must be noted that for prasinophytes, cryptophytes and haptophytes, the December averages were enhanced by the exceptional population densities of December 2003, although all these groups presented a peak in December, even if that sample was eliminated from the calculations. Regarding the cyanobacteria, *Prochlorococcus* practically disappeared from the surface waters between February and August, and *Synechococcus* presented their highest contributions in April and between July and October.

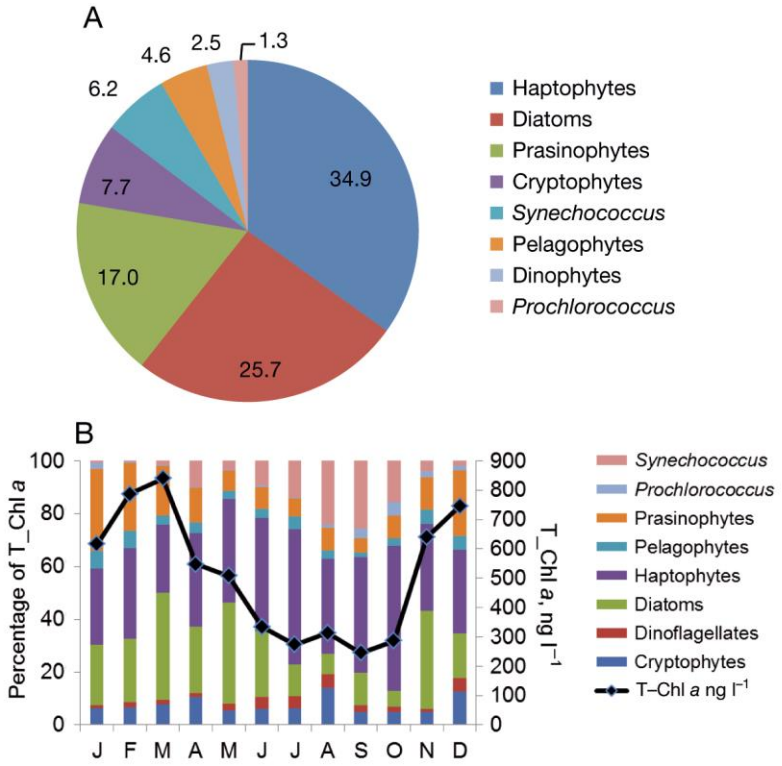

Figure 5. Contribution to T_Chl *a* of the CHEMTAX-derived phytoplankton groups. (A), for the whole data set and (B) monthly averages.

Counts of selected phytoplankton taxa were compared with their CHEMTAX-derived contribution to Chl *a*. The square of the correlation coefficients between flow cytometry counts of *Prochlorococcus* and *Synechococcus* and their contributions to Chl *a* were 0.63 ($N = 151$, $p < 0.0001$) and 0.60 ($N = 151$, $p < 0.0001$), respectively (Fig. S4). For diatom and dinoflagellate abundances, the square of the correlation coefficients with their corresponding Chl *a* contributions were 0.19 ($N = 126$, $p < 0.0001$) and 0.13 ($N = 126$, $p < 0.0001$), respectively (data not shown).

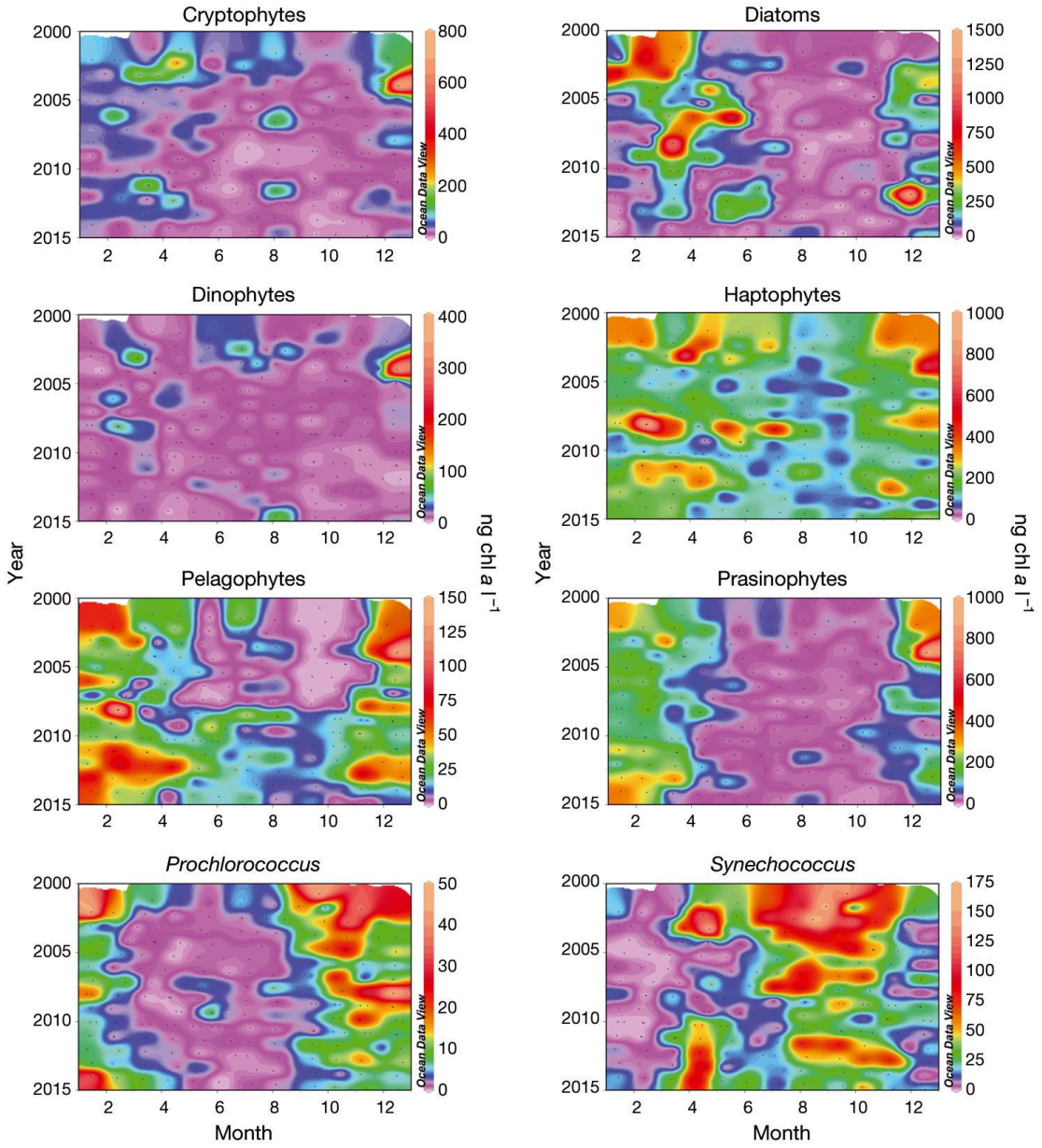

Figure 6. Seasonal and interannual variation of the contribution to T_Chl *a* by the CHEMTAX-derived phytoplankton groups. Pras = prasinophytes, Dino = dinoflagellates, Hapto 6+7+8 = haptophytes, Diat = diatoms, Crypto = cryptophytes, Pelago = pelagohytes, *Syn* = *Synechococcus*, *Prochl* = *Prochlorococcus*. Figure produced using the Ocean Data View software (Schlitzer, 2016).

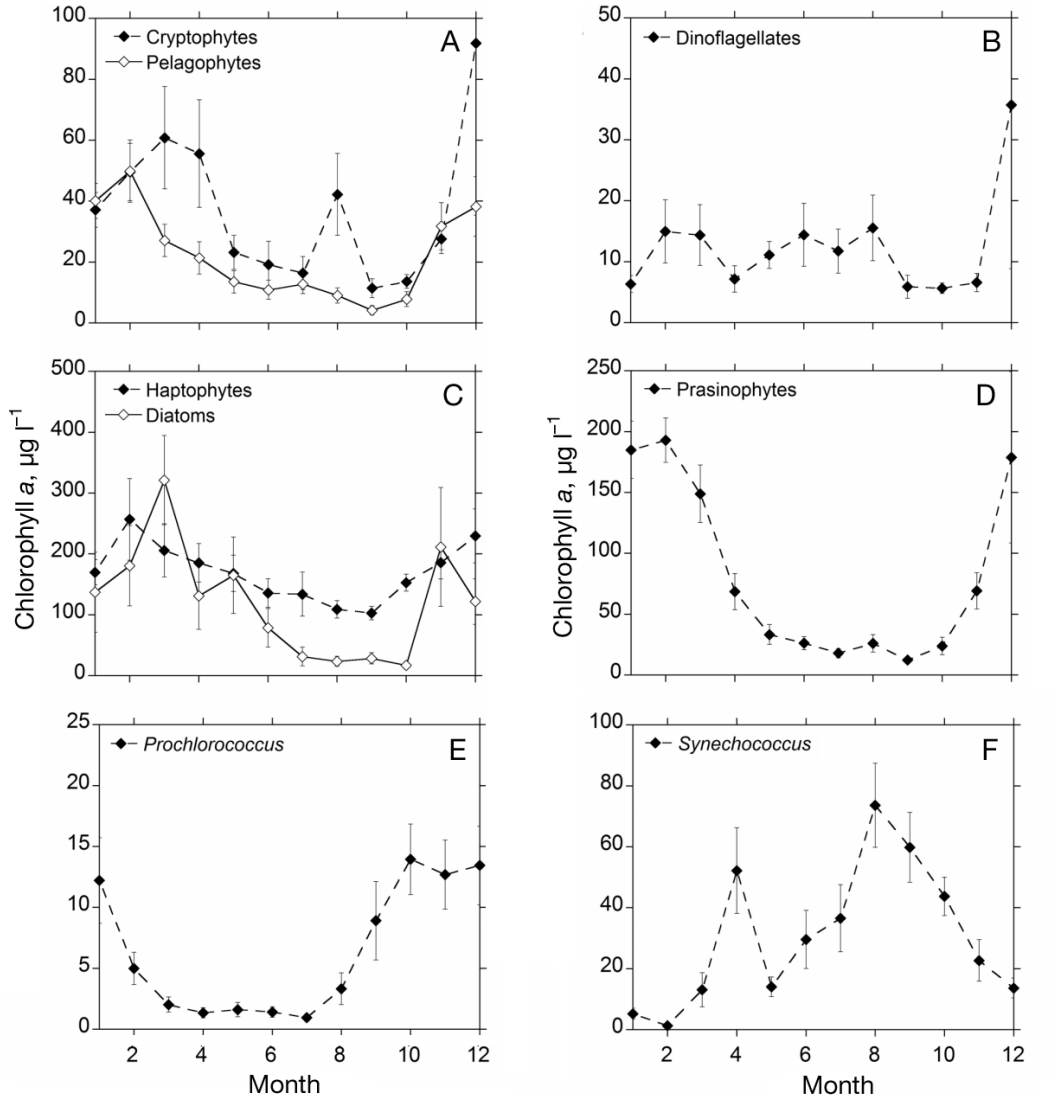

Figure 7. Monthly climatologies of the contribution to T_Chl *a* by prasinophytes (A), dinoflgellates (B), haptophytes and diatoms (C), cryptophytes and pelagophytes (D), *Synechococcus* (E) and *Prochlorococcus* (F). Error bars indicate the standard error of the mean.

2.3.4. Interannual variability

The time series of temperature (Fig. 8A), PI7 precipitation index (the total amount of precipitation during the 7 days ending two days before each sampling date), wind speed at 2 m (2000-2005) and 10 m (2005- 2014) above the ground, and anomalies of salinity and ammonium did not present any statistically significant interannual trend (data not shown). In contrast, phosphate, nitrate, nitrite (data not shown) and silicate anomalies decreased with time (Figs. 8B, 8C and 8D Table 2), as happened also for the anomalies

(after square root transformation of the data) of TMV_Chl *a*, T_Chl *a*, Fl_Chl_*a* and all CHEMTAX groups except pelagophytes, which increased with time, and haptophytes and prasinophytes, for which correlations were not significant (Figs. 6, 9, 10, Table 2). Comparable results were obtained for the winter (January-March) and summer (July-September) data subsets (data not shown), although in this case, with reduced number of observations, many of the relationships became not significant. A correlation analysis among potential factors influencing the variability of Chl *a* concentration anomalies, such as temperature, the PI7 precipitation index, wind speed (only 2005-2014) and major nutrient (phosphate, nitrate and silicate) concentrations revealed some interesting patterns (Table 3). The temperature anomaly was only significantly negatively correlated with the PI7 index, whereas all nutrient anomalies were significantly positively correlated among themselves. In turn, the nitrate and silicate anomalies were positively correlated with that of the PI7 index and the phosphate anomaly was positively correlated with wind speed (2005-2014). When these same relationships were calculated separately for the winter (January-March) and summer (July-August) periods of 2005-2014, the results were qualitatively similar, but the only significant correlations were the winter ones between silicate and PI7 anomalies ($N = 26$, $R^2 = 0.20$, $p<0.01$) and between phosphate and wind speed anomalies ($N = 26$, $R^2 = 0.24$, $p<0.05$). Based on the findings for the whole data set, time and the PI7 index were used as predictor variables in bivariate linear regressions with the group Chl *a* concentration anomalies as dependent variables. The standardized slopes, shown in Table 4, can be used as an indication of the relative importance of long-term (time) versus episodic (PI7) environmental forcing. As expected, the slopes with respect to time in the bivariate regression are close to the corresponding ones in Table 2.

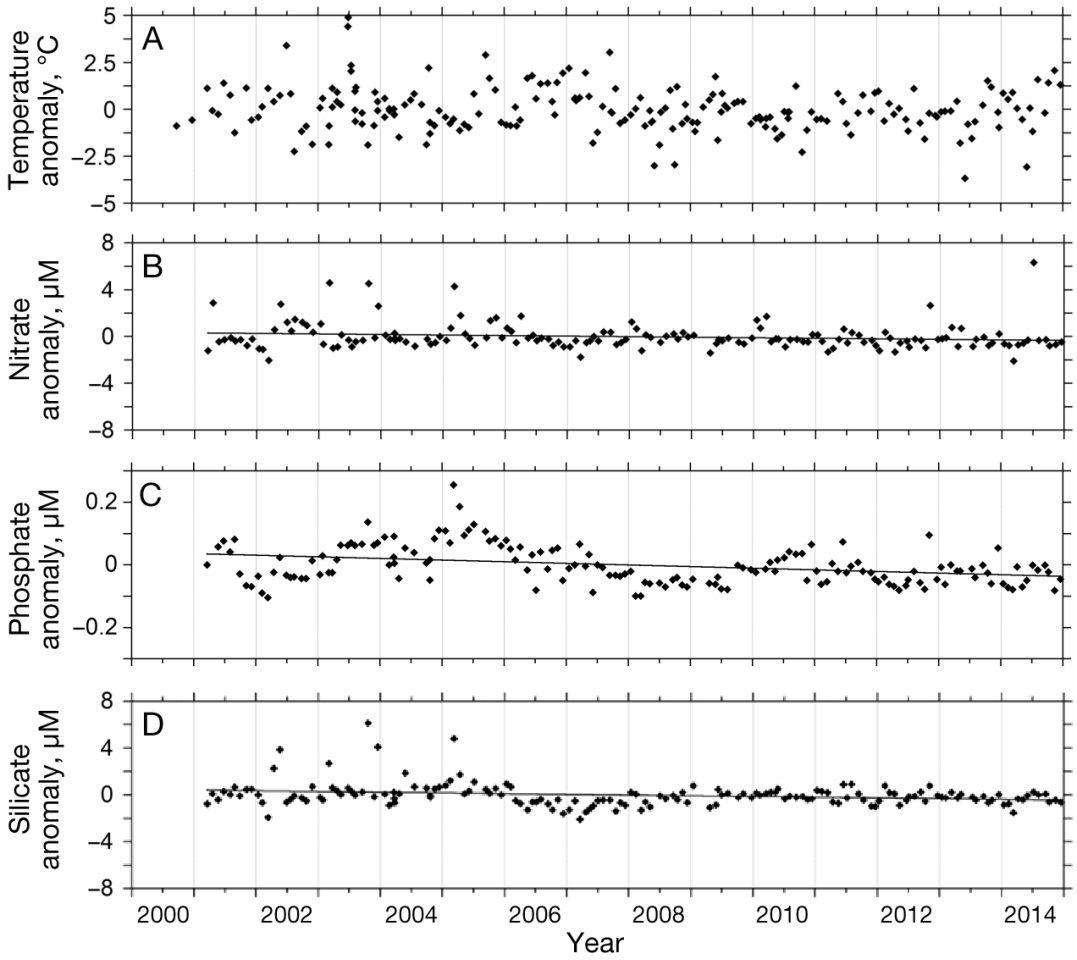

Figure 8. Temporal variation of the monthly anomalies of surface water temperature (A), phosphate (B) and silicate (C). The regression lines were significant in (B) and (C) and are indicated in the graphs; the corresponding equations are shown in Table 2.

2.4. DISCUSSION

2.4.1. Seasonal patterns

In agreement with the findings of previous studies, Blanes Bay presented a strong seasonality with a marked yearly cycle of warm summers and cool winters (Margalef 1957, 1964; Cebrián et al. 1996, Duarte et al. 1999). Salinity values lower than 38 are typical of coastal surface waters in the region. The relatively high autumn and winter salinities can be associated to intrusions of oceanic waters (Cebrián et al 1996); local freshwater discharges may induce sporadic low salinity values at the sampling station,

but are generally insufficient to affect the seasonal salinity patterns. The salinity minimum in June may be related to spring increases of freshwater inputs from upstream rivers (in particular the Rhône) influenced by snow melt (Masó and Tintoré 1991); in addition, seasonal stratification hinders the mixing of freshwaters entering at surface, therefore contributing to maintain relatively low salinity values. Monthly Fl_Chla and T_Chl *a* averages in Blanes Bay present a winter maximum that starts to build up in October and a summer minimum, coinciding with a similar variation in the concentration of nitrate, silicate and, to a minor extent, phosphate. These seasonal patterns are typical of the Catalan Sea (Estrada 1999, Segura-Noguera et al. 2011, Arin et al. 2013) and other Mediterranean marine areas (D'Ortenzio and Ribera d'Alcalà 2009, Siokou-Frangou et al. 2010, Estrada and Vaqué 2014). The occurrence of a winter bloom in the Mediterranean, before the establishment of thermal stratification has been related to the recurrent periods of calm weather during this season (D'Ortenzio and Ribera d'Alcalà 2009). In addition, in shallow waters like those of the Blanes station, it may be facilitated by the practically year-round existence of sufficient light availability (Gasol et al., 2016).

Haptophytes were the globally most abundant group (Fig. 5A), while the most important components of the Chl *a* maxima were the diatoms, which showed a strong global correlation ($r = 0.79$, $p < 0.0001$) with T_Chl *a* and accounted for 44% of the March T_Chl *a* peak (Fig. 5B). This dominance of diatoms in phytoplankton bloom situations is a general finding in coastal and open sea areas of the NW Mediterranean (Ribera d'Alcalà et al 2004; Estrada & Vaqué 2014). The prevalence of *Chaetoceros* spp. and *Asterionellopsis glacialis* in the late winter peaks and the contribution of *Lioloma pacificum* and *Thalassionema nitzschioides* in autumn agree with findings from

previous studies (Margalef 1964). Prasinophytes, haptophytes and pelagophytes (Fig. 7) presented also winter maxima and summer minima.

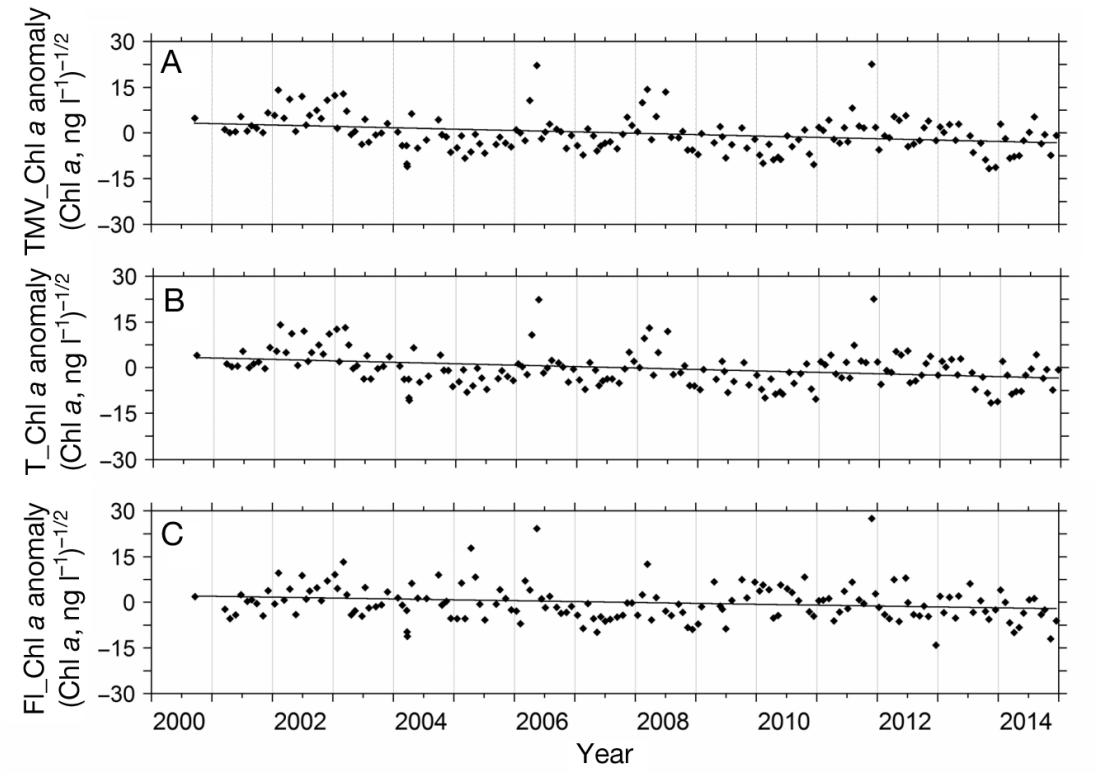

Figure 9. Temporal variation of the monthly anomalies (after square root transformation of the data) of TMV_Chl *a* (A), T_Chl *a* (B) and Fl_Chl *a* (C). The significant regression lines are indicated in the graphs; the corresponding coefficients are shown in Table 2.

Cryptophytes showed a comparable pattern, but with an additional peak in August. The association of diatoms, prasinophytes and haptophytes in the autumn to late-winter bloom period had been already noted by Gutiérrez-Rodríguez et al. (2011), who linked the dominance of these groups to high nutrient and moderately mixed conditions. According to Unrein et al. (2014), haptophytes (in particular the 3- 5 µm size class) are present in Blanes year-round and account for a high proportion of the bacterivory at the site. In our study, the seasonal variability of haptophytes was relatively small and the monthly variability was high, as evidenced by large error bars (Fig. 7), a finding that may be related to the ecological heterogeneity of this chemotaxonomic group, which included forms such as *Emiliana huxleyi* and *Chrysochromulina* (haptophytes 6+7), as

well as *Phaeocystis* (haptophytes 8). The pelagophytes were classified among the "mesotrophic" groups by Latasa et al. (2010), and in fact Marty et al. (2002) found a spring increase of their pigment marker 19'-butanoyloxyfucoxanthin in the DYFAMED site. The presence of cryptophytes in Blanes Bay during the coldest months had been noted by Unrein et al. (2014), but Cerino & Zingone (2006) reported maximum concentrations in the Gulf of Naples in spring-summer and autumn. This diversity of observations concerning HPLC-derived groups such as pelagophytes and cryptophytes highlights the need of gathering information to improve our insight into their taxonomical composition and associated ecological traits. The remaining eukaryotic group, that of dinoflagellates, was more abundant between May and August and, with the exception of the December average value, influenced by the high concentrations observed in December 2003, their calculated monthly average contribution to total Chl *a* did not exceed 20 ng L^{-1} and was always < 5% (Table 1, Fig. 5B, 7). The presence of dinoflagellates in summer, under stratified, nutrient-poor conditions (Margalef 1978), can be related to their potential mixotrophy and to their ability to undergo vertical migrations. However, some dinoflagellate taxa may also proliferate in winter, in particular following prolonged periods of good weather, as has been shown for *Alexandrium minutum* in some Catalan harbors (Van Lenning et al. 2007, Estrada et al. 2008). Note also that the CHEMTAX method takes into account only peridinin-containing dinoflagellates; many dinoflagellate taxa do not contain this pigment or are heterotrophic and would not be accounted for by CHEMTAX. The photosynthetic cyanobacteria, *Synechococcus* and *Prochlorococcus*, showed quite distinct seasonal distributions in Blanes Bay (Table 1, Figs. 5B, 7). *Synechococcus* presented their highest concentrations during the warmer months and accounted for 39% of T_Chl *a* in September, while *Prochlorococcus* was generally present in low concentrations and

increased between autumn and early winter, with a maximum contribution to T_Chl *a* of 5% in October. Both genera are favored by their small size under low nutrient conditions (Moutin et al 2002; Lomas et al. 2014), although *Prochlorococcus* has been associated with more oligotrophic situations than *Synechococcus* (Partensky et al. 1999; Latasa et al. 2010). Based on a seasonal survey in the Bay of Banyuls-sur-mer (a coastal site in the Mediterranean Sea, at the northern foothills of the Pyrenees), Charles et al. (2005) observed that *Prochlorococcus* and *Synechococcus* peaked between August and November, and suggested that the dominance of cyanobacteria over eukaryotes was associated with low nutrient concentrations and N:P ratios below 10. In Blanes Bay, average N:P ratios below 10 were recorded in May and between August and November (fig. 3D). These periods coincide in part with times of high *Synechococcus* abundance, but *Prochlorococcus* concentrations are still significant in December and January, when N:P ratios are relatively high. It is likely that relative nutrient availability is only one of the many factors affecting picophytoplankton abundance. Several studies have addressed the positive relationship between temperature and picocyanobacteria abundance (Flombaum et al. 2013, Hunter-Cevera et al. 2016). Agawin et al. (1998) illustrated the relationship between temperature and *Synechococcus* variability in Blanes Bay and Šantić et al. (2011) reported that both *Synechococcus* and *Prochlorococcus* tended to increase in several stations of the Adriatic Sea during the warmer period. However, as noted by Vaulot et al. (1990) and Šantić et al. (2011) among others, both cyanobacterial taxa were able to grow across a wide temperature range. This feature is illustrated by the occurrence of the autumn to early winter maximum of *Prochlorococcus* in Blanes Bay. A similar timing for the highest presence of prochlorophytes (divinyl-Chl *a*) was documented by Marty et al., (2002) in open waters of the NW Mediterranean. However, temperature, nutrient availability, irradiance in

surface waters and a number of biotic factors, such as grazing intensity vary in close association along the seasonal cycle of the coastal Mediterranean and it is difficult to disentangle their various effects. In addition, the two genera present a diversity of ecotypes that show spatio-temporal variability and preferences for different levels of the water column (Garczarek et al. 2007, Latasa et al. 2010, Mella-Flores et al. 2011, van de Poll et al. 2015). This genetic diversity is likely to underlie the two *Synechococcus* maxima in April and August. On the other hand, the modest abundance of *Prochlorococcus* in the summer samples could perhaps be related to their susceptibility to the high solar UV radiation in the surface waters (Sommaruga et al. 2005, Llabrés et al. 2010).

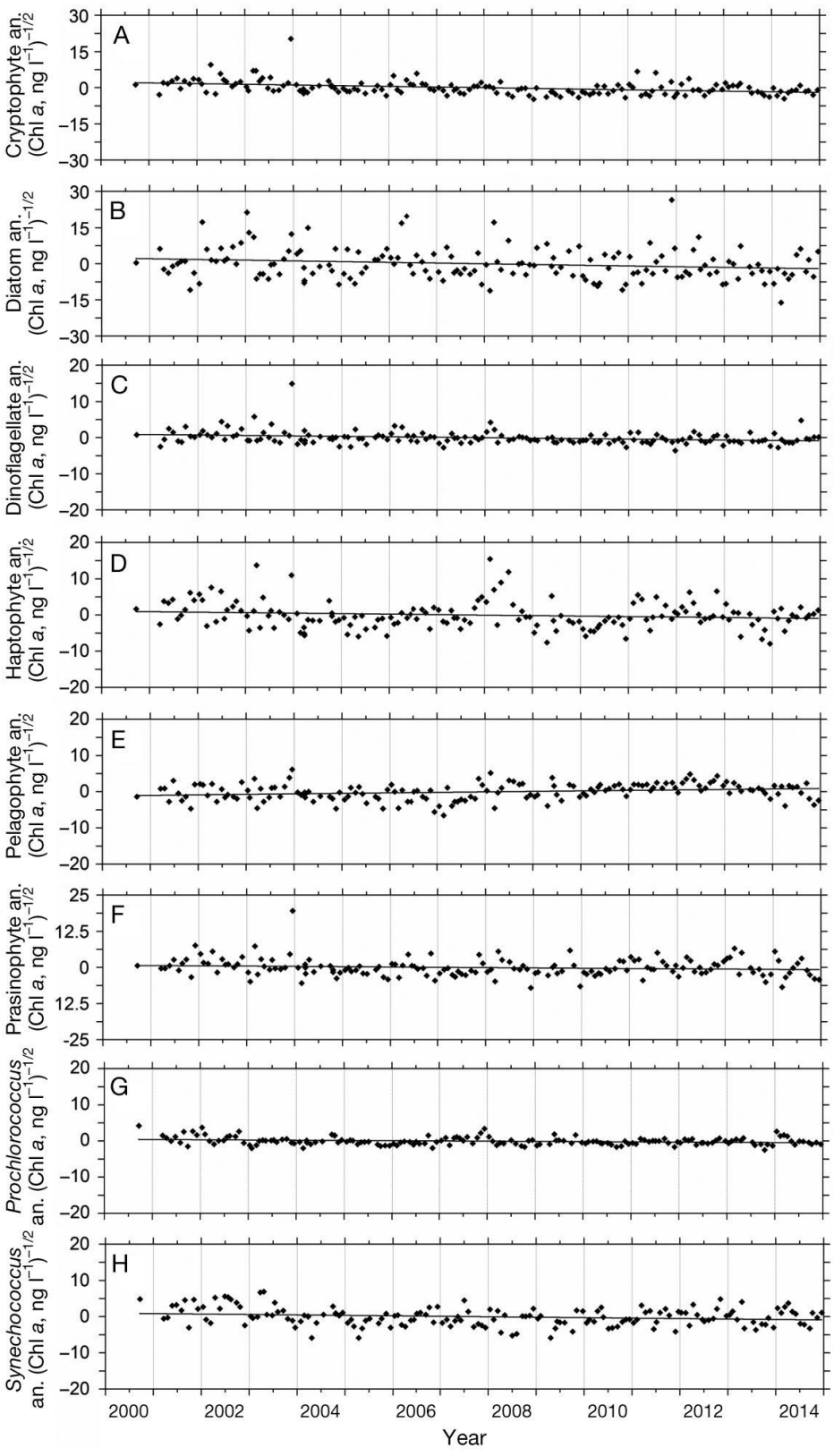

Figure 10. Temporal variation of the monthly anomalies (after square root transformation of the data) of cryptophytes (A), diatoms (B), dinoflagellates (C), haptophytes (D), pelagophytes €, prasinophytes (F), P*rochlorococcus* (G) and *Synechococcus* (H). The significant regression lines are indicated in the graphs; the corresponding coefficients are shown in Table 2.

2.4.2. Episodic nutrient enrichment and interannual variability

Significant linearly decreasing temporal trends were identified (Table 2) for the monthly anomalies of phosphate, nitrate, nitrite (data not shown) and silicate, pooled Chl *a* concentrations (TMV_Chl *a*, T_Chl *a*, FL_Chl *a*) and all CHEMTAX-derived groups except haptophytes, prasinophytes and pelagophytes. Haptophytes and prasinophytes, as well as ammonium concentration anomalies (data not shown) presented also negative albeit non-significant trends, while pelagophyte anomalies increased with time. Superimposed to the general temporal trends, the monthly sampling recorded isolated events with T_Chl *a* concentrations exceeding 1.5 µg L^{-1}. Comparison of Figs. 2B and 2C suggests that particularly intense rain storms may have fuelled some of these high Chl *a* blooms, as appears to be the case for the samples taken on 4 March 2003 (T_Chl *a* = 1.68 µg L^{-1}), 16 December 2003 (T_Chl *a* = 3.37 µg L^{-1}) and 29 November 2011 (T_Chl *a* = 2.15 µg L^{-1}), which followed heavy rains on 25-26 February 2003, 1-7 December 2003 and 4-6 and 15 November 2011, respectively. The significant relationships between precipitation (as represented by the PI7 index, see Material and Methods) and the Chl *a* concentration of the various CHEMTAX groups were positive, except for *Prochlorococcus*, as shown by the PI7 slopes in the bivariate linear regression of CHEMTAX Chl *a* concentrations with time and PI7 anomaly as independent variables (Table 4). In this context, it must be noted that although the plume of the main river close to Blanes, the Tordera (Fig. 1) tends to go to the south without affecting Blanes Bay, heavy rains may originate localized freshwater discharges and runoff. Due to the shortness of the record, the effect of wind events is more difficult to ascertain, although there it is hinted by the positive correlation between phosphate and wind speed anomalies for the winter data subset of 2005-2014. The influence of

continental runoff and wind storms (which may appear in association) for the phyto- and bacterioplankton community of Blanes Bay was studied by Guadayol et al (2009) for the period between December 1997 and September 2006 (with a 2 year gap in 1999 and 2000); they found that in this particular location river runoff was very important for phytoplankton dynamics, whereas resuspension events caused by waves had a secondary importance. Winter wind events of certain intensity and direction could also be important in introducing nutrient-rich oceanic waters, as shown by Arin et al. (2013) for the coastal area of Barcelona and by Goffart et al (2015) for the Bay of Calvi (Corsica). However, our data for Blanes Bay do not have enough spatio-temporal resolution to document this point. The fertilization effect of freshwater runoff in Catalan coastal waters has also been discussed by Estrada (1979), which documented a *Skeletonema costatum* proliferation off Arenys de Mar (about 30 km to the south of Blanes) following a heavy rainfall event in the region. In addition, precipitation may contribute to wet nutrient input from the atmosphere and together with dry deposition processes may be important in Blanes Bay, as shown by Marín (2017). We do not have information on long-term trends in our study region; according to Goffart et al. (2015), atmospheric deposition values seem to present decadal fluctuations and have recently (2003-2007) shown high variability (Ternon et al. 2010).

The general decreasing trends in nutrient and phytoplankton group concentrations could be due to several causes, including changes in stratification (due to increased temperature or freshwater input) and variations in episodic forcing factors such as those discussed above (continental runoff, wind events, atmospheric deposition). However, there was no relationship between nutrient concentration and temperature anomalies. The water column in Blanes Bay is mixed during most of the year and, during our study period, temperature did not present any significant trend, a finding that can be explained

by the relatively short period of observation; indeed, the study of a long-term (since 1974) series measured at l'Estartit marine station (43º 03' N, 03º 15' 15'' E), located to the north of Blanes, has shown a temperature increase of 0.3ºC per decade for the shallower 50 m of the water column (Martin-Vide 2016). Among nutrient concentration anomalies, phosphate showed the strongest negative correlation with time (Table 2) while, as discussed above, nitrate and silicate were positively correlated with the precipitation index anomaly, and phosphate (period 2005-2014) was correlated with the wind speed anomaly (Table 3). However, there were no significant interannual trends in PI7 and wind speed, an observation that in the case of PI7 (no comparable information is available for wind speed) is consistent with conclusions from longer precipitation time series in the region (BAIC 2017). Another possibility for explaining the decreasing nutrient and Chl *a* concentrations in Blanes Bay waters is the implementation of policies of wastewater treatment and phosphate reduction during the last decades (Rygaard et al. 2009; Gasol et al. 2012). A first sewage treatment plant started to operate in Blanes in 1972 and was replaced by an improved facility in 1997; in 2003 it was upgraded to tertiary reclamation treatment that was interrupted in 2012 (Rygaard et al. 2009, E. Sallarès, Agència Catalana de l'Aigua, unpubl. data). A reduction in anthropogenic nutrient inputs could be a plausible factor behing the general oligotrophication trend in Blanes Bay, but longer time series are needed to ascertain the relative importance of climatic and anthropogenic forcing. Our findings agree with those of Mozetič et al. (2012), who concluded that anthropogenic drivers (the ban on phosphorus in late 80s and improvement of sewage treatment), together with reduced precipitation in the surrounding continental area could be responsible for the nutrient and Chl *a* reduction trends detected in the Northern Adriatic for the period 1970-2007.

Inspection of Table 4 indicates that the relative importance of the temporal trends and the runoff events was different for the various CHEMTAX groups. Taking into account the classification of Latasa et al. (2010), who assigned a "trophic preference index" (TPI) to different phytoplankton groups (cryptophytes, dinoflagellates, prasinophytes and diatoms were considered as "eutrophic", *Synechococcus*, pelagophytes and haptophytes as "mesotrophic" and *Prochlorococcus* as "oligotrophic"), it appears that the response to short-term fertilization events associated with freshwater runoff was strongest for the most "eutrophic" taxa, prasinophytes, diatoms, dinoflagellates and cryptophytes, and lowest for *Prochlorococcus*, as shown by their highest standardized slopes for the PI7 precipitation index. In contrast, there was little relationship between the effects of nutrient reduction (as expressed by standardized slopes with respect to time) and the TPI classification. In this context, the positive temporal trend of the "mesotrophic" pelagophytes is difficult to explain; it could indicate a need to revise the grouping of Latasa et al. (2010) or could be a result of other ecological changes in the Blanes Bay ecosystem. As noted above, the lack of significant slopes in the haptophytes could be a result of the heterogeneity of this group, which is likely to include taxa with substantial ecological differences.

2.5. CONCLUDING REMARKS

The nano- and microphytoplanton succession in the waters of Blanes Bay had been previously characterized, by means of optical microscopic observations, as typical of temperate marine ecosystems: dominated by diatoms in the winter- spring bloom, followed by haptophytes and dinoflagellates later in the season (Margalef 1964, Mura et al. 1996, Estrada 1999, Sioukou-Frangou et al. 2009, Estrada and Vaqué 2014). This

study, using HPLC pigment chemotaxonomy and flow cytometry, provides a more comprehensive view of the composition of the phytoplankton community, including cells in the picoplankton size range. Our data confirmed the prevalence of diatoms in the winter-spring bloom and in most episodic high-biomass situations, and indicated the occurrence of more or less marked winter-spring maxima and summer minima in cryptophytes, haptophytes, pelagophytes prasinophytes, in agreement with the variability in the concentrations of major nutrients. *Prochlorococcus* showed a fall-winter maximum and a spring-summer minimum, while dinoflagellates did not decrease their contribution in summer and *Synechococcus* presented peaks in April and August. . On the other hand, the abundance of diatoms, prasinophytes, cryptophytes and dinoflagellates responded positively to episodic coastal fertilization associated with precipitation events. Most phytoplankton groups presented a decreasing interannual trend that could be attributed to a reduction in nutrient availability, as suggested by the coincidence with decreasing concentrations of phosphate and the other major nutrients. A possible driver for this oligotrophication trend is the improvement in wastewater treatment, but longer time series are needed to ascertain the role of climatic factors. Our results highlight the need for sustained ecosystem observations at adequate temporal resolution. In the context of coastal management, our findings suggest, on one side, that in spite of increasing human pressure, coastal eutrophication can be controlled if appropriate management of continental nutrient inputs is performed, and on the other side, highlight the importance of considering not only warming (Doney 2006), but also the potential effects of extremes of precipitation or other meteorological events (Lavaysse et al. 2012) in a context of climate change.

Table 1. Global monthly means ± standard deviation (SD) and medians, (in terms of ng L^{-1} of Chl *a*), and percentage contribution to T_Chl *a* (%) of the CHEMTAX-derived phytoplankton groups.

Month	Cryptophytes			Diatoms			Dinoflagellates			Haptophytes		
	Mean ± SD	Median	%	Mean ± SD	Median	%	Mean ± SD	Median	%	Mean ± SD	Median	%
January	37.1 ± 21.4	36.1	6	137.06 ± 245.8	41	22.3	6.3 ± 5.2	4.9	1	170.1 ± 77.1	161.8	27.6
February	49.5 ± 32.5	45.8	6.3	180.6 ± 228.5	102.2	23	14.7 ± 17.9	7.2	1.9	256.9 ± 232.0	181.9	32.7
March	60.8 ± 67.2	32.9	7.2	321.3 ± 292.9	230.6	38.3	14.4 ± 20.0	5.7	1.7	205.9 ± 174.9	128.2	24.5
April	55.6 ± 66.0	29.8	10.2	131.1 ± 206.5	27	24	7.1 ± 8.1	4.3	1.3	185.2 ± 118.3	167.5	33.9
May	23.2 ± 21.5	11.3	5.5	165.1 ± 243.6	73.5	38.4	11.1 ± 8.6	8.8	2.6	167.9 ± 115.1	121.5	39.1
June	19.2 ± 25.5	9.1	6.1	78.5 ± 105.2	28.6	24.8	14.4 ± 17.1	9.9	4.6	135.8 ± 78.9	123.1	43
July	16.4 ± 18.8	9.9	6	11.7 ± 12.5	6.1	4.3	32.0 ± 54.1	8.6	11.6	134.0± 125.5	101.7	49.1
August	42.2 ± 48.6	17.6	13.5	15.5 ± 19.4	6.9	5	23.6 ± 29.5	15.3	7.5	109.0 ± 51.5	92.5	34.8
September	11.4 ± 11.5	5.2	4.7	5.9 ± 7.0	4.1	2.4	28.5 ± 34.3	20.2	11.6	102.7 ± 41.7	88.1	41.9
October	13.6 ± 8.5	16.5	4.8	5.7 ± 3.3	5.1	2	16.8 ± 21.9	9.2	5.9	152.8 ± 52.5	147.4	53.3
November	27.6 ± 17.9	22.3	4.3	6.6 ± 5.6	6.3	1	211.4 ± 365.1	47.9	33.1	185.7 ± 100.1	148.9	29.1
December	91.8 ± 203.3	29.7	12.3	35.7 ± 96.8	10.3	4.8	121.9 ± 135.3	66.3	16.4	229.6 ± 159.2	192.2	30.8

Month	Pelagophytes			Prasinophytes			*Prochlorococcus*			*Synechococcus*		
	Mean ± SD	Median	%	Mean ± SD	Median	%	Mean ± SD	Median	%	Mean ± SD	Median	%
January	40.1 ± 21.6	37.9	6.5	185.0 ± 88.2	144.7	30	12.2 ± 13.1	7	2	5.7 ± 6.7	2.6	0.9
February	49.8 ± 35.5	36.5	6.3	193.1 ± 63.1	184.7	24.5	5.0 ± 4.5	3.9	0.6	1.3 ± 1.7	0.5	0.2
March	27.1 ± 21.2	27.9	3.2	148.9 ± 94.6	129.5	17.7	2.0 ± 2.5	1.3	0.2	13.1 ± 22.5	5.7	1.6
April	21.4 ± 19.9	17.6	3.9	68.5 ± 55.9	49.4	12.5	1.4 ± 1.5	1	0.2	52.2 ± 52.7	40.4	9.5
May	12.9 ± 14.5	11.6	2.4	33.3 ± 31.4	28.2	7.7	1.7 ± 2.3	0.9	0.3	14.4 ± 12.8	13.2	2.7
June	11.9 ± 10.7	10.9	3.7	27.2 ± 17.8	22.4	8.3	1.3 ± 1.4	1.3	0.4	28.0 ± 30.7	15.8	8.8

July	12.8 ± 11.0	12.5	4.7	17.9 ± 12.8	16.3	6.6	1.0 ± 1.0	0.7	0.3	36.6 ± 38.1	18.7	13.4
August	9.0 ± 9.1	7.8	2.9	26.1 ± 26.0	17.4	8.3	3.3 ± 4.7	1.3	1.1	73.6 ± 49.6	85.2	23.5
September	4.2 ± 5.6	0	1.7	12.5 ± 9.5	8.3	5.1	8.9 ± 12.1	4.1	3.6	59. 8 ± 42.8	50	24.4
October	7.8 ± 9.0	3	2.7	23.9 ± 26.8	19.8	8.3	13.9 ± 10.8	10.5	4.9	43. 7± 23.5	43.4	15.2
November	31.8 ± 29.0	26.8	5	69.2 ± 55.5	58.9	10.8	12.7 ± 10.6	8.5	2	22.7 ± 25.6	14.7	3.6
December	38.2 ± 35.2	29.2	5.1	178.9 ± 254.0	94	24	13.4 ± 11.6	9.9	1.8	13.7 ± 11.8	17.2	1.8

Table 2. Slope (time units are year^{-1}), standardized (Std.) slope, squared correlation coefficient and p-values corresponding to the regression lines, with respect to sampling date (in years), of the monthly anomalies of phosphate and silicate, and the anomalies (after square root transformation) of the CHEMTAX groups, total monovinyl-Chl_*a* (TMV Chl *a*), total Chl *a* (T_Chl *a*) and flurometric Chl *a* (Fl_Chl *a*). The number of observations ranged from 216 for temperature to 157 – 162 for the other variables. Only values corresponding to significant correlation coefficients are shown. "NS": non significant. The second row for cryptophytes and dinoflagellates gives the values after deletion of the November 2003 sample, which had unusually high abundances of these groups (see text).

Variable	Units	Slope (change per year)	Std. slope	r^2	p
Phosphate	µM	-0.005	-0.275	0.076	<0.001
Nitrate	µM	-0.045	-0.157	0.025	<0.05
Silicate	µM	-0.060	-0.232	0.054	<0.01
Cryptophytes	(Chl *a*, ng L^{-1})$^{-1/2}$	-0.277	-0.373	0.139	<0.0001
		-0.247	-0.393	0.155	<0.0001
Diatoms		-0.311	-0.188	0.035	<0.05
Dinoflagellates		-0.128	-0.273	0.074	<0.0001
		-0.106	-0.286	0.082	<0.0001
Haptophytes		-0.136	-0.144	0.021	NS
Pelagophytes		0.139	0.245	0.06	<0.01
Prasinophytes		-0.108	-0.138	0.019	NS
Prochlorococcus		-0.06	-0.217	0.047	<0.01
Synechococcus		-0.131	-0.210	0.044	<0.01
TMV_Chl *a*		-0.462	-0.291	0.085	<0.0001
T_Chl *a*		-0.444	-0.279	0.078	<0.0001
Fl_Chl *a*		-0.27	-0.166	0.027	<0.05

Table 3. Correlation coefficients among phosphate, nitrate, silicate, precipitation index (PI7), temperature and wind speed (WS, 2005-2014) anomalies. N = 159-161 for all coefficients, except those involving WS (*in Italics*), for which N = 110-111; in this case, anomalies of all the other variables were recalculated for the period 2005-2014. Significant values ($p<0.05$) are highlighted in bold type.

Variable		Phosphate anomaly	Nitrate anomaly	Silicate anomaly	PI7 anomaly	WS anomaly
Nitrate anomaly		**0.345**				
Silicate anomaly		**0.456**	**0.632**			
PI7 anomaly	Lm^{-2}	0.055	**0.208**	**0.332**		
Temperature anomaly	ºC	0.018	0.018	0.092	**-0.2**	
WS anomaly	ms^{-1}	***0.191***	*0.02*	*-0.041*	*0.044*	*0.064*

Table 4. Slopes (units are year^{-1}), standardized (Std.) slopes, *p*-values for the t-statistic, squared correlation coefficients and *p*-values of the F-ratio corresponding to the bivariate linear regression lines, with respect to sampling date (in years) and to the precipitation index (PI7) anomaly (units are Lm^{-2}), of the monthly anomalies (after square root transformation) of the CHEMTAX groups. The number of observations was 162. "NS": non-significant. The second row for cryptophytes and dinoflagellates gives the values after deletion of the December 2003 sample, which had unusually high abundances of these groups (see text). Significant positive slopes with respect to time and negative with respect to PI7 have been highlighted in bold type.

Dependent variable (Chl *a*, ng L^{-1})$^{-1/2}$	Time (years)			PI7 anomaly (Lm^{-2})			Multiple r^2	p-value
	Slope	Std. Slope	p-value	Slope	Std. Slope	p-value		
Cryptophytes	-0.273	-0.367	<0.0001	0.027	0.185	<0.05	0.174	<0.0001
	-0.236	-0.378	<0.0001	0.016	0.132	NS	0.163	<0.0001
Diatoms	-0.303	-0.183	<0.05	0.055	0.172	<0.05	0.065	<0.01
Dinoflagellates	-0.121	-0.254	<0.001	0.021	0.224	<0.01	0.119	<0.0001
	-0.092	-0.257	<0.001	0.009	0.131	NS	0.085	<0.001
Haptophytes	-0.137	-0.145	NS	-0.002	-0.012	NS	0.021	NS
Pelagophytes	**0.142**	**0.250**	**<0.001**	0.014	0.125	NS	0.076	<0.01
Prasinophytes	-0.099	-0.126	NS	0.037	0.242	<0.001	0.077	N<0.01
Prochlorococcus	-0.062	-0.225	<0.01	**-0.010**	**-0.194**	**<0.05**	0.085	<0.001
Synechococcus	-0.131	-0.211	<0.01	-0.009	-0.073	NS	0.048	<0.05

SUPLEMENTARY MATERIAL

Table S1. Dates of collection of the samples used in this work

Year	Day/Month
2000	21/09
2001	20/03; 19/04; 23/05; 25/06; 02/08; 29/08; 27/09; 06/11; 04/12
2002	14/01; 07/02; 12/03; 15/04; 22/05; 27/06; 24/07; 14/08; 26/09; 23/10; 27/11
2003	13/01; 28/01; 04/03; 25/03; 22/04; 13/05; 25/06; 14/07, 04/08; 16/09; 21/10; 25/11; 16/12
2004	26/01; 23/02; 22/03; 23/03; 24/03; 20/04; 26/05; 19/07; 29/09; 19/10; 20/10; 16/11, 14/12
2005	20/01, 15/02; 09/03; 13/04; 10/05; 07/06; 05/07; 13/09; 04/10; 08/11; 12/12
2006	11/01; 07/02; 07/03; 04/04; 16/05; 13/06; 05/07; 01/08; 12/09; 09/10; 10/11; 11/12
2007	16/01; 20/02; 20/03; 24/04; 15/05; 05/06; 03/07; 01/08; 12/09; 16/10; 13/11; 11/12
2008	09/01; 13/02; 12/03; 10/04; 10/05; 02/07; 06/08; 12/09; 08/10; 05/11; 10/12
2009	14/01; 05/02; 16/04; 26/05; 09/06; 30/06; 04/08; 14/10; 04/11; 14/12
2010	13/01; 10/02; 09/03; 06/04; 04/05; 01/06; 06/07; 03/08; 15/09; 06/10; 10/11; 15/12
2011	12/01; 08/02; 14/03; 12/04; 17/05; 15/06; 05/07; 02/08; 13/09; 10/10; 29/11; 19/12
2012	10/01; 14/02; 13/03; 11/04; 11/05; 20/06; 03/07; 07/08; 13/09; 09/10; 06/11; 21/12
2013	15/01; 06/02; 12/03; 17/04; 07/05; 13/07; 01/08; 17/09; 15/10; 05/11; 15/12
2014	14/01; 11/02; 10/03; 07/04; 05/05; 02/06; 07/07; 04/08; 16/09; 07/10; 11/11; 16/12

Table S2. Phytoplankton pigments detected in this study. Range, average and standard deviation (SD) in ng L^{-1}.

Abbreviation	Pigment	Range (ng L^{-1})		Average (ng L^{-1})	SD (ng L^{-1})
		Maximum	Minimum		
19 - But	19'-Butanoyloxyfucoxanthin	136.37	1.25	23.35	18.21
19 - Hex	19'-Hexanoyloxyfucoxanthin	467.57	9.51	73.36	55.95
α-Car	α-Carotene	49.96	0.1	3.97	4.75
Allo	Alloxanthin	400.95	0.45	18.79	34.92
β-Car	β-Carotene	58.45	1.46	12.85	8.23
Chl *b*	Chlorophyll *b*	518.25	1.42	57.05	60.31
Chl c_1	Chlorophyll c_1	41.81	0.05	6.02	7.13
Chl c_2	Chlorophyll c_2	433.61	0.75	55.66	58.84
Chl c_2-MGDG [14/18]*	Chl c_2-monogalactosyldiacylglyceride ester [14/18]	109.75	0.26	9.6	16.7
Chl c_3	Chlorophyll c_3	167.71	1.9	31.77	29.05
Chl c_2-MGDG [14/14]	Chl c_2-monogalactosyldiacylglyceride ester [14/14]	70.54	0.53	9.17	9.74
Chlide *a*	Chlorophyllide *a*	609.08	0.12	22.43	67.11
cis-fuco*	Cis - fucoxanthin	66.33	0	5.88	10.6
cis-hex*	Cis 19-hexanoyloxyfucoxanthin	43.45	0.43	4.93	5.88
Ddx	Diadinoxanthin	205.52	2.47	30.42	28.74
DVChl *a*	Divinyl chlorophyll *a*	47.95	0.1	6.56	9.24
Fuco	Fucoxanthin	961.42	3.7	90.31	116.11
MV_Chl *a*	Monovinyl chlorophyll *a*	3178.87	58.03	460.45	375.5
MV_Chl c_3	Monovinyl chlorophyll c_3	26.91	0.15	3.88	3.89
MV_Chl *a*-allomer1	Monovinil chlorophyll *a* allomer 1	92.61	0.08	11.94	12.12

MV_Chl *a*-allomer2	Monovinyl chlorophyll *a* allomer 2	37.83	0.05	7.83	7.84
MV_Chl *a*-epimer	Monovinyl chlorophyll *a* epimer	22.75	0.49	4.19	3.8
Neo	Neoxanthin	54.09	0.12	4.13	5.23
Per	Peridinin	222.72	0.47	8.24	18.72
Pras	Prasinoxanthin	62.15	0	7.3	8.53
Uri	Uriolide	40.4	0	3.53	4.6
Viol	Violaxanthin	59.15	0.22	4.28	5.42
Zea	Zeaxanthin	104.27	0.39	21.24	21.2

* Measurement started in 2008

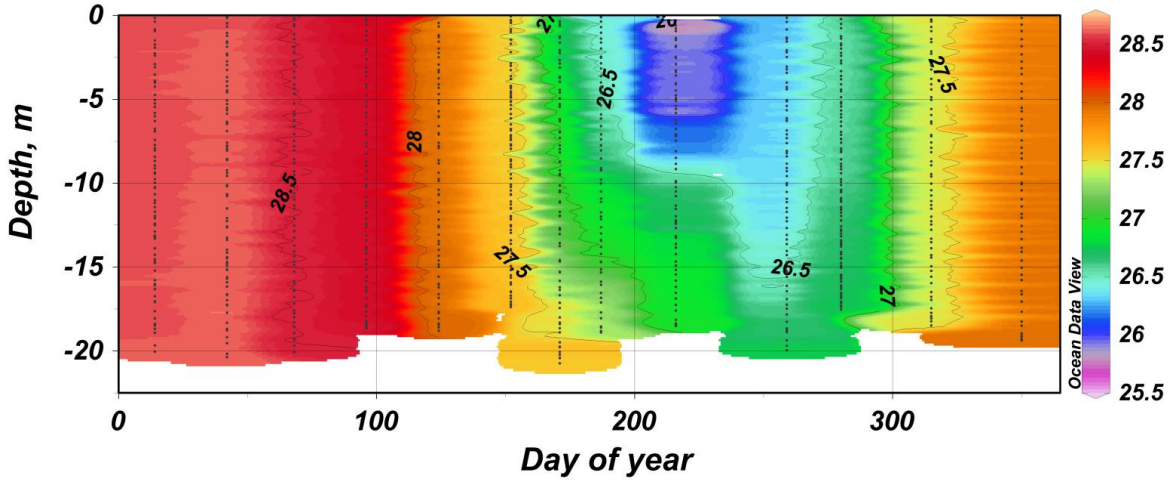

Figure S1. Example of seasonal cycle of the seawater potential density anomaly (σ_θ) for Blanes Bay (2014). Figure produced using the Ocean Data View software (Schlitzer, 2016).

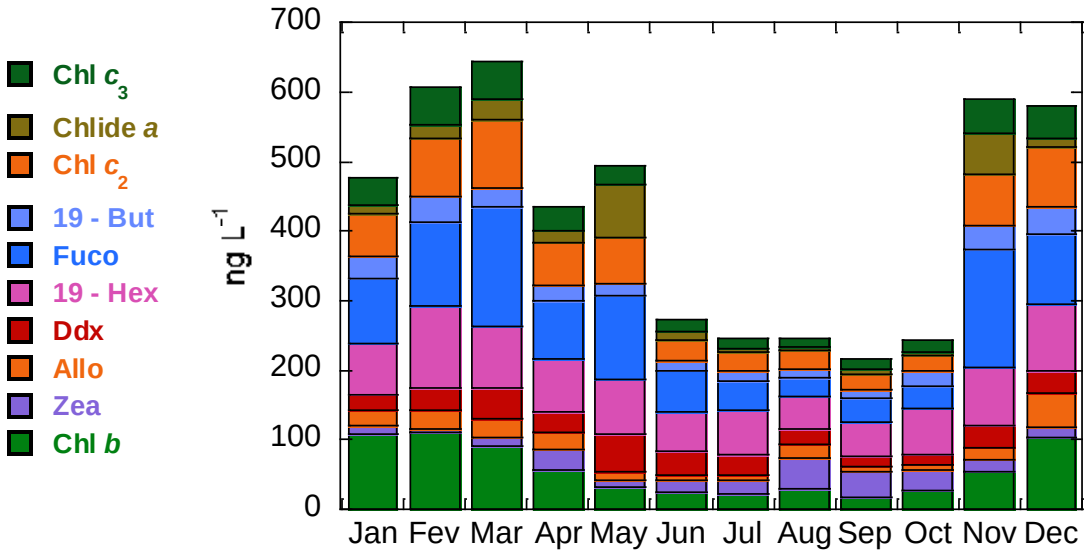

Figure S3. Average monthly concentration of the main pigments determined by HPLC. See Table S2 for the explanation of the abbreviations.

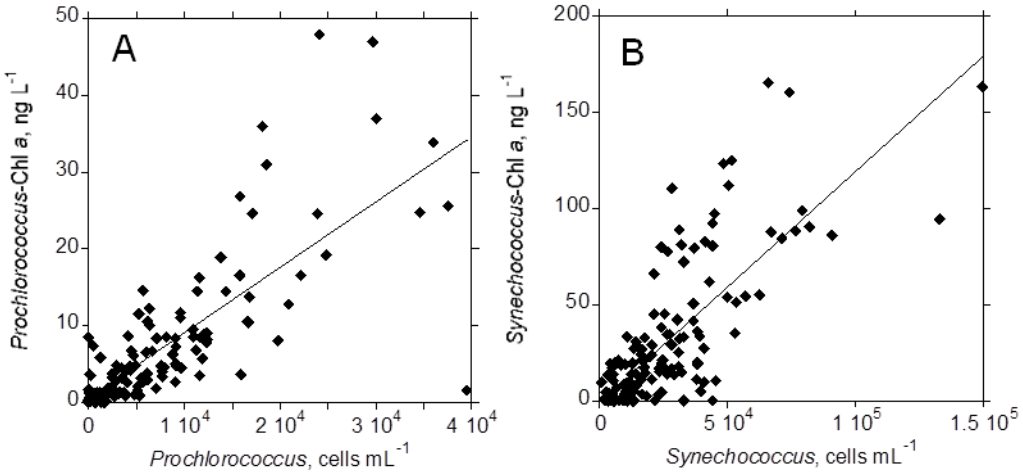

Figure S4. Relationship between flow cytometric cell counts and CHEMTAX-derived contribution to T_Chl *a* of *Prochlorococcus* (A) and *Synechococcus* (B). The equations of the regression lines are and $y = 0.00086x + 0.520$ (N=XX, $R^2 = 0.63$, $p < 0.001$) for *Prochlorococcus* and $y = 0.00120x - 0.723$ (N = 151, $R^2 = 0.60$, $p < 0.001$) for *Synechococcus*.

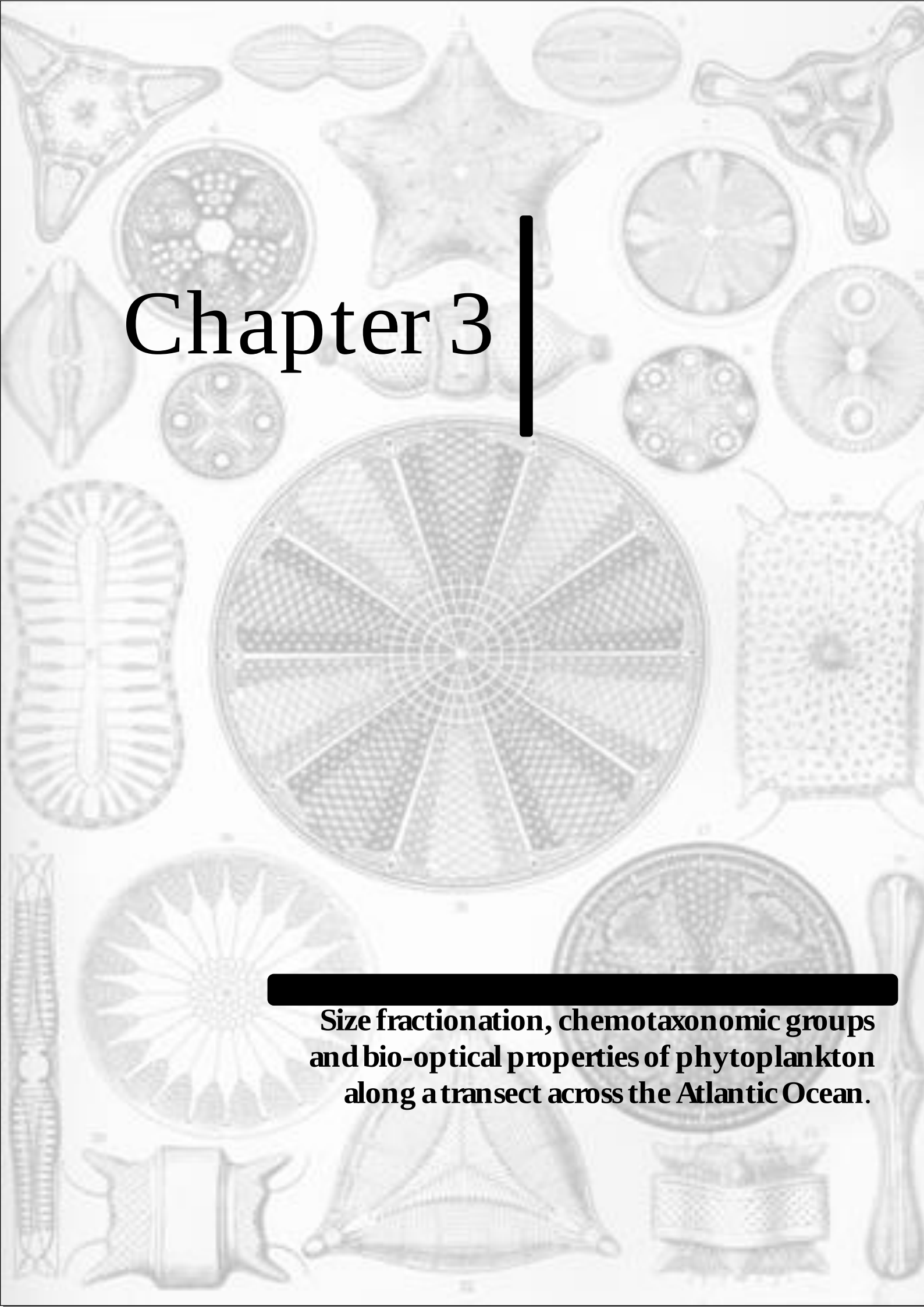

Chapter 3

Size fractionation, chemotaxonomic groups and bio-optical properties of phytoplankton along a transect across the Atlantic Ocean.

The scientific contribution of this work has resulted in of this chapter as a manuscript entitled: Nunes, S.**;** Perez, G.L, Latasa, M.; Zamanillo, M. Delgado, M.; Ortega-Retuerta, E.; Marrasé, C.; Simó, R.; Estrada, M. (2018). **Size fractionation, chemotaxonomic groups and bio-optical properties of phytoplankton along a transect across the Atlantic Ocean.** Scientia Marina. *Aceptado.*

CHAPTER 3

Size fractionation, chemotaxonomic groups and bio-optical properties of phytoplankton along a transect across the Atlantic Ocean

Abstract

The relationships between the structure of the phytoplankton community and the bio-optical properties of surface waters were studied during the TransPEGASO cruise, along a transect through the Atlantic Ocean that sampled seven biogeographycal provinces, from the Alboran Sea (SW Mediterranean) to the Patagonian Shelf. We characterized the composition of the phytoplankton community by means of microscopic observations and HPLC - CHEMTAX pigment analyses applied to whole water and two filtration size fractions (>3 and < 3 µm), and measured the absorption of particulate matter and colored dissolved organic matter (CDOM). The Chl *a* size class distribution obtained from the fractionated filtrations was compared with those resulting from the diagnostic pigment algorithms (VU) developed by Vidussi et al. (2001) and Uitz et al. (2006), and the total Chl *a*-based approach (HI) of Hirata et al. (2011). The seven provinces covered by the transect could be divided in an oligotrophic group, with Chl *a* < 0.25 mg m^{-3}, comprising the Tropical and Subtropical Atlantic (including the Canary Current Coastal province), and a eutrophic group (Chl *a* > 0.5 mg m^{-3}) with a single Mediterranean (MEDI) sample and those from the Southwestern Atlantic Shelf (SWAS). According to CHEMTAX, the most important taxa in the Tropical and Subtropical Atlantic were *Prochlorococcus* spp., haptophytes and *Synecoccoccus* spp., while MEDI and SWAS were dominated by diatoms and haptophytes. Both the VU and HI algorithms, which are based on pigment composition or Chl *a* concentration, predicted for SWAS a high proportion of nano- and microphytoplankton. However, microscopic observations found only small concentrations of nano- or microplankton-sized cells in several stations of this region and the results of the size-fractionated filtrations, indicated dominance of the < 3 µm fraction. This discrepancy appeared to be due to the presence, confirmed by scanning electron microscopy, of picoplankton-sized forms such as cells of Parmales (a group sharing the pigment composition with the diatoms) and the diatom *Minidiscus* sp.

The total non-water absorption in the water column was dominated by CDOM. Average phytoplankton absorption for the different provinces ranged between 19.3% in MEDI to 45.7% in SWAS and 47% in the Western Tropical Atlantic (WTRA). The Chl

a-specific phytoplankton absorption [a_{ph}*(443)] was lower in MEDI and SWAS than in the oligotrophic provinces. a_{ph}*(443) was positively correlated to the package index [Qa*(443)] but was only weakly related to the photosynthetic (PSC) and non-photynthetic (PPC) carotinoid to Chl *a* ratios (PSC/Chl *a* and PPC/Chl *a*, respectively) and was not correlated with indicators of size structure such as the proportion of Chl *a* in the < 3 µm fraction or a VU-derived size index. These findings suggest that cell size did not exert a marked influence on Qa*(443) and that the variability observed in a_{ph}*(443) was mainly related to differences in intracellular pigment concentration and possibly to photoacclimation processes.

Keywords: Chemotaxonomic, CHEMTAX, Size-fractionation, Bio-optics, Atlantic Ocean, CDOM

3.1. INTRODUCTION

The organisms of the phytoplankton, microscopic photosynthetic protists and cyanobacteria that inhabit the illuminated layers of water bodies, represent the main primary producers in the marine ecosystem, are a crucial agent in biogeochemical cycles and influence processes linking atmosphere and ocean. They are the main protagonists of the biological uptake of atmospheric CO_2 in the ocean and play an important role in aerosol generation through the production of dymethyl sulphoproprionate (DMSP), a precursor of dimethyl sulphide (DMS), and other volatile compounds.

The phytoplankton includes an enormous variety of taxa; descriptions based on morphology included around 4000 species when reviewed by Sournia et al. (1991) but current molecular techniques are uncovering a large amount of novel genetic diversity (Vargas et al, 2015; Farrant et al., 2016). A way to manage this diversity, in particular regarding the biogeochemical and trophic flow roles played by different groups, has been the recognition of life-forms or functional types of phytoplankton (PFTs), which consist of groupings of organisms based on some common traits of interest (Margalef, 1978, Litchman andf Klausmeier, 2008), rather than on explicit taxonomy. PFTs may be defined by properties such as the posession of flagella and the ability to migrate in the water column (as in the dinoflagellates), by the role played in biogeochemical cycles or by size, which is in itself an important functional trait that influences other phytoplankton properties. Examples of biogeochemical PFTs are the silicifyers (diatoms), calcifyers (such as coccolithophores) or nitrogen fixers (certain cyanobacteria) (Le Queré et al., 2005; Zeng et al., 2018). Concerning size, phytoplankton is traditionally divided in three categories: micro- (20 - 200 µm, nano- (2

- 20 µm) and picophytoplankton (0.2 - 2 µm). PFTs defined on a biogeochemical basis may include components of different size classes. For example, diatoms characterized by the presence of siliceous frustules, comprise micro- and nanophytoplankton-sized forms.

Phytoplankton size, in combination with other traits such as the presence of mineral walls, determines sinking rates and is a key factor influencing energy flows in the food web and the potential export of carbon to the sediment (Kiørboe, 1993; Klaas and Archer, 2002). Thus, knowing the PSC distribution in a community is necessary for improving our knowledge of ecosystem dynamics and for ascertaining the effects of climate and anthropogenic changes on the marine environment.

Using the PCS´s classification as reference, Vidussi et al. (2001) proposed a method to distribute phytoplankton populations in size categories according to their HPLC (High-Pressure Liquid Chromatography) pigment signatures. Their equations were updated by Uitz et al. (2006), based in Gieskes et al. (1988), by assigning weights to each of seven diagnostic pigment markers and allowing the total chlorophyll *a* (Chl *a*) concentration to be reconstructed from the knowledge of the concentration of these pigments (Vega-Moreno et al., 2012). Further refinements to these methods of diagnostic pigment analysis (DPA) were introduced by Hirata et al., (2008, 2011), who defined ten pigment groups to represent three size categories (micro-, nano- and picoplankton) and seven PFTs, and observed that the Chl *a* of the whole community could be used as an index not only of phytoplankton biomass but also of their community structure in terms offunctional type and size distributions.

As the optical properties of a water body are strongly associated with the pigment composition and the size structure of the phytoplankton assemblages, the study of these community traits has relevant applications in the development of algorithms for the

detection of chlorophyll, the modelling of primary production and the identification of phytoplankton functional types (PFTs) by remote sensing (Perez et al, 2016; Falkowski et al., 2003; Brewing et al., 2010, Taylor et al., 2011).

In this study, we present information on the relationships between environmental parameters, CDOM variability and phytoplankton size and community structure in the surface waters along a transect from the Mediterranean to the southwest Atlantic that covered several biogeochemical provinces (Longhurst, 2007) in the southern spring of 2014. We examined the phytoplankton composition by means of microscopic and flow cytometric observations, and by HPLC pigment analysis followed by the application of the CHEMTAX algorithm (Mackey et al., 1996). Pigment measurements were carried out for whole water samples and for size-fractionated filtrations and the results were compared with size distribution estimates derived from the composition of diagnostic pigments (Vidussi et. al., 2001; Uitz et al., 2006; Hirata et al., 2011). We also explored the relationships between CDOM absorption, bio-optical properties of the water and phytoplankton size distribution and chemotaxonomic characteristics.

3.2. MATERIAL AND METHODS

3.2.1 TransPEGASO cruise: Sampling and physical measurements

The TransPEGASO cruise, carried out on board the R/V Hesperides between 21 October 21 and 21 November 2014, sampled 42 oceanographic stations along a transect (Fig. 1) across the Mediterranean and the Atlantic Ocean, from Cartagena (Spain) to Punta Arenas (Chile), with a stopover in Brazil from 8 to 16 November (Table S1). Based on geographic location and Chl *a* concentration, we assigned the stations to seven biogeographical provinces (Longhurst, 2007): Mediterranean (MEDI), Atlantic

Subtropical Gyre East (NAST- E), Canary Current Coastal (CNRY), North Atlantic Tropical Gyre (NATR), Western Tropical Atlantic (WTRA), South Atlantic Tropical Gyre (SATL) and South West Atlantic Continental Shelf (SWAS) (Table S1).

Water samples were obtained twice a day, at 9 a.m. - 3 p.m. - local time (Table S1), through an underway flow-through system that collected water from 4 m depth and included a SBE 21 SeaCAT thermosalinograph. The water was screened *in situ* through a 150 μm nylon mesh to remove the larger zooplankton and the total sampling time did not exceed 90 seconds. Temperature, salinity and conductivity were determined from the continuous records of the SBE 21 thermosalinograph.

3.2.2 Nutrients, Flow Cytometry (FC), Fluorometric Chl *a* (Fl_Chl *a*)

For determination of nitrate, nitrite, silicate and phosphate concentrations, 100 mL of seawater were introduced in Falcon vials that were kept frozen (−20 °C) until analysis in the home laboratory. There, the nutrient concentrations were measured colorimetrically with an Alliance Evolution II autoanalyser, following the procedures described in Hansen & Koroleff (1999).

Samples for flow cytometric analysis consisted of 4.5 ml of water that were preserved with 1% paraformaldehyde plus 0.05 % glutaraldehyde (final concentrations), left to fix for 15 min, deep frozen in liquid nitrogen and stored at −80 °C until analysis (Zamanillo et al., submited). The concentration of autotrophic prokaryotes and picoeukaryotes was determined 6 months after the cruise, in the home laboratory, with a Becton Dickinson FACScalibur flow cytometer provided with with a laser emitting at 488 nm (Gasol and Del Giorgio, 2000). For analysis, the samples were thawed and 10 μL of a 10^5 mL^{-1} solution of yellow-green 0.92 μm Polysciences latex beads were added per 600 μL

sample as an internal standard. *Synechococcus*, *Prochlorococcus* and picoeukaryotes were identified on the basis of their autofluorescence and scattering properties.

For fluorometric Chl *a* (Chl *a*_Fl) determinations, 250 ml of seawater were filtered through 25 mm Whatman GF/F glass fiber filters (nominal pore size 0.7 μm), using a <200 mm Hg vacuum. The filters were subsequently frozen at − 20°C and, after one day, introduced into 90% acetone and kept in the dark at 4°C for 24 hours. The Chl *a*_Fl concentrations were determined fluorometrically using a calibrated Turner Designs fluorometer (Yentsch and Menzel, 1963). No phaeopigment "correction" was carried out.

3.2.3 Phytoplankton identification

Approximately 250 ml of seawater were placed in glass bottles, preserved with formaldehyde solution (4%) and stored in the dark until analysis on land. Phytoplankton examination was carried out by means of the inverted microscope method (Utermöhl, 1958); 100 ml of water were introduced in composite chambers and left to settle for 48 h. Subsequently, the entire base of the chambers was scanned at 125X to quantify the larger, less abundant organisms of the microphytoplankton (> 20 μm), and at least two transects were examined at 312X to enumerate the smaller and more frequent nanophytoplankton forms (<20 μm). When possible, phytoplankton was identified to the species level, but many organisms could not be adequately classified and were pooled in categories such as "small dinoflagellates (< 20 μm)", "unidentified centric diatoms" or "unidentified small coccolithophores (< 10 μm)". For scanning electron microscopy (SEM) examination. 40-50 ml of water from the fixed phytoplankton samples were filtered thorugh polycarbonate filters of 0.8 μm pore size and 14 mm

diameter that were subsequently washed with bottled water, dried and prepared as described in Cros and Estrada (2013).

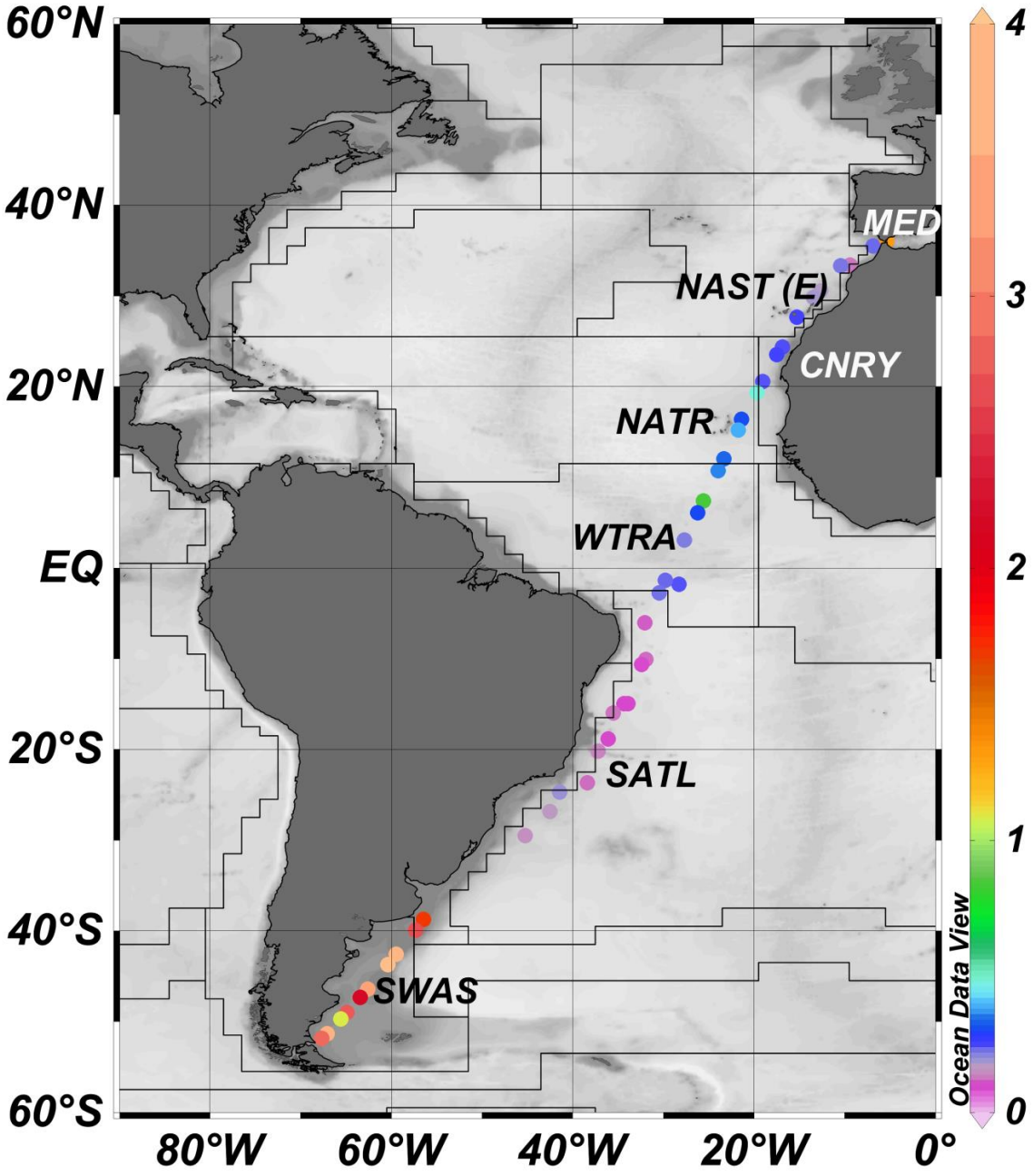

Figure 1. Position and biogeochemical provinces (Longhurst, 2007) of the sampling stations of the "TransPEGASO" cruise (21/10/2014- 21/11/2014). The province names and abbreviations are: Mediterranean (MEDI), Atlantic Subtropical Gyre East (NAST- E), Canary Current Coastal (CNRY), North Atlantic Tropical Gyre (NATR), Western Tropical Atlantic (WTRA), South Atlantic Tropical Gyre (SATL) and South West Atlantic Continental Shelf (SWAS).

3.2.4 Size-fractionated pigments estimates from HPLC

Pigment analysis by high-performance liquid chromatography (HPLC) following the method from Latasa (2014) was carried out for three phytoplankton size fractions (SFF) obtained on board by filtration: Chl *a*_tot (total phytoplankton), Chl *a*_n+m>3 (nano and microphytoplankton) and Chl *a*_pico<3 (picophytoplankton). For Chl *a*_tot, we filtered 0.35 - 2 L) onto 25 mm Whatman GF/F glass fiber filters. For the Chl *a*_n+m>3 fraction we filtered 0.2 – 1.8 L of seawater in the SWAS province stations and 2.5 L in the others onto a 25 mm Nuclepore polycarbonate filter of 3 μm pore size. The resulting filtrate was filtered again through 25 mm Whatman GF/F filters, corresponding to the Chl *a*_pico<3 samples. Immediately after filtration, the filters were introduced into criovials and stored frozen at -80°C until analysis in the laboratory of the Instituto Español de Oceanografia (Xixón/Gijón laboratory). The procedure for pigment extraction began with wetting the filters with 2.5 mL acetone 90% that contained an internal standard of trans-β-apo-8'-carotenal Sigma, followed by sonication (30 seconds, 8 x 10 cycle and 40 intensity). After keeping the filters in acetone at -20°C during 24 h y, the samples were vortexed, filtered again through Whatman GF/F glass fiber filters to remove debris and placed in amber cryovials.. The extracts were analyzed by HPLC using an Agilent series (Waldbronn, Germany) 1200 chromatographic system with a G1311A quaternary pump, a G1367C autosampler with a 100 _L capillary loop, a G1316B column thermostat, and a G1315C diode array detector. The sample volume injected was 100 μL and the sequence of sample withdrawal and injection was: sample-water-sample-water and ejection into seat; the composition of the eluents is detailed in Latasa (2014). A total of 36 pigments (Tables 1 and S2) were detected at 440 and 665 nm, and identified by retention time and online diode array detector- DAD. The peak

area of the pigments was calculated with the Agilent ChemStation software. The chlorophyll *a* concentration in total (Chl *a*_tot) and size-fractionated samples (Chl *a*_n+m>3 for the > 3 μm and Chl *a*_pico<3 for the < 3 μm fractions) was estimated as the sum of monovinyl chlorophyll *a* (MV_Chl *a*), divinyl chlorophyll *a* (DV_Chl *a*), chlorophyllide *a* (Chlide *a*), and chlorophyll *a* allomers and epimers. DV_Chl *a* was not detected in the SWAS region.

3.2.5 Pigment-based estimation of phytoplankton size classes and physiological state

An estimate of the size structure of the phytoplankton assemblages was obtained from pigment concentrations quantified by HPLC, by means of the diagnostic pigment algorithms (Table 2) of Vidussi et al. (2001) and Uitz et al. (2006). In this approach, an estimate of the total Chl *a* concentration can be obtained as a weighted sum of the seven diagnostic pigments considered (ΣDP, see Table 2). An additional evaluation of the three phytoplankton size fractions was obtained using the Chl *a* -based approach (Table 2) of Hirata et al. (2011). The size-fractionated Chl *a* concentrations derived from the Uitz et al. and Hirata et al. estimates were compared with the filtration results using the standard major axis regression method, which is appropriate (Falster et al., 2006) to test whether the slope fits a specific value (1 in this case).

A size index (SI) based on an expression derived by Bricaud et al. (2004) was used to synthesize the size structure of each algal assemblage:

$$SI = (1*f\_pico+5*f\_nano+50*f\_micro) \quad (1)$$

where 1 μm, 5 μm and 50 μm are taken as representative sizes for the picophytoplankton (f_pico), nanophytoplankton (f_nano) and microphytoplankton (f_micro) fractions.

To assess the photoacclimation response to irradiance of the phytoplankton groups containing diadinoxanthin (Ddx) as the main light-protecting pigment, which include diatoms, dinoflagellates, haptophytes and pelagophytes, we calculated the ratio Ddx/LHC between the concentration of Ddx and the sum of the concentrations (LHC) of four major light-harvesting carotenoids: fucoxanthin, 19'-butanoyloxyfucoxanthin, 19'-hexanoyloxyfucoxanthin and peridinin. In order to assess the effect of accesory pigment composition on phytoplankton absorption properties we grouped the carotinoids in two categories: non-photosynthetic carotinoids (PPC, including zeaxanthin, diadinoxanthin and *β*-carotene, and photosynthetic carotinoids (PSC), comprising fucoxanthin, peridinin, 19'-butanoyloxyfucoxanthin, and 19'-hexanoyloxyfucoxanthin (Bricaud et al. 2004).

3.2.6 CHEMTAX processing

Based on the main pigment markers, the contribution of different phytoplankton groups to total Chl *a* was calculated using version 1.95 of the CHEMTAX chemical taxonomy software (Mackey et al., 1996). Essentially, the CHEMTAX algorithm uses one or several initial matrices of pigment:Chl *a* ratios for the selected phytoplankton groups to derive the contribution of each pigmentary class to the total Chl *a*. The samples corresponding to Chl *a*_tot, Chl *a*_n+m>3 and Chl *a*_pico<3 were clustered separately according to the contribution of the pigments 19'-Butanoyloxyfucoxanthin (19 - but), 19'-Hexanoyloxyfucoxanthin (19 - hex), alloxanthin (allo), chlorophyll *b* (Chl *b*), chlorophyll *c*2 (Chl *c*2), Chl *c*2-monogalactosyldiacylglyceride ester [14/14] (Chl c2-MGDG [14/14]), divinyl chlorophyll *a* (DV_Chl *a*, fucoxanthin (fuco), neoxanthin (neo), peridinin (per), prasinoxanthin (pras), violaxanthin (viol) and zeaxanthin (zea); DV_Chl *a* was removed in SWAS because it was below detection level. Each fraction

data set could be grouped in two clusters, one containing the SWAS samples (cluster 2) and another (cluster 1) with the remaining ones (Table S3). CHEMTAX was run following the procedures of Latasa (2007) and Latasa et al. (2010). Briefly, we created 29 randomized copies of the initial ratio matrix and we ran the program for eight successive times. After the eighth run, a single average matrix was made and used again for a final run. Nine pigmentary classes were quantified in MEDI, NAST-E, CNRY, NATR, WTRA and SATL Zones: Chlorophytes (Chloro), Cryptophytes (Chrypto), Diatoms, Dinoflagellate (Dino), Haptophytes (Haptos), Prasinophytes (Prasinos), Pelagophytes (Pelagos), *Prochlorococcus* spp. and *Synechococcus* spp., while *Prochlorococcus* was not found in SWAS.

3.2.6 Bio-Optical estimates of phytoplankton

Water samples of 37 TransPEGASO cruise station were collected and filtered through 47 mm Whatman GF/F glass fiber filters, precombusted at 450 °C for 4 h (Romera-Castillo et al., 2011), in an acid-cleaned all-glass filtration system and under positive pressure with low N_2 flow. CDOM absorbance was measured onboard immediately after filtration in the spectral range between 240 and 700 nm at 1 nm intervals in a Lambda 800 (Perkin-Elmer) dual beam spectrophotometer equipped with 10 cm quartz cells. Blank spectra of filters (prepared in the field) with pre-filtered (0.2 μm) seawater was used as a reference blank and were subtracted after each scan. The baseline variations were automatically corrected. The CDOM absorption coefficients were calculated as follows:

$$a_{CDOM}(\lambda) = 2.303 * Afiltrate(\lambda)/\iota \qquad (2)$$

where Afiltrate(λ) is the absorbance of the filtrate and ι is the path length (in m) and 2.303 converts between log10 and natural log.

The λ chosen for the study were 443 nm because of its use in remote sensing and 325 nm because of its application in estimates of DOC concentration (Baker aand Spencer, 2004).

For determination on-board of total particulate matter absorption coefficients ([a_p (λ)] with m^{-1} as units)), samples of 0.85 to 2 L were filtered through 25 mm-diameter GF/F filters. Immediately after filtration absorbance scans were measured from 300 to 750 nm at 1 nm intervals. Absorbance was checked to be lower than 0.4 (Cleveland and Weidemann, 1993). The [a_p (λ)] were determined by the quantitative filter technique (QFT), using the simple transmittance method in a Lambda 800 (Perkin-Elmer) dual beam spectrophotometer. The QFT method was applied according to NASA's optics protocols for absorption coefficient measurements (Mitchell et al., 2000). Blank scan filter wetted with filtered (0.2 μm) seawater were subtracted. Absorption coefficients of non-algal particles [a_{nap} (λ)] (i.e., non-chlorophyllous, unpigmented particles) were determined by using the methanol extractive method following the procedures of Kishino et al. (1985). Absorption coefficients of a_p (λ) (first measurement) and a_{nap} (λ) (measurement after methanol extraction) were estimated according the equation:

$$a_{p,}\, a_{nap}\, (\lambda) = 2.303 * Afilter(\lambda) * S / V\beta\, (\lambda) \qquad (3)$$

where Afilter (λ) is the measured absorbance with QFT, S is the clearance area of the filter, V is the volume of filtered water, and β (λ) is the amplification factor vector (Mitchell and Kiefer, 1984). The β (λ) factor was calculated following Bricaud and Stramski (1990) with the equation:

$$\beta\, (\lambda) = 1.63\ Afilter(\lambda)^{-0.22} \qquad (4)$$

In order to correct for residual offsets in the sample filter relative to the reference and for scattering artifacts due to particle loading (Mitchel et al., 2000), the optical density

of all spectra was corrected subtracting the readings at 750 nm where absorbance by particles was assumed to be negligible.

Phytoplankton absorption coefficients [$a_{ph}(\lambda)$] were obtained by subtracting a_{nap} (λ) from $a_p(\lambda)$. The Chl *a*-specific phytoplankton absorption coefficient [$a_{ph}^*(\lambda)$] was estimated as: $a_{ph}(\lambda)$/Chl *a*_tot. Finally, total absorption coefficients [a_t (λ)] were calculated based on equation:

$$a_t(\lambda) = a_{CDOM}(\lambda) + a_p(\lambda) + a_w(\lambda) \qquad (5)$$

where a_w (λ), the absorption coefficient of pure water, was taken from Pope and Fry (1997) and from Morel et al. (2007) for the UV-blue range (see a_{w1} values in Morel et al., 2007).

In general, $a_{ph}^*(\lambda)$ depends not only on the pigmentary composition of the cells, but also on the so-called package effect, which consists on a reduction in the absorption of pigmented particles relative to the absorption of the pigments in solution. The package effect is stronger when either cell size or intracellular pigment concentration increase and can be estimated by means of the package index $Qa^*(443)$. This index can be calculated as the ratio of the phytoplankton absorption $a_{ph}(\lambda)$ and the absorption of pigments in solution $a_{sol}(\lambda)$, according to the eexpressions (Bricaud et al., 2004):

$$a_{pig}(\lambda) = \Sigma\, C_i\, a^w_{sol,i}(\lambda)$$

$$a_{sol}(\lambda) = a_{pig}(\lambda) + a_{miss}(\lambda)$$

where $a_{pig}(\lambda)$ is the sum of pigment-specific absorption coefficient of the i th pigment multiplied by their concentrations (C_i, mg m^{-3}) in the medium, following the approach of Bricaud et al. (2004) based on the weight-specific absorption coefficients proposed by Goericke and Repeta (1993) and Bidigare et al. (1990). The $a_{miss}(\lambda)$ expression is a so-called "missing term" that depends on total Chl *a* concentration (Bricaud et al.,

2004). The $Qa^*(\lambda)$ index can increase from 0 (maximum package effect) to 1 (no package effect).

3.3. RESULTS

3.3.1 Oceanographic characterization of the transect

The TransPEGASO transect crossed seven biogeochemical provinces between the Mediterranean (MEDI) and the Southwestern Atlantic Shelf (Fig. 1) and encountered a wide range of hydrographical properties (Fig. 2, Table 3). Temperature (Fig, 2a) was about 21ºC in MEDI, increased to mean values (Table 3) of 28.7 and 28.2 in NATR and WTRA, respectively, and decreased to 8-14ºC in SWAS. Salinity (Fig. 2a, Table 3) ranged from 34.8 to 36.8 between MEDI and CNRY, presented a minimum of 34.8 in WTRA, increased again in SATL (36.3-37.4) and decreased to 32.6-33.6 in SWAS.

Nitrate, nitrite, and phosphate concentrations (Fig. 2b, c, Table 3) were generally low from MEDI to NATL and relatively high in SWAS, where the mean concentrations of these nutrients were respectively 4.08 µM, 0.13 µM and 0.57 µM. Silicate (Fig. 2c) concentrations were low (0.2-1.42 µM) and very variable across the whole transect. The N:P ratio [(nitrate+nitrite)/phosphate] was always lower than the Redfield value of 16 (Table 3).

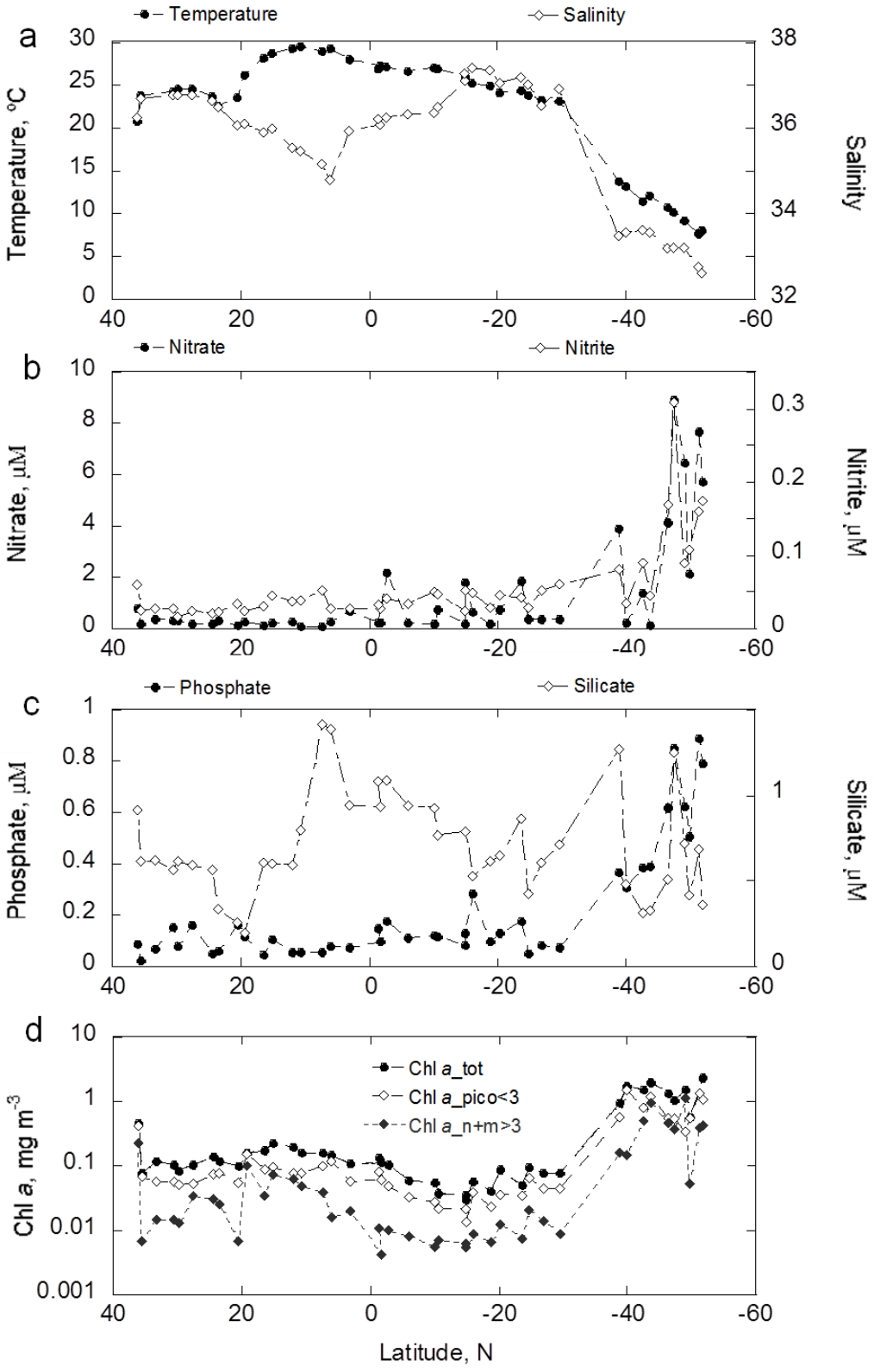

Figure 2. Variations of (a) temperature (ºC) and salinity, (b) nitrate (µM) and nitrite (µM, right ordinate scale), (c) phosphate (µM) and silicate (µM, right ordinate scale) and (d) Chl *a* (mg m^{-3}) of the total community (Chl *a*_tot) and of the < 3 µ (Chl *a*_pico<3) and > 3 µm (Chl *a*_n+m>3) size fractions, in the TransPEGASO transect.

3.3.2. Chl *a* and HPLC pigments

There was a good correlation (Fig. S2b) between Chl *a*_Fl (fluorometric readings) and Chl *a*_tot (HPLC), although fluorometric readings tended to be substantially higher (Chl *a*_Fl = 1.76*Chl *a*_tot + 0.17, n = 41, r^2 = 0.96, p < 0.0001; one Chl *a*_tot outlier for station 41, with a value much smaller than the sum of Chl *a*_pico<3 and Chl *a*_n+m>3 was excluded), and (Fig. S2c) between Chl *a*_tot and the sum of the HPLC-measured Chl *a*_pico<3 and Chl *a*_n+m>3 fractions (Chl *a*_pico<3 + Chl *a*_n+m>3 = 0.85+ Chl *a*_tot + 0.005; n = 41, r^2 = 0.95, p < 0.0001; the same outlier was also excluded). Hereafter, for simplicity unless otherwise stated, Chl *a* concentrations will refer to the HPLC determinations.

The highest Chl *a*_tot concentrations (fig. 2d) were recorded in the shelf waters of SWAS (mean 1.40 mg m^{-3} ± 0.45, 2.7 mg m^3 ± 0.71 Chl*a*_tot), followed by MEDI (0.47 mg m^{-3} Chl *a*_tot). In the remaining regions, Chl *a*_tot ranged from 0.03 mg m^{-3} (SATL) to 0.22 mg m^{-3} (WTRA). The Chl *a*_pico<3 and Chl *a*_n+m>3 fractions followed a comparable pattern (Fig. 2d), with the highest values in SWAS and MEDI and low values elsewhere. There were appreciable differences between the size structure of the various regions, with more nano + microplankton contribution in SWAS and MEDI Fig. 3a). However, there were no significant trends when comparing the percentage of Chl *a* in the picoplankton size fraction (f_pico<3) with Chl *a*_tot (Fig. S1).

The principal phytoplankton pigments determined by HPLC in each zone (and the name abbreviations used hereafter) are presented in Table 1 for the whole water and in Table S2 for the nano + microphytoplankton (n+m>3) and picophytoplankton (pico<3) fractions. Overall, apart of monovinyl Chl *a* (MV-Chl *a*), which was dominant in all

zones, the most important pigments in the whole community were Chl *b*, Fuco and 19 - Hex in SWAS, and Fuco, 19 – Hex and Chl *c*2 in MEDI (Fig. 4a). In contrast, the other provinces, with the exception of CNRY, were characterized by the dominance of Zea, DV_Chl *a* and 19 – Hex. In CNRY, the most important pigments were Zea, Phaeop, 19 – Hex and DV_Chl *a* (Fig. 4b; Table 1).

In general, the most abundant pigments in the n+m>3 size class (excluding MV_Chl *a*) were Fuco (dominant in MEDI and SWAS), Phaeop and 19 – Hex, with Chl *c*2 in MEDI, β Car in CNRY and Chl *c*2-MGDG [14/14] in NATR and WTRA (Table S2). In the pico<3 size class, Zea, DV_Chl *a*, MV_Chl *a* and 19 – Hex were the most abundant pigments in NAST-E, NATR, WTRA and SATL. In the other provinces, MV_Chl *a* was always the most abundant pigment, followed by Chl *b* and 19 – Hex in MEDI, by Phaeop and Zea in CNRY and by 19- hex and Fuco in SWAS (Table S2).

The ratio Ddx/LHC ranged from a low value of 0.09 in MEDI to a peak of 0.40 in SWAS and showed short-term fluctuations, generally in phase with those of PAR (Fig. 5a); there was a weak but significant correlation ($n = 40$, $r^2 = 0.10$, $p < 0.05$; Fig. S1a) between solar radiation and the Ddx/LHC ratio. Both the the PPC/Chl *a*_tot (data not shown) and the PPC/PSC (Fig. 5b) pigment ratio peaked in the Tropical and Subtropical Atlantic and presented their lowest values in the MEDI and SWAS.

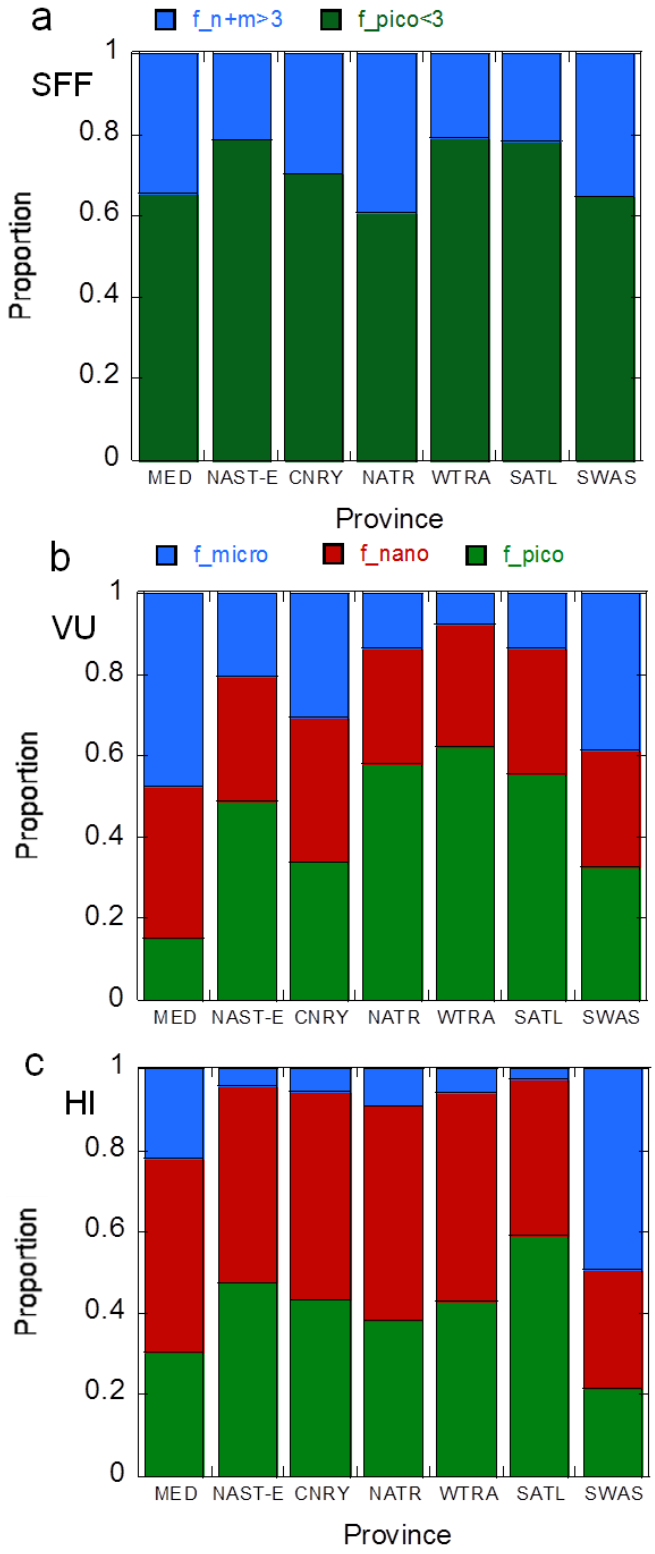

Figure 3. Size-distribution of Chl *a* determined by different approaches; (a) Proportion of nano+microphytoplankton (fn+m>3) and picophytoplankton (fpico<3) derived from fractionated filtration, (b) proportion of microphytoplankton (fmicro), nanophytoplankton (fnano) and picophytoplankton (fpico) estimated by the Vidussi et al. (2001)- Uitz et al. (2006) algorithm, (c) as in (b), but estimated by the Hirata et al. (2011) algorithm.

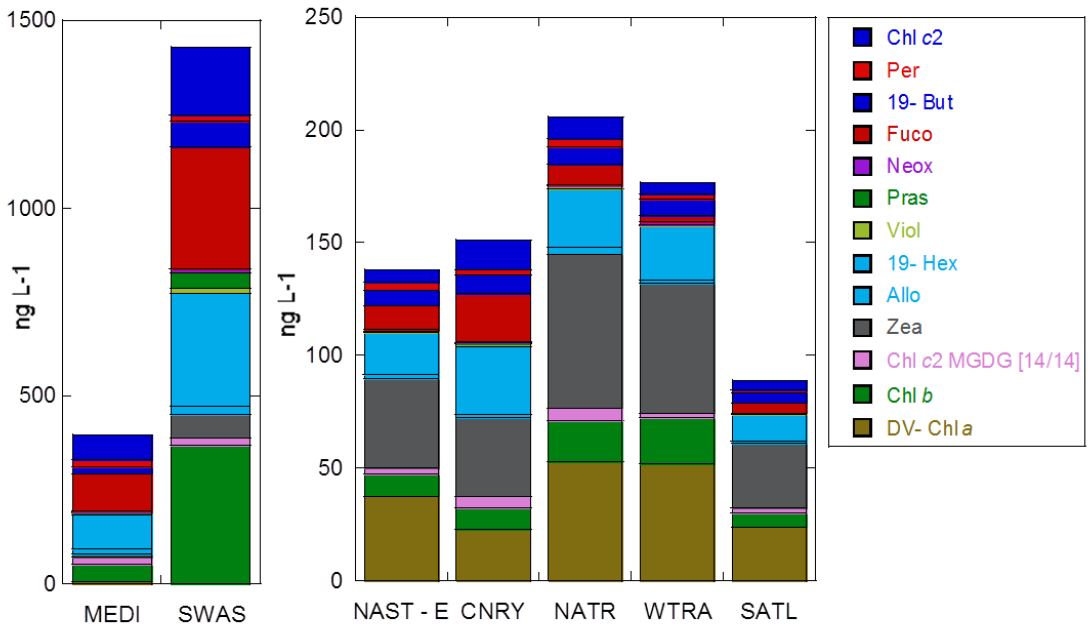

Figure 4. Averge concentration of the twelf most abundant pigments determined by HPLC in the seven provinces. Province name abbreviations as in Fig. 1.

3.3.3 Phytoplankton composition

All CHEMTAX groups except *Synechococcus* and *Prochlorococcus* presented generally low abundances in the Tropical and Subtropical Atlantic, and increased markedly in SWAS and to a smaller extent in MEDI (Figs. 6-8). *Prochlorococcus* showed maximum abundances in WTRA and did not occur in SWAS (Fig. 6a), and *Synechococcus* peaked in NATR around 15.1º N, and in several SWAS stations (Fig. 6b). In terms of relative contribution to total Chl *a* (Chl *a*_tot), the most important taxa in the Equatorial and Tropical Atlantic (NAST-E, CNRY, NATR, WTRA and SALT) were *Prochlorococcus* spp., haptophytes and *Synecoccoccus* spp., while MEDI and SWAS were dominated by diatoms and haptophytes (Fig. 8a). Superimposed to these general characteristics, there was noticeable heterogeneity within stations of the same province, in particular in SWAS which presented an haptophyte Chl *a* maximum at station 34 (39.56º S) and a diatom peak based both in Chl *a* and in cell counts at station 36 (-43.43º S).

The distribution was similar for the pico<3 fraction (Fig. 8b), although the overall abundance of *Synechococcus* in this fraction (Syn_<3) was lower than in Chl *a*_tot (Syn_tot); the resulting expression was: Syn_<3 = 0.25* Syn_tot + 8.36 (n = 41, r2 = 0.38; Wilcoxon's test for comparison of the means, n = 41, p< 0.05). In contrast, there were no significant differences in the abundance of *Prochlorococcus* in the two fractions. In the n+m>3 fraction (Fig. 8c), the most important groups were diatoms and haptophytes in MEDI, NAST-E, CNRY, NATR and SWAS, haptophytes, chlorophytes and dinoflagellates in WTRA, and haptophytes, dinoflagellates and prasinophytes in SATL.

There was a significant correlation between CHEMTAX-derived contribution to Chl *a*_tot and cell counts (microscopy for eukaryotes and flow cytometry for the prokaryotes) of cryptophytes (n = 20, r^2 = 0.2), dinoflagellates (n = 29, r^2 = 0.24, p < 0.01), *Prochlorococcus* (n = 31, r^2 = 0.70, p < 0.0001) and *Synechococcus* (n = 41, r^2 = 0.44, p < 0.0001, one outlier excluded). The global correlation was also significant for diatoms (n = 29, r^2 = 0.15, p < 0.05), but in particular in the SWAS region, there were marked discrepancies between the Chl *a* contribution and the cell counts for this group (Figs. 6b and 8).

According to the microscopy (Table S4), the most abundant diatom taxa in MEDI was *Guinardia striata*; the CNRY diatom peak was mainly contributed by *Chaetoceros* spp. < 20 µm and *Pseudo-nitzschia* spp. (thin). In most of the Subtropical and Tropical Atlantic diatoms were represented by low densities of forms like *Cylindrotheca closterium*, *Hemiaulus hauckii*, *Thalassiosira/Porosira* spp. > 20 µm, *Proboscia alata* and *Pseudosolenia calcaravis*. The CHEMTAX algorithm indicated that diatoms were dominant in many SWAS stations, but this abundance was not always associated with large microscopic counts for this zone, where the most abundant taxa were *Chaetoceros*

criophilus, C. lorenzianus, and *Chaetoceros* <20 µm, *Thalassiosira* <20 µm and *Eucampia* spp. Flow cytometric counts revealed a substantial increase of pico- and nanoeukaryotes in several stations of the SWAS Zone (Fig. 6d); a high presence of cells in the picoplankton size range could also be seen by optical microscopy in some SWAS samples (data not shown), but their concentration could not be properly quantified. SEM examination of water from these samples revealed the presence of the diatom genus *Minidiscus* and of *Triparma laevis*, a member of the Parmales (Fig. S3) a phytoplankton group monophyletic with the Bolidophyceae and genetically very close to the diatoms, with which it shares a similar pigmentary suite (Ichinomiya et al., 2010). The Parmales have small cells with siliceous plates and are ubiquitous in marine waters(Ichinomiya and Kuwata, 2015; Ichinomiya et al, 2016). Both, *Minidiscus* and the Parmales (Kaczsmarska et al., 2016; Jewson et al, 2016) have sizes of 2-3 µm and could have been part of the unidentified picoplanktonic cells in SWAS.

Most haptophytes large enough to be counted by microscopy were likely to be pooled into the "Nanoflagellates 3 - 20 µm" category (which comprised the majority of "Other" in Table S4), but part of them could be identified as *Phaeocystis* colonies or coccolithophores. Colonial *Phaeocystis* occurred in stations 33, 35 and 36, in the northern part of SWAS, at concentrations ranging from $5*10^6$ to $89*10^6$ in terms of individual cells L^{-1} (data not shown). Coccolithophore concentrations ranged between 70 and 30000 cells L^{-1} throughout most of transect (Table S4), but reached a peak of $0.6*10^6$ cells L^{-1} at station 36 (SWAS). A total of 18 coccolithophore taxa were recorded; the dominant group were the "Unidentified small coccolithophores (< 10 µm)" (mostly *Emiliania huxleyi* and probably *Gephyrocapsa* spp.) but, in particular in the Tropical Atlantic Ocean, other forms, such as *Calcidiscus leptoporus, Discophera tubifera, Syracosphaera pulcha and Umbellosphaera irregularis*, could be abundant.

The CHEMTAX dinoflagellate group was well represented in the n+m>3 fraction of all regions except SWAS, where they contributed only a small percentage of the total Chl *a* (fig. 8b). Apart of the ubiquitous "Unidentified small dinoflagellates (< 20 µm)" and "Unidentified large dinoflagellates", a high diversity of dinoflagellate taxa (89 in total) was identified by microscopy in the tropical and Subtropical Atlantic provinces, including *Karlodinium* spp. and several species of *Ceratium*, *Dynophysis*, *Gonyaulax*, *Oxytoxum* and *Protoperidiniu*m (Table S4). In contrast, only a few taxa, such as *Dinophysis acuminata*, *Karlodinium* spp., *Prorocentrum balticum* and *Protoperidinium pacificum*, but at relatively high abundances were present in SWAS. As mentioned for haptophytes, other CHEMTAX groups comprising cells of generally small size such as chlorophytes, pelagophytes and prasinophytes are likely to have been included in pooled microscopy categories such as the "Nanoflagellates 3 - 20 µm".

3.3.4. Size structure estimation of the phytoplankton community based on fractionated filtration and diagnostic pigment approaches

The correlations between the picophytoplankton (fpico) and microphytoplankton (fmicro) fractions calculated by the Vidussi et al. (2001) - Uitz et al. (2006) and Hirata models (hereafter referred to as VU and HI, see Table 2) were all significant, but the standard major axis slope of the regression between fmicro from VU (fmicroVU) and fmicro from HI (fmicroHI) was lower than unity (Table 4). The relationships of the VU and HI estimates with the results obtained by filtration were only significant (Table 4) between the nano+microphytoplankton fractions from Hirata (fn+mHI) and the filtrations (fn+m>3). However, the large range of Chl *a* concentrations in the data set led to significant correlations among estimates of the contribution of each size fraction to toal Chl *a* (Fig. S3).

The size distribution for each province resulting from the application of the VU and HI procedures and the proportion of Chl *a*_pico<3 and Chl *a*_n+m>3 derived from the filtrations can be seen in Figs. 3b and 3c. A rough comparison betwen these size fraction distributions and the CHEMTAX results can be done using the approach of Taylor et la. (2011), who classified diatoms and dinoflagellates as microphytoplankton, cryptophytes, chlorophytes, haptophytes, pelagophytes and prasinophytes as nanophytoplankton, and *Synechococcus* and *Prochlorococcus* as picophytoplankton. The color codes in Figs. 3 and 8 have been adjusted to facilitate this comparison (greenish for picoplankton, reddish for nanoplankton and bluish for microplankton).

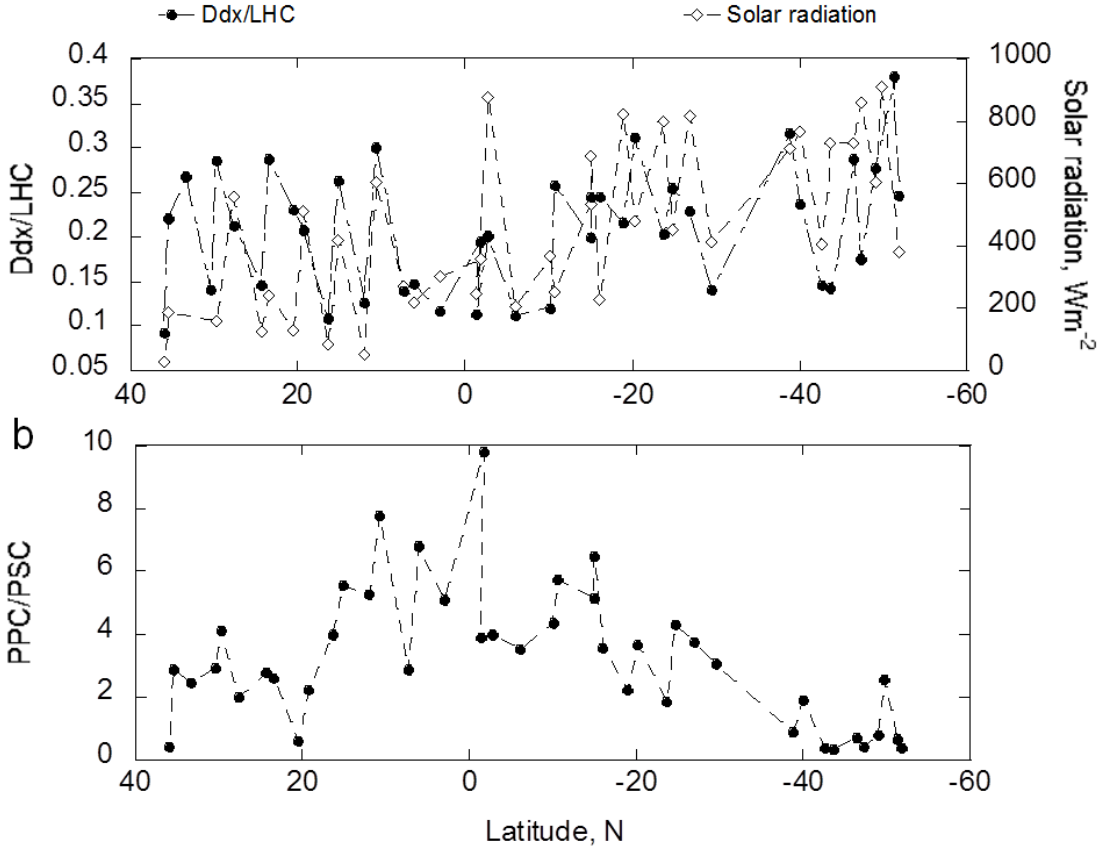

Figure 5. Variation of (a) Ddx/LHC and solar radiation (Wm^{-2}) and (b) PPC/PSC along the TransPEGASO transect.

3.3.3 Variation of CDOM and light absorption properties

Average CDOM absorption of the filtrates at 325 nm [$a_{CDOM}(325)$] and 443 nm [$a_{CDOM}(443)$] ranged from 0.02 m^{-1} (WTRA) to 0.16 m^{-1} (MEDI) and from 0.09 m^{-1} (SATL) to 0.43 m^{-1} (MEDI) respectively (Fig. 9a, Table 5). There was a significant correlation between CDOM absorption and Chl *a*_tot, although with important dispersion (Fig. 9b).

At 443 nm, CDOM was in general the largest component of total light absorption, in particular at the MEDI station and some of the low Chl *a* provinces (Fig. 10). The average CDOM contribution ranged from 74% at MEDI and 69% at NATR, to 34% at WTRA, while phytoplankton absorption accounted for 47% of the total at WTRA and SWAS and for 18-24% at the other provinces (Fig. 10, Table 5).

When the whole data set was considered, phytoplankton absorption at 443 nm [$a_{ph}(443)$] showed a positive correlation with Chl *a*_tot [Fig. 11a; $a_{ph}(443) = 0.098 + Chl\ a\_tot\text{^}0.88$, n = 37; $r^2 = 0.93$, $p < 0.0001$). However, the relationship between the Chl *a* -specific absorption by phytoplankton [$a_{ph}^*(443)$] and Chl *a*_tot (Fig. 11b) distinguished two well-defined situations, the more oligotrophic regions (NAST-E, CNRY, NATR, WTRA and SATL) with relatively high $a_{ph}^*(443)$ and SWAS and MEDI with relatively low $a_{ph}^*(443)$ (Fig. 11b, Table 5). The package index, $Qa^*(443)$ was correlated with aph*(443) (fig. 11c; $aph^*(443) = 0.11*Qa^*(443) + 0.11$, n = 35: $r^2 = 0.53$, $p<0.0001$), but not with Chl *a*_tot (data not shown).

To ascertain the effect of pigment composition on absorption properties, we studied the relationships between $a_{ph}(443)$ and the non-photosynthetic (PPC) and photosynthetic (PSC) carotinoid concentrations, and between $a_{pig}(443)$ and $a_{ph}(443)$ [we avoided correlating aph*(443) with apig*(443) because the common denominator (Chl *a*_tot)

induces spurious statistical relationship between the two ratio variables (Kim, 1999)]. As shown in Fig. 12, two clusters could be clearly distinguished, one with the high Chl *a* provinces (MEDI and SWAS in Fig. 12a and SWAS in Fig. 12b) and another with the low Chl *a* provinces (and MEDI as an outlier in 12b); the lower than 1 slope of the log-log relationship between $a_{ph}(443)$ and PPC reflected a decrease in the ratio of total phytoplankton pigment absorption to PPC concentration for increasing Chl *a*_tot concentration. As can be seen in Fig. 11d, the slope of the regression of $\log[a_{ph}(443)]$ on $\log[a_{pig}(443)]$ was lower for the high Chl *a* (MEDI and SWAS) than for the low Chl *a* provinces. In addition, the slope of the regression of $\log[a_{ph}(443)]$ on log(Chl *a*_tot) (0.88, Fig. 11a) was only slightly lower that that of $\log[a_{pig}(443)]$ on log[Chl *a*_tot], (Fig. 12a, $\log[a_{pig}(443)] = 0.94*\log[\text{Chl } a\text{\_tot}] + 0.059$, n = 40, $r^2 = 0.95$, $p < 0.0001$), although in all these cases the slope differences were not significant.

We explored the potential influence of cell size on aph*(443) and $Qa^*(443)$ by examining the relationships between aph*(443) and the size structure of the phytopankton community, as described by the diagnostic pigment approach (SI index) and by size-fractionated filtrations (fpico<3). Si was higher in the high Chl *a* provinces (Fig.12c). However, the relationships of aph*(443) with SI and with fpico<3, as well as those of $Qa^*(443)$ with SI and with fpico<3 (Fig. S4) were not significant.

3.4. DISCUSSION

3.4.1. Oceanographic characteristics of surface waters

Most of the TransPEGASO cruise crossed oligotrophic waters of the Tropical and Subtropical Atlantic gyre. During our survey, the CNRY stations could also be considered as oligotrophic, although this region is affected by stational coastal

upwelling, which may cause the sporadic offshore export of filaments of nutrient-rich waters (Longhurst, 2007; Menna et al., 2016). Average nitrate concentrations (Table 3) approached or exceeded 1 µM only in MEDI (0.8 µM) and SWAS (4.1 µM), average silicate ranged between 0.3 and 0.7 µM except in WTRA (1.1 µM) and average phosphate was lower than 0.12 µM in all provinces except SWAS. Only MEDI, with a Chl *a*_tot concentration of 0.5 mg m^{-3} and SWAS, with an average Chl *a*_tot of 1.4 mg m^{-3} could be considered as high Chl *a* regions. The MEDI sample was taken in the Alboran Sea, a zone of strong mesoscale variability in which the influence of the Atlantic jet coming through the Strait of Gibraltar and wind forcing originate coastal upwelling and other hydrodynamic structures associated with nutrient fertilization and relatively high Chl *a* concentrations (Tintoré et al., 1991; Macías et al., 2007). The eutrophic condition of SWAS, already described in previous studies (Gibb et al., 2000, Vega-Moreno et al., 2012) reflects the strong hydrodynamism of this region, subjected to tidal mixing and the interactions of the Brazil and Malvinas Currents with the waters over the continental shelf. During our study, the influence of the Sub Antarctic Surface Waters associated with the Malvinas Current could be seen the in temperature and salinity minima (fig 2a) and the high concentrations of nutrients (Fig 2 b, c) found in the southern part of the transect.

We used HPLC to study the distribution of total (Chl *a*_tot) and size-fractionated Chl *a* (Chl *a*_pico<3 and Chl *a*_n+m>3) across the TransPEGASO transect. Additionally, we performed flurometric total Chl *a* (Chl *a*_Fl) measurements, to facilitate comparisons with older works. As mentioned in 3.2, there was a good correlacion between Chl *a*_Fl and Chl *a*_tot (Chl *a*_Fl = 1.76*Chl *a*_tot + 0.17, $r^2 = 0.96$, n = 41, $p < 0.0001$), but the slope of the relationship was higher than 1, indicating that Chl *a*_Fl overestimated Chl *a*_tot; this is a common finding (Nunes et al., submitted) that, apart of calibration or

other experimental problems, may be due to the overlap of fluorescence bands of other chlorophylls and accessory pigments (Kumari, 2005). On the other hand, the sum of the HPLC determinations of the < 3 and > 3 Chl *a* size fractions (Chl *a*_pico<3 and Chl *a*_n+m>3, respectively) did not reveal any substantial bias when compared with the independently determined Chl *a*_tot (the 95% confidence limits for the slope of the lineal regression of Chl *a*_pico<3 + Chl *a*_n+m>3 on Chl *a*_tot (Chl *a*_pico<3 + Chl *a*_n+m>3 = 0.85+ Chl *a*_tot + 0.005; n = 41, r^2 = 0.95, p < 0.0001) were 0.79-0.92).

Based on the observed Chl *a* and nutrient concentrations, the oceanographic provinces encountered during TransPEGASO were operationally classified into a low Chl *a* (< 0.5 mg m^{-3}) and a high Chl *a* (≥ 0.5 mg m^{-3}) category. The first or "oligotrophic" group includes the Tropical and Subtropical Atlantic provinces, from 35°N to 29°S, with NAST-E, CNRY, NATR, WTRA and SATL, and the second or "eutrophic" one comprises SWAS and the single MEDI station. As discussed below, these fertility differences had a crucial influence on the structure of the phytoplankton community. However, an important part of the pigment variability encountered during the cruise was associated with short-term physiological responses. The morning-afternoon changes of Ddx/LHC and its positive correlation with solar radiation (Fig. S1a) reflect the photoacclimation role of the Ddx – diatoxanthin intercoversion in the xanthophyll cycle (Falkowski and Raven, 1997). Both high light and low nutrient environments were likely to be associated with the relative increases in the proportion of PPC/PSC (and PPC/Chl *a*_tot, data not shown) found in the oligotrophic provinces of our transect (Fig. 5b). Timescales for interconversion in the xanthophyll cycle are of the order of seconds to minutes (Ferris and Christian, 1991), while those for pigment synthesis are of minutes – hours for photoprotective carotinoids (PPCs) and of hours –days for light-harvesting pigments (Ferris and Christian, 1991; Bidigare et al., 2014).

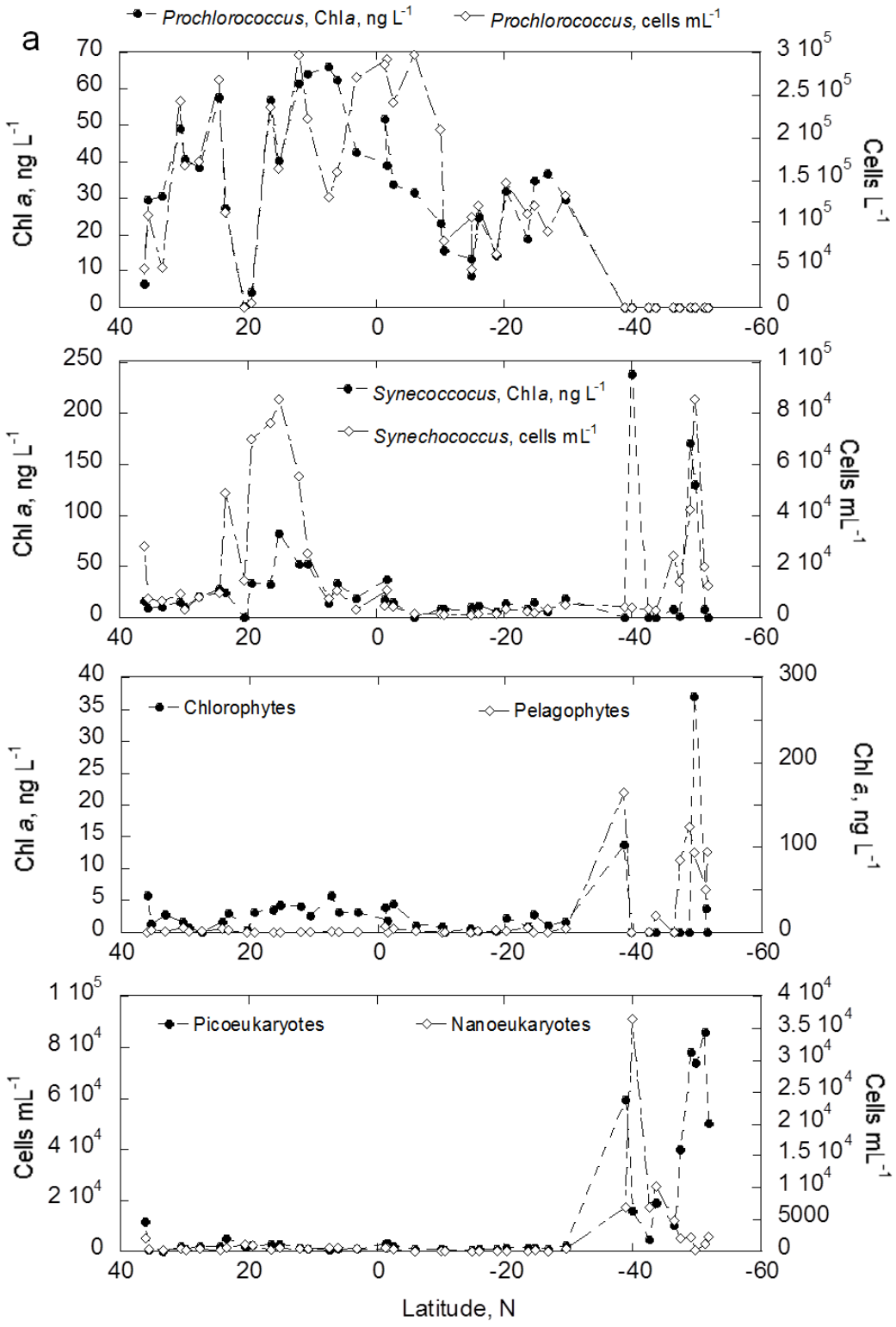

Figure 7. Variation of CHEMTAX-derived Chl *a* (ng L^{-1}) and cell counts (cells L^{-1}) for (a) cryptophytes, (b) diatoms, (c) dinoflagellates. Variation of CHEMTAX-derived Chl *a* (ng L^{-1}) for (d) haptophytes (left ordinate scale) and prasinophytes (right ordinate scale).

3.4.2. Size-fractionated Chl *a* and comparison between phytoplankton size structure estimates

Although with limited verification (see Brewin et al., 2014), the diagnostic pigment algorithms of Vidussi et al. (2001) - Uitz et al. (2006) and the total Chl *a* –based expressions of Hirata et al. (2011) (referred to respectively as VU and HI, Table 2) have been widely used to infer the size structure of phytoplankton communities (Taylor et al., 2011; Zeng et al., 2017). In both the VU and HI models (Fig. 3a, b), the nanophytoplankton showed the smallest range of variation and the microphytoplankton comprised only a small fraction of the total in the Subtropical and Tropical Atlantic. However, VU gave more weight to picoplankton than HI, and both approaches predicted a lower proportion of small cells than that found in the filtration results (fig. 3a). This discrepancy can arise in part because our filtrations used a limit of 3 μm between the small and large fractions instead of the 2 μm threshold of the VU and HI approximations, so that the f_pico<3 fraction of Fig. 3a includes part of the nanophytoplankton size class of the other methods. This difference is not trivial, as suggested by the extense list of phytoplankton taxa with sizes ranging from < 2 μm to 3 μm (Vaulot et al., 2008). It must also be taken into account that estimation of phytoplankton size based on pigment composition is challenging because many pigments are shared by small and large phytoplankton forms (Jeffrey et al., 1997; Roy et al., 2011) and approaches like that of Hirata et al. (2011) based on the relationship of the proportion of PFTs or size classes with total Chl *a* are influenced by the phytoplankton composition in the data sets used to derive the model parameters. On the other hand, filtration procedures have their own problems (e. g., due to cell breakage), especially when dealing with low Chl *a* concentrations (Brewin et al., 2014).

All size distributions (Fig. 3a-c) presented a greater proportion of nano and microphytoplankton cells in MEDI and SWAS (together with NATR for the filtration data) than in the other provinces, but the relatively large importance of picophytoplankton in the VU and Hi models and in the filtration results for SWAS did not agree with the HPLC findings for this province, in which *Prochlorococcus*, which accounted for most of the picophytoplankton in the other regions was absent and *Synechococcus* represented only a small fraction of total Chl *a*. The total Chl *a* (ΣDP) estimated by the VU algorithm was in very good agreement with Chl *a*_tot from HPLC (ΣDP = 0.96*Chl *a*_tot - 0.01, n = 41, r^2 = 0.88, p < 0.0001, Fig. S2c), indicating that the discrepancy derived from a mis-allocation of part of the Chl_*a* pool between the pico- and microphytoplankton size fractions. In addition, diatoms accounted for a larger proportion of the total in the CHEMTAX results (Fig. 8a) than the sum of the nano and microphytoplankton fractions in the filtrations (Fig. 3a. Optical microscopy observations showed relatively low concentrations of nano- and micro-sized diatom in several SWAS stations in which diatom contribution to Chl *a*_tot was important according to CHEMTAX (Table 4). This discrepancy could be explained by the presence of Parmales and of picoplankton-sized diatoms like *Minidiscus*, which could have been part of the high picophytoplankton densitties found in SWAS. As the VU approach to estimate taxonomic composition through diagnostic pigments is based on the premise that organisms with diatom pigments belong to the microplankton size class, picophytoplankton forms with diatom pigments will be incorrectly classified as microphytoplankton.

3.4.3. The phytoplankton community in the oligotrophic Atlantic Ocean

The tropical and subtropical low Chl *a* provinces were generally dominated by pico- and nanophytoplankton. However, microphytoplankton was relatively important in CNRY, where diatoms presented a marked abundance peak at stations 9 and 10 (19º 02' W, 20º 33 '02' N and 19º 39' 26" W, 19º 19' 54" N; respectively) that did not translate into high Chl *a* concentrations. The taxa forming these maxima were mainly thin *Pseudo-nitzschia* spp. that because of their elongated shape would likely pass through 3 μM pore filters and small *Chaetoceros* (< 20 μM). This observation could explain the low fmicro estimated for the CNRY province by the Chl *a*-based HI algorithm (Fig. 3c). The dominance of Zea and DV_Chl *a* in the oligotrophic provinces agrees with the prominent contribution of *Synechoccus* and *Prochlorococcus* to Chl *a*_tot and with abundance and biomass estimates derived from flow cytometric counts (Fig. 6d; Zamanillo et al., submitted). However, our filtration results indicate that pore sizes of 2 or 3 μm may retain a part of the *Synechococcus* population, suggesting the need of caution when interpreting fractionation data. Due to their small size, both *Prochlorococcus* and *Synechococcus* have relatively high surface to volume ratios and can thrive in nutrient-poor situations, although *Prochlorococcus* seems to be associated with more oligotrophic conditions than *Prochlorococcus* spp (Latasa et al., 2010). This observation could explain the higher relative importance of *Synechococcus* in CNRY, which may be affected by occasional upwelling filaments (Menna et al., 2016).

Comparable results concerning pigment and phytoplankton distributions have been reported in other studies based on HPLC analysis (Gibb et al., 2000), remote-sensing (Uitz et al., 2006) and or modeling (Acevedo-Trejos et al., 2014). Gibb et al. (2000), who sampled the Atlantic Ocean bewteen 50º N and 50º S, recorded a shift from

dominance of PSCs to PPCs around 27º N, a few degrees to the north of the start of our survey.

3.4.4. The phytoplankton community in the high Chl *a* regions

CHEMTAX results for MEDI and SWAS indicated a high contribution in the total and fn+m>3 size fractions of diatoms, haptophytes and prasinophytes (Fig. 8). Prokaryotic phytoplankton, probably outcompeted by other groups (Partensky et al., 1999), accounted only for a small proportion of Chl *a*_tot in both provinces. The absence of *Prochlorococcus* in SWAS agrees with a lower temperature limit of 15º C for this genus (Johnson et al., 2006). Our microscopic observations for SWAS revealed that the most abundant diatom taxa were several *Chaetoceros* species, small *Thalassiosira* < 20 μm) and *Eucampia* spp., whereas haptophytes were partially represented by *Phaeocystis* colonies and coccolithophores. García et al. (2008), in their spring survey of the Patagonian Shelf noted the occurrence of large diatom and dinoflagellate blooms, accompanied by nanoflagellates including *Phaeocystis* cf. *antarctica*. Similarly, Ferreira et al. (2013) mentions the dominance of nanoplankton-sized *Thalassiosira* spp. in the same area in spring, while Souza et al. (2012) studied a summer bloom dominated by the coccolithophore *Emiliania huxleyi*, the haptophyte *Phaeocystis antarctica* and other microalgal taxa. As mentioned above, the discrepancy between the high contribution of diatom Chl *a* and the relatively low proportion of microplankton estimated by size fractionation and by the HI and HIRATA models in SWAS could be explained by the presence of Parmales and picoplankton-sized diatoms like *Minidiscus*. These findings would support the observations of Ferreira et al. (2013) who noted that the size of phytoplankton cells in Patagonian waters tended to be smaller that that found in other areas with similar Chl *a* concentration.

3.4.5. Variability of CDOM and phytoplankton absorption

Except in SWAS, $a_{CDOM}(443)$ accounted for more than 50% of total non-water absorption (Table 5), as found in other sudies (Nelson et al., 1998; Gonçalves-Araujo et findings of Pérez et al. (2016). Detrital particulate absorption was generally a minor component and the highest relative contributions of $a_{ph}(443)$ were found both in an oligotrophic province (WTRA) and in an eutrophic one (SWAS). Both $a_{CDOM}(443)$ and $a_{CDOM}(325)$ were significantly correlated with Chl *a*_tot but there was substantial dispersion (Fig. 9b) and the slope of the relationship between $a_{CDOM}(443)$ and Chl *a*_tot ($a_{CDOM}(443)$= 0.078*Chl *a*_tot^0.39, n = 34, r^2 = 0.42, p < 0.0001) was lower than that ($a_{CDOM}(440)$ = 0.034*Chl *a*_tot^0.62, n = 45, r^2 = 0.72, p < 0.0001) found by Bricaud et al. (2010) in the Southeast Pacific. The positive relationship between a_{CDOM} and Chl *a*_tot suggests CDOM production by phytoplankton, while the low a_{CDOM} values in WTRA, wich included the most distant stations from the continents might indicate a terrestrial influence. However, the available data do not allow a reliable discrimination between allochthonous and autochtonous DOM sources. There was a significant negative correlation between $a_{CDOM}(325)$ and salinity (data not shown), but this finding derived from the association of low salinity with high Chl *a* in the SWAS waters.

As reported by Bricaud et al. (2004) and others, we found that $a_{ph}(443)$ could be expressed as a power function of Ch *a* ($a_{ph}(443)$ = 0.098*Chl *a*_tot^0.88, n = 37; r^2 = 0.93, p < 0.0001; Fig. 11a). The slope of the relationship was similar to that determined by Bricaud et al (2010) for southern Pacific waters [$a_{ph}(440)$ = 0.0617*Chl *a*_tot^0:93]. The presence of outliers could be due to natural variability or to some analytical problem. Variability in the relationship between $a_{ph}(443)$ and Chl *a*_tot may result mainly from changes in the contribution of non-photosynthetic pigments, from package

effects related to cell size or from a combination of both. We explored the potential influence of these factors in our data set.

The < 1 value of the slope of the relationship between $a_{ph}(443)$ and Chl *a*_tot (Fig. 11a) implies that the Chl *a*-specific absorption coefficient, $a_{ph}^*(443)$ decreases with increasing Chl *a*, as seen in Fig. 11b, which highlights the differences between the oligotrophic and the eutrophic waters sampled in our study. This pattern is a common in absorption studies because high Chl *a* values tend to be associated with a lower contribution of accessory pigments and larger cells (and therefore a higher package effect due to size) than low Chl *a* concentrations, so that the specific absorption tends to decrease with increasing Chl *a* (Bricaud et al., 1995).

We found (Fig. 11c) a positive relationship between $a_{ph}^*(443)$ and the package effect index $Qa^*(443)$, indicating the occurrence of package effects, but $Qa^*(443)$ was not correlated with Chl *a*_tot, in contrast with the findings of Bricaud et al. (2004), and there was no clustering of the $Qa^*(443)$ values for the diffferent provinces. The high correlation between $a_{ph}(443)$ and $a_{pig}(443)$ (Fig. 11d), and $a_{ph}(443)$ and $a_{pig}(443)$ with PPC and PSC (Figs. 12b and 12c) suggest a strong influence of the pigment composition of the phytoplankton community on the specific pigment absorption, $a_{ph}^*(443)$. On the other hand, the regression coefficients of $a_{ph}(443)$ and $a_{pig}(443)$ with Chl *a*_tot (0.88 and 0.94, respectively) were similar and $a_{ph}^*(443)$ and $Qa^*(443)$ were not correlated with SI and fpico<3 (Fig. 14). Altogether, our observations suggest that cell size was not an important factor in structuring the variation of $Qa^*(443)$. It may be that the variability observed in $a_{ph}^*(443)$ responds not only to changes in pigment composition, but also to differences in intracellular pigment concentration related to photoacclimation processes.

3.5. CONCLUSION

During the TransPEGASO cruise, that covered seven biogeographycal provinces across Atlantic Ocean, the composition of the phytoplankton community was characterized by means of microscopic observations and the application of HPLC - CHEMTAX pigment analyses to whole water and two filtration size fractions (> 3 and < 3 µm), and measured the absorption of particulate matter and colored dissolved organic matter (CDOM). The most important taxa in the Tropical and Subtropical Atlantic were *Prochlorococcus* spp., haptophytes and *Synecoccoccus* spp., while MEDI and SWAS were dominated by diatoms and haptophytes. The Chl *a* size class distribution obtained from the fractionated filtrations was compared with with those resulting from the diagnostic pigment algorithms (VU) developed by Vidussi et al. (2001) and Uitz et al. (2006), and the total Chl *a*-based approach (HI) of Hirata et al. (2011). Both the VU and HI algorithms predicted for SWAS a high proportion of nano- and microphytoplankton, in contrast with microscopic observations and the results of the size-fractionated filtrations, which indicated dominance of the < 3 µm fraction. This discrepancy appeared to be due to the presence, confirmed by scanning electron microscopy, of picoplankton-sized forms such as cells of Parmales (a group sharing the pigment composition with the diatoms) and the diatom *Minidiscus* sp. These observations indicate that the occurrence of diatom pigment markers cannot be systematically associated with the presence of large cells. In this study, CDOM dominated the total non-water absorption in the water column. a_{ph}*(443) was positively related to the package index [Qa*(443)] but was not correlated with indicators of size structure and apparently it was mainly related to differences in intracellular pigment concentration and possibly to photoacclimation processes.

Table 1. Range (minimum: Min and maximum: Max), mean and standard deviation (SD) of pigment concentrations (ng L^{-1}) and pigment ratios in surface seawater for the seven study provinces. LHC = Light Harvesting Pigments (19 - But + 19 - Hex + Fuco + Per), PPC = non-photosynthetic carotinoids (Zea, DDx and *β*-car), PSC = photosynthetic carotinoids (Fuco, Per, 19 - But, and 19- Hex). For province names, see the explanation of Fig. 1.

		MEDI	**NAST - E**			
Pigment	**Abbreviation**		Min	Max	Mean	SD
19'-Butanoyloxyfucoxanthin	19 - But	18,50	4,89	14,71	6,87	1,44
19'-Hexanoyloxyfucoxanthin	19 - Hex	91,77	13,93	55,20	18,50	4,91
α-Carotene	α-Car	7,99	5,60	20,62	7,82	2,23
Alloxanthin	Allo	13,44	0,37	3,87	2,10	1,09
β-Carotene	β-Car	15,45	3,26	30,45	4,29	0,81
Chl *c*2-monogalactosyldiacylglyceride ester [14/14]	Chl *c*2-MGDG [14/14]	11,14	0,39	11,33	0,85	0,38
Chl *c*2-monogalactosyldiacylglyceride ester [14/18]	Chl *c*2-MGDG [14/18]	18,56	1,04	13,70	2,88	1,91
Chlorophyll *c*1	Chl *c*1	3,67	0,86	3,69	1,25	0,28
Chlorophyll *c*2	Chl *c*2	64,70	0,43	23,07	5,75	3,53
Chlorophyll *c*3	Chl *c*3	24,88	0,86	11,70	2,72	1,30
Monovinyl chlorophyll a epimer	MV-Chl *a*-epimer	3,23	0,35	9,08	0,63	0,27
Chlorophyll *b*	Chl *b*	46,42	6,49	21,85	9,16	2,72
Cis – fucoxanthin	cis-fuco	10,49	0,92	3,64	1,35	0,49
Cis 19'-hexanoyloxyfucoxanthin	cis-hex	9,08	0,41	1,99	0,70	0,38
Diadinoxanthin	Ddx	21,25	5,06	17,76	8,82	2,94
Divinyl chlorophyll *a*	DV-Chl *a*	6,42	29,76	65,98	37,77	7,16
Divinyl chlorophyll *a* allomer 1	DV-Chl *a*-allomer1	5,66	0,28	2,29	0,73	0,47
Divinyl chlorophyll *a* allomer 2	DV-Chl *a*-allomer2	0,19	0,27	1,39	0,37	0,14
Divinyl Chlorophyllide *a*	DV-Chlide *a*	17,58	0,29	12,36	0,68	0,40

Fucoxanthin	Fuco	99,02	4,11	42,77	10,34	6,57
Unidentified carotenoid	M-car	1,45	0,27	3,71	0,46	0,14
Micromonal	Micr	2,27	0,23	5,29	0,80	0,88
Monovinyl chlorophyll *a* allomer 1	MV-Chl *a*-allomer1	4,66	0,11	2,50	0,48	0,35
Monovinyl chlorophyll *a* allomer 2	MV-Chl *a*-allomer2	4,99	0,13	1,99	0,36	0,32
Monovinyl chlorophyll *c*3	MV-Chl *c*3	2,92	0,50	2,23	1,36	0,61
Monovinyl chlorophyll *a*	MV-Chl *a*	425,13	41,67	157,80	57,29	15,21
Monovinyl chlorophyllide *a*	MV-Chlide *a*	3,40	0,13	2,04	0,50	0,42
Neoxanthin	Neo	2,43	0,24	1,04	0,39	0,10
Peridinin	Per	18,81	1,92	6,04	3,44	1,47
Prasinoxanthin	Pras	5,28	0,11	0,97	0,18	0,09
Uriolide	Uri	2,30	0,13	0,63	0,19	0,07
Violaxanthin	Viol	2,97	0,48	1,34	0,74	0,22
Zeaxanthin	Zea	7,13	28,85	86,04	39,88	7,61
Unidentified zeaxanthin derivative	Zea-der	1,47	0,11	1,47	0,47	0,51
∑ pheophorbide *a*	Phaeob	2,89	1,29	14,47	4,34	5,09
∑ phaeophytin *a*	Phaeop	50,16	2,87	106,95	6,32	4,91
Total chlorophyll *a*	Chl *a*_tot	471,24	76,67	224,37	98,83	15,29

	CNRY				NATR				WTRA			
Abbreviation - Pigment	Min	Max	Mean	SD	Min	Max	Mean	SD	Min	Max	Mean	SD
19 - But	2,47	14,71	8,28	4,41	6,37	9,54	7,81	1,31	4,83	9,59	6,86	1,72
19 - Hex	19,58	55,20	30,20	14,55	23,45	40,35	26,06	1,89	15,14	40,35	24,18	7,87
α-Car	0,47	16,12	6,06	6,16	10,03	16,44	12,27	1,72	10,81	20,62	15,58	3,27
Allo	0,52	2,74	1,98	0,86	2,61	3,87	3,25	0,52	0,73	2,05	1,32	0,52
β-Car	5,45	14,40	8,94	3,39	15,91	30,45	23,79	6,00	1,17	13,30	5,52	3,78
Chl *c*2-MGDG [14/14]	1,60	10,09	5,15	3,09	1,01	11,33	2,05	0,74	0,65	11,33	3,13	3,49
Chl *c*2-MGDG [14/18]	0,86	13,70	5,12	5,08	4,44	8,25	6,02	1,62	0,97	4,91	2,70	1,43
Chl c1	0,75	3,69	2,40	1,06	0,78	1,12	0,95	0,14	0,67	0,99	0,78	0,11
Chl c2	7,20	23,07	12,98	6,34	8,51	10,54	9,36	0,86	2,60	9,38	5,16	2,06
Chl c3	1,59	11,70	5,27	3,86	3,89	4,96	4,26	0,49	1,19	4,93	2,94	1,05
MV-Chl *a*-epimer	1,03	3,34	1,93	0,88	2,28	9,08	5,74	2,78	0,69	2,65	1,36	0,60
Chl *b*	3,95	12,85	9,73	3,45	13,84	21,85	17,89	2,90	13,79	31,00	20,52	4,99
cis-fuco	1,36	3,34	2,12	0,76	1,35	3,64	1,89	0,43	0,56	3,64	1,93	0,94
cis-hex	0,50	1,99	1,16	0,53	0,64	1,04	0,83	0,14	0,29	1,04	0,59	0,25
Ddx	6,68	17,76	13,59	4,18	5,07	13,58	7,94	3,99	3,27	12,16	6,34	2,74
DV-Chl *a*	0,50	57,80	22,55	22,82	40,48	65,98	53,05	9,09	34,04	65,98	51,48	12,13
DV-Chl *a*-allomer1	1,30	2,21	1,86	0,35	1,03	2,29	1,58	0,43	0,41	2,29	1,36	0,57
DV-Chl *a*-allomer2	0,06	0,55	0,26	0,21	0,42	1,39	0,87	0,40	0,09	0,61	0,31	0,20
DV-Chlide *a*	1,08	8,35	3,21	2,99	0,90	12,36	6,05	4,75	0,80	1,92	1,32	0,39
Fuco	12,62	42,77	21,32	12,42	6,67	10,58	8,83	1,62	1,98	5,04	3,36	1,11
M-car	0,69	1,72	0,98	0,43	0,79	3,71	1,86	1,32	0,38	0,84	0,63	0,16
Micr	0,29	0,69	0,46	0,16	1,58	5,29	3,43	1,51	0,10	1,60	0,54	0,47
MV-Chl *a*-allomer1	0,75	2,50	1,61	0,70	0,80	1,64	1,29	0,36	0,11	1,29	0,72	0,40
MV-Chl *a*-allomer2	0,32	1,17	0,71	0,30	0,46	1,99	0,65	0,25	0,33	2,41	1,18	0,69
MV-Chl *c*3	0,25	1,97	1,09	0,66	0,87	1,72	1,26	0,35	0,51	1,56	0,97	0,32

MV-Chl *a*	75,38	148,13	97,31	29,51	105,36	157,80	128,06	21,98	62,88	85,93	75,19	8,90
MV-Chlide *a*	0,32	2,04	0,84	0,70	0,68	1,83	1,20	0,48	0,21	0,78	0,44	0,18
Neo	0,23	1,04	0,64	0,34	0,44	0,95	0,64	0,23	0,48	0,70	0,59	0,07
Per	0,56	3,16	2,46	1,10	3,26	4,53	3,71	0,45	1,18	4,77	2,72	1,37
Pras	0,12	0,97	0,59	0,35	0,22	0,39	0,29	0,07	0,12	0,24	0,15	0,04
Uri	0,02	0,29	0,14	0,10	0,02	0,63	0,39	0,26	0,25	0,63	0,49	0,13
Viol	0,48	1,34	0,82	0,33	0,69	0,90	0,75	0,06	0,34	0,90	0,58	0,16
Zea	5,83	55,07	34,54	18,02	56,72	86,04	67,80	13,00	31,85	80,11	57,33	18,32
Zea-der	0,15	0,92	0,35	0,33	0,02	0,31	0,20	0,13	0,16	1,06	0,39	0,30
Phaeob	2,48	3,55	2,81	0,43	3,18	5,98	4,39	1,04	2,00	5,98	3,23	1,40
Phaeop	3,79	106,95	32,47	43,16	22,07	29,93	25,29	3,36	5,28	15,94	9,02	3,69
Chl *a*_tot	99,26	162,68	130,28	23,92	173,52	224,37	198,49	20,77	103,47	158,15	133,37	21,58
Ddx/LHC	0,15	0,29	0,22	0,06	0,11	0,26	0,17	0,09	0,11	0,30	0,17	0,07
PPC/Chl *a*_tot	0,30	0,57	0,45	0,11	0,47	0,60	0,51	0,07	0,33	0,78	0,53	0,15
PPC/PSC	0,61	2,80	2,06	1,00	4,00	5,57	4,95	0,84	2,86	9,82	5,75	2,49

	SATL				SWAS			
Abbreviation - Pigment	Min	Max	Mean	SD	Min	Max	Mean	SD
19 - But	2,70	7,86	4,72	1,39	27,44	173,03	68,18	42,68
19 - Hex	8,44	18,49	11,99	3,38	37,07	1414,47	302,67	395,92
α-Car	1,92	7,17	4,89	1,87	0,49	10,23	5,01	2,93
Allo	0,09	2,02	0,76	0,57	6,89	58,26	23,43	15,22
β-Car	1,25	3,73	2,32	0,86	18,03	119,57	49,78	29,26
Chl *c*2-MGDG [14/14]	0,47	5,56	1,69	1,41	2,78	324,20	83,61	97,35
Chl *c*2-MGDG [14/18]	0,44	3,52	2,04	0,87	1,93	90,36	21,66	28,76
Chl c1	0,35	2,29	0,99	0,54	6,03	63,31	26,14	17,07
Chl c2	1,08	7,04	3,87	1,70	49,87	349,74	181,83	97,55
Chl c3	0,74	2,74	1,55	0,56	22,30	327,43	124,62	107,96
MV-Chl *a*-epimer	0,37	1,30	0,72	0,26	11,94	73,41	29,73	15,95
Chl *b*	2,41	12,59	6,56	3,29	27,61	829,00	367,71	236,63
cis-fuco	0,37	1,68	0,83	0,37	15,70	122,70	42,12	30,55
cis-hex	0,16	0,45	0,30	0,09	3,54	23,89	11,07	6,98
Ddx	2,62	8,09	4,70	1,81	78,73	418,93	188,57	95,15
DV-Chl *a*	8,92	36,72	23,65	9,00	0,00	0,00	0,00	0,00
DV-Chl *a*-allomer1	0,19	0,95	0,49	0,24	0,00	20,27	7,71	7,21
DV-Chl *a*-allomer2	0,00	0,57	0,22	0,15	0,00	55,69	11,34	15,71
DV-Chlide *a*	0,24	0,77	0,44	0,15	9,33	91,77	36,76	25,12
Fuco	1,32	10,25	4,43	2,70	60,78	740,28	323,96	181,45
M-car	0,12	0,72	0,27	0,15	1,01	7,01	3,38	1,85
Micr	0,11	0,21	0,15	0,03	1,54	28,02	8,51	7,38
MV-Chl *a*-allomer1	0,00	1,13	0,48	0,29	0,55	79,41	25,67	26,01
MV-Chl *a*-allomer2	0,00	1,74	0,44	0,45	3,79	130,98	24,98	37,13
MV-Chl *c*3	0,39	1,52	0,88	0,37	1,79	42,16	16,52	11,76

MV-Chl *a*	18,78	56,80	32,50	11,91	539,78	2176,21	1259,48	483,37
MV-Chlide *a*	0,08	0,53	0,28	0,13	0,64	19,95	7,70	6,31
Neo	0,20	0,42	0,30	0,07	3,84	24,71	11,20	6,39
Per	0,61	1,79	1,12	0,34	3,54	54,27	15,91	15,43
Pras	0,12	0,24	0,16	0,04	14,09	83,28	39,68	22,00
Uri	0,15	0,84	0,32	0,19	3,80	36,14	13,24	9,28
Viol	0,29	0,91	0,47	0,19	1,18	47,72	12,57	14,88
Zea	20,54	35,43	28,74	4,23	5,28	215,49	60,10	70,74
Zea-der	0,10	2,20	0,34	0,57	0,70	2,06	1,28	0,42
Phaeob	0,91	2,75	1,69	0,59	1,80	17,04	8,86	5,18
Phaeop	1,82	10,91	5,09	2,25	40,01	135,65	88,45	30,17
Chl *a*_tot	29,98	95,65	59,23	20,76	578,75	2408,19	1403,37	536,81
Ddx/LHC	0,11	0,31	0,21	0,06	0,14	1,19	0,34	0,31
PPC/Chl *a*_tot	0,49	1,15	0,67	0,20	0,09	0,71	0,27	0,19
PPC/PSC	1,84	6,48	3,98	1,35	0,33	2,53	0,89	0,74

Table 2. Expressions for the estimation of the proportion of phytoplankton in the microplanktonic, nanoplanktonic and picoplanktonic size fractions (f_micro, f_nano and f_pico, respectively), based on diagnostic pigments [Vidussi et al. (2001) and Uitz et al. (2006)], and on the Chl *a*_tot concentration (Hirata et al., 2011). □DP is the total Chl *a* concentration recostructed from the concentrations of the considered diagnostic pigments.

Size fractions	Vidussi et al., 2001/Uitz et al., 2006	Hirata et al., 2011
f_Micro	1.41 (Fuco + Perid)/ΣDP	[0.9117 + exp (-2.733x + 0.4003)]
f_Nano	(1.27 19'-Hex + 0.35 19- But + 0.60 Allo)/ΣDP	1-f_Micro-f_Nano
f_Pico	(1.01 T_Chl *a* + 0.86 Zea)/□DP	$(-[0.1529+ \exp (1.0306x - 1.5576)]^{-1}$ - 1.8597x+2.9954
∑DP	1.41 Fuco + 1.41 Per + 1.27 19- Hex + 0.6 Allo + 0.35 19 - But + 1.01 Chl b + 0.86 Zea	
X	log 10(T_Chl*a*)	

Table 3. Range (minimum: Min and maximum: Max), mean and standard deviation (SD) of temperature (1 C), salinity, particulate organic nitrogen (PON, µM) particulate organic carbon (POC, µM), ratio between the sum of nitrite + nitrate and phosphate (P/N) and major nutrients (nitrate, nitrite, silicate and phosphate, µM) for the seven study provinces. For province names, see the explanation of Fig. 1.

	MEDI	**NAST - E**				**CNRY**				**NATR**			
Variables		Min	Max	Mean	SD	Min	Max	Mean	SD	Min	Max	Mean	SD
Temperature [°C]	20,75	23,83	24,62	24,31	0,35	22,63	26,21	24,05	1,53	28,13	29,59	28,72	0,57
Salinity	36,25	36,70	36,77	36,75	0,04	36,07	36,65	36,33	0,29	35,56	35,99	35,82	0,24
PON µM						0,71	0,94	0,83	0,16	0,90	0,90	0,90	.
POC µM						5,86	7,07	6,47	0,86	6,79	6,79	6,79	.
N/P	9,5	1,23	9,09	4,56	3,11	1,00	6,07	3,56	2,23	2,62	5,65	3,90	1,57
Nitrate µM	0,78	0,18	0,40	0,28	0,10	0,13	0,35	0,24	0,09	0,14	0,27	0,22	0,07
Nitrite µM	0,06	0,02	0,05	0,02	0,01	0,02	0,04	0,03	0,01	0,03	0,05	0,04	0,01
Silicate µM	0,92	0,57	1,42	0,60	0,02	0,20	0,57	0,34	0,16	0,59	1,42	0,60	0,01
Phosphate µM	0,09	0,02	0,16	0,10	0,06	0,05	0,16	0,10	0,05	0,05	0,11	0,07	0,03

Variables	WTRA				SATL				SWAS			
	Min	Max	Mean	SD	Min	Max	Mean	SD	Min	Max	Mean	SD
Temperature [°C]	26,89	29,59	28,20	1,12	23,21	27,08	25,16	1,38	7,63	13,88	10,74	2,18
Salinity	34,80	36,23	35,70	0,56	36,32	37,41	36,92	0,40	32,62	33,62	33,25	0,36
PON µM	0,42	0,75	0,60	0,17	0,22	0,29	0,27	0,03	1,43	8,16	2,87	2,96
POC µM	4,21	5,81	4,95	0,71	1,74	3,01	2,29	0,49	6,82	44,34	16,60	15,82
N/P	1,86	12,56	5,07	4,22	1,89	14,50	5,81	3,91	0,53	10,87	6,53	3,92
Nitrate µM	0,09	2,18	0,55	0,75	0,18	1,89	0,65	0,60	0,16	8,92	4,08	3,08
Nitrite µM	0,03	0,05	0,04	0,01	0,03	0,06	0,04	0,01	0,04	0,31	0,13	0,08
Silicate µM	0,79	1,42	1,09	0,23	0,43	0,94	0,72	0,16	0,32	1,27	0,63	0,36
Phosphate µM	0,05	0,18	0,10	0,05	0,05	0,29	0,12	0,06	0,31	0,89	0,57	0,21

Table 4. Standard major axis regression lines between the proportions of picophytoplankton (fpico), nanophytoplankton (fnano) and microphytoplankton (fmicro) estimated by the Vidussi et al. (2001) - Uitz et al. (2006) diagnostic pigment method (VU) and the Hirata et al. (2011) total Chl *a*-based method, among them and with respect to the values for the > 3 (fpico<3) and > 3 (fn+m>3) fractions determined by filtration. Probability values of the test for slope = 1 are based on the F-statistic.

Dependent variable	Independent variable	r^2	Slope	Low CI	High CI	Intercept	p for slope = 1
f_picoVU	f_pico<3	ns					
f_picoHI	f_pico<3	ns					
f_n+mVU	f_n+m>3	ns					
f_n+mHI	f_n+m>3	0.17*	1,10	0,82	1,47	0,28	>0.99
f_picoVU	f_picoHI	0.25**	1,11	0,84	1,46	0,01	0,45
f_microVU	f_microHI	0.32***	0,82	0,63	1,06	0,09	0,13

ns: non-significant, * p < 0.005, ** p < 0.001, *** p < 0.001

SUPPLEMENTARY MATERIAL

Table S1. Province allocation, position and sampling date and time of the TransPEGASO stations.

Biogeographical provinces	Station number	Date	Longitude [º W]	Latitude [º N]	Local time	GMT time
MEDI	1	10/21/2014	-5,21	36,02	9:00 AM	8:00 AM
NAST	2	10/21/2014	-6,51	35,30	4:00 PM	3:00 PM
NAST	3	10/22/2014	-9,23	33,23	9:00 AM	8:00 AM
NAST	4	10/23/2014	-12,40	30,32	9:00 AM	8:00 AM
NAST	5	10/23/2014	-13,28	29,49	4:00 PM	3:00 PM
NAST	6	10/24/2014	-15,17	27,38	4:00 PM	4:00 PM
CNRY	7	10/25/2014	-16,52	24,22	9:00 AM	9:00 AM
CNRY	8	10/25/2014	-17,30	23,30	4:00 PM	4:00 PM
CNRY	9	10/26/2014	-19,02	20,33	9:00 AM	8:00 AM
CNRY	10	10/26/2014	-19,39	19,20	4:00 PM	3:00 PM
NATR	11	10/27/2014	-21,23	16,23	9:00 AM	8:00 AM
NATR	12	10/27/2014	-21,44	15,11	4:00 PM	3:00 PM
NATR	13	10/28/2014	-23,18	12,01	9:00 AM	8:00 AM
WTRA	14	10/28/2014	-23,57	10,43	4:00 PM	3:00 PM
WTRA	15	10/29/2014	-25,34	7,24	9:00 AM	8:00 AM
WTRA	16	10/29/2014	-26,12	6,05	4:00 PM	3:00 PM
WTRA	17	10/30/2014	-27,40	3,03	9:00 AM	9:00 AM
WTRA	18	10/30/2014	-28,16	-1,48	4:00 PM	4:00 PM
WTRA	19	10/31/2014	-29,47	-1,21	9:00 AM	9:00 AM
WTRA	20	10/31/2014	-30,28	-2,45	4:00 PM	4:00 PM
SATL	21	11/01/2014	-32,02	-6,02	9:00 AM	9:00 AM
SATL	22	11/02/2014	-31,56	-10,06	9:00 AM	9:00 AM
SATL	23	11/02/2014	-32,23	-10,39	4:00 PM	5:00 PM
SATL	24	11/03/2014	-33,54	-14,57	9:00 AM	10:00 AM
SATL	25	11/03/2014	-34,20	-14,57	4:00 PM	5:00 PM
SATL	26	11/04/2014	-35,32	-15,60	9:00 AM	10:00 AM
SATL	27	11/04/2014	-36,05	-18,51	4:00 PM	5:00 PM
SATL	28	11/05/2014	-37,12	-20,12	9:00 AM	10:00 AM
SATL	29	11/05/2014	-38,22	-23,41	4:00 PM	5:00 PM
SATL	30	11/06/2014	-41,26	-24,43	9:00 AM	10:00 AM
SATL	31	11/06/2014	-42,29	-26,51	4:00 PM	5:00 PM
SATL	32	11/07/2014	-45,15	-29,30	9:00 AM	11:00 AM
SWAS	33	11/17/2014	-56,27	-38,45	9:00 AM	12:00 PM
SWAS	34	11/17/2014	-57,19	-39,56	4:00 PM	7:00 PM
SWAS	35	11/18/2014	-59,27	-42,35	9:00 AM	12:00 PM
SWAS	36	11/18/2014	-60,22	-43,43	4:00 PM	7:00 PM
SWAS	37	11/19/2014	-62,36	-46,26	9:00 AM	12:00 PM
SWAS	38	11/19/2014	-63,25	-47,19	4:00 PM	7:00 PM
SWAS	39	11/20/2014	-64,54	-48,59	9:00 AM	12:00 PM
SWAS	40	11/20/2014	-65,33	-49,42	4:00 PM	7:00 PM

SWAS	41	11/21/2014	-67,05	-51,20	8:00 AM	11:00 AM
SWAS	42	11/21/2014	-67,41	-51,52	3:00 PM	6:00 PM

Table S2A. Range (minimum: Min and maximum: Max), mean and standard deviation (SD) of pigment concentrations (ng L-1) and pigment ratios in the <3 µM size fraction of surface seawater for the seven study provinces. LHC = Light harvesting pigments (19 - But + 19 - Hex + Fuco + Per). For province names, see the explanation of Fig. 1.

Pigment	**Abbreviation**	**MEDI**	**NAST - E**			
			Min	Max	Mean	SD
19'-Butanoyloxyfucoxanthin	19 - But	35,69	3,11	7,19	5,11	1,55
19'-Hexanoyloxyfucoxanthin	19 - Hex	81,00	6,57	27,16	10,68	3,83
α-Carotene	α-Car	14,71	5,26	13,88	6,01	0,70
Alloxanthin	Allo	10,86	0,13	2,03	0,64	0,40
β-Carotene	β-Car	14,42	1,74	20,11	2,27	0,29
Chl c2-monogalactosyldiacylglyceride ester [14/14]	Chl c2-MGDG [14/18]	5,87	0,27	8,39	2,78	1,89
Chl c2-monogalactosyldiacylglyceride ester [14/18]	Chl c2-MGDG [14/14]	12,87	0,42	5,13	1,45	0,98
Chlorophyll c1	Chl c1	4,79	0,43	2,07	0,54	0,10
Chlorophyll c2	Chl c2	40,66	1,04	14,61	2,72	1,14
Chlorophyll c3	Chl c3	28,92	0,96	15,71	4,35	5,70
Monovinyl chlorophyll *a* epimer	MV-Chl *a*-epimer	4,91	0,19	6,91	0,25	0,04
Chlorophyll *b*	Chl *b*	96,63	4,07	15,48	4,84	0,64
Cis – fucoxanthin	cis-fuco	3,80	0,25	1,94	0,57	0,31
Cis 19'-hexanoyloxyfucoxanthin	cis-hex	7,29	0,24	0,72	0,32	0,11
Diadinoxanthin	Ddx	12,01	2,31	10,77	4,33	1,45
Divinyl chlorophyll *a*	DV-Chl *a*	46,24	23,46	54,93	28,60	2,76

Divinyl chlorophyll *a* allomer 1	DV-Chl *a*-allomer1	3,69	0,17	4,99	0,30	0,17
Divinyl chlorophyll *a* allomer 2	DV-Chl *a*-allomer2	1,00	0,20	0,56	0,29	0,08
Divinyl Chlorophyllide *a*	DV-Chlide *a*	3,92	0,30	7,22	0,70	0,33
Fucoxanthin	Fuco	44,30	3,50	25,37	4,47	0,86
Unidentified carotenoid	M-car	1,05	0,19	1,00	0,25	0,04
Micromonal	Micr	4,32	0,09	3,87	0,14	0,04
Monovinyl chlorophyll *a* allomer 1	MV-Chl *a*-allomer1	3,03	0,06	7,69	0,17	0,10
Monovinyl chlorophyll *a* allomer 2	MV-Chl *a*-allomer2	4,29	0,09	1,17	0,18	0,06
Monovinyl chlorophyll *c*3	MV-Chl *c*3	3,48	0,36	1,01	0,67	0,16
Monovinyl chlorophyll *a*	MV-Chl *a*	363,31	18,10	124,08	27,16	7,16
Monovinyl Chlorophyllide *a*	MV-Chlide *a*	1,02	0,06	1,04	0,20	0,08
Neoxanthin	Neo	4,80	0,14	0,93	0,19	0,05
Peridinin	Per	2,88	0,11	3,60	0,41	0,42
Prasinoxanthin	Pras	13,53	0,09	0,71	0,11	0,02
Uriolide	Uri	6,41	0,11	0,31	0,13	0,03
Violaxanthin	Viol	5,63	0,29	1,08	0,46	0,10
Zeaxanthin	Zea	24,57	26,04	59,60	30,21	3,84
Unidentified zeaxanthin derivative	Zea-der	0,42	0,04	0,52	0,08	0,04
∑ pheophorbide *a*	Phaeob	8,24	0,51	5,14	0,90	0,48
∑ phaeophytin *a*	Phaeop	15,37	2,52	78,16	3,27	0,63
Total chlorophyll *a*	T_Chl *a*	431,41	50,56	151,06	57,86	6,59

Table S2A. Range (minimum: Min and maximum: Max), mean and standard deviation (SD) of pigment concentrations (ng L-1) and pigment ratios in the <3 µM size fraction of surface seawater for the seven study provinces. LHC = Light harvesting pigments (19 - But + 19 - Hex + Fuco + Per). For province names, see the explanation of Fig. 1.

Pigment	**Abbreviation**	**MEDI**	**NAST - E**			
			Min	Max	Mean	SD
19'-Butanoyloxyfucoxanthin	19 - But	35,69	3,11	7,19	5,11	1,55
19'-Hexanoyloxyfucoxanthin	19 - Hex	81,00	6,57	27,16	10,68	3,83
α-Carotene	α-Car	14,71	5,26	13,88	6,01	0,70
Alloxanthin	Allo	10,86	0,13	2,03	0,64	0,40
β-Carotene	β-Car	14,42	1,74	20,11	2,27	0,29
Chl *c*2-monogalactosyldiacylglyceride ester [14/14]	Chl *c*2-MGDG [14/18]	5,87	0,27	8,39	2,78	1,89
Chl *c*2-monogalactosyldiacylglyceride ester [14/18]	Chl *c*2-MGDG [14/14]	12,87	0,42	5,13	1,45	0,98
Chlorophyll *c*1	Chl *c*1	4,79	0,43	2,07	0,54	0,10
Chlorophyll *c*2	Chl *c*2	40,66	1,04	14,61	2,72	1,14
Chlorophyll *c*3	Chl *c*3	28,92	0,96	15,71	4,35	5,70
Monovinyl chlorophyll a epimer	MV-Chl *a*-epimer	4,91	0,19	6,91	0,25	0,04
Chlorophyll *b*	Chl *b*	96,63	4,07	15,48	4,84	0,64
Cis – fucoxanthin	cis-fuco	3,80	0,25	1,94	0,57	0,31
Cis 19'-hexanoyloxyfucoxanthin	cis-hex	7,29	0,24	0,72	0,32	0,11
Diadinoxanthin	Ddx	12,01	2,31	10,77	4,33	1,45
Divinyl chlorophyll *a*	DV-Chl *a*	46,24	23,46	54,93	28,60	2,76
Divinyl chlorophyll *a* allomer 1	DV-Chl *a*-allomer1	3,69	0,17	4,99	0,30	0,17
Divinyl chlorophyll *a* allomer 2	DV-Chl *a*-allomer2	1,00	0,20	0,56	0,29	0,08

Divinyl Chlorophyllide *a*	DV-Chlide *a*	3,92	0,30	7,22	0,70	0,33
Fucoxanthin	Fuco	44,30	3,50	25,37	4,47	0,86
Unidentified carotenoid	M-car	1,05	0,19	1,00	0,25	0,04
Micromonal	Micr	4,32	0,09	3,87	0,14	0,04
Monovinyl chlorophyll *a* allomer 1	MV-Chl *a*-allomer1	3,03	0,06	7,69	0,17	0,10
Monovinyl chlorophyll *a* allomer 2	MV-Chl *a*-allomer2	4,29	0,09	1,17	0,18	0,06
Monovinyl chlorophyll *c*3	MV-Chl *c*3	3,48	0,36	1,01	0,67	0,16
Monovinyl chlorophyll *a*	MV-Chl *a*	363,31	18,10	124,08	27,16	7,16
Monovinyl Chlorophyllide *a*	MV-Chlide *a*	1,02	0,06	1,04	0,20	0,08
Neoxanthin	Neo	4,80	0,14	0,93	0,19	0,05
Peridinin	Per	2,88	0,11	3,60	0,41	0,42
Prasinoxanthin	Pras	13,53	0,09	0,71	0,11	0,02
Uriolide	Uri	6,41	0,11	0,31	0,13	0,03
Violaxanthin	Viol	5,63	0,29	1,08	0,46	0,10
Zeaxanthin	Zea	24,57	26,04	59,60	30,21	3,84
Unidentified zeaxanthin derivative	Zea-der	0,42	0,04	0,52	0,08	0,04
∑ pheophorbide *a*	Phaeob	8,24	0,51	5,14	0,90	0,48
∑ phaeophytin *a*	Phaeop	15,37	2,52	78,16	3,27	0,63
Total chlorophyll *a*	T_Chl *a*	431,41	50,56	151,06	57,86	6,59

	CNRY				NATR				WTRA			
Abbreviation - Pigment	Min	Max	Mean	SD	Min	Max	Mean	SD	Min	Max	Mean	SD
19 - But	1,56	7,19	4,99	2,35	3,64	6,33	4,78	0,97	2,68	6,33	4,59	1,29
19 - Hex	11,73	27,16	16,85	6,10	13,75	25,56	14,90	0,97	7,17	25,56	14,22	6,45
α-Car	0,40	11,10	4,32	4,29	7,56	12,64	8,38	0,69	5,67	13,88	10,10	2,82
Allo	0,15	2,03	1,15	0,75	0,16	0,83	0,40	0,31	0,17	0,75	0,42	0,21
β-Car	2,35	20,11	7,94	7,15	4,60	9,60	6,90	2,06	0,39	6,94	2,59	2,14
Chl *c*2-MGDG [14/18]	1,17	7,48	3,93	2,80	0,39	7,34	0,45	0,08	0,43	8,39	3,05	3,13
Chl *c*2-MGDG [14/14]	2,15	5,13	3,27	1,14	0,90	4,94	2,01	0,94	0,71	4,94	2,33	1,44
Chl *c*1	0,56	2,07	1,22	0,63	0,48	0,80	0,54	0,04	0,33	0,80	0,48	0,15
Chl *c*2	3,47	14,61	8,67	4,94	3,45	4,37	3,66	0,22	1,22	5,43	3,14	1,39
Chl *c*3	1,94	5,92	3,60	1,47	2,01	2,77	2,46	0,32	1,31	2,55	1,76	0,44
MV-Chl *a*-epimer	0,31	6,91	2,28	2,69	0,77	1,24	1,06	0,21	0,31	1,75	0,61	0,47
Chl *b*	2,71	9,05	6,64	2,52	8,21	15,48	10,37	1,52	8,41	18,35	11,98	3,49
cis-fuco	0,32	1,94	1,08	0,61	0,88	1,85	1,01	0,11	0,46	1,85	1,04	0,53
cis-hex	0,25	0,72	0,50	0,17	0,22	0,41	0,29	0,09	0,14	0,45	0,27	0,12
Ddx	2,54	10,77	7,95	3,26	2,04	6,47	3,54	2,08	1,32	5,69	3,50	1,55
DV-Chl *a*	0,08	43,43	17,29	17,46	30,59	51,55	37,13	4,92	32,50	54,93	44,41	8,46
DV-Chl *a*-allomer1	0,34	4,99	1,81	1,86	0,32	1,09	0,51	0,18	0,15	1,09	0,59	0,29
DV-Chl *a*-allomer2	0,06	0,42	0,19	0,14	0,34	0,56	0,47	0,10	0,08	0,49	0,25	0,13
DV-Chlide *a*	0,47	7,22	2,95	2,61	0,38	1,64	0,99	0,51	0,22	1,10	0,66	0,30
Fuco	4,91	25,37	14,56	8,39	1,80	3,35	2,69	0,66	0,74	3,86	1,94	0,97
M-car	0,35	1,00	0,64	0,26	0,36	0,58	0,47	0,09	0,24	0,50	0,37	0,09
Micr	0,13	3,87	1,08	1,61	0,12	0,30	0,19	0,08	0,07	0,41	0,15	0,11
MV-Chl *a*-allomer1	0,07	7,69	2,38	3,10	0,44	0,65	0,57	0,10	0,08	3,21	0,69	1,03
MV-Chl *a*-allomer2	0,09	0,57	0,35	0,17	0,19	1,17	0,31	0,09	0,13	1,38	0,63	0,43
MV-Chl *c*3	0,35	1,01	0,76	0,25	0,68	0,90	0,81	0,10	0,46	0,88	0,65	0,14

MV-Chl *a*	28,03	124,08	62,15	36,83	31,64	60,39	45,58	11,75	13,37	58,04	29,12	15,03
MV-Chlide *a*	0,09	1,04	0,51	0,37	0,08	0,62	0,28	0,22	0,10	0,62	0,25	0,17
Neo	0,19	0,58	0,41	0,15	0,33	0,51	0,42	0,07	0,15	0,93	0,38	0,25
Per	0,07	3,60	1,47	1,48	0,05	0,98	0,12	0,06	0,11	1,84	0,51	0,61
Pras	0,13	0,71	0,38	0,21	0,13	0,31	0,18	0,04	0,09	0,31	0,17	0,07
Uri	0,06	0,27	0,13	0,08	0,10	0,19	0,15	0,04	0,13	0,43	0,22	0,10
Viol	0,33	1,08	0,56	0,30	0,35	0,41	0,39	0,03	0,10	0,55	0,31	0,13
Zea	3,88	36,78	25,01	13,33	37,24	59,60	46,15	9,68	26,83	54,95	39,45	11,09
Zea-der	0,09	0,52	0,25	0,16	0,07	0,16	0,09	0,02	0,04	0,25	0,12	0,06
Phaeob	0,96	5,14	2,26	1,70	0,83	1,48	1,11	0,27	0,08	1,98	0,84	0,61
Phaeop	2,91	78,16	30,92	31,11	4,15	8,11	5,12	0,95	0,68	9,05	4,35	3,26
T_Chl *a*	55,62	151,06	89,90	36,35	78,91	98,60	86,91	6,47	48,24	117,56	77,21	22,68

Abbreviation - Pigment	**SATL**				**SWAS**			
	Min	Max	Mean	SD	Min	Max	Mean	SD
19 - But	1,82	5,65	3,02	1,04	8,90	170,08	59,96	56,49
19 - Hex	4,18	12,05	6,36	2,17	8,43	1235,18	210,54	350,58
α-Car	0,22	5,69	3,22	1,54	1,24	11,02	4,20	3,11
Allo	0,09	1,38	0,33	0,36	2,24	49,40	11,95	13,42
β-Car	0,39	2,66	1,27	0,66	9,54	47,73	26,72	13,26
Chl *c*2-MGDG [14/18]	0,35	3,81	1,94	1,13	0,41	105,94	35,61	38,29
Chl *c*2-MGDG [14/14]	0,71	2,29	1,24	0,43	1,58	44,93	11,32	12,64
Chl *c*1	0,21	1,83	0,66	0,41	1,32	31,42	10,30	8,92
Chl *c*2	0,79	4,33	1,96	0,89	6,31	182,68	68,51	56,20
Chl *c*3	0,24	2,47	0,84	0,57	2,88	200,37	57,41	70,53
MV-Chl *a*-epimer	0,18	0,67	0,33	0,15	6,32	38,05	17,13	10,51
Chl *b*	0,75	5,83	2,67	1,59	6,60	317,62	106,94	96,11
cis-fuco	0,17	0,88	0,36	0,18	1,05	111,47	25,39	34,61
cis-hex	0,11	0,66	0,23	0,15	1,01	23,00	6,37	6,13
Ddx	1,38	4,73	2,51	1,01	17,48	363,10	105,98	98,32
DV-Chl *a*	4,47	29,19	15,93	6,68	0,00	0,00	0,00	0,00
DV-Chl *a*-allomer1	0,04	1,01	0,25	0,26	1,90	36,59	13,85	10,32
DV-Chl *a*-allomer2	0,04	0,93	0,20	0,24	0,29	3,47	1,68	0,97
DV-Chlide *a*	0,09	0,72	0,38	0,15	4,73	25,67	14,40	7,97
Fuco	0,86	6,08	2,31	1,51	23,83	379,91	189,80	120,86
M-car	0,07	0,29	0,17	0,06	1,11	3,47	1,90	0,76
Micr	0,06	0,12	0,10	0,02	0,37	18,97	6,33	5,30

MV-Chl *a*-allomer1	0,09	0,98	0,27	0,22	1,87	46,31	14,96	12,94
MV-Chl *a*-allomer2	0,06	0,51	0,18	0,12	1,47	10,69	4,85	2,69
MV-Chl *c*3	0,13	1,37	0,47	0,34	0,57	16,69	7,58	6,17
MV-Chl *a*	8,42	33,06	16,21	6,41	328,23	1434,55	783,64	351,03
MV-Chlide *a*	0,10	0,35	0,17	0,07	0,74	6,57	3,51	2,00
Neo	0,11	0,24	0,16	0,03	3,49	17,55	8,40	4,69
Per	0,11	0,28	0,18	0,06	0,19	71,31	14,17	20,00
Pras	0,07	0,26	0,11	0,05	0,51	64,37	29,44	18,25
Uri	0,09	0,18	0,13	0,03	2,25	28,95	12,12	8,38
Viol	0,17	0,60	0,31	0,12	3,21	39,64	17,50	13,86
Zea	9,30	24,62	19,23	4,44	2,61	64,86	21,23	19,30
Zea-der	0,07	0,97	0,20	0,25	0,25	4,71	1,61	1,45
Phaeob	0,21	1,05	0,50	0,25	3,06	36,40	16,52	9,36
Phaeop	0,66	3,98	1,92	0,98	7,33	81,47	37,30	21,42
T_Chl *a*	13,78	64,76	33,93	13,19	349,55	1508,16	854,02	377,59

Table S2B. Range (minimum: Min and maximum: Max), mean and standard deviation (SD) of pigment concentrations (ng L-1) and pigment ratios in the >3 µM size fraction of surface seawater for the seven study provinces. LHC = Light Harvesting Pigments (19 - But + 19 - Hex + Fuco + Per). For province names, see the explanation of Fig. 1.

Pigment	**Abbreviation**	**MEDI**	**NAST - E**			
			Min	Max	Mean	SD
19'-Butanoyloxyfucoxanthin	19 - But	3,74	0,50	1,99	0,68	0,12
19'-Hexanoyloxyfucoxanthin	19 - Hex	25,94	2,58	10,50	3,67	0,71
α-Carotene	α-Car	1,41	0,12	0,51	0,20	0,07
Alloxanthin	Allo	1,11	0,11	2,03	0,40	0,22
β-Carotene	β-Car	6,50	0,24	11,33	0,89	0,45
Chl *c*2-monogalactosyldiacylglyceride ester [14/14]	Chl *c*2-MGDG [14/14]	2,47	0,25	6,02	0,33	0,05
Chl *c*2-monogalactosyldiacylglyceride ester [14/18]	Chl *c*2-MGDG [14/18]	4,12	0,38	2,31	0,86	0,40
Chlorophyll *c*1	Chl *c*1	11,54	0,34	3,55	0,54	0,19
Chlorophyll *c*2	Chl *c*2	32,53	0,79	9,79	2,07	1,08
Chlorophyll *c*3	Chl *c*3	19,31	0,40	4,32	0,62	0,17
Monovinyl chlorophyll a epimer	MV-Chl *a*-epimer	2,17	0,08	7,16	0,19	0,13
Chlorophyll *b*	Chl *b*	9,92	0,92	5,07	1,43	0,31
Cis – fucoxanthin	cis-fuco	3,01	0,12	1,06	0,18	0,06
Cis 19'-hexanoyloxyfucoxanthin	cis-hex	1,09	0,08	0,57	0,16	0,08
Diadinoxanthin	Ddx	10,75	1,53	8,33	2,28	0,65
Divinyl chlorophyll *a*	DV-Chl *a*	0,51	0,08	1,23	0,22	0,12

Divinyl chlorophyll *a* allomer 1	DV-Chl *a*-allomer1	2,57	0,06	3,97	0,20	0,19
Divinyl chlorophyll *a* allomer 2	DV-Chl *a*-allomer2	0,21	0,05	0,24	0,10	0,06
Divinyl Chlorophyllide *a*	DV-Chlide *a*	2,06	0,06	1,49	0,41	0,54
Fucoxanthin	Fuco	61,83	0,70	18,08	3,37	4,54
Unidentified carotenoid	M-car	0,56	0,09	0,81	0,19	0,14
Micromonal	Micr	0,12	0,19	2,99	0,35	0,12
Monovinyl chlorophyll *a* allomer 1	MV-Chl *a*-allomer1	3,55	0,11	7,27	0,25	0,21
Monovinyl chlorophyll *a* allomer 2	MV-Chl *a*-allomer2	2,36	0,06	0,41	0,13	0,11
Monovinyl chlorophyll *c*3	MV-Chl *c*3	3,73	0,18	1,46	0,32	0,10
Monovinyl chlorophyll *a*	MV-Chl *a*	212,17	5,62	80,09	14,97	7,83
Monovinyl Chlorophyllide *a*	MV-Chlide *a*	0,53	0,03	0,75	0,21	0,26
Neoxanthin	Neo	0,32	0,11	0,47	0,14	0,02
Peridinin	Per	15,18	0,33	6,63	1,23	0,55
Prasinoxanthin	Pras	0,52	0,08	0,25	0,11	0,02
Uriolide	Uri	0,41	0,10	0,40	0,19	0,11
Violaxanthin	Viol	0,86	0,16	0,50	0,23	0,04
Zeaxanthin	Zea	0,66	0,11	4,72	0,39	0,24
Unidentified zeaxanthin derivative	Zea-der	0,41	0,05	4,22	0,08	0,02
∑ pheophorbide *a*	Phaeob	7,51	0,46	4,73	0,73	0,31
∑ phaeophytin *a*	Phaeop	28,79	1,21	31,61	3,33	2,70
Total chlorophyll *a*	T_Chl *a*	226,13	6,75	101,39	16,68	9,17

	CNRY				NATR				WTRA			
Abbreviation	Min	Max	Mean	SD	Min	Max	Mean	SD	Min	Max	Mean	SD
19 - But	0,32	1,99	1,08	0,61	1,17	1,72	1,38	0,25	0,31	1,31	0,83	0,31
19 - Hex	2,23	10,50	5,75	3,20	3,55	6,03	4,62	0,86	1,87	6,03	4,58	1,31
α-Car	0,10	0,34	0,26	0,10	0,32	0,51	0,40	0,08	0,10	0,70	0,32	0,18
Allo	0,11	1,57	0,64	0,56	0,56	2,03	1,19	0,62	0,09	3,09	0,77	0,97
β-Car	0,21	10,11	3,49	3,88	3,68	11,33	8,28	3,31	0,20	7,20	2,13	2,31
Chl *c*2-MGDG [14/14]	0,37	6,02	2,03	2,32	1,01	3,46	1,50	0,46	0,42	6,91	2,91	2,06
Chl *c*2-MGDG [14/18]	0,28	1,51	1,09	0,48	0,47	2,31	0,77	0,21	0,25	2,64	1,18	0,86
Chl *c*1	0,28	3,55	1,48	1,25	0,62	1,12	0,84	0,21	0,24	1,36	0,70	0,35
Chl *c*2	0,95	9,79	4,09	3,40	3,04	3,74	3,39	0,29	0,41	3,28	1,54	0,97
Chl *c*3	0,36	4,32	1,59	1,59	0,68	1,15	0,91	0,19	0,36	5,80	1,43	1,80
MV-Chl *a*-epimer	0,32	7,16	2,23	2,86	1,80	6,96	4,44	2,11	0,06	2,80	0,84	0,91
Chl *b*	0,26	5,07	2,70	1,75	2,25	2,60	2,40	0,15	0,74	2,60	1,89	0,60
cis-fuco	0,09	1,06	0,53	0,37	0,33	0,66	0,46	0,14	0,14	0,42	0,30	0,09
cis-hex	0,11	0,57	0,29	0,18	0,16	0,45	0,30	0,10	0,04	0,45	0,27	0,12
Ddx	1,39	8,33	3,98	2,65	2,40	4,02	2,94	0,76	1,01	3,87	2,03	0,90
DV-Chl *a*	0,12	0,59	0,39	0,17	0,26	1,23	0,38	0,09	0,09	1,23	0,31	0,38
DV-Chl *a*-allomer1	0,20	3,97	1,22	1,59	0,45	1,59	0,89	0,50	0,15	0,67	0,37	0,19
DV-Chl *a*-allomer2	0,00	0,24	0,06	0,11	0,00	0,10	0,05	0,04	0,00	0,60	0,09	0,21
DV-Chlide *a*	0,20	1,03	0,49	0,32	0,40	1,03	0,74	0,26	0,19	0,68	0,42	0,19
Fuco	2,76	18,08	7,65	6,17	3,57	5,00	4,28	0,58	0,19	2,35	1,24	0,75
M-car	0,12	0,53	0,27	0,16	0,32	0,81	0,54	0,20	0,06	0,48	0,18	0,14
Micr	0,14	0,26	0,21	0,04	1,16	2,99	2,13	0,75	0,08	1,37	0,38	0,41
MV-Chl *a*-allomer1	0,19	7,27	2,11	2,98	0,62	2,71	1,44	0,91	0,19	1,10	0,49	0,32
MV-Chl *a*-allomer2	0,00	0,41	0,17	0,15	0,23	0,34	0,29	0,04	0,04	0,19	0,11	0,05
MV-Chl *c*3	0,12	1,46	0,62	0,52	0,27	0,42	0,34	0,06	0,11	0,46	0,31	0,11

MV-Chl *a*	5,36	80,09	34,11	27,82	30,92	60,10	48,81	12,79	2,87	41,21	18,40	13,53
MV-Chlide *a*	0,06	0,75	0,27	0,28	0,07	0,26	0,16	0,07	0,05	0,26	0,16	0,08
Neo	0,17	0,41	0,25	0,10	0,16	0,47	0,19	0,03	0,11	0,47	0,24	0,11
Per	0,14	6,63	2,69	2,41	3,08	3,68	3,17	0,07	0,26	3,68	1,90	1,33
Pras	0,09	0,25	0,15	0,06	0,09	0,24	0,10	0,01	0,10	0,24	0,16	0,05
Uri	0,10	0,40	0,20	0,12	0,09	0,35	0,11	0,02	0,20	0,47	0,36	0,09
Viol	0,11	0,50	0,29	0,14	0,23	0,45	0,29	0,05	0,13	0,45	0,27	0,11
Zea	0,16	3,78	1,38	1,42	0,10	4,72	2,39	1,88	0,08	2,74	1,07	0,90
Zea-der	0,07	0,14	0,11	0,02	0,18	4,22	1,54	1,89	0,07	0,33	0,17	0,09
Phaeob	0,18	4,73	1,67	1,79	1,33	3,32	2,55	0,87	0,41	2,59	1,33	0,72
Phaeop	1,79	31,61	11,20	11,90	9,42	21,61	14,00	5,44	1,09	9,94	5,33	2,84
T_Chl *a*	6,89	101,39	41,06	35,93	34,81	73,47	57,21	16,37	4,26	47,79	21,20	15,13

	SATL				SWAS			
Abbreviation	Min	Max	Mean	SD	Min	Max	Mean	SD
19 - But	0,30	1,16	0,49	0,23	1,61	70,12	19,60	18,53
19 - Hex	1,90	6,17	2,79	1,18	1,28	139,37	67,99	53,65
α-Car	0,09	0,32	0,12	0,06	0,14	2,46	1,07	0,58
Allo	0,03	0,78	0,30	0,21	1,47	29,43	10,66	8,59
β-Car	0,30	1,25	0,61	0,28	1,23	45,99	12,37	12,14
Chl *c*2-MGDG [14/14]	0,24	17,81	1,99	4,80	0,34	75,95	26,31	24,16
Chl *c*2-MGDG [14/18]	0,26	5,69	0,85	1,47	0,45	6,21	3,41	1,66
Chl *c*1	0,18	1,91	0,57	0,47	1,49	73,23	18,99	21,66
Chl *c*2	0,59	3,16	1,12	0,68	3,43	149,67	44,59	40,44
Chl *c*3	0,21	3,80	0,58	0,97	0,94	140,33	36,93	42,42
MV-Chl *a*-epimer	0,05	0,81	0,24	0,20	1,62	33,34	12,30	8,59
Chl *b*	0,45	1,61	0,95	0,33	1,79	134,02	29,36	36,43
cis-fuco	0,10	0,35	0,19	0,08	0,15	12,42	6,76	3,97
cis-hex	0,10	0,19	0,14	0,03	0,19	10,95	3,28	2,83
Ddx	1,17	2,84	1,75	0,51	5,32	151,73	52,36	37,69
DV-Chl *a*	0,06	0,36	0,15	0,09	0,00	0,00	0,00	0,00
DV-Chl *a*-allomer1	0,05	0,46	0,14	0,12	0,44	34,93	9,08	9,95
DV-Chl *a*-allomer2	0,00	0,15	0,04	0,05	0,00	8,50	1,41	2,49
DV-Chlide *a*	0,03	0,38	0,16	0,11	0,74	26,69	9,39	8,71
Fuco	0,28	2,26	0,88	0,60	15,02	524,80	156,45	150,71
M-car	0,05	0,15	0,08	0,03	0,10	3,53	1,06	0,93
Micr	0,05	0,10	0,08	0,01	0,32	5,46	2,00	1,38
MV-Chl *a*-allomer1	0,06	0,52	0,18	0,12	0,73	51,01	11,96	14,27
MV-Chl *a*-allomer2	0,00	0,46	0,10	0,12	0,28	15,05	5,27	5,13
MV-Chl *c*3	0,03	0,60	0,15	0,17	0,21	47,43	11,84	14,50

MV-Chl *a*	4,66	18,21	8,18	3,86	50,13	1042,81	411,62	290,09
MV-Chlide *a*	0,03	0,16	0,08	0,03	0,15	9,78	3,87	3,17
Neo	0,10	0,24	0,14	0,03	0,51	10,50	3,07	3,20
Per	0,37	1,43	0,84	0,31	0,13	23,90	7,90	8,71
Pras	0,08	0,23	0,11	0,04	0,96	32,78	10,77	10,63
Uri	0,10	0,23	0,15	0,04	0,26	7,95	2,38	2,11
Viol	0,09	0,30	0,17	0,06	0,21	9,70	2,58	2,65
Zea	0,07	0,70	0,21	0,16	0,84	37,81	5,76	10,74
Zea-der	0,01	0,38	0,10	0,09	0,11	1,70	0,60	0,44
Phaeob	0,41	1,11	0,62	0,17	1,05	48,32	12,85	12,86
Phaeop	0,56	4,41	2,43	0,88	7,75	184,51	74,02	68,28
T_Chl *a*	5,45	20,34	9,27	4,16	54,09	1155,08	464,91	329,15

Table S3. Pigment ratios used for the runs of the different CHEMTAX clusters (cluster 1 includes MEFI ans SWAS; cluster 2, the other provinces). The numbers indicate the amount of pigment per unit of Chl *a*. See Table 1 for pigment name abbreviations.

	Chl *c*2	Per	19but	Fuco	Neo	Pras	Viol	19 - Hex	Allox	Zeax	Chl *b*	DV-Chl *a*	Chl *c*2-MGDG [14/14]
PRASINOPHYTES													
pico<3													
Cluster 1	-	-	-	-	0,11	0,28	0,07	-	-	0,13	0,74	-	-
Cluster2	-	-	-	-	0,07	0,20	0,10	-	-	0,10	0,68	-	-
n+m>3													
Cluster 1	-	-	-	-	0,13	0,21	0,08	-	-	0,13	0,80	-	-
Cluster2	-	-	-	-	0,05	0,07	0,03	-	-	0,08	0,20	-	-
Total													
Cluster 1	-	-	-	-	0,12	0,27	0,08	-	-	0,13	0,69	-	-
Cluster2	-	-	-	-	0,08	0,19	0,07	-	-	0,11	1,46	-	-
CHLOROPHYTES													
pico<3													
Cluster 1	-	-	-	-	0,24	0,00	0,07	-	-	0,13	0,31	-	-
Cluster2	-	-	-	-	0,21	0,00	0,07	-	-	0,13	0,35	-	-
n+m>3													
Cluster 1	-	-	-	-	0,19	0,00	0,08	-	-	0,13	0,31	-	-
Cluster2	-	-	-	-	0,05	0,00	0,04	-	-	0,07	0,20	-	-
Total													
Cluster 1	-	-	-	-	0,23	0,00	0,07	-	-	0,12	0,30	-	-
Cluster2	-	-	-	-	0,23	0,00	0,08	-	-	0,13	0,33	-	-
DINOFLAGELLATES													
pico<3													
Cluster 1	0,13	0,61	-	-	-	-	-	-	-	-	-	-	-
Cluster2	0,13	0,66	-	-	-	-	-	-	-	-	-	-	-
n+m>3													
Cluster 1	0,12	0,63	-	-	-	-	-	-	-	-	-	-	-

Cluster2	0,06	0,37	-	-	-	-	-	-	-	-	-	-	-
Total													
Cluster 1	0,13	0,67	-	-	-	-	-	-	-	-	-	-	-
Cluster2	0,12	0,56	-	-	-	-	-	-	-	-	-	-	-
CRYPTOPHYTES													
pico<3													
Cluster 1	0,18	-	-	-	-	-	-	-	0,54	-	-	-	-
Cluster2	0,18	-	-	-	-	-	-	-	0,56	-	-	-	-
n+m>3													
Cluster 1	0,18	-	-	-	-	-	-	-	0,56	-	-	-	-
Cluster2	0,09	-	-	-	-	-	-	-	0,41	-	-	-	-
Total													
Cluster 1	0,18	-	-	-	-	-	-	-	0,61	-	-	-	-
Cluster2	0,18	-	-	-	-	-	-	-	0,61	-	-	-	-
HAPTOPHYTES													
n+m>3													
Cluster 1	0,14	-	0,24	0,14	-	-	-	0,66	-	-	-	-	0,13
Cluster2	0,08	-	0,19	0,12	-	-	-	0,92	-	-	-	-	0,05
P_n+m													
Cluster 1	0,14	-	0,10	0,14	-	-	-	0,61	-	-	-	-	0,14
Cluster2	0,08	-	0,09	0,08	-	-	-	0,04	-	-	-	-	0,04
Total													
Cluster 1	0,13	-	0,17	0,13	-	-	-	0,63	-	-	-	-	0,11
Cluster2	0,15	-	0,11	0,13	-	-	-	0,74	-	-	-	-	0,06
PELAGOPHYTES													
pico<3													
Cluster 1	0,51	-	0,65	0,26	-	-	-	-	-	-	-	-	-
Cluster2	0,45	-	0,61	0,27	-	-	-	-	-	-	-	-	-
n+m>3													
Cluster 1	0,51	-	0,65	0,27	-	-	-	-	-	-	-	-	-

Cluster2	0,17	-	0,30	0,13	-	-	-	-	-	-	-	-	-
Total													
Cluster 1	0,42	-	0,65	0,27	-	-	-	-	-	-	-	-	-
Cluster2	0,38	-	0,68	0,25	-	-	-	-	-	-	-	-	-
DIATOMS													
pico<3													
Cluster 1	0,26	-	0,00	0,70	-	-	-	-	-	-	-	-	-
Cluster2	0,12	-	0,00	0,46	-	-	-	-	-	-	-	-	-
n+m>3													
Cluster 1	0,12	-	0,00	0,53	-	-	-	-	-	-	-	-	-
Cluster2	0,06	-	0,00	0,34	-	-	-	-	-	-	-	-	-
Total													
Cluster 1	0,17	-	0,00	0,70	-	-	-	-	-	-	-	-	-
Cluster2	0,12	-	0,00	0,41	-	-	-	-	-	-	-	-	-
Synecoccoccus													
pico<3													
Cluster 1	-	-	-	-	-	-	-	-	-	1,05	-	-	-
Cluster2	-	-	-	-	-	-	-	-	-	0,64	-	-	-
Total													
Cluster 1	-	-	-	-	-	-	-	-	-	0,74	-	-	-
Cluster2	-	-	-	-	-	-	-	-	-	0,66	-	-	-
Phroclorococcus													
pico<3													
Cluster 1	-	-	-	-	-	-	-	-	-	0,71	0,20	1,00	-
Total													
Cluster 1	-	-	-	-	-	-	-	-	-	0,80	0,28	1,00	-

Table S4. Abundance, in cells L^{-1} of selected frequent phytoplankton taxa (the 10 most frequent in the case of dinoflagellates, diatoms and coccolithophores) and total values for major groups.

Sample date	21.10 A	21.10 B	22.10 A	23.10 A	23.10 B
Station	1	2	3	4	5
Dinoflagellates, cells L^{-1}					
Gonyaulax spp.	10	0	0	0	0
Gymnodinium elongatum	20	50	10	20	20
Oxytoxum minutum	10	40	70	0	0
Oxytoxum spp.		0	20	30	20
Oxytoxum variabile	30	80	20	0	10
Pronoctiluca acuta		0		20	30
Protoperidinium spp. (Large)	40	0	0	0	0
Scrippsiella spp.		90	10	30	100
Unidentified large dinoflagellates	180	450	320	340	330
Unnidentified small dinoflagellates (<20 µm)	6850	4247	2192	1507	3699
Diatoms, cells L^{-1}					
Chaetoceros spp. Large (>20 µm)	0	0	0	0	0
Chaetoceros spp. Small (<20 µm)	0	0	0	10	0
Hemiaulus hauckii		0	10	0	10
Proboscia alata	90	0	0	0	0
Pseudo-nitzschia spp. (Thin)	30	60	0	0	0
Pseudo-nitzschia spp. (Wide)	160	40	10	0	0
Thalassiosira spp. Small (<20 µm)	411	0	0	0	0
Thalassiosira/*Porosira* spp. (>20 µm)	0	0	0	0	0
Unidentified centric diatoms	10	0	0	0	0
Unidentified pennate diatoms	10	0	0	0	0
Coccolithophores, cells L^{-1}					
Unidentified small coccolithophores (< 10 µm)	15344	4521	5617	1233	2603
Unidentified large coccolithohores	822	510	274	130	850
Discosphaera tubifera	60	230	220	110	360
Calcidiscus leptoporus	110	300	490	150	120
Umbellosphaera irregularis		274	685	137	137
Syracosphaera pulchra HET	260	170	160	30	20
Rhabdosphaera clavigera	822	160	548	80	60
S. pulchra HOL	0	50	710	30	0
Syracosphaera spp.	50	0	30	0	0
Helicosphaera carteri	20	10	40	0	0
Other groups, cells L^{-1}					
Criptophytes	1370	137	548	0	137
Nanoflagellates (3-20 µm)	86520	14933	35020	63860	18906
Group totals, cells L^{-1}					
Dinoflagellates	7260	5217	2872	2237	4339
Diatoms	13969	952	200	621	648
Coccolithophores	17498	6245	8794	1900	4150
Criptophytes	1370	137	548	0	137
Others	86660	14953	35030	63900	18926

Sample date	24.10 B	25.10 A	25.10 B	26.10 A	26.10 B
Station	6	7	8	9	10
Dinoflagellates, cells L^{-1}					
Gonyaulax spp.	0	30	0	20	10
Gymnodinium elongatum	10	90	10	10	20
Oxytoxum minutum	20	40	10	0	0
Oxytoxum spp.	0	10	0	0	10
Oxytoxum variabile	20	959	0	0	10
Pronoctiluca acuta	20	40	10	110	0
Protoperidinium spp. (Large)	0	0	30	100	50
Scrippsiella spp.	80	0	890	50	170
Unidentified large dinoflagellates	420	540	780	1880	970
Unnidentified small dinoflagellates (<20 µm)	1781	4384	4384	4932	3425
Diatoms, cells L^{-1}					
Chaetoceros spp. Large (>20 µm)	160	80	0	50	0
Chaetoceros spp. Small (<20 µm)	1918	430	70	25345	250
Hemiaulus hauckii	0	0	0	0	0
Proboscia alata	0	0	0	40	50
Pseudo-nitzschia spp. (Thin)	0	0	10	10823	822
Pseudo-nitzschia spp. (Wide)	0	10	70	2329	120
Thalassiosira spp. Small (<20 µm)	0	137	0	1918	137
Thalassiosira/*Porosira* spp. (>20 µm)	0	0	10	0	20
Unidentified centric diatoms	10	0	0	80	60
Unidentified pennate diatoms	50	0	40	10	90
Coccolithophores, cells L^{-1}					
Unidentified small coccolithophores (< 10 µm)	2192	5343	14796	2055	21509
Unidentified large coccolithohores	590	280	430	60	50
Discosphaera tubifera	110	500	360	0	0
Calcidiscus leptoporus	70	130	0	30	10
Umbellosphaera irregularis	130	137	685	137	0
Syracosphaera pulchra HET	20	30	80	20	20
Rhabdosphaera clavigera	40	130	250	20	0
S. pulchra HOL	20	0	10	0	0
Syracosphaera spp.	20	70	0	0	0
Helicosphaera carteri	0	0	0	0	0
Other groups, cells L^{-1}					
Criptophytes	0	137	0	822	685
Nanoflagellates (3-20 µm)	12467	16480	19454	23564	16440
Group totals, cells L^{-1}					
Dinoflagellates	2541	6884	6611	7996	5035
Diatoms	2635	1097	550	43594	8692
Coccolithophores	3202	6640	16631	2342	21649
Criptophytes	0	137	0	822	685
Others	12467	16510	19494	23574	16460

Sample date	27.10 A	28.10 A	28.10 B	29.10 A	29.10 B
Station	12	13	14	15	16
Dinoflagellates, cells L^{-1}					
Gonyaulax spp.	0	60	10	30	10
Gymnodinium elongatum	20	0	10	30	30
Oxytoxum minutum	10	10	10	20	60
Oxytoxum spp.	0	0	30	0	30
Oxytoxum variabile	0	40	20	0	20
Pronoctiluca acuta	30	40	10	10	10
Protoperidinium spp. (Large)	10	10	10	10	0
Scrippsiella spp.	80	10	370	110	190
Unidentified large dinoflagellates	210	440	290	360	220
Unnidentified small dinoflagellates (<20 µm)	3973	4384	4247	4247	5206
Diatoms, cells L^{-1}					
Chaetoceros spp. Large (>20 µm)	20	0	0	20	0
Chaetoceros spp. Small (<20 µm)	130	274	20	0	10
Hemiaulus hauckii	10	0	10	180	50
Proboscia alata	210	30	80	0	50
Pseudo-nitzschia spp. (Thin)	40	20	10	30	0
Pseudo-nitzschia spp. (Wide)	10	10	0	0	0
Thalassiosira spp. Small (<20 µm)	0	137	0	0	0
Thalassiosira/*Porosira* spp. (>20 µm)	0	10	0	20	0
Unidentified centric diatoms	20	0	0	20	0
Unidentified pennate diatoms	210	20	30	40	70
Coccolithophores, cells L^{-1}					
Unidentified small coccolithophores (< 10 µm)	7946	4795	5206	4932	4932
Unidentified large coccolithohores	80	190	200	240	110
Discosphaera tubifera	10	30	260	390	340
Calcidiscus leptoporus	10	20	0	10	0
Umbellosphaera irregularis	20	0	150	274	70
Syracosphaera pulchra HET	10	0	0	10	20
Rhabdosphaera clavigera	0	0	0	10	0
S. pulchra HOL	20	0	0	40	0
Syracosphaera spp.	0	20	0	30	0
Helicosphaera carteri	0	0	20	20	0
Other groups, cells L^{-1}					
Criptophytes	548	137	137	274	411
Nanoflagellates (3-20 µm)	23701	15618	7261	42196	21509
Group totals, cells L^{-1}					
Dinoflagellates	4483	5291	5207	5234	5886
Diatoms	2648	2418	1463	3511	3351
Coccolithophores	8116	5055	5836	5976	5472
Criptophytes	548	137	137	274	411
Others	23711	15648	7291	42226	21539

Sample date	30.10 A	30.10 B	31.10 A	1.11 A	2.11 A
Station	17	18	19	21	22
Dinoflagellates, cells L^{-1}					
Gonyaulax spp.	20	30	20	30	0
Gymnodinium elongatum	10	0	0	0	30
Oxytoxum minutum	80	20	70	70	50
Oxytoxum spp.	0	0	10	10	0
Oxytoxum variabile	70	50	10	90	40
Pronoctiluca acuta	0	0	0	0	30
Protoperidinium spp. (Large)	0	10	10	10	0
Scrippsiella spp.	20	140	20	40	0
Unidentified large dinoflagellates	90	180	160	70	370
Unnidentified small dinoflagellates (<20 µm)	3288	3151	1233	1096	2329
Diatoms, cells L^{-1}					
Chaetoceros spp. Large (>20 µm)	0	0	40	0	20
Chaetoceros spp. Small (<20 µm)	0	0	0	0	0
Hemiaulus hauckii	0	0	0	0	0
Proboscia alata	0	30	0	10	0
Pseudo-nitzschia spp. (Thin)	0	0	0	0	0
Pseudo-nitzschia spp. (Wide)	0	20	0	0	0
Thalassiosira spp. Small (<20 µm)	0	0	0	0	0
Thalassiosira/*Porosira* spp. (>20 µm)	10	110	10	10	20
Unidentified centric diatoms	0	30	0	0	0
Unidentified pennate diatoms	30	60	20	20	30
Coccolithophores, cells L^{-1}					
Unidentified small coccolithophores (< 10 µm)	3151	4658	5069	6165	2740
Unidentified large coccolithohores	460	150	750	260	430
Discosphaera tubifera	190	40	560	870	170
Calcidiscus leptoporus	20	150	290	320	70
Umbellosphaera irregularis	20	10	50	685	2740
Syracosphaera pulchra HET	0	20	0	0	40
Rhabdosphaera clavigera	0	0	0	90	10
S. pulchra HOL	0	0	0	0	10
Syracosphaera spp.	20	0	10	0	10
Helicosphaera carteri	50	50	60	0	0
Other groups, cells L^{-1}					
Criptophytes	0	0	0	0	0
Nanoflagellates (3-20 µm)	7398	26304	4384	8494	8631
Group totals, cells L^{-1}					
Dinoflagellates	3805	3858	1623	1496	3069
Diatoms	1988	2258	1714	2379	2018
Coccolithophores	3921	5148	6999	8580	6270
Criptophytes	0	0	0	0	0
Others	7428	26334	4394	8504	8631

Sample date	2.11 B	3.11 A	3.11 B	4.11 A	4.11 B
Station	23	24	25	26	27
Dinoflagellates, cells L^{-1}					
Gonyaulax spp.	0	20	0	0	10
Gymnodinium elongatum	20	20	60	50	70
Oxytoxum minutum	10	50	10	30	0
Oxytoxum spp.	20	10	30	20	10
Oxytoxum variabile	0	0	10	60	10
Pronoctiluca acuta	0	0	10	10	20
Protoperidinium spp. (Large)	0	10	0	10	20
Scrippsiella spp.	60	20	10	10	10
Unidentified large dinoflagellates	200	90	80	170	230
Unnidentified small dinoflagellates (<20 µm)	1918	548	1096	3151	2329
Diatoms, cells L^{-1}					
Chaetoceros spp. Large (>20 µm)	0	0	0	0	10
Chaetoceros spp. Small (<20 µm)	30	0	20	0	0
Hemiaulus hauckii	0	20	0	0	20
Proboscia alata	0	0	0	0	0
Pseudo-nitzschia spp. (Thin)	0	0	0	0	0
Pseudo-nitzschia spp. (Wide)	0	0	10	0	0
Thalassiosira spp. Small (<20 µm)	10	0	0	0	0
Thalassiosira/*Porosira* spp. (>20 µm)	50	30	30	10	10
Unidentified centric diatoms	0	0	10	0	0
Unidentified pennate diatoms	20	0	40	30	20
Coccolithophores, cells L^{-1}					
Unidentified small coccolithophores (< 10 µm)	3288	3425	3973	3562	2877
Unidentified large coccolithohores	690	480	980	190	320
Discosphaera tubifera	150	620	140	110	160
Calcidiscus leptoporus	80	70	60	60	20
Umbellosphaera irregularis	2192	274	137	548	0
Syracosphaera pulchra HET	30	40	70	20	20
Rhabdosphaera clavigera	60	10	0	0	0
S. pulchra HOL	80	60	100	10	100
Syracosphaera spp.	20	90	10	0	10
Helicosphaera carteri	30	10	0	10	10
Other groups, cells L^{-1}					
Criptophytes	0	0	137	137	0
Nanoflagellates (3-20 µm)	3562	4795	6576	13152	10960
Group totals, cells L^{-1}					
Dinoflagellates	2338	938	1356	3748	2829
Diatoms	942	1283	414	1694	561
Coccolithophores	6640	5079	5480	4530	3537
Criptophytes	0	0	137	137	0
Others	3572	4805	6576	13172	10960

Sample date	5.11 A	5.11 B	6.11 B	7.11 A	17.11 A
Station	28	29	31	32	33
Dinoflagellates, cells L^{-1}					
Gonyaulax spp.	10	0	0	10	0
Gymnodinium elongatum	60	0	80	50	0
Oxytoxum minutum	60	10	10	60	0
Oxytoxum spp.	20	10	130	20	
Oxytoxum variabile	70	40	30	0	
Pronoctiluca acuta	10	10	20	10	
Protoperidinium spp. (Large)	0	20	0	0	0
Scrippsiella spp.	40	110	80	40	
Unidentified large dinoflagellates	230	260	430	240	30
Unnidentified small dinoflagellates (<20 µm)	2466	3836	3014	2466	685
Diatoms, cells L^{-1}					
Chaetoceros spp. Large (>20 µm)	70	10	0	0	0
Chaetoceros spp. Small (<20 µm)	80	0	30	0	0
Hemiaulus hauckii	60	80	30	0	
Proboscia alata	30	0	0	30	0
Pseudo-nitzschia spp. (Thin)	0	0	0	0	0
Pseudo-nitzschia spp. (Wide)	0	0	0	0	0
Thalassiosira spp. Small (<20 µm)	0	0	0	0	0
Thalassiosira/*Porosira* spp. (>20 µm)	0	0	0	0	0
Unidentified centric diatoms	10	10	0	0	0
Unidentified pennate diatoms	0	20	0	0	0
Coccolithophores, cells L^{-1}					
Unidentified small coccolithophores (< 10 µm)	3836	3288	3836	7672	29866
Unidentified large coccolithohores	200	570	990	170	0
Discosphaera tubifera	320	390	880	590	
Calcidiscus leptoporus	0	10	30	20	
Umbellosphaera irregularis	411	137	137	1644	
Syracosphaera pulchra HET	0	30	40	40	
Rhabdosphaera clavigera	10	30	40	50	
S. pulchra HOL	120	30	60	50	
Syracosphaera spp.	0	0	0	0	
Helicosphaera carteri	0	0	0	0	
Other groups, cells L^{-1}					
Criptophytes	0	0	137	0	1644
Nanoflagellates (3-20 µm)	13837	12878		9316	8768
Group totals, cells L^{-1}					
Dinoflagellates	3036	4386	3994	3163	1694
Diatoms	1650	1647	290	1313	548
Coccolithophores	4897	4485	6023	10256	29866
Criptophytes	0	0	137	0	1644
Others	13887	12888	9366	8818	418150

Sample date	17.11 B	18.11 A	18.11 B	19.11 B	20.11 A
Station	34	35	36	38	39
Dinoflagellates, cells L^{-1}					
Gonyaulax spp.	0	0	0	0	0
Gymnodinium elongatum	0	170	210	0	0
Oxytoxum minutum	0	60	0	0	0
Oxytoxum spp.	0		0	0	
Oxytoxum variabile	0	3425	0	0	0
Pronoctiluca acuta	0		0	0	
Protoperidinium spp. (Large)	0	140	60	0	0
Scrippsiella spp.	0		30	0	
Unidentified large dinoflagellates	20	6302	13426	270	60
Unnidentified small dinoflagellates (<20 µm)	274	50416	22331	1918	0
Diatoms, cells L^{-1}					
Chaetoceros spp. Large (>20 µm)	0	2466	5891	20	0
Chaetoceros spp. Small (<20 µm)	0	685	3425	40	0
Hemiaulus hauckii	0		0	0	
Proboscia alata	0	0	0	0	0
Pseudo-nitzschia spp. (Thin)	0	959	4521	10	20
Pseudo-nitzschia spp. (Wide)	0	3425	11371	0	20
Thalassiosira spp. Small (<20 µm)	0	0	411	5206	50
Thalassiosira/*Porosira* spp. (>20 µm)	0	20	20	0	0
Unidentified centric diatoms	0	50	3151	10	10
Unidentified pennate diatoms	10	0	90	0	10
Coccolithophores, cells L^{-1}					
Unidentified small coccolithophores (< 10 µm)	1507	2192	599716	3425	69
Unidentified large coccolithohores	0	10	20	0	0
Discosphaera tubifera	0		0	0	
Calcidiscus leptoporus	0		10	0	
Umbellosphaera irregularis	0		0	0	
Syracosphaera pulchra HET	0		0	0	
Rhabdosphaera clavigera	0		0	0	
S. pulchra HOL	0		0	0	
Syracosphaera spp.	0		0	0	
Helicosphaera carteri	0		0	0	
Other groups, cells L^{-1}					
Criptophytes	274	0	0	685	0
Nanoflagellates (3-20 µm)	407880	588183	1656240	1418559	184528
Group totals, cells L^{-1}					
Dinoflagellates	304	75249	47976	3735	80
Diatoms	421	8400	58121	5556	110
Coccolithophores	1507	2212	599746	3425	69
Criptophytes	274	0	0	685	0
Others	588203	1662269	1419579	184528	3014

Sample date	20.11 B	21.11 A	21.11 B
Station	40	41	42
Dinoflagellates, cells L^{-1}			
Gonyaulax spp.	0	0	0
Gymnodinium elongatum	0	0	0
Oxytoxum minutum	0	0	0
Oxytoxum spp.	0		0
Oxytoxum variabile	0	0	0
Pronoctiluca acuta	0		0
Protoperidinium spp. (Large)	0	0	70
Scrippsiella spp.	0		0
Unidentified large dinoflagellates	40	20	50
Unnidentified small dinoflagellates (<20 µm)	20	30	685
Diatoms, cells L^{-1}			
Chaetoceros spp. Large (>20 µm)	0	80	0
Chaetoceros spp. Small (<20 µm)	70	40	0
Hemiaulus hauckii	0		0
Proboscia alata	0	0	0
Pseudo-nitzschia spp. (Thin)	0	20	0
Pseudo-nitzschia spp. (Wide)	0	0	0
Thalassiosira spp. Small (<20 µm)	548	1233	0
Thalassiosira/*Porosira* spp. (>20 µm)	0	0	0
Unidentified centric diatoms	0	20	0
Unidentified pennate diatoms	10	10	0
Coccolithophores, cells L^{-1}			
Unidentified small coccolithophores (< 10 µm)	274	2466	3014
Unidentified large coccolithohores	0	0	0
Discosphaera tubifera	10		0
Calcidiscus leptoporus	0		0
Umbellosphaera irregularis	0		0
Syracosphaera pulchra HET	0		0
Rhabdosphaera clavigera	0		0
S. pulchra HOL	0		0
Syracosphaera spp.	0		0
Helicosphaera carteri	0		0
Other groups, cells L^{-1}			
Criptophytes	0	0	274
Nanoflagellates (3-20 µm)	3014	3288	24934
Group totals, cells L^{-1}			
Dinoflagellates	220	15668	1510
Diatoms	638	1553	2653
Coccolithophores	284	2466	3014
Criptophytes	0	0	274
Others	3288	24934	165222

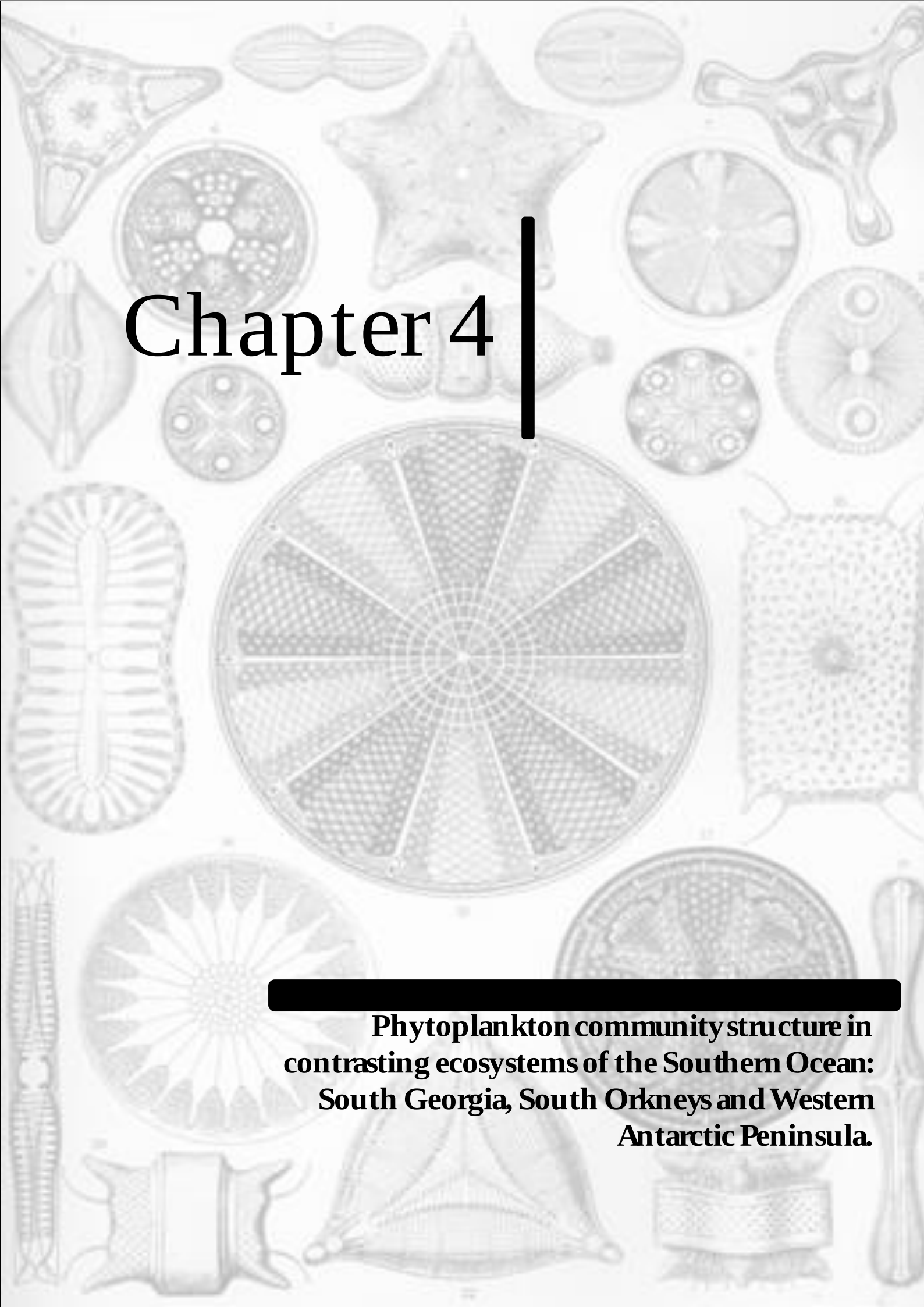

Chapter 4

Phytoplankton community structure in contrasting ecosystems of the Southern Ocean: South Georgia, South Orkneys and Western Antarctic Peninsula.

The scientific contribution of this work has resulted of this chapter as a manuscript entitled: Nunes, S.**;** Latasa, M.; Delgado, M. Simó, R.; Estrada, M. (2018). **Phytoplankton community structure in contrasting ecosystems of the Southern Ocean: South Georgia, South Orkneys and Western Antarctic Peninsula.** Deep-Sea Research Part I - *Enviado*

CHAPTER 4

Phytoplankton community structure in contrasting ecosystems of the Southern Ocean: South Georgia, South Orkneys and Western Antarctic Peninsula

ABSTRACT

The taxonomy and distribution of the phytoplankton in four contrasting regions (North of the South Orkney Islands= NSO, Southeast of the South Orkney Islands = SSO, Northwest of South Georgia = NSG and West of Anvers = WA) of the Atlantic sector of the Southern Ocean was studied by microscopic examination and pigment analyses using high-performance liquid chromatography (HPLC) followed by the CHEMTAX algorithm, during the PEGASO cruise of the BIO Hespérides (January-February 2015). Overall, a statistically significant association was found between fluorometric and HPLC determinations of chlorophyll *a*, and between chemotaxonomic and microscopy-derived estimates of the contribution of diatoms, dinoflagellates and cryptophytes, although the latter appeared to be underestimated by the microscopic observations. The highest average levels of fluorometric chlorophyll *a* (517 mg m^{-2}) were found at NSG, followed by WA (132 mg m^{-2}), NSO (120 mg m^{-2}) and SSO (34 mg m^{-2}). The phytoplankton community at NSG was dominated by diatoms like *Eucampia Antarctica* and *Thalassiosira* spp. Cryptophytes and diatoms (mainly *Corethron pennatum*, small *Thalassiosira* spp. and *Fragilariopsis* spp.) were the most abundant chemotaxonomic groups at NSO, followed by haptophytes types 6 + 7, *Phaeocystis* and, especially in the deeper levels of the euphotic zone, pelagophytes. At SSO, the most important groups were haptophytes types 6 + 7, followed by diatoms (with a combination of taxa similar to that of NSO) and *Phaeocystis*. At both NSO and SSO, microscopic observations revealed a substantial contribution of heterotrophic dinoflagellates. The main CHEMTAX groups at WA were cryptophytes (between surface and about 40 m depth), haptophytes types 6 + 7 and diatoms. The ratio between the photoprotective pigment diadinoxanthin and the sum of the light harvesting pigments of phytoplankton sharing diadinoxanthin (sum of 19'-butanoyloxyfucoxanthin, 19'-hexanoyloxyfucoxanthin, fucoxanthin and peridinin) presented a significant positive correlation with the euphotic zone depth, indicating an enhancement due to exposure to a relatively high irradiance environment.

KEYWORDS: Southern Ocean; phytoplankton distribution; microscopy; HPLC; CHEMTAX; pigments

4. 1. INTRODUCTION

The Southern Ocean (SO), which surrounds Antarctica, plays a substantial role in regulating and controlling the climate in the world. One of its main features is the Antarctic Circumpolar Current (ACC), which flows clockwise around Antarctica, connecting the Atlantic, Indian and Pacific oceans. The SO covers about 30% of the global ocean and large parts of it are high-nutrient low-chlorophyll (HNLC) areas, mainly due to the co-limitation of light and micronutrients such as iron. Despite widespread limitation to productivity, it is a large sink for anthropogenic CO_2 in the world and accounts for about 43% of the ocean uptake of anthropogenic CO_2 released to the atmosphere over the historical period (Frölicher et al., 2015). This control occurs mainly through CO_2 solubility in the water and by action of the so-called biological pump – CO_2 capture by phytoplankton photosynthesis in surface waters of localized high-productivity areas, vertical transport of organic matter and carbon sequestration in the deep ocean and the sediment (Boyd and Trull, 2007; Marinov et al., 2008). Besides contributing to ocean carbon sequestration, phytoplankton plays a key role in the metabolism of sulfur compounds and may contribute to the formation of organic aerosols. In particular, some phytoplankton groups, such as prymnesiophytes and dinoflagellates, synthesize substantial quantities of dimethylsulfoniopropionate (DMSP), which by enzymatic action can form dimethylsulfide (DMS). These and other biogenic organic emissions can influence the optical properties of the atmosphere and the Earth radiative budget (Simó, 2001) and might be important in climate regulation (Charlson et al., 1987; Quinn and Bates, 2011).

The SO contains very diverse environments, which influence the function and structure of the corresponding phytoplankton communities. One of the key factors appears to be

the availability of iron. Open waters of the ACC are generally iron-limited, while coastal regions influenced by terrestrial sources, such as areas neighbouring subantarctic islands or the Antarctic Peninsula, may have adequate iron supply (Martin et al., 1990; Moore et al., 2013). Another major abiotic factor influencing phytoplankton growth in the SO is light availability and its interaction with water column mixing, in turn affected by wind forcing and stabilization associated with ice melt (Vernet et al., 2008; Cassar et al., 2011). Phytoplankton blooms in the Atlantic sector of the SO tend to be dominated by diatoms or haptophytes like *Phaeocystis* spp. (Estrada and Delgado, 1990; Mendes et al., 2013) but cryptophyte proliferations may also be important, in particular in areas influenced by melting ice (Schloss and Estrada, 1994; Moline et al., 2004). Documenting the composition of the phytoplankton communities is important for understanding aerosol production, food web dynamics and biogeochemical cycling, and for projecting potential responses of the ecosystem to climate change.

The PEGASO oceanographic cruise, on board the RV Hespérides was conducted in the Atlantic sector of the Southern Ocean as part of the PEGASO project, which investigated the role of planktonic community structure, activity and physiological state in controlling the emission of trace gases, semivolatile organics and microgels from the surface waters. The survey included series of oceanographic stations in four contrasting zones of the SO, located in the vicinity of the South Orkneys, the South Georgia and the Anvers Islands. The reasoning for selecting these zones was a combination of differences in nutrient conditions (in particular with respect to iron availability), relatively high chlorophyll concentrations and relatively slow currents without stable direction. Within each zone, a Lagrangian approach was applied to locate the stations. At each station and during transits, physical, chemical and biological measurements were conducted in parallel to atmospheric measurements of aerosol chemistry and

physics. Within this context, this work reports the quantitative distribution and taxonomic composition of the phytoplankton community in the study region, with the aim of contributing to document the links between phytoplankton community structure and aerosol composition. We used High Performance Liquid Chromatography (HPLC) analysis of phytoplankton pigments (Roy et al., 2011), followed by application of the CHEMTAX algorithm (Mackey et al., 1996) to estimate the quantitative contribution of major phytoplankton groups to total chlorophyll a (Chl *a*) and we combined these results with microscopic observations of nano- and microphytoplankton to refine the identification of the main phytoplankton taxa.

4. 2. MATERIAL AND METHODS

4.2.1. PEGASO expedition and study location

This survey was conducted on board the B.I.O. Hespérides in the austral summer of 2015 (From January, 02 to February, 12). Four zones (Fig. 1) were chosen for a several-day study following a Lagrangian approach: north of the South Orkney Islands (NSO), southeast of the South Orkney Islands (SSO), northwest of South Georgia (NSG) and west of Anvers (WA). The position of the main hydrographic fronts during the cruise (Figs. 2 and S1) was determined, following the scheme of Orsi et al. (1995), with reference to the continuous records of temperature and salinity (thermosalinograph SBE 21 SeaCAT), current velocity and direction measured with the Shipboard Acoustic Doppler Current Profiler (SADCP) "Ocean Surveyor" at 75 khz, and the synoptic modeling data obtained from the Global Real-Time Ocean Forecast System (Global RTOFS) (Dall'Osto et al., 2017). We also used 8-day average satellite images of chlorophyll *a* concentration and sea surface temperature obtained from the Visible and

Infrared Scanner (VIRS), NASA. We did not measure micronutrients, but evidence from prior studies places NSG as iron-sufficient and considers open sea areas of the ACC as HNLC regions due to iron limitation (Martin et al., 1990; Nielsdóttir et al., 2012). In three of the zones (NSO, NSG and WA), the studied water bodies were marked by means of WOCE (World Ocean Circulation Experiment) standard drifters provided with Iridium communication system; in SSO, icebergs were used as Lagrangian "markers". CTD casts using a SBE 911 Plus sonde attached to a rosette of 24 12-L PVC Niskin bottles were carried out at least once a day, around 8:30 solar (local) time. In addition, a 36-hour cycle was sampled in each zone, with CTD casts every 4 hours starting generally at 9:30 and ending at 17:00 (solar times) the day after (see Table S1 for station information). Solar time calculations were performed by means of the NASA Solar Calculator (https://www.esrl.noaa.gov/gmd/grad/solcalc/, accessed on 15 December 2017). Conductivity, temperature, depth, *in vivo* fluorescence (with a WET Labs ECO-AFL/FL fluorometer) and photosynthetically active radiation (PAR, measured with a LI-COR Biospherical PAR Sensor) profiles were recorded down to 400 m. Water samples were taken from the Niskin bottles, at six different depths. These included generally "surface" (4 m depth), a "deep" level ranging between 120 m and 150 m, and four additional levels in between (Table S1). Fluorometric Chl *a* (Fl_Chl *a*) determination and phytoplankton pigment analyses were carried out for all six depths. Major nutrients were analyzed for surface samples. Water samples for phytoplankton identification by microscopy were collected from surface and the depth of maximum fluorescence, generally the 1% light depth. Mixed layer depth was estimated in as the first depth for which water density was 0.125 kg m^{-3} higher than at surface (Monterey and Levitus, 1997).

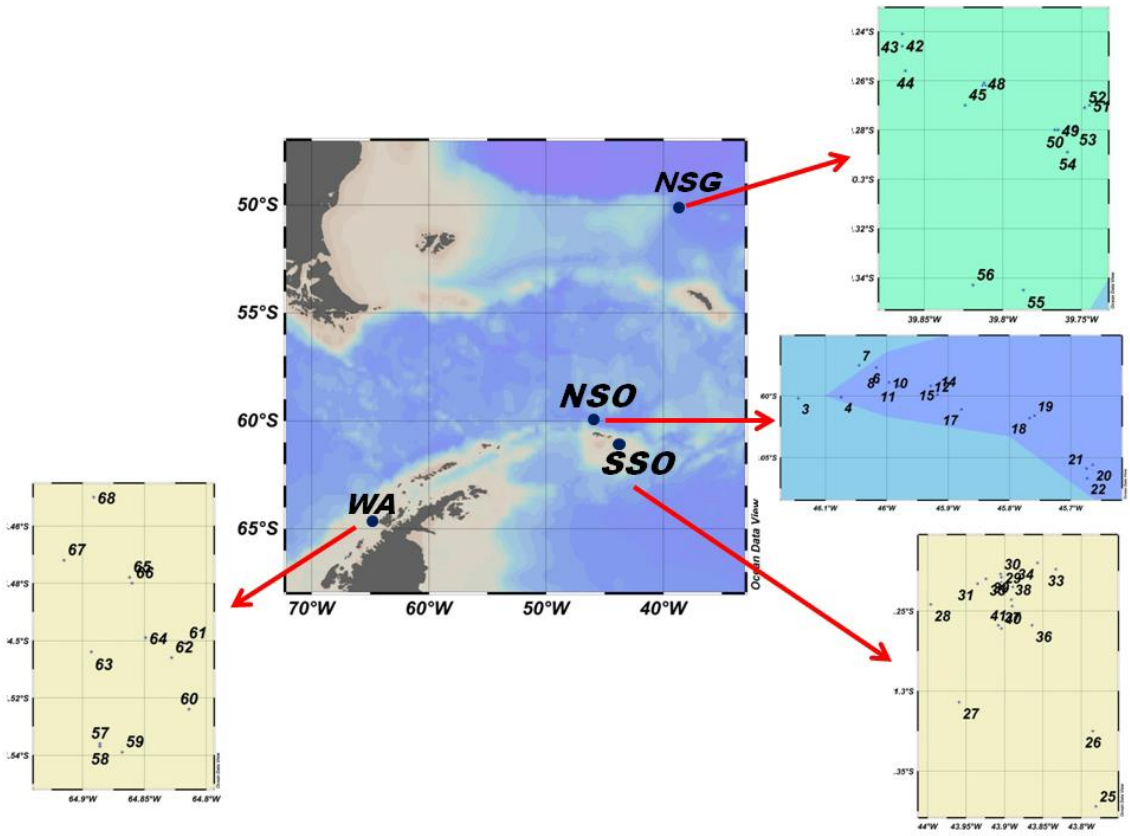

Fig. 1. Position of the sampling stations in the four visited zones: NSO = North of the South Orkney Islands, SSO = South of the South Orkney Islands, NSG = Northwest of South Georgia Island, WA = West of Anvers Island.

4.2.2. Nutrient concentration and Fluorometric Chl *a* (Fl_Chl *a*)

Water for nutrient analyses was placed in Falcon vials and kept frozen at -20ºC until processing on land. Phosphate, nitrate, nitrite and silicate concentrations were determined (only for the surface samples) with an Alliance Evolution II autoanalyser, following the procedures of Hansen & Koroleff (1999).

For Fl_Chl *a* determination, 100 cm^3 of water were filtered through Whatman GF/F fibre filters (25 mm diameter) which were subsequently placed in a freezer at −20 °C. After several hours, the filters were introduced in vials with 90% acetone and left in the dark at 4°C for about 24 hours. The fluorescence of the extracts was measured with a Turner Designs fluorometer according to the procedure described in Yentsch and Menzel (1963). No “phaeophytin” correction was applied.

4.2.3. Phytoplankton identification

Immediately after collection, 250 cm^3 of seawater were placed in amber glass flasks, preserved with formalin-hexamine solution to a final concentration of 1% formalin and stored in the dark until analysis. For phytoplankton identification 100 cm^3 methacrylate settling chambers were filled with water sample. After 48 hours of sedimentation, the chamber bottom was separated and examined under a XSB-1A inverted microscope (Utermöhl, 1958) . The entire base of the chambers was scanned at 125X to quantify the less abundant and larger organisms of the microphytoplankton (> 20 μm), and at least two transects were examined at 312X to enumerate the smaller and more abundant organisms of the nanoplankton (< 20 μm). On accasion of exceptionally high concentrations, 6 fields were counted at 312x. Phytoplankton was identified to the species level, when possible. However, many organisms could no be adequately classified and were pooled in categories such as “small dinoflagellates (< 20 μm)”, “unidentified centric diatoms” or “unidentified small coccolithophores (< 10 μm)”. The inverse microscope method is not adequate for the small organisms of the picoplankton. Our counts, thus, include nano- and microplankton. For the purpose of comparison with the pigment data, we classified the organisms into the following groups: dinoflagellates, diatoms, coccolithophores, cryptophytes and other. For brevity, we will refer to these groups as “phytoplankton”, although many dinoflagellates are heterotrophs. For biovolume estimation, maximum and minimum length and maximum and minimum observed width were recorded for each taxon; average values from these data were used to calculate the volume of approximate geometric shapes: elipsoid for dinoflagellates, coccolithophores and flagellates, cylinder for centric diatoms and prisma for pennate diatoms.

4.2.4. HPLC pigment analysis

Pigment composition was determined by HPLC (Latasa, 2014). Briefly, 0.65 – 1 L of seawater were filtered onto Whatman GF/F (nominal pore size 0.7 µm; 25 mm diameter) glass fiber filter under dim light. The filters were folded, introduced into cryovials and frozen at -80ºC until analysis on land, at the Centro Oceanográfico de Gijón (IEO, Instituto Español de Oceanografía, Spain). For analysis, the filters were placed in Nalgene tubes with with 2.5 cm^3 of 90% acetone in which an internal standard of apo-8'-carotenal (Fluka) had been dissolved. The tubes were chilled in ice, sonicated during 30 seconds and stored for 24 hours at - 20 °C. Afterwards, the samples were vortexed, filtered through Whatman GF/F glass fiber filters to remove filter debris and immediately injected into the HPLC instrument [Agilent series (Waldbronn, Germany) 1200 chromatographic system with a G1311A quaternary pump, a G1367C autosampler with a 100 _L capillary loop, a G1316B column thermostat, and a G1315C diode array detector]. Sample extract/water ratios of 60/40 were used, according to Latasa (2014). We identified 32 pigments (Table 1) at 474 and 664 nm. The total monovinyl-chlorophyll *a* concentration (T_Chl *a*) was estimated as the sum of monovinyl-chlorophyll *a*, chlorophyllide *a*, chlorophyll *a* epimer and chlorophyll *a* allomers. No divinyl-chlorophyll *a* was detected.

4.2.5. Photoprotective pigment index

The response to variations in irradiance intensity of phytoplankton may alter their pigment concentrations and composition (Higgins et al., 2011). To assess the photoacclimation response of at least a part of the phytoplankton (the groups sharing diadinoxanthin as the main light-protecting pigment, which include diatoms, dinoflagellates, haptophytes and pelagophytes), we calculated the ratio Ddx/(LHC)

between the concentration of diadinoxanthin (Ddx) and the sum of the concentrations (LHC) of the main light-harvesting carotenoids fucoxanthin, 19'-butanoyloxyfucoxanthin, 19'-hexanoyloxyfucoxanthin and peridinin).

4.2.5. CHEMTAX

The relative abundance of microalgal groups contributing to total Chl *a* biomass was derived from pigment concentration data using version 1.95 of the CHEMTAX chemical taxonomy software (Mackey et al., 1996). This program uses one or several initial matrices of pigment/T_Chl *a* ratios for the selected phytoplankton groups and performs iterations to optimize the proportion of T_Chl *a* accounted for by these groups. The final result of the CHEMTAX program consists of a new adjusted matrix of pigment quotients and a list of the contribution of each pigmentary class to the concentration of each pigment. The initial pigment ratios used in this work were based on diagnostic pigments and pigment matrices used in studies from the Antarctic region (Rodríguez et al, 2002; Kozlowski et al, 2011). The pigments considered were peridinin (Per), 19'-butanoyloxyfucoxanthin (19-But), 19'- hexanoyloxyfucoxanthin (19-Hex), alloxanthin (Allo), chlorophyll *b* (Chl *b*), chlorophyll *c*2 (Chl *c*2), fucoxanthin (Fuco), lutein (Lut), prasinoxanthin (Pras), violaxanthin (Viol) and zeaxanthin (Zea). The haptophytes, characterized by the occurrence of 19-Hex, were divided in two groups, according to the important presence of 19-But (type 8, which comprises *Phaeocystis*) or to the negligible content of this pigment (a combination of types 6 and 7, including the coccolithophores and *Chrysochromulina*). The samples of each study region were clustered according to the application of Ward's method to a similarity matrix based on Manhattan distances, using the Statistica v.5.5 software. A total of 13 clusters was identified, corresponding 3 to NSO and SSO, 5 to NSG and 2 to WA. For each cluster,

we followed the procedures of Latasa (2007) and Latasa et al. (2010), i.e. we created 29 randomized copies of the initial ratio matrix and we ran the program for eight successive times. After the eighth run, a single average matrix was made and used again for a final run of each cluster (Table S2). Eight pigmentary classes were quantified: Chlorophytes, cryptophytes, diatoms, dinoflagellates, haptophytes types 6 + 7, prasinophytes, haptophytes type 8 (hereafter "*Phaeocystis*") and pelagophytes.

4.3. RESULTS

4.3.1. General characterization of the study regions

The surface temperature and salinity records and the position of the main hydrographic fronts during the PEGASO cruise are shown in Figs. 2 and S1. The NSO and the NSG zones were located within meanders of the Southern Boundary of the ACC (SBACC) and the Polar Front (PF), respectively. SSO, some 60 nautical miles to the north of the Weddell Front, was next to the marginal ice zone of the Weddell Sea. In January 2015, the characteristic position of the Weddell Front coincided with the perimeter of the >25% ice cover (https://seaice.uni-bremen.de – data not shown). WA was placed on the Southern Boudary (SB) and was influenced by relatively colder and less saline coastal waters of Anvers Island.

The distributions of temperature, salinity potential density and fluorescence during the time-series sampling in the four zones are presented in Figs. 3-6. In NSO and SSO (Figs. 3-4), the layer of relatively cold Winter Water (WW), centered around 70 m depth, was underlain by a relatively warm and saline Warm Deep Water (WDW), derived from the Circumpolar Deep Water (CDW) of the ACC (Meredith et al. 2011) and was covered by surface layers seasonally warmed in NSO and influenced by low

salinity ice-melt water in SSO. Mean values (± standard deviation, SD) of surface temperature and salinity were, respectively, 0.58 ± 0.1 and 33.84 ± 0.07 for NSO, and -0.75 ± 0.10 and 33.16 ± 0.06 for SSO (Table 2). The mean mixed layer depth (MLD) was 30 m in NSO and 16 m in SSO, where it was located below the ice-melt surface water layer. NSG (Fig. 5) was located outside the main bloom area, which was closer to the continental shelf, according to climatological data (Borrione and Schlitzer, 2013) and recent satellite images (data not shown); on the third day of the series, there was a marked change towards warmer, more saline and chlorophyll-poorer surface waters, presumably linked to movements across PF gradients. Mean surface temperature and salinity were, respectively, 4.73 ± 0.44 and 33.74 ± 0.02, and the MLD was approximately 50 m. The hydrography of the WA (Fig. 6) zone is complex (Dinniman and Klinck, 2004); water masses on the shelf are episodically influenced by intrusions of Circumpolar Deep Water. During our visit, surface temperature ranged between 1.4 and 1.6, and surface salinity between 33.36 and 33.45, and mean MLD was 23 m. Surface nitrate concentrations were ca. 27 µM in NSO and SSO, and ca. 17-19 µM in NSG and WA (Table 2). Silicate concentration was 47-49 µM in all regions except NSG, where it was around 2 µM. All zones presented subsurface fluorescence maxima (Figs. 3-6), partly related to decreases in the Fluorescence/Chl *a* ratio in the upper surface waters (Fig. S2), as will be commented later.

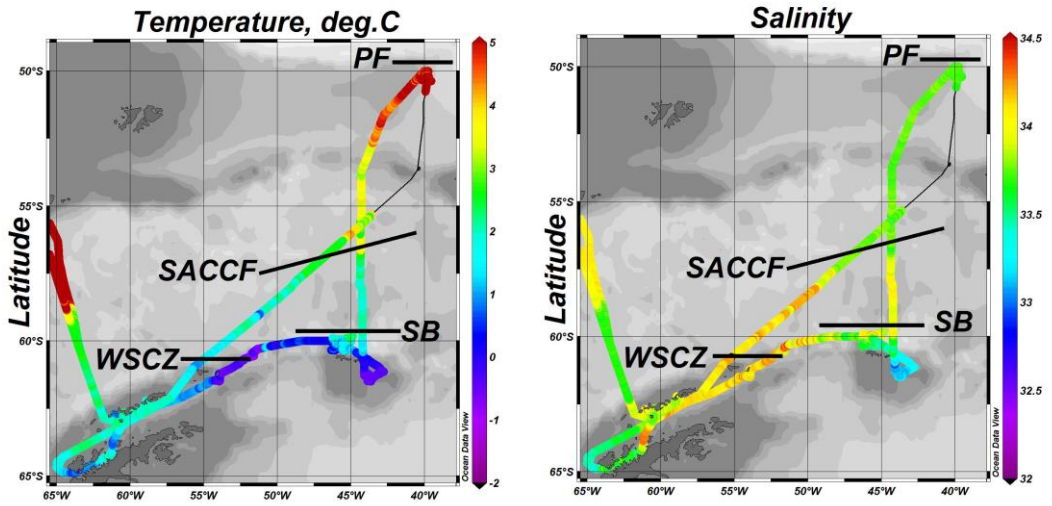

Figure 2. Track of the research vessel, with sea surface temperatures (left) and salinity (right), recorded with a flow-through termosalinograph, coded in color. The position of the main oceanic fronts across the track is indicated: Polar Front (PF; 50ºS), Southern Antarctic Circumpolar Current Front (SACCF¸56.8ºS-57.2ºS), Southern Boundary of the Antarctic Circumpolar Current (SB; 59.9ºS), and Weddell Scotia Confluence Zone (WSCZ; 60.0ºS-60.8ºS). Figure producedwith the Ocean Data View software (Schlitzer, 2016).

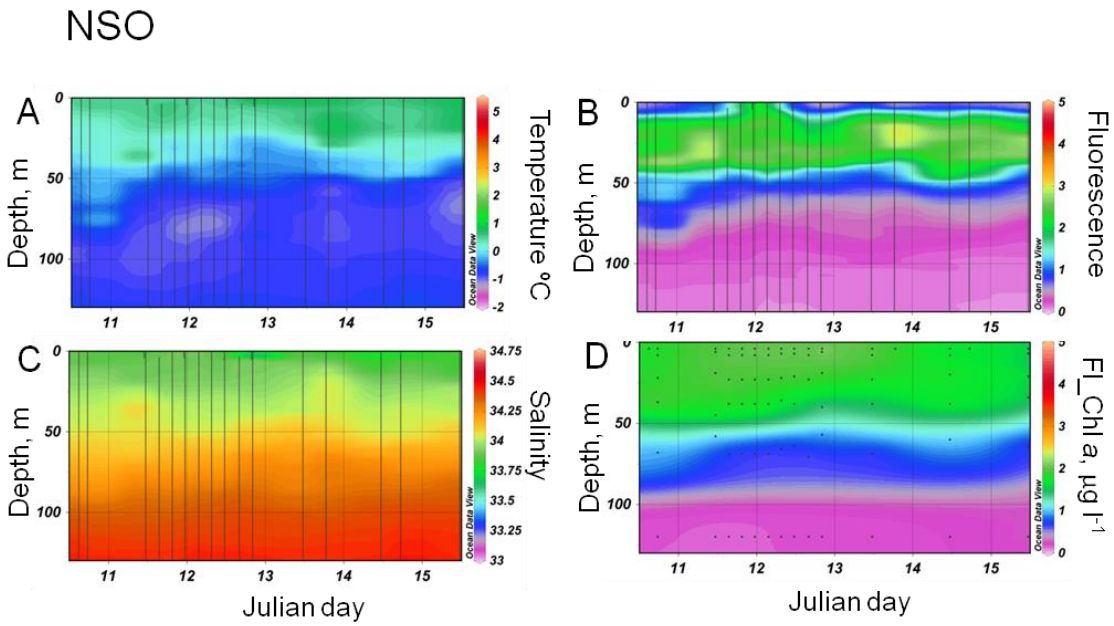

Figure 3. Temporal variation of (A) temperature (ºC), (B) fluorescence (arbitray units), (C) salinity and (D) fluorometric Chl *a* (Fl_Chl *a*, µg l-3) during the visit to the NSO (North of the South Orkney Islands) region. Figure produced with the Ocean Data View software (Schlitzer, 2016).

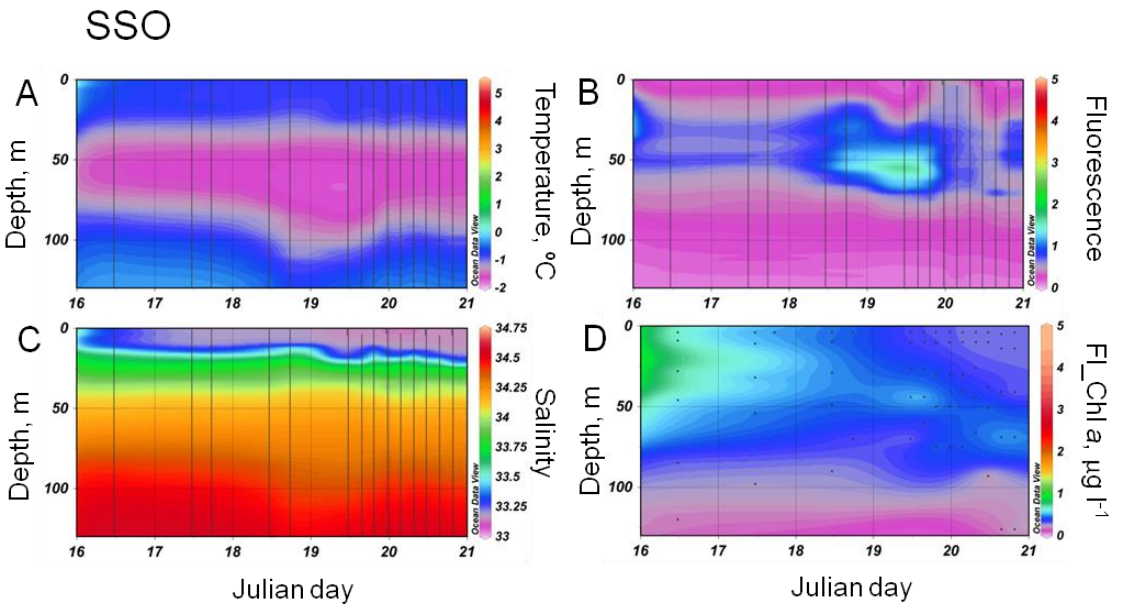

Figure 4. Variability of (A) temperature (ºC), (B) fluorescence (arbitray units), (C) salinity and (D) fluorometric Chl *a* (Fl_Chl *a*, µg l-3) during the visit to the SSO (South of the South Orkney Islands) region. Figure produced with the Ocean Data View software (Schlitzer, 2016).

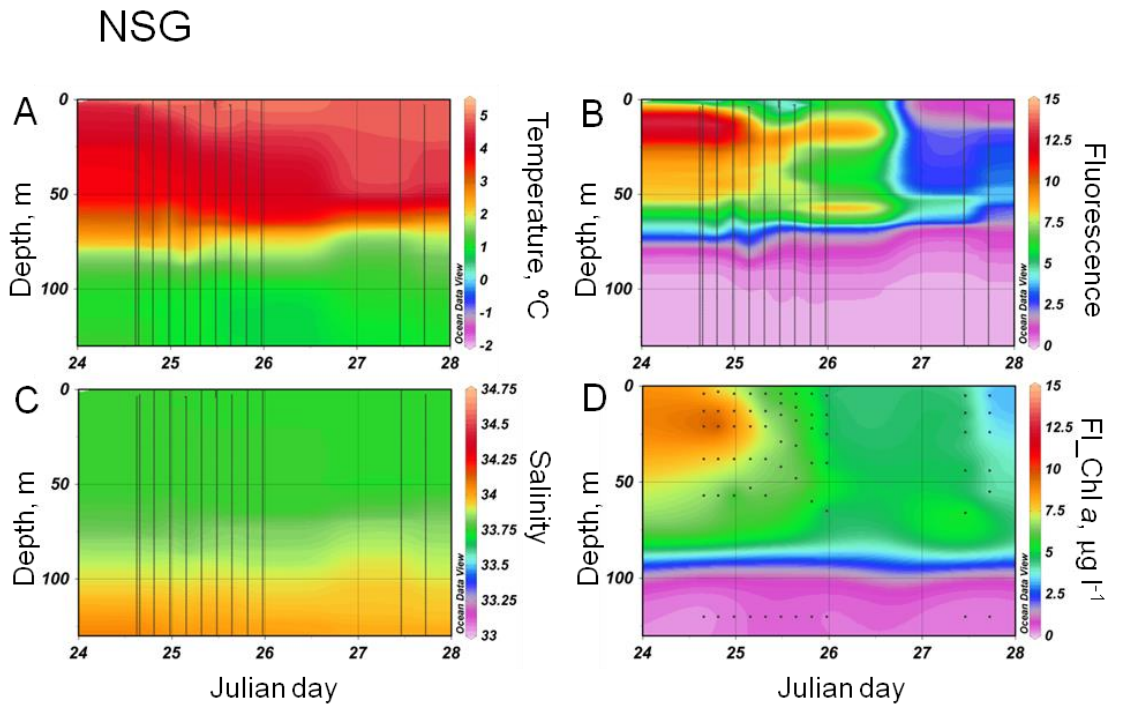

Figure 5. Variability of (A) temperature (ºC), (B) fluorescence (arbitray units), (C) salinity and (D) fluorometric Chl *a* (Fl_Chl *a*, µg l-3) during the visit to the NSG (Northwest of South Georgia Island) region. Figure produced with the Ocean Data View software (Schlitzer, 2016).

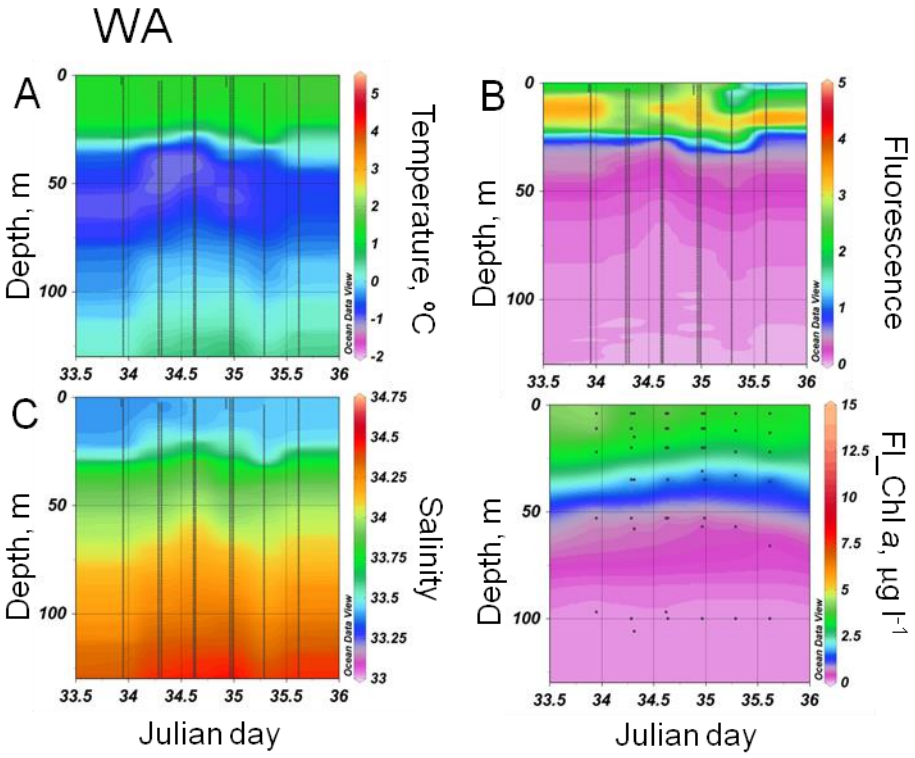

Figure 6. Variability of (A) temperature (ºC), (B) fluorescence (arbitray units), (C) salinity and (D) fluorometric Chl *a* (Fl_Chl a, µg l-3) during the visit to the WA (West of Anvers Island) region.

4.3.2. Phytoplankton pigments

Mean Fl_Chl *a* concentrations at surface (Table 2) ranged (mean ± SD) from 0.32 ± 0.06 µg L^{-1} at SSO to 5.05 ± 1.98 µg L^{-1} at NSG, with intermediate values for NSO (1.95 ± 0.17 µg L^{-1}) and WA (4.05 ± 0.48 µg L^{-1}). Integrated Fl_Chla values (0–100 m depth) were 33.6 ± 6.2 mg m^{-2} for SSO, 119.8 ± 11 mg m^{-2} for NSO, 132 ± 22.6 mg m^{-2} for WA and 516.8 ± 149.8 mg m^{-2} for NSG. The vertical distribution of Fl_Chl *a* (Figs. 3D, 4D, 5D, 6D and S2) was fairly homogeneous troughout the mixed layer in NSO and NSG, tended to attain the highest values at surface (4 m depth) in WA and presented weak subsurface maxima below the MLD in SSO. In contrast with *in vivo* fluorescence, Fl_Chl *a* did not present marked surface minima. The ratio Fluo/Fl_Chl *a* between in vivo fluorescence (Fluo) and Fl_Chl *a* for the two upper sampling depths showed appreciable circadian variability, with lower values around noon in all regions, as

higlighted by significant 2-degree polynomial regressions (Fig. S3A), while for the deeper samples there were no comparable significant relationships (Fig. S3B).

There was a good correlation between Fl_Chl *a* and T_Chl *a* as determined by HPLC (Fl_Chl *a* = 1.65 *T_Chl *a* + 0.30, n = 268, r^2 = 0.83, p <0.0001) (Fig. S4), although the Fl_Chl *a* values were higher than the corresponding T_Chl *a* ones. Excluding monovinyl Chl *a* (MV-Chl *a*) and the phaeopigments, the most abundant pigments (Table 1, Fig. S5) according to their vertically-integrated values were fucoxanthin (Fuco), chlorophyll *c*2 (Chl *c*2), 19-butanoyloxyfucoxanthin (19-But) and 19'-hexanoyloxyfucoxanthin (19-Hex) in NSO; 19-Hex, Fuco, diadinoxanthin (Ddx) and Chl *c*2 in SSO; Fuco, Chl *c*2, chlorophyll *c*3 (Chl *c*3) and Ddx in NSG, and finally alloxanthin (Allo), Fuco, Chl *c*2 and 19-Hex in WA. Fuco was dominant at all depths in NSO and NSG, while 19-Hex and Allo were more abundant from 4 m down to 22-41 m depth at SSO and to 11-15 m at WA, respectively (data not shown).

The ratio Ddx/LHC, between the concentration of the photoprotective carotenoid Ddx and the sum of the concentrations of the chromophyte light-harvesting carotenoids 19-But, 19-Hex, Fuco and Per, decreased strongly below 20-40 m depth in all regions and presented the highest values in the upper mixed layer of SSO (Table 3, Fig. S6A, B). The circadian variability of Ddx/LHC in surface waters was fairly small, with slightly higher noon values in SSO and WA (Fig. S6C).

The average values for each region of the ratio between the sum of pheophorbides and phaeophytines and T_Chl *a* (Phaeo/T_Chl *a*) for the two shallower sampling levels of the stations ranged from 10% at WA to 22% at NSG (Table 3). Phaeo/T_Chl *a* was relatively homogeneous in the upper water layers but increased considerably below 50 m at NSG and WA and in the deeper samples of NSO and SSO (Fig. S7).

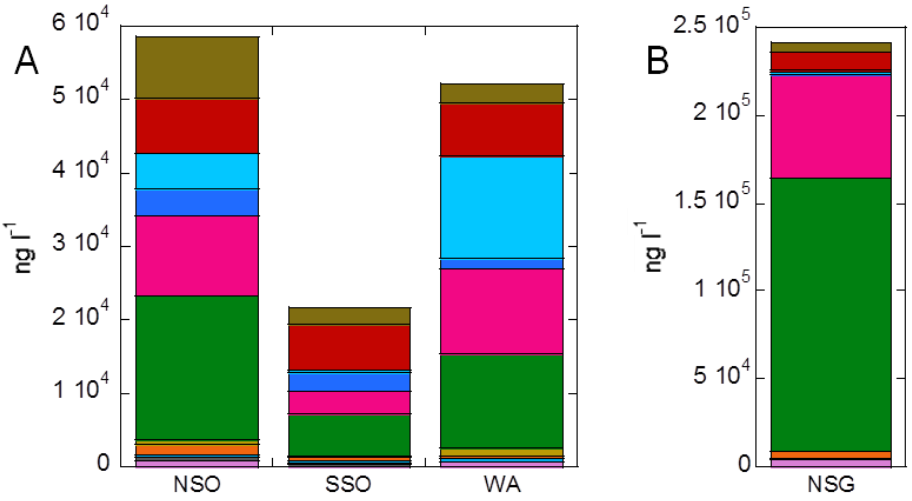

Figure 7. Biovolume of selected taxa and major phytoplankton groups in the surface (4 m) and subsurface (deep) samples taken in the four study regions. NSO = North of the South Orkney Islands, SSO = South of the South Orkney Islands, NSG = Northwest of South Georgia Island,WA = West of Anvers Island.

4.3.3. Phytoplankton assemblages.

A total of 116 taxa, including several microzooplankton groups (such as ciliates and radiolaria), were identified by optical microscopy in the surface and subsurface phytoplankton samples of the different stations. For each region, the average abundance and biovolume of the most important taxa (in terms of biovolume) that were present in at least 25% of the samples are presented in Table S3; the biovolume contribution of some selected taxa and major groups is shown in Fig. 7. The temporal variability of the Chl *a* contribution (hereafter, referred to as Chl *a* concentration) of the eight phytoplankton groups determined by CHEMTAX are shown in Figs. 8-11 and the corresponding average Chl *a* concentrations for each depth is shown in Fig. 12. Comparisons between the contribution to total Chl *a* of the chemotaxonomic groups and microscopy-estimated biovolumes could be attempted for diatoms, autotrophic (and mixotrophic) dinoflagellates and cryptophytes (Fig. S8). The relationship was

significant for all three groups (diatoms, $r^2 = 0.68$; autotrophic dinoflagellates, $r^2 = 0.23$; cryptophytes, $r^2 = 0.68$, $p < 0.0001$; $N = 105$, $p < 0.0001$ for all groups).

The four studied regions presented marked differences in phytoplankton composition. Cryptophytes, wich decreased with depth, and diatoms, which showed the opposite pattern, were the most abundant CHEMTAX groups at NSO, followed by haptophytes types 6 + 7, *Phaeocystis* and pelagophytes (figs. 8, 12); the most important taxa in the surface microscopy samples (Table S3; Fig. 7) were the diatoms *Corethron pennatum*, *Thalassiosira* spp. (small) and *Fragilariopsis* spp., heterotrophic *Gyrodinium* spp. and large and small (< 20 µm) unidentified dinoflagellates, cryptophytes and nanoflagellates; at depth there were more diatoms and less dinoflagellates and cryptophytes (Table S3, Figs. 7, 8, 12). Haptophytes types 6 + 7, followed by diatoms and *Phaeocystis*, both of which increased their contribution deeper in the water column, were the most important CHEMTAX groups at SSO (Figs. 9, 12). This region presented a combination of microscopy taxa similar to that of NSO (Table S3, Fig. 7), but with lower *C. pennatum* and *Thalassiosira* spp. (small), and higher *Fragilariopsis* spp. abundances, and a smaller contribution of cryptophytes; as at NSO, diatoms were relatively more important at depth (Table S3, Figs. 7, 9, 12). NSG, the zone with highest T_Chl *a* concentration, was dominated by diatoms at all depths, both in terms of CHEMTAX-derived Chl *a* and of phytoplankton abundance and biovolume (Figs. 7, 10, 12), but the the warmer water body encountered after day 27 (Fig. 5) was associated to a marked change in the phytoplankton composition, with higher concentrations of chlorophytes and *Phaeocystis* and lower concentrations of the other CHEMTAX groups. The main microscopy taxa both at surface and subsurface levels (Table S3) were *Eucampia antarctica*, *Fragilariopsis kerguelensis*, *Thalassiosira* spp. small, *Thalassiosira* and *Porosira* spp., *Odontella weissflogii* and *Trichotoxon reinboldii*, but

there was also a substantial contribution of nanoflagellates. In turn, coccolithophores were practically only present in this region. The main CHEMTAX groups at WA (Figs. 11-12) were cryptophytes and haptophytes types 6 + 7 at the shallowest layers, and haptophytes, diatoms and prasinophytes at depth (below 22 m), while microscopic observations (Table S3, Fig. 7) revealed cryptophytes and nanoflagellates, heterotrophic *Gyrodinium* spp., unidentified dinoflagellates and, in particular at the subsurface levels, diatoms such as *Eucampia antarctica*, *Fragilariopsis kerguelensis* and *Thalassiosira* spp. small. At stations 60 to 68, subsurface samples from 20 m depth presented a microscopy-estimated phytoplankton biovolume comparable to that at surface, while the deeper subsurface samples of stations 58 and 59 (taken from 53 and 35 m depth, respectively) showed a much lower biomass (Fig. 7).

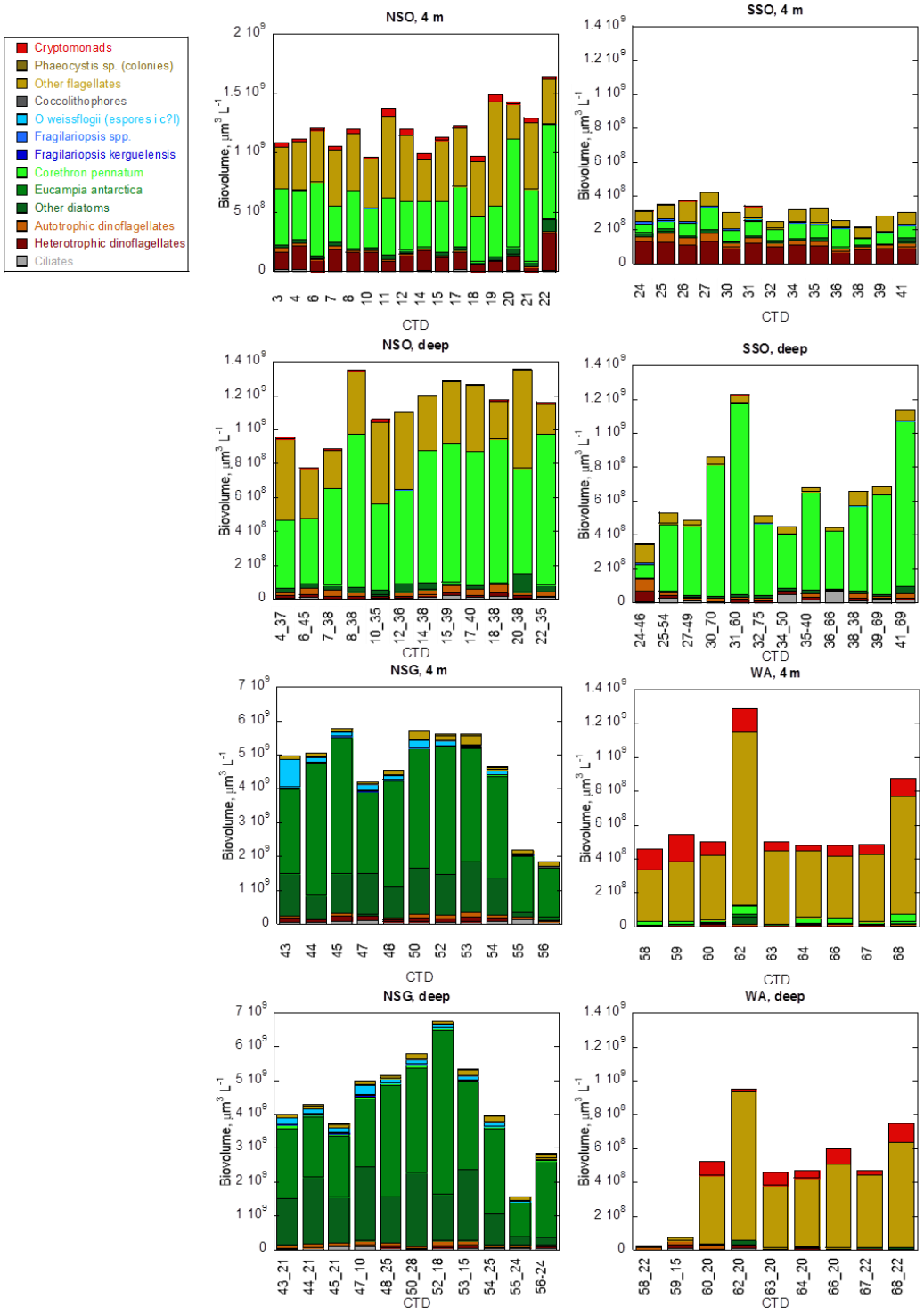

Figure 8. Temporal variation of the contribution to total chlorophyll a by the CHEMTAX-derived phytoplankton groups (in ng l−1) in the NSO (North of the South Orkney Islands) region. Figure produced using the Ocean Data View software (Schlitzer, 2016).

4.4. DISCUSSION

4.4.1. Microscope *vs* pigment-based quantification of phytoplankton taxa

Microscopic observations and the HPLC analysis of biomarker pigments followed by the CHEMTAX algorithm have been successfully used in many phytoplankton studies, either separately or complementing each other (Rodriguez et al., 2002; Kozlowski et al, 2011; Cassar et al., 2015; Mendes el al, 2012; Mendes et al 2017). Microscopy may provide more precise taxonomic classification but is biased towards relatively large forms (> 5 µm) of phytoplankton groups with identifiable morphological characteristics, is time-consuming and needs a high level of expertise. In contrast, HPLC / CHEMTAX tecniques can provide a comprehensive account of the main phytoplankton groups present in a particular sample, including those collected in oligotrophic areas (Roy et al., 2011). In the present work, we combined HPLC/CHEMTAX with microscopical observations of selected samples to obtain a robust and consistent view of the phytoplankton composition in the study zones. Comparisons between the two techniques must be interpreted with caution due to taxonomically and environmentally-related variability in biomarker pigments and Chl *a* content per biovolume and to problems in biovolume estimates and in the microscopical identification of naked and small-celled groups (Kozlowski et al., 2011; Cassar et al., 2015). In this work, we found significant relationships between microscopy and chemotaxonomy for diatoms, autotrophic dinoflagellates and cryptophytes (Fig. S8). A strong correlation (r^2 = 0.68) was observed for diatoms, although there were some points, all belonging to the same station, for which the biovolume estimate was substantially lower than the CHEMTAX estimate, a discrepancy which could be attributed to sampling variability, errors in microscopy or overestimation by CHEMTAX due to contribution to fucoxanthin from

unidentified nanoplankton (Cassar et al., 2015). The correlation (r^2 = 0.23) was lower for autotrophic dinoflagellates, a finding that could be attributed to errors in the classification of auto- or heterotrophic forms and to the presence of peridinin-lacking species (Garibotti et al., 2003). The correlation coefficient (r^2 = 0.68) was relatively high for cryptophytes, but there was a disagreement between the two methods concerning their relative contribution to the phytoplankton community, especially at NSO (global average of 2% for microscopy vs 24% for CHEMTAX), an inconsistency which is likely to be caused by underestimation of the cryptophytes in the microscopic samples, as noted also by Rodríguez et al. (2002) and Cassar et al. (2015). A coarse check of those biovolume vs. Chl *a* relationships (ignoring intercept values) could be obtained from calculations of a theoretical Chl *a* to biovolume ratios, which could be estimated using a standard C/Chl *a* ratio of 50 and the C to biovolume equations from Table 2 of Davies et al. (2016). For cells between 5 and 20 µm of diameter this Chl *a*/biovolume value would span from $8.0*10^{-7}$ to $1.8*10^{-6}$ (ng μm^{-3}) for diatoms, $2.3*10^{-6}$ to $4.9*10^{-6}$ for dinoflagellates and $2.3*10^{-6}$ to $2.9*10^{-6}$ for cryptophytes ("others"), slightly above the slopes (Fig. S8) obtained from our field samples for diatoms ($6.4*10^{-7}$) and dinoflagellates ($1.35*10^{-6}$), and well below the values estimated for cryptophytes ($1.0*10^{-5}$), adding support to a possible underestimation of the latter by microscopy. The HPLC-CHEMTAX approach used in our study provided a comprehensive analysis of the phytoplankton composition and highlighted the importance of groups like cryptophytes, chlorophytes, haptophytes types 6 + 7, *Phaeocystis*, pelagophytes and prasinophytes in the global community (Fig. 13). Organisms of these groups tend to deteriorate easily in fixed samples and are difficult to identify by microscopy. In particular, cryptophytes were more important at NSO, SSO and WA than suggested by the microscopic observations, probably due to underestimation in the microscopic

observations as discussed above, while most forms from the other groups that endured fixation became presumably pooled into nano- or microflagellate categories. The detection of *Phaeocystis* by HPLC but not by microscopy could be explained the presence of non-colonial forms of *Phaeocystis* spp., which would have been counted as unidentified flagellates.

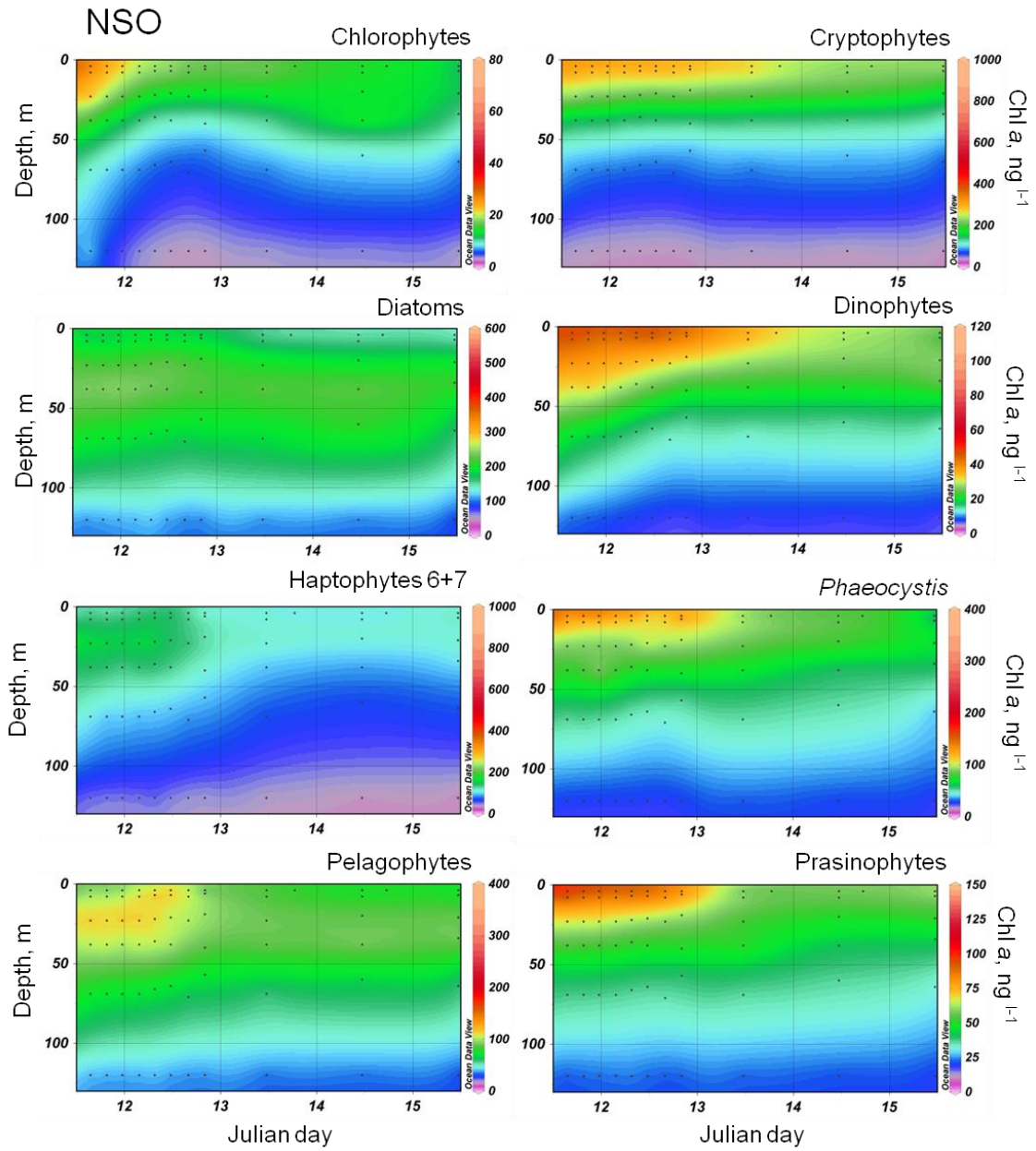

Figure 8. Temporal variation of the contribution to total chlorophyll a by the CHEMTAX-derived phytoplankton groups (in ng l−1) in the NSO (North of the South Orkney Islands) region. Figure produced using the Ocean Data View software (Schlitzer, 2016).

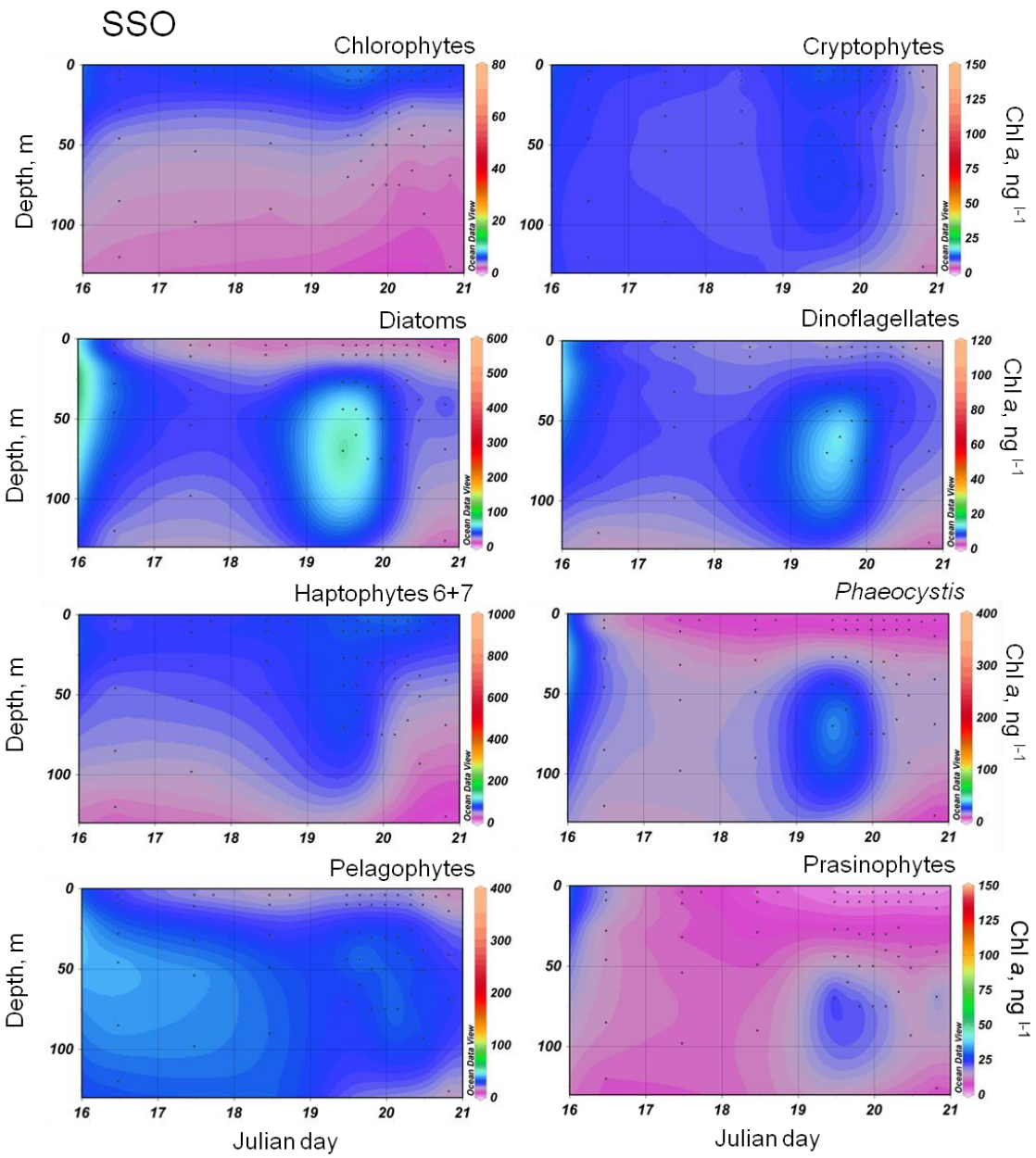

Figure 9. Temporal variation of the contribution to total chlorophyll a by the CHEMTAX-derived phytoplankton groups (in ng l−1) in the SSO (South of the South Orkney Islands) region. Figure produced using the Ocean Data View software (Schlitzer, 2016).

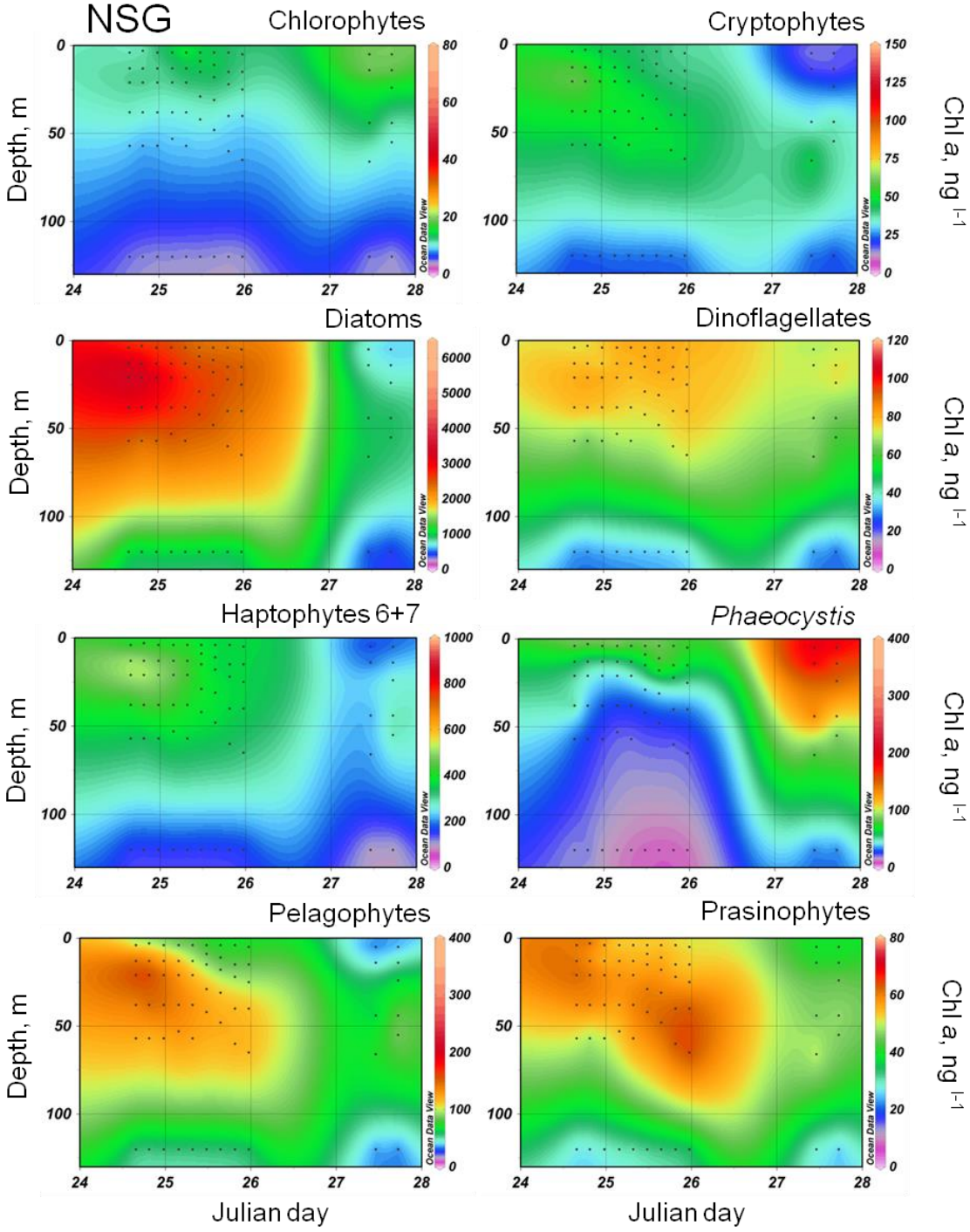

Figure 10. Temporal variation of the contribution to total chlorophyll a by the CHEMTAX-derived phytoplankton groups (in ng l−1) in the NSG (Northwest of South Georgia Island) region. Figure produced using the Ocean Data View software (Schlitzer, 2016).

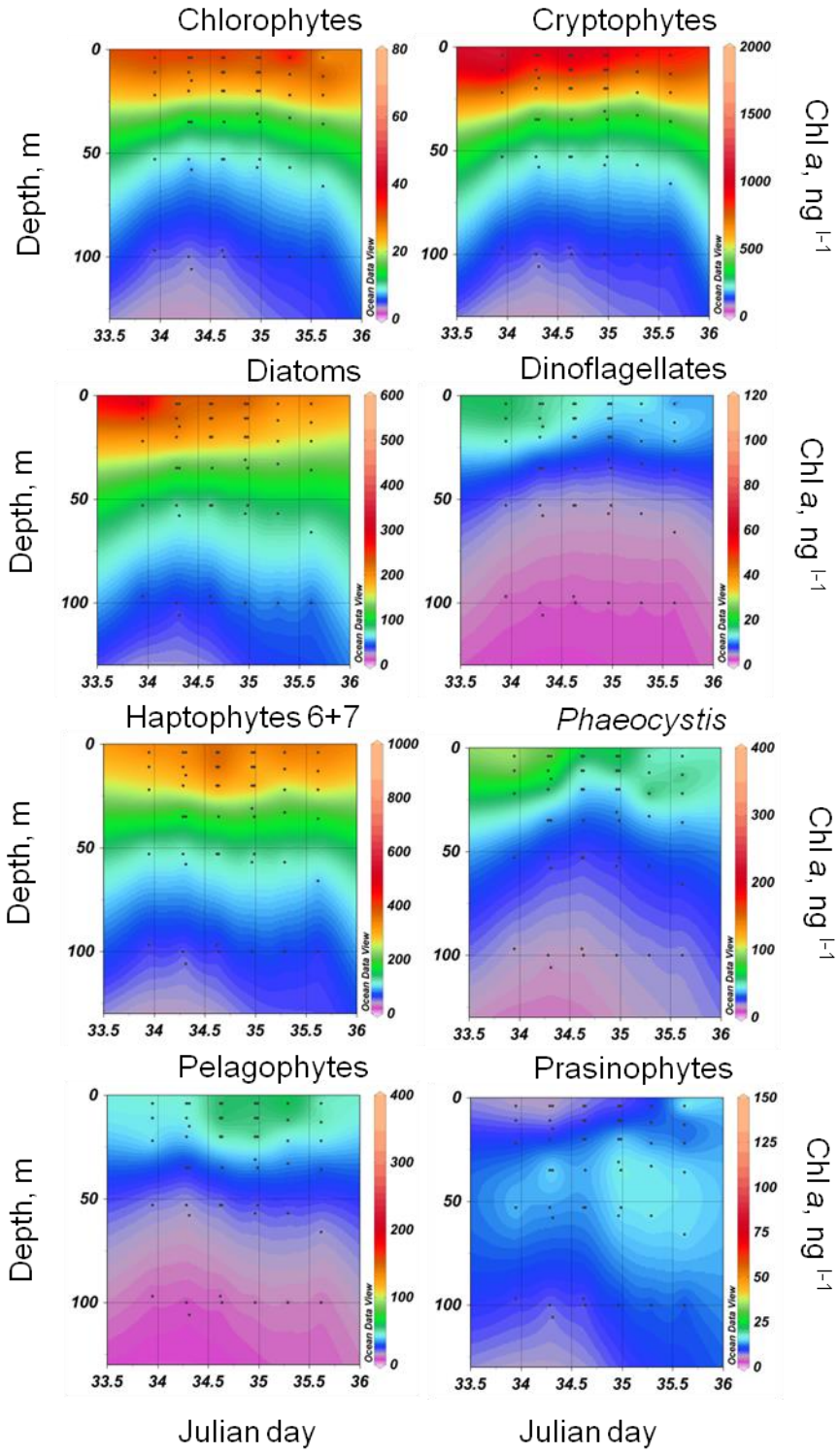

Figure 11. Temporal variation of the contribution to total chlorophyll a by the CHEMTAX-derived phytoplankton groups (in ng l−1) in the WA (West of Anvers Island) region. Figure produced using the Ocean Data View software (Schlitzer, 2016).

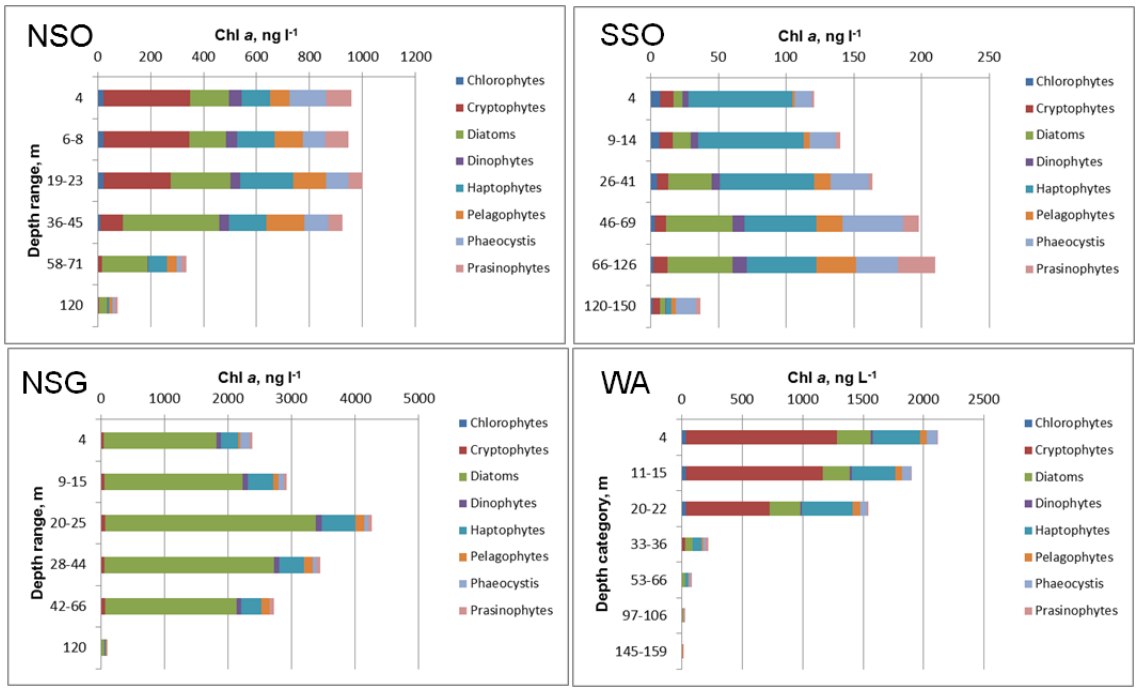

Figure 12. Vertical distribution of the mean contribution to total chlorophyll a by the CHEMTAX-derived phytoplankton groups (in ng l−1) in the four study regions. NSO = North of the South Orkney Islands, SSO = South of the South Orkney Islands, NSG = Northwest of South Georgia Island, WA = West of Anvers Island.

4.4.2. Phytoplankton assemblages and their drivers

The four zones visited in this study encompassed a wide spectrum of hydrographic and biological characteristics. NSG was placed between the Polar Front and the Southern ACC Front (SACCF), in a region characterized by the regular occurrence of spring and summer phytoplankton blooms, fuelled by the high concentrations of major nutrients and the availability of iron contributed by the ACC after its passage over the shelf waters around South Georgia (Korb et al., 2004; Whitehouse et al., 2008; Nielsdóttir et al., 2012). The relatively high temperatures in this region (mean ± SD, 4.73ºC ± 0.44) in comparison with other SO areas may also contribute to enhanced phytoplankton proliferation (Korb et al., 2004). The PEGASO stations were outside the main bloom area as seem from satellite imagery (Borrione and Schlitzer, 2013), but presented high Chl *a* concentrations (Tables 1 and 2, Figs. 5 and 12). Moderately lower nitrate and

phosphate and much lower silicate concentrations at NSG than in the zones around the South Orkney Islands were consistent with a phytoplankton community dominated by well-silicified diatoms like *Eucampia antarctica*, *Thalassiosira* and *Porosira* spp. and *Odontella weissflogii*, typical of blooms in the area (Atkinson et al., 2001), complemented by substantial populations of haptophytes, including coccolithophores, and pelagophytes, as shown by our microscopy and HPLC-CHEMTAX analyses. However, at the time of our visit, the deep mixing layer of about 50 m compared with an average euphotic depth of 26 m (Table 2), and the relatively low silicate concentrations (average of 2 ± 0.4 µM at surface, Table 2) at the threshold for diatom dominance (Egge and Aksnes, 1992; Atkinson et al., 2001) were probably restricting phytoplankton growth.

The other three regions visited in this study, NSO, SSO and WA presented macronutrient-replete conditions and integrated T_Chl *a* concentrations ranging from 20.8 mg m^{-2} at SSO to 60 and 67 mg m^{-2} at WA and NSO, respectively (Tables 1, 2). Surface silicate concentrations exceeded 47 µM in all three regions (Table 2), reflecting a relatively low diatom contribution (Figs. 7 and 12). Lack of macronutrient depletion is typical of iron-limited regions of the SO (Venables et al., 2010). However, marine areas in the vicinity of islands and the West Antarctic Peninsula region may benefit from some benthic supply of iron from continental shelves (Nielsdóttir et al., 2012), a situation that can explain the relatively high Chl *a* concentrations in NSO and WA (Nielsdóttir et al., 2012; Murphy et al., 2013).

The main nano- and microplankton forms recorded by microscopy in NSO and SSO included the diatoms *Corethron pennatum* and *Fragilariopsis* spp., heterotrophic dinoflagellates like *Gyrodinium* spp. and *Protoperidinium* spp., unidentified autotrophic dinoflagellates, nanoflagellates and cryptophytes, all of which have been recorded in the

region. Some differences, like the higher proportion of *Fragilariopsis* spp. in SSO could be attributed to the stronger sea ice influence (Cefarelli et al., 2010) in this zone. In transects across the Scotia Sea, from the vicinity of South Georgia to the South Orkney Islands, Korb et al. (2010) noted the abundance of *Corethron pennatum* and *Fragilariopsis* spp. and suggested that iron limitation could account for the high proportion of heterotrophic dinoflagellates, in agreement with our findings at SSO. On the other hand, some microscopy-based surveys in the South Orkney region encountered a dominance of cryptophytes, prasinophytes and other nanoflagellates (Kopczyńska, 1991; Nielsdóttir et al., 2012). At WA, our CHEMTAX results highlighted the dominance of flagellates like cryptophytes and haptophytes 6 + 7, in agreement with the microscopic observations, which showed a high contribution of unidentified flagellates and cryptophytes, while diatoms, represented mainly by *Corethron pennatum* and small pennates, and dinoflagellates, with heterotrophic *Gyrodinium* spp. and unidentified small forms, were scarce. Several studies have shown the association of cryptophyte populations with shallow mixed layers influenced by ice melting (Schloss and Estrada, 1994; Mendes et al., 2017) and a shift from diatoms to cryptophytes has been described as characteristic of the seasonal phytoplankton succession in the West Antarctic Peninsula region (Garibotti et al., 2003; Moline et al., 2004; Ducklow et al., 2007; Murphy et al., 2013). The gradient of increased T_Chl *a* concentrations and cryptophyte contribution from SSO to NSO and WA was associated with increased temperatures (Fig. S9), suggesting that it could be related, at least in part, to seasonal succession.

An examination of the vertical distribution of the different phytoplankton categories reveals some consistent trends in the different study zones. Some groups, like haptophytes types 6 + 7 and *Phaeocystis* did not show marked vertical gradients within

the euphotic zone. Cryptophytes, as noted above, tended to be more important in surface layers, while diatoms and pelagophytes increased their contribution at subsurface levels (Fig. 12). The ability of diatoms to thrive in relatively low light environments has been noted by a number of authors and has been attributed to features such as increased efficiency of ATP production (Fisher and Halsey, 2016). The increased abundance of pelagophytes in subsurface layers agrees with the observations of Latasa et al. (2017), who noted their preference for deeper levels within the deep chlorophyll maximum.

4.4.3. Ecophysiological hints from pigment composition

The mid-day decline of the ratio Fluo/Fl_Chl *a* (Fig. S3A) for the shallow samples is a common finding (Estrada et al., 1996; Mignot et al., 2011) and has been related to non-photochemical fluorescence quenching processes (Falkowski and Kolber, 1995; Sackmann et al., 2008), which in turn are influenced by factors such as community and pigment composition, and nutrient and light conditions. In our data set, the variability of the Fluo/Fl_Chl *a* ratio was particularly marked for SSO (Fig. S3). This was the region with lowest beam attenuation coefficients and the highest average $Z_{1\%}$/MLD relationship (Table 2), suggesting a higher potential for fluorescence quenching.

Consistent with the variation of specific fluorescence, the highest values of the ratio Ddx/LHC, indicative of the proportion of the photoprotective pigment Ddx with respect to the sum of the light-harvesting carotenoids 19-But, 19-Hex, Fuco and Per, were found throughout the shallow mixed layer of SSO (Fig. S6); at NSO, NSG and WA, the ratios were lower and started to decrease with depth within the upper part of the mixed layer, suggesting a faster time scale of photoacclimation relative to that of vertical mixing in the mixed layer of these regions. The surface Ddx/LHC ratio (Fig. S6A, B) decreased with increasing MLD (Fig. S6D) and beam attenuation coefficient (data not

shown), and was positively associated (r^2 = 0.78, N = 35, p < 0.0001) with $Z_{1\%}$ (Fig. 13) in agreement with the expected enhancement of photoprotective pigment concentration with increased exposure to a relatively high irradiance environment (Goericke and Montoya, 1997; Cheah et al., 2017).

We found a rather high Phaeo/T_Chl *a* (Table 3) at all four regions (Table 3, Fig. S7); although no grazing data are available, this observation could be related to an important contribution of herbivory, as noted by Mendes et al. (2015).

4.5. CONCLUSION

As part of the PEGASO project, the aim of this work was to characterize the planktonic community of the study areas, in order to investigate its role in controlling the emission of trace gases, semivolatile organics and microgels from the marine surface. Microscopical observations and chemotaxonomic pigment analyses were used to ascertain the quantitative and qualitative composition of the phytoplankton in four contrasting regions in the vicinity of South Georgia (NSG), the South Orkneys (NSO and SSO) and Anvers Islands (WA). Our findings confirmed previous observations such as the dominance of diatoms in the iron-rich South Georgia bloom region and the association of cryptophytes with well-illuminated stratified surface waters influenced by ice melting, but also highlighted the subtantial contribution of less well-studied forms such as the pelagophytes, important components of the picoplankton. The light stress condition of the phytoplankton community, an ecophysiological factor that is an important modulators of DMS metabolism (Bell et al., 2010) was investigated by means of a photoprotective pigment index, which showed the highest values at SSO, the region with the shallowest mixed layer and the deepest euphotic zone.

SUPLEMENTARY MATERIAL

Table S1. Position, date, time and sampled depths of the PEGASO stations considered in this work. Regions are (See Fig. 1): NSO = North of the South Orkney Islands, SSO = South of the South Orkney Islands, NSG = Northwest of South Georgia Island, WA = West of Anvers Island. *Time of 2 February 2015.

Region	Station number	Latitude ºN	Longitude ºE	Date Day	Month	Year	UTC time h	Solar time h	Sampled depths m
NSO	3	-60.002	-46.088	10	January	2015	14.88	11.68	4
NSO	4	-60.008	-46.040	10	January	2015	17.52	14.32	4
NSO	4	-60.008	-46.040	10	January	2015	17.52	14.32	8
NSO	4	-60.008	-46.040	10	January	2015	17.52	14.32	22
NSO	4	-60.008	-46.040	10	January	2015	17.52	14.32	37
NSO	4	-60.008	-46.040	10	January	2015	17.52	14.32	68
NSO	4	-60.008	-46.040	10	January	2015	17.52	14.32	120
NSO	6	-59.587	-46.010	11	January	2015	11.37	8.17	6
NSO	6	-59.587	-46.010	11	January	2015	11.37	8.17	19
NSO	6	-59.587	-46.010	11	January	2015	11.37	8.17	45
NSO	6	-59.587	-46.010	11	January	2015	11.37	8.17	58
NSO	6	-59.587	-46.010	11	January	2015	11.37	8.17	120
NSO	7	-59.585	-46.027	11	January	2015	15.50	12.30	4
NSO	7	-59.585	-46.027	11	January	2015	15.50	12.30	8
NSO	7	-59.585	-46.027	11	January	2015	15.50	12.30	38
NSO	7	-59.585	-46.027	11	January	2015	15.50	12.30	23
NSO	7	-59.585	-46.027	11	January	2015	15.50	12.30	69
NSO	7	-59.585	-46.027	11	January	2015	15.50	12.30	120
NSO	8	-59.594	-46.009	11	January	2015	19.55	16.35	4

NSO	8	-59.594	-46.009	11	January	2015	19.55	16.35	8
NSO	8	-59.594	-46.009	11	January	2015	19.55	16.35	23
NSO	8	-59.594	-46.009	11	January	2015	19.55	16.35	38
NSO	8	-59.594	-46.009	11	January	2015	19.55	16.35	69
NSO	8	-59.594	-46.009	11	January	2015	19.55	16.35	120
NSO	10	-59.593	-45.593	11	January	2015	23.45	20.25	4
NSO	10	-59.593	-45.593	11	January	2015	23.45	20.25	8
NSO	10	-59.593	-45.593	11	January	2015	23.45	20.25	23
NSO	10	-59.593	-45.593	11	January	2015	23.45	20.25	38
NSO	10	-59.593	-45.593	11	January	2015	23.45	20.25	69
NSO	10	-59.593	-45.593	11	January	2015	23.45	20.25	120
NSO	11	-59.594	-45.582	12	January	2015	3.65	0.45	4
NSO	11	-59.594	-45.582	12	January	2015	3.65	0.45	8
NSO	11	-59.594	-45.582	12	January	2015	3.65	0.45	35
NSO	11	-59.594	-45.582	12	January	2015	3.65	0.45	23
NSO	11	-59.594	-45.582	12	January	2015	3.65	0.45	69
NSO	11	-59.594	-45.582	12	January	2015	3.65	0.45	120
NSO	12	-59.596	-45.550	12	January	2015	7.55	4.35	4
NSO	12	-59.596	-45.550	12	January	2015	7.55	4.35	7
NSO	12	-59.596	-45.550	12	January	2015	7.55	4.35	22
NSO	12	-59.596	-45.550	12	January	2015	7.55	4.35	36
NSO	12	-59.596	-45.550	12	January	2015	7.55	4.35	66
NSO	12	-59.596	-45.550	12	January	2015	7.55	4.35	120
NSO	14	-59.594	-45.550	12	January	2015	11.53	8.33	4
NSO	14	-59.594	-45.550	12	January	2015	11.53	8.33	7
NSO	14	-59.594	-45.550	12	January	2015	11.53	8.33	21
NSO	14	-59.594	-45.550	12	January	2015	11.53	8.33	38

NSO	14	-59.594	-45.550	12	January	2015	11.53	8.33	64
NSO	14	-59.594	-45.550	12	January	2015	11.53	8.33	120
NSO	15	-59.595	-45.550	12	January	2015	15.97	12.77	4
NSO	15	-59.595	-45.550	12	January	2015	15.97	12.77	8
NSO	15	-59.595	-45.550	12	January	2015	15.97	12.77	39
NSO	15	-59.595	-45.550	12	January	2015	15.97	12.77	23
NSO	15	-59.595	-45.550	12	January	2015	15.97	12.77	71
NSO	15	-59.595	-45.550	12	January	2015	15.97	12.77	120
NSO	17	-60.006	-45.527	12	January	2015	20.08	16.88	4
NSO	17	-60.006	-45.527	12	January	2015	20.08	16.88	6
NSO	17	-60.006	-45.527	12	January	2015	20.08	16.88	19
NSO	17	-60.006	-45.527	12	January	2015	20.08	16.88	40
NSO	17	-60.006	-45.527	12	January	2015	20.08	16.88	57
NSO	17	-60.006	-45.527	12	January	2015	20.08	16.88	120
NSO	18	-60.041	-45.461	13	January	2015	11.48	8.28	4
NSO	18	-60.041	-45.461	13	January	2015	11.48	8.28	8
NSO	18	-60.041	-45.461	13	January	2015	11.48	8.28	23
NSO	18	-60.041	-45.461	13	January	2015	11.48	8.28	38
NSO	18	-60.041	-45.461	13	January	2015	11.48	8.28	69
NSO	18	-60.041	-45.461	13	January	2015	11.48	8.28	120
NSO	19	-60.611	-45.453	13	January	2015	18.53	15.33	4
NSO	20	-60.034	-45.397	14	January	2015	11.38	8.18	4
NSO	20	-60.034	-45.397	14	January	2015	11.38	8.18	8
NSO	20	-60.034	-45.397	14	January	2015	11.38	8.18	20
NSO	20	-60.034	-45.397	14	January	2015	11.38	8.18	38
NSO	20	-60.034	-45.397	14	January	2015	11.38	8.18	60
NSO	20	-60.034	-45.397	14	January	2015	11.38	8.18	120

NSO	21	-60.037	-45.405	14	January	2015	17.42	14.22	4
NSO	22	-60.040	-45.404	15	January	2015	11.38	8.18	4
NSO	22	-60.040	-45.404	15	January	2015	11.38	8.18	7
NSO	22	-60.040	-45.404	15	January	2015	11.38	8.18	21
NSO	22	-60.040	-45.404	15	January	2015	11.38	8.18	35
NSO	22	-60.040	-45.404	15	January	2015	11.38	8.18	64
NSO	22	-60.040	-45.404	15	January	2015	11.38	8.18	120
SSO	24	-61.114	-43.013	16	January	2015	11.47	8.36	4
SSO	24	-61.114	-43.013	16	January	2015	11.47	8.36	9
SSO	24	-61.114	-43.013	16	January	2015	11.47	8.36	28
SSO	24	-61.114	-43.013	16	January	2015	11.47	8.36	46
SSO	24	-61.114	-43.013	16	January	2015	11.47	8.36	85
SSO	24	-61.114	-43.013	16	January	2015	11.47	8.36	120
SSO	25	-61.224	-43.468	17	January	2015	11.42	8.31	4
SSO	25	-61.224	-43.468	17	January	2015	11.42	8.31	11
SSO	25	-61.224	-43.468	17	January	2015	11.42	8.31	32
SSO	25	-61.224	-43.468	17	January	2015	11.42	8.31	54
SSO	25	-61.224	-43.468	17	January	2015	11.42	8.31	98
SSO	25	-61.224	-43.468	17	January	2015	11.42	8.31	140
SSO	26	-61.195	-43.471	17	January	2015	17.42	14.31	4
SSO	27	-61.184	-43.576	18	January	2015	11.15	8.04	4
SSO	27	-61.184	-43.576	18	January	2015	11.15	8.04	29
SSO	27	-61.184	-43.576	18	January	2015	11.15	8.04	10
SSO	27	-61.184	-43.576	18	January	2015	11.15	8.04	49
SSO	27	-61.184	-43.576	18	January	2015	11.15	8.04	90
SSO	27	-61.184	-43.576	18	January	2015	11.15	8.04	150
SSO	27	-61.146	-44.002	18	January	2015	17.52	14.41	4

SSO	30	-61.136	-43.543	19	January	2015	11.47	8.36	4
SSO	30	-61.136	-43.543	19	January	2015	11.47	8.36	10
SSO	30	-61.136	-43.543	19	January	2015	11.47	8.36	27
SSO	30	-61.136	-43.543	19	January	2015	11.47	8.36	44
SSO	30	-61.136	-43.543	19	January	2015	11.47	8.36	70
SSO	30	-61.136	-43.543	19	January	2015	11.47	8.36	150
SSO	31	-61.138	-43.560	19	January	2015	15.60	12.49	4
SSO	31	-61.138	-43.560	19	January	2015	15.60	12.49	19
SSO	31	-61.138	-43.560	19	January	2015	15.60	12.49	27
SSO	31	-61.138	-43.560	19	January	2015	15.60	12.49	44
SSO	31	-61.138	-43.560	19	January	2015	15.60	12.49	60
SSO	32	-61.139	-43.542	19	January	2015	19.28	16.17	4
SSO	32	-61.139	-43.542	19	January	2015	19.28	16.17	10
SSO	32	-61.139	-43.542	19	January	2015	19.28	16.17	30
SSO	32	-61.139	-43.542	19	January	2015	19.28	16.17	50
SSO	32	-61.139	-43.542	19	January	2015	19.28	16.17	75
SSO	32	-61.139	-43.542	19	January	2015	19.28	16.17	150
SSO	34	-61.134	-43.507	19	January	2015	23.53	20.42	4
SSO	34	-61.134	-43.507	19	January	2015	23.53	20.42	10
SSO	34	-61.134	-43.507	19	January	2015	23.53	20.42	30
SSO	34	-61.134	-43.507	19	January	2015	23.53	20.42	50
SSO	34	-61.134	-43.507	19	January	2015	23.53	20.42	75
SSO	34	-61.134	-43.507	19	January	2015	23.53	20.42	150
SSO	35	-61.137	-43.552	20	January	2015	3.57	0.46	4
SSO	35	-61.137	-43.552	20	January	2015	3.57	0.46	10
SSO	35	-61.137	-43.552	20	January	2015	3.57	0.46	30
SSO	35	-61.137	-43.552	20	January	2015	3.57	0.46	40

SSO	35	-61.137	-43.552	20	January	2015	3.57	0.46	75
SSO	35	-61.137	-43.552	20	January	2015	3.57	0.46	150
SSO	36	-61.153	-43.514	20	January	2015	7.60	4.49	4
SSO	36	-61.153	-43.514	20	January	2015	7.60	4.49	10
SSO	36	-61.153	-43.514	20	January	2015	7.60	4.49	26
SSO	36	-61.153	-43.514	20	January	2015	7.60	4.49	44
SSO	36	-61.153	-43.514	20	January	2015	7.60	4.49	66
SSO	36	-61.153	-43.514	20	January	2015	7.60	4.49	150
SSO	38	-61.146	-43.535	20	January	2015	11.43	8.32	4
SSO	38	-61.146	-43.535	20	January	2015	11.43	8.32	38
SSO	38	-61.146	-43.535	20	January	2015	11.43	8.32	10
SSO	38	-61.146	-43.535	20	January	2015	11.43	8.32	51
SSO	38	-61.146	-43.535	20	January	2015	11.43	8.32	93
SSO	38	-61.146	-43.535	20	January	2015	11.43	8.32	150
SSO	39	-61.142	-43.533	20	January	2015	15.52	12.41	4
SSO	39	-61.142	-43.533	20	January	2015	15.52	12.41	150
SSO	41	-61.156	-43.545	20	January	2015	19.63	16.52	4
SSO	41	-61.156	-43.545	20	January	2015	19.63	16.52	14
SSO	41	-61.156	-43.545	20	January	2015	19.63	16.52	41
SSO	41	-61.156	-43.545	20	January	2015	19.63	16.52	69
SSO	41	-61.156	-43.545	20	January	2015	19.63	16.52	126
SSO	41	-61.156	-43.545	20	January	2015	19.63	16.52	150
NSG	43	-50.148	-39.519	24	January	2015	15.77	13.62	4
NSG	43	-50.148	-39.519	24	January	2015	15.77	13.62	13
NSG	43	-50.148	-39.519	24	January	2015	15.77	13.62	21
NSG	43	-50.148	-39.519	24	January	2015	15.77	13.62	38
NSG	43	-50.148	-39.519	24	January	2015	15.77	13.62	57

NSG	43	-50.148	-39.519	24	January	2015	15.77	13.62	120
NSG	44	-50.154	-39.517	24	January	2015	19.45	17.30	4
NSG	44	-50.154	-39.517	24	January	2015	19.45	17.30	13
NSG	44	-50.154	-39.517	24	January	2015	19.45	17.30	21
NSG	44	-50.154	-39.517	24	January	2015	19.45	17.30	38
NSG	44	-50.154	-39.517	24	January	2015	19.45	17.30	57
NSG	44	-50.154	-39.517	24	January	2015	19.45	17.30	120
NSG	45	-50.163	-39.495	25	January	2015	23.53	21.38	4
NSG	45	-50.163	-39.495	25	January	2015	23.53	21.38	13
NSG	45	-50.163	-39.495	25	January	2015	23.53	21.38	21
NSG	45	-50.163	-39.495	25	January	2015	23.53	21.38	38
NSG	45	-50.163	-39.495	25	January	2015	23.53	21.38	57
NSG	45	-50.163	-39.495	25	January	2015	23.53	21.38	120
NSG	47	-50.157	-39.458	25	January	2015	3.73	1.58	4
NSG	47	-50.157	-39.458	25	January	2015	3.73	1.58	13
NSG	47	-50.157	-39.458	25	January	2015	3.73	1.58	20
NSG	47	-50.157	-39.458	25	January	2015	3.73	1.58	38
NSG	47	-50.157	-39.458	25	January	2015	3.73	1.58	57
NSG	47	-50.157	-39.458	25	January	2015	3.73	1.58	120
NSG	48	-50.155	-39.491	25	January	2015	7.67	5.52	4
NSG	48	-50.155	-39.491	25	January	2015	7.67	5.52	13
NSG	48	-50.155	-39.491	25	January	2015	7.67	5.52	20
NSG	48	-50.155	-39.491	25	January	2015	7.67	5.52	38
NSG	48	-50.155	-39.491	25	January	2015	7.67	5.52	57
NSG	48	-50.155	-39.491	25	January	2015	7.67	5.52	120
NSG	50	-50.168	-39.460	25	January	2015	11.60	9.45	4
NSG	50	-50.168	-39.460	25	January	2015	11.60	9.45	9

NSG	50	-50.168	-39.460	25	January	2015	11.60	9.45	15
NSG	50	-50.168	-39.460	25	January	2015	11.60	9.45	28
NSG	50	-50.168	-39.460	25	January	2015	11.60	9.45	42
NSG	50	-50.168	-39.460	25	January	2015	11.60	9.45	120
NSG	52	-50.163	-39.450	25	January	2015	15.50	13.35	4
NSG	52	-50.163	-39.450	25	January	2015	15.50	13.35	11
NSG	52	-50.163	-39.450	25	January	2015	15.50	13.35	18
NSG	52	-50.163	-39.450	25	January	2015	15.50	13.35	32
NSG	52	-50.163	-39.450	25	January	2015	15.50	13.35	48
NSG	52	-50.163	-39.450	25	January	2015	15.50	13.35	120
NSG	53	-50.168	-39.452	25	January	2015	19.53	17.38	4
NSG	53	-50.168	-39.452	25	January	2015	19.53	17.38	15
NSG	53	-50.168	-39.452	25	January	2015	19.53	17.38	22
NSG	53	-50.168	-39.452	25	January	2015	19.53	17.38	46
NSG	53	-50.168	-39.452	25	January	2015	19.53	17.38	60
NSG	53	-50.168	-39.452	25	January	2015	19.53	17.38	120
NSG	54	-50.174	-39.456	25	January	2015	23.42	21.27	4
NSG	54	-50.174	-39.456	25	January	2015	23.42	21.27	15
NSG	54	-50.174	-39.456	25	January	2015	23.42	21.27	25
NSG	54	-50.174	-39.456	25	January	2015	23.42	21.27	40
NSG	54	-50.174	-39.456	25	January	2015	23.42	21.27	65
NSG	54	-50.174	-39.456	25	January	2015	23.42	21.27	120
NSG	55	-50.208	-39.472	27	January	2015	11.10	8.95	4
NSG	55	-50.208	-39.472	27	January	2015	11.10	8.95	14
NSG	55	-50.208	-39.472	27	January	2015	11.10	8.95	44
NSG	55	-50.208	-39.472	27	January	2015	11.10	8.95	66
NSG	55	-50.208	-39.472	27	January	2015	11.10	8.95	120

NSG	56	-50.206	-39.491	27	January	2015	17.40	15.25	4
NSG	56	-50.206	-39.491	27	January	2015	17.40	15.25	14
NSG	56	-50.206	-39.491	27	January	2015	17.40	15.25	24
NSG	56	-50.206	-39.491	27	January	2015	17.40	15.25	44
NSG	56	-50.206	-39.491	27	January	2015	17.40	15.25	55
NSG	56	-50.206	-39.491	27	January	2015	17.40	15.25	120
WA	58	-64.322	-64.532	2	February	2015	11.38	6.82	4
WA	58	-64.322	-64.532	2	February	2015	11.38	6.82	11
WA	58	-64.322	-64.532	2	February	2015	11.38	6.82	22
WA	58	-64.322	-64.532	2	February	2015	11.38	6.82	53
WA	58	-64.322	-64.532	2	February	2015	11.38	6.82	97
WA	58	-64.322	-64.532	2	February	2015	11.38	6.82	146
WA	59	-64.324	-64.519	2	February	2015	15.75	11.19	4
WA	59	-64.324	-64.519	2	February	2015	15.75	11.19	15
WA	59	-64.324	-64.519	2	February	2015	15.75	11.19	35
WA	59	-64.324	-64.519	2	February	2015	15.75	11.19	58
WA	59	-64.324	-64.519	2	February	2015	15.75	11.19	106
WA	59	-64.324	-64.519	2	February	2015	15.75	11.19	150
WA	60	-64.315	-64.489	2	February	2015	19.43	14.87	4
WA	60	-64.315	-64.489	2	February	2015	19.43	14.87	11
WA	60	-64.315	-64.489	3	February	2015	19.43	14.87	20
WA	60	-64.315	-64.489	3	February	2015	19.43	14.87	53
WA	60	-64.315	-64.489	3	February	2015	19.43	14.87	97
WA	60	-64.315	-64.489	3	February	2015	19.43	14.87	150
WA	62	-64.304	-64.496	3	February	2015	23.87	19.31	4
WA	62	-64.304	-64.496	3	February	2015	23.87	19.31	11
WA	62	-64.304	-64.496	3	February	2015	23.87	19.31	20

WA	62	-64.304	-64.496	3	February	2015	23.87	19.31	35
WA	62	-64.304	-64.496	3	February	2015	23.87	19.31	53
WA	62	-64.304	-64.496	3	February	2015	23.87	19.31	100
WA	63	-64.302	-64.536	3	February	2015	3.42	22.86*	4
WA	63	-64.302	-64.536	3	February	2015	3.42	22.86*	11
WA	63	-64.302	-64.536	3	February	2015	3.42	22.86*	20
WA	63	-64.302	-64.536	3	February	2015	3.42	22.86*	35
WA	63	-64.302	-64.536	3	February	2015	3.42	22.86*	53
WA	63	-64.302	-64.536	3	February	2015	3.42	22.86*	100
WA	64	-64.296	-64.505	3	February	2015	7.62	3.06	4
WA	64	-64.296	-64.505	3	February	2015	7.62	3.06	11
WA	64	-64.296	-64.505	3	February	2015	7.62	3.06	22
WA	64	-64.296	-64.505	3	February	2015	7.62	3.06	53
WA	64	-64.296	-64.505	3	February	2015	7.62	3.06	97
WA	64	-64.296	-64.505	3	February	2015	7.62	3.06	100
WA	66	-64.288	-64.516	3	February	2015	11.58	7.02	4
WA	66	-64.288	-64.516	3	February	2015	11.58	7.02	11
WA	66	-64.288	-64.516	3	February	2015	11.58	7.02	20
WA	66	-64.288	-64.516	3	February	2015	11.58	7.02	31
WA	66	-64.288	-64.516	3	February	2015	11.58	7.02	57
WA	66	-64.288	-64.516	3	February	2015	11.58	7.02	100
WA	67	-64.290	-64.549	3	February	2015	15.45	10.89	4
WA	67	-64.290	-64.549	3	February	2015	15.45	10.89	12
WA	67	-64.290	-64.549	3	February	2015	15.45	10.89	22
WA	67	-64.290	-64.549	3	February	2015	15.45	10.89	33
WA	67	-64.290	-64.549	3	February	2015	15.45	10.89	60
WA	67	-64.290	-64.549	3	February	2015	15.45	10.89	100

WA	68	-64.271	-64.534	3	February	2015	19.40	14.84	4
WA	68	-64.271	-64.534	3	February	2015	19.40	14.84	13
WA	68	-64.271	-64.534	3	February	2015	19.40	14.84	22
WA	68	-64.271	-64.534	3	February	2015	19.40	14.84	36
WA	68	-64.271	-64.534	3	February	2015	19.40	14.84	66
WA	68	-64.271	-64.534	3	February	2015	19.40	14.84	100

Table S2. Pigment ratios used for the runs of the different CHEMTAX clusters. The numbers indicate the amount of pigment per unit of Chl *a*. See Table 1 for pigment name abbreviations.

	Chl c_2	Per	19-But	Fuco	Pras	Viol	19-Hex	Allox	Zea	Lut	Chl *b*
PRASINOPHYTES											
NSO											
Cluster 1	-	-	-	-	0.10	0.08	-	-	0.20	-	0.72
Cluster 2	-	-	-	-	0.08	0.08	-	-	0.14	-	0.84
Cluster 3	-	-	-	-	0.11	0.06	-	-	0.35	-	0.82
SSO											
Cluster 1	-	-	-	-	0.12	0.07	-	-	0.07	-	1.40
Cluster 2	-	-	-	-	0.16	0.07	-	-	0.09	-	1.01
Cluster 3	-	-	-	-	0.12	0.08	-	-	0.12	-	1.09
NSG											
Cluster 1	-	-	-	-	0.17	0.06	-	-	0.62	-	0.30
Cluster 2	-	-	-	-	0.03	0.06	-	-	0.63	-	0.78
Cluster 3	-	-	-	-	0.18	0.06	-	-	0.51	-	0.32
Cluster 4	-	-	-	-	0.13	0.06	-	-	0.54	-	0.19
Cluster 5	-	-	-	-	0.22	0.07	-	-	0.34	-	0.53
WA											
Cluster 1	-	-	-	-	0.14	0.06	-	-	0.15	-	0.72
Cluster 2	-	-	-	-	0.15	0.07	-	-	0.10	-	1.30
CHLOROPHYTES											
NSO											
Cluster 1	-	-	-	-	-	0.08	-	-	0.13	0.71	0.29
Cluster 2	-	-	-	-	-	0.16	-	-	0.12	0.53	0.30
Cluster 3	-	-	-	-	-	0.07	-	-	0.13	1.21	0.29

SSO											
Cluster 1	-	-	-	-	-	0.08	-	-	0.29	0.43	0.30
Cluster 2	-	-	-	-	-	0.08	-	-	0.74	0.31	0.22
Cluster 3	-	-	-	-	-	0.07	-	-	0.97	0.21	0.19
NSG											
Cluster 1	-	-	-	-	-	-	-	-	0.17	0.22	0.83
Cluster 2	-	-	-	-	-	0.07	-	-	0.13	0.61	0.41
Cluster 3	-	-	-	-	-	0.08	-	-	0.51	0.51	0.20
Cluster 4	-	-	-	-	-	0.08	-	-	0.22	0.22	0.58
Cluster 5	-	-	-	-	-	0.08	-	-	0.15	0.69	0.30
WA											
Cluster 1	-	-	-	-	-	0.08	-	-	0.28	0.65	0.27
Cluster 2	-	-	-	-	-	0.07	-	-	0.37	0.75	0.19
DINOFLAGELLATES											
NSO											
Cluster 1	0.12	0.61	-	-	-	-	-	-	-	-	-
Cluster 2	0.13	0.67	-	-	-	-	-	-	-	-	-
Cluster 3	0.12	0.66	-	-	-	-	-	-	-	-	-
SSO											
Cluster 1	0.12	0.63	-	-	-	-	-	-	-	-	-
Cluster 2	0.13	0.58	-	-	-	-	-	-	-	-	-
Cluster 3	0.12	0.65	-	-	-	-	-	-	-	-	-
NSG											
Cluster 1	0.13	0.56	-	-	-	-	-	-	-	-	-
Cluster 2	0.13	0.73	-	-	-	-	-	-	-	-	-
Cluster 3	0.12	0.52	-	-	-	-	-	-	-	-	-
Cluster 4	0.12	0.65	-	-	-	-	-	-	-	-	-

Cluster 5	0.13	0.58	-	-	-	-	-	-	-	-	-
WA											
Cluster 1	0.12	0.79	-	-	-	-	-	-	-	-	-
Cluster 2	0.12	0.62	-	-	-	-	-	-	-	-	-
CRYPTOPHYTES											
NSO											
Cluster 1	0.08	-	-	-	-	-	-	0.56	-	-	-
Cluster 2	0.20	-	-	-	-	-	-	0.40	-	-	-
Cluster 3	0.19	-	-	-	-	-	-	0.30	-	-	-
SSO											
Cluster 1	0.18	-	-	-	-	-	-	0.34	-	-	-
Cluster 2	0.18	-	-	-	-	-	-	0.35	-	-	-
Cluster 3	0.19	-	-	-	-	-	-	0.31	-	-	-
NSG											
Cluster 1	0.21	-	-	-	-	-	-	0.68	-	-	-
Cluster 2	0.24	-	-	-	-	-	-	0.40	-	-	-
Cluster 3	0.18	-	-	-	-	-	-	0.24	-	-	-
Cluster 4	0.18	-	-	-	-	-	-	0.27	-	-	-
Cluster 5	0.19	-	-	-	-	-	-	0.27	-	-	-
WA											
Cluster 1	0.19	-	-	-	-	-	-	0.41	-	-	-
Cluster2	0.24	-	-	-	-	-	-	0.55	-	-	-
DIATOMS											
NSO											
Cluster 1	0.11	-	-	0.63	-	-	-	-	-	-	-
Cluster 2	0.08	-	-	0.68	-	-	-	-	-	-	-
Cluster 3	0.11	-	-	0.71	-	-	-	-	-	-	-

SSO											
Cluster 1	0.17	-	-	0.84	-	-	-	-	-	-	-
Cluster 2	0.13	-	-	0.64	-	-	-	-	-	-	-
Cluster 3	0.15	-	-	0.68	-	-	-	-	-	-	-
NSG											
Cluster 1	0.22	-	-	0.57	-	-	-	-	-	-	-
Cluster 2	0.21	-	-	1.04	-	-	-	-	-	-	-
Cluster 3	0.22	-	-	0.68	-	-	-	-	-	-	-
Cluster 4	0.19	-	-	0.65	-	-	-	-	-	-	-
Cluster 5	0.21	-	-	0.95	-	-	-	-	-	-	-
WA											
Cluster 1	0.13	-	-	1.14	-	-	-	-	-	-	-
Cluster 2	0.20	-	-	0.97	-	-	-	-	-	-	-
Phaeocystis											
NSO											
Cluster 1	0.08	-	0.35	0.22	-	-	0.42	-	-	-	-
Cluster2	0.10	-	0.42	0.27	-	-	0.53	-	-	-	-
Cluster 3	0.12	-	0.26	0.28	-	-	0.97	-	-	-	-
SSO											
Cluster 1	0.13	-	0.27	0.28	-	-	0.82	-	-	-	-
Cluster 2	0.13	-	0.26	0.30	-	-	0.86	-	-	-	-
Cluster 3	0.14	-	0.24	0.28	-	-	0.81	-	-	-	-
NSG											
Cluster 1	0.16	-	0.23	0.27	-	-	0.65	-	-	-	-
Cluster 2	0.15	-	0.36	0.31	-	-	0.75	-	-	-	-
Cluster 3	0.12	-	0.21	0.25	-	-	0.52	-	-	-	-

Cluster 4	0.14	-	0.21	0.24	-	-	0.49	-	-	-	-
Cluster 5	0.14	-	0.25	0.26	-	-	0.70	-	-	-	-
WA											
Cluster 1	0.12	-	0.41	0.51	-	-	0.83	-	-	-	-
Cluster 2	0.15	-	0.24	0.33	-	-	0.75	-	-	-	-
PELAGOPHYTES											
NSO											
Cluster 1	0.74	-	0.67	0.24	-	-	-	-	-	-	-
Cluster 2	0.59	-	0.79	0.26	-	-	-	-	-	-	-
Cluster 3	0.33	-	0.67	0.27	-	-	-	-	-	-	-
SSO											
Cluster 1	0.35	-	0.65	0.24	-	-	-	-	-	-	-
Cluster 2	0.51	-	0.62	0.25	-	-	-	-	-	-	-
Cluster 3	0.56	-	0.68	0.23	-	-	-	-	-	-	-
NSG											
Cluster 1	0.83	-	0.75	0.53	-	-	-	-	-	-	-
Cluster 2	0.42	-	0.75	0.25	-	-	-	-	-	-	-
Cluster 3	0.72	-	0.61	0.24	-	-	-	-	-	-	-
Cluster 4	0.63	-	0.59	0.26	-	-	-	-	-	-	-
Cluster 5	1.21	-	0.38	0.25	-	-	-	-	-	-	-
WA											
Cluster 1	0.46	-	0.76	0.27	-	-	-	-	-	-	-
Cluster 2	0.65	-	0.58	0.25	-	-	-	-	-	-	-
HAPTOPHYTES											
TYPES 6+7											
NSO											
Cluster 1	0.21	-	-	0.20	-	-	0.46	-	-	-	-

Cluster 2	0.24	-	-	0.20	-	-	0.32	-	-	-	-
Cluster 3	0.16	-	-	0.14	-	-	0.46	-	-	-	-
SSO											
Cluster 1	0.16	-	-	0.15	-	-	0.32	-	-	-	-
Cluster 2	0.18	-	-	0.17	-	-	0.47	-	-	-	-
Cluster 3	0.14	-	-	0.13	-	-	0.58	-	-	-	-
NSG											
Cluster 1	0.24	-	-	0.42	-	-	0.59	-	-	-	-
Cluster 2	0.12	-	-	0.12	-	-	0.26	-	-	-	-
Cluster 3	0.14	-	-	0.16	-	-	0.33	-	-	-	-
Cluster 4	0.15	-	-	0.15	-	-	0.28	-	-	-	-
Cluster 5	0.13	-	-	0.13	-	-	0.28	-	-	-	-
WA											
Cluster 1	0.19	-	-	0.17	-	-	0.39	-	-	-	-
Cluster 2	0.13	-	-	0.15	-	-	0.37	-	-	-	-

Table S3. Mean and standard deviation (SD) of (A) the abundance in cells l^{-1} and (B) biovolume in μm^3 cm^{-3} of selected taxa and major phytoplankton groups identified in the microscopic observations for the surface (4 m depth) and subsurface (depths as indicated in Fig. 7) samples of the four studied regions. The chosen taxa were those with total biovolume (for the whole data set) exceeding $3*10^5$ μm^3 cm^{-3} and present in at least 25 % of the samples.

A, cells l^{-1}

4 m	**NSO Mean**	**NSO SD**	**SSO Mean**	**SSO SD**	**NSG Mean**	**NSG SD**	**WA Mean**	**WA SD**
Diatoms								
Chaetoceros dichaeta	2	8	30	72	26558	20781	6	17
Chaetoceros spp., small (<20 µm)	0	0	1	3	2279	2216	0	0
Corethron inerme	0	0	0	0	786	536	1	3
Corethron pennatum	1154	382	193	88	57	21	59	37
Dactyliosolen antarcticus	0	0	0	0	52	47	0	0
Unidentified pennate diatom No. 2	26	17	69	26	105	68	0	0
Eucampia antarctica	4	15	23	73	54654	16108	36	107
Fragilariopsis kerguelensis	0	0	1	3	15630	8101	16	47
Fragilariopsis spp.	3160	1378	12105	3248	6427	4258	412	519
Guinardia cylindrus	0	0	0	0	3500	1423	1	3
Odontella weissflogii	2	8	11	37	1683	2117	8	23
Unidentified pennate diatom No. 3	538	350	115	75	15	21	2	4
Thalassiosira spp. small (<20 µm)	18371	13486	2574	3474	414323	232185	280	389
Thalassiosira spp. large (>20 µm) chain-forming	0	0	10	15	486	312	3	10
Thalassiosira/Porosira spp. (>20 µm)	25	21	46	31	17013	9035	286	845
Trichotoxon reinboldii	12	17	29	23	1069	603	8	23
Dinoflagellates								

Unidentified dinoflagellates, large	917	377	1356	544	4944	2890	117	70
Unidentified dinoflagellates, small (< 20 µm)	7800	4223	6987	4003	11508	3266	2238	906
Gyrodinium spp. (heterotrophic)	1561	739	1211	207	342	172	106	34
Protoperidinium spp., large (heterotrophic)	0	0	0	0	1202	495	1	3
Other								
Phaeocystis spp.	0	0	0	0	1961	1582	0	0
Unidentified coccolithophores (<10 µm)	0	0	10	37	182870	78655	0	0
Cryptophytes	240028	124242	9568	8216	461	992	631615	292195
Dictyocha speculum	0	0	11	37	1121	470	0	0
Unidentified microflagellates	5115	4693	1086	1439	0	0	1066	473
Unidentified nanoflagellates (3-20 µm)	705146	222457	106139	30331	162029	104334	721825	347230
Major groups								
Total dinoflagellates	10576	4832	10138	4438	21572	7014	2520	943
Total diatoms	30383	16946	69566	82198	561945	270928	425513	372392
Total coccolithophores	0	0	9	35	182870	78655	0	0
Cryptophytes	240028	124242	9479	7924	461	992	631615	292195
Total others without cryptophytes	711619	220819	103769	32936	164791	105377	722921	347131
SUBSURFACE	NSO mean	NSO SD	SSO mean	SSO SD	NSG mean	NSG SD	WA mean	WA SD
Diatoms								
Chaetoceros dichaeta	0	0	43	48	53985	40202	917	3536
Chaetoceros spp., small (<20 µm)	0	0	118	189	10113	18362	24	90
Corethron inerme	0	0	0	0	1562	697	113	439
Corethron pennatum	1579	472	1201	688	141	81	63	64

Dactyliosolen antarcticus	0	0	0	0	58	47	5	18
Unidentified pennate diatom No. 2	32	23	12	14	229	153	17	64
Eucampia antarctica	3	10	13	36	49474	17105	5438	18007
Fragilariopsis kerguelensis	29	103	1	3	26749	11184	1559	6012
Fragilariopsis spp.	2183	2154	4753	3787	8511	4253	1157	2827
Guinardia cylindrus	0	0	0	0	3451	2401	493	1910
Odontella weissflogii	1	5	3	6	1920	1364	23	88
Unidentified pennate diatom No. 3	780	206	140	166	12	19	11	12
Thalassiosira spp. small (<20 µm)	19896	14811	5469	5654	404069	325769	10114	38679
Thalassiosira spp. large (>20 µm) chain-forming	0	0	21	50	621	429	3	10
Thalassiosira/Porosira spp. (>20 µm)	69	66	66	54	25987	18506	862	3324
Trichotoxon reinboldii	9	12	11	28	2559	1512	64	245
Dinoflagellates								
Unidentified dinoflagellates, large	961	299	929	437	2808	2113	439	355
Unidentified dinoflagellates, small (< 20 µm)	4581	1425	4732	3689	5163	3405	3242	4072
Gyrodinium spp. (heterotrophic)	344	261	208	194	246	129	89	70
Protoperidinium spp., large (heterotrophic)	1	3	4	7	771	394	42	122
Other								
Phaeocystis spp.	0	0	0	0	1410	1375	15	55
Unidentified coccolithophores (<10 µm)	0	0	0	0	74955	55671	11533	44667
Cryptophytes	70682	47435	6557	12543	248	564	427463	544779
Dictyocha speculum	0	0	67	189	1070	605	37	141
Unidentified microflagellates	1772	2450	632	766	0	0	1516	1638
Unidentified nanoflagellates (3-20 µm)	550784	208897	69537	39817	114784	60923	490127	405595
Major groups								
Total dinoflagellates	6576	2080	6666	4393	11174	5973	3268	2667

Total diatoms	29796	17744	17465	11449	619348	375981	460253	642802
Total coccolithophores	0	0	1	3	74955	55671	1	3
Cryptophytes	59592	40621	6557	12543	248	564	412381	341404
Total others without cryptophytes	513045	240934	70268	40012	117120	61608	608157	381715

B, $\mu m^3\ cm^{-3}$

4 m	**NSO Mean**	**NSO SD**	**SSO Mean**	**SSO SD**	**NSG Mean**	**NSG SD**	**WA Mean**	**WA SD**
Diatoms								
Chaetoceros dichaeta	2	7	29	71	26074	20401	5	16
Chaetoceros spp., small (<20 µm)	0	0	2	6	5499	5347	0	0
Corethron inerme	0	0	0	0	30656	20904	43	130
Corethron pennatum	496211	164329	82900	37942	24619	8828	25314	15859
Dactyliosolen antarcticus	0	0	0	0	2661	2396	0	0
Unidentified pennate diatom No. 2	1485	1066	4222	1576	6425	4172	0	0
Eucampia antarctica	238	819	1260	3998	2976265	877181	1936	5809
Fragilariopsis kerguelensis	0	0	1	2	12712	6589	13	38
Fragilariopsis spp.	2436	1062	9334	2504	4955	3283	318	401
Guinardia cylindrus	0	0	0	0	27206	11062	9	26
Odontella weissflogii	199	795	1055	3878	168196	223634	643	1930
Unidentified pennate diatom No. 3	663	432	142	92	18	25	3	5
Thalassiosira spp. small (<20 µm)	28180	20687	3948	5329	635566	356167	429	597
Thalassiosira spp. large (>20 µm) chain-forming	0	0	174	296	9860	6319	68	203
Thalassiosira/Porosira spp. (>20 µm)	188	156	345	232	128275	68122	2153	6375
Trichotoxon reinboldii	577	836	1388	1125	51940	29314	378	1134
Dinoflagellates								

Unidentified dinoflagellates, large	6439	2643	9521	3817	34705	20287	819	491
Unidentified dinoflagellates, small (< 20 µm)	9410	5095	8429	4829	13883	3940	2699	1093
Gyrodinium spp. (heterotrophic)	136216	64477	105737	18060	29835	14970	9213	2995
Protoperidinium spp., large (heterotrophic)	0	0	0	0	57399	23630	53	159
Other								
Phaeocystis spp.	0	0	0	0	84	85	0	0
Unidentified coccolithophores (<10 µm)	0	0	1	4	20682	8896	0	0
Cryptophytes	34562	17890	1378	1183	66	143	90946	42073
Dictyocha speculum	0	0	148	516	15847	6643	0	0
Unidentified microflagellates	12710	12487	2879	3815	0	0	2824	1255
Unidentified nanoflagellates (3-20 µm)	468118	147680	70461	20136	107565	69263	479191	230512
Major groups								
Total dinoflagellates	153021	68145	128651	37666	174516	67008	12997	3715
Total diatoms	532246	180538	132353	99331	4153332	1288190	36476	32164
Total coccolithophores	0	0	1	4	20682	8896	0	0
Cryptophytes	482156	142721	71209	22196	140555	80325	482039	230278
Total others without cryptophytes	34562	17890	1365	1141	66	143	90946	42073
SUBSURFACE	NSO mean	NSO SD	SSO mean	SSO SD	NSG mean	NSG SD	WA mean	WA SD
Diatoms								
Chaetoceros dichaeta	0	0	284	455	24399	44302	58	218
Chaetoceros spp., small (<20 µm)	0	0	0	0	60971	27191	4423	17129
Corethron inerme	678898	203010	516220	295678	60448	34726	27224	27460
Corethron pennatum	0	0	0	0	2953	2434	240	928

Dactyliosolen antarcticus	1828	1425	703	856	13938	9344	1056	3925
Unidentified pennate diatom No. 2	170	552	712	1968	2694187	931458	217180	839778
Eucampia antarctica	24	84	1	2	21755	9096	1268	4889
Fragilariopsis kerguelensis	1684	1661	3665	2920	6563	3279	892	2179
Fragilariopsis spp.	0	0	0	0	26825	18664	3834	14849
Guinardia cylindrus	133	530	326	668	148997	111605	1097	4250
Odontella weissflogii	962	253	173	204	15	24	13	15
Unidentified pennate diatom No. 3	30520	22720	8390	8673	619836	499725	15515	59333
Thalassiosira spp. small (<20 µm)	0	0	359	941	12582	8691	68	212
Thalassiosira spp. large (>20 µm) chain-forming	523	499	499	409	195939	139531	6498	25064
Thalassiosira/Porosira spp. (>20 µm)	456	574	523	1352	124317	73468	3110	11910
Trichotoxon reinboldii	6745	2102	6521	3065	19711	14829	3084	2494
Dinoflagellates								
Unidentified dinoflagellates, large	5526	1720	5708	4450	6229	4108	3911	4912
Unidentified dinoflagellates, small (< 20 µm)	30058	22823	18195	16965	21493	11250	7797	6132
Gyrodinium spp. (heterotrophic)	30	119	184	311	36832	18815	2006	5816
Protoperidinium spp., large (heterotrophic)	0	0	0	0	65	72	1	3
Other								
Phaeocystis spp.	0	0	0	0	8477	6296	1304	5052
Unidentified coccolithophores (<10 µm)	10177	6830	944	1806	36	81	61550	78443
Cryptophytes	0	0	948	2678	15131	8552	526	1998
Dictyocha speculum	4403	6383	1676	2030	0	0	4019	4341
Unidentified microflagellates	365643	138678	46163	26433	76200	40444	325375	269258
Unidentified nanoflagellates (3-20 µm)	6928	5459	4942	2311	2163	1638	1327	1098
Major groups								
Total dinoflagellates	39797	14753	36010	29753	110432	54368	15312	7630

Total diatoms	656844	230333	535395	297848	4135635	1290472	35586	36118
Total coccolithophores	0	0	1	5	8477	6296	2	6
Cryptophytes	343843	160157	48812	26229	106064	51427	407013	254833
Total others without cryptophytes	8581	5849	944	1806	36	81	59379	49159

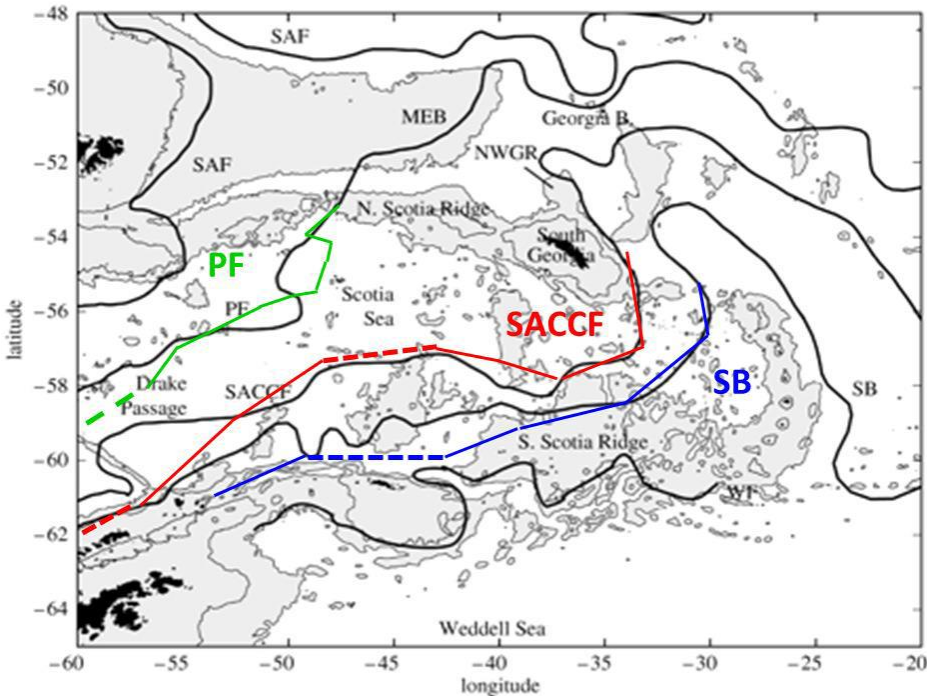

Figure S1. Main fronts in the PEGASO campaign area (from Dall'Osto et al., 2017). Fronts of the ACC are marked (Polar Front, PF; Southern ACC Front, SACCF), as is the southernmost limit of the ACC (Southern Boundary, SB). The Weddell Front (WF), marking the southern limit of the Weddell–Scotia Confluence is shown. The background plot shows the average position of the fronts as depicted by Orsi et al (1995); the color lines are the positions of the fronts nearest to the PEGASO cruise track in Jan-Feb 2015, as reconstructed from underway measurements, satellite data and synoptic modelling (see Dall'Osto et al., 2017). Dashed lines show the portions of the fronts that were crossed by the ship track.

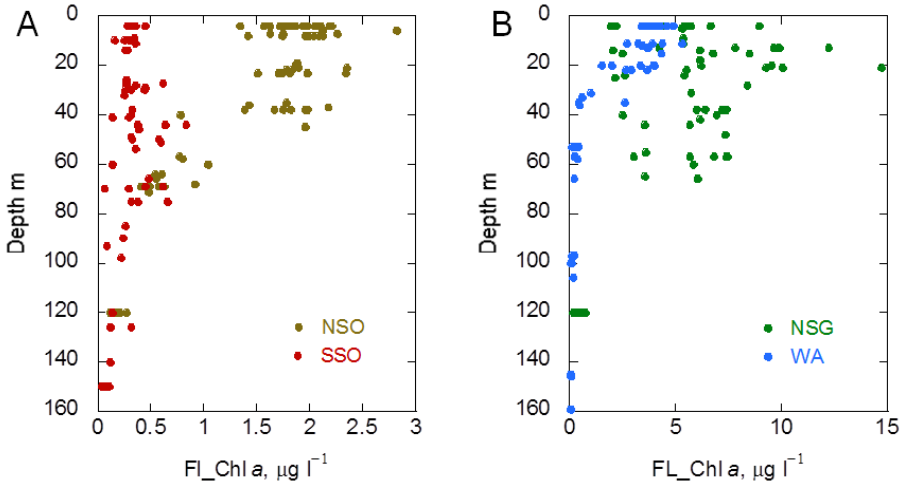

Figure S2. Vertical distribution of the concentration of fluorometric chlorophyll *a* (Fl_Chl *a*, ng 13 l^{-1}) in (A), NSO (North of the South Orkney Islands) and SSO (South of the South Orkney Islands) regions, and (B), NSG (Northwest of South Georgia Island) and WA (West of Anvers Island) regions.

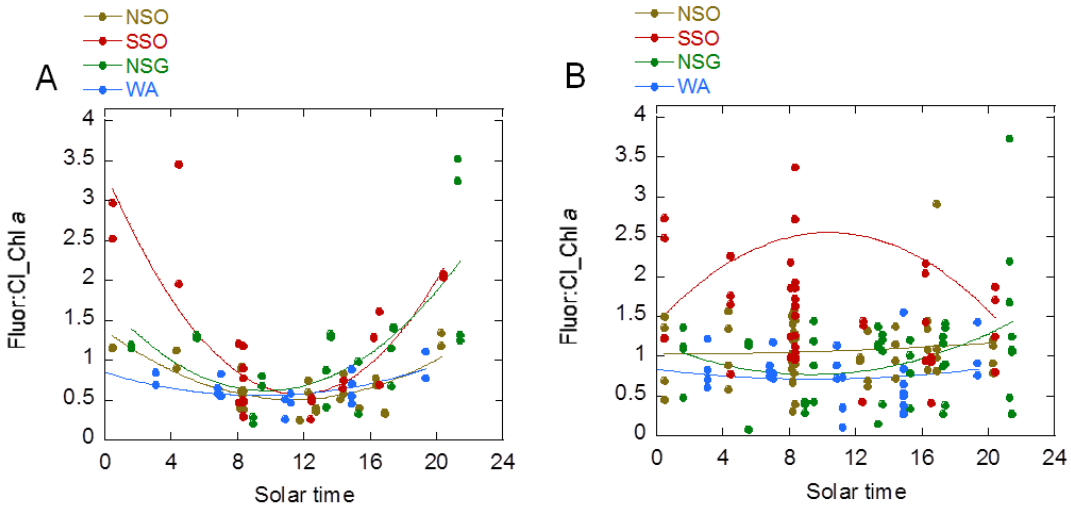

Figure S3. Variation of the Fluorescence/Fl_Chl *a* (Fluo/Fl_Chl *a*) ratio with solar time in (A) the two upper sampling depths and (B) the deeper sampling depths of the four study regions.NSO = North of the South Orkney Islands, SSO = South of the South Orkney Islands, NSG = Northwest of South Georgia Island, WA = West of Anvers Island. The fitted lines are 2-degree polinomials with the following equations: (A) NSO, y = -0.15*x + 0.0067*x2 + 1.37, r^2 = 0.55, p^2 22 < 0.0001; SSO, y = -0.48*x + 0.02*x^2 + 3.37, r^2 = 0.69, p < 0.0001; NSG, y = -0.23*x + 0.12*x^2 23 + 1.73, r^2 = 0.49, p < 0.01; WA, y = -0.063*x + 0.0034*x^2 + 0.85, r^2 = 0.45, p < 0.05. The polynomial regressions were not significant for the deep data in B.

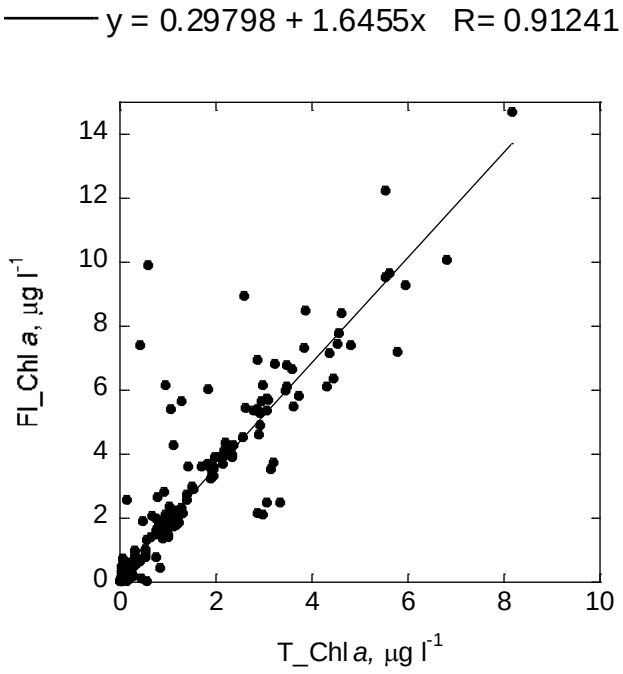

Figure S4. Relationship between fluorometric chlorophyll *a* (Fl_Chl *a*) and HPLC-measured total chlorophyll *a* (T_Chl *a*). The equation of the regression line is Fl_Chl *a* = 1.65* T_Chl *a* +28 0.30 (n = 268, r^2 = 0.83, p < 0.0001).

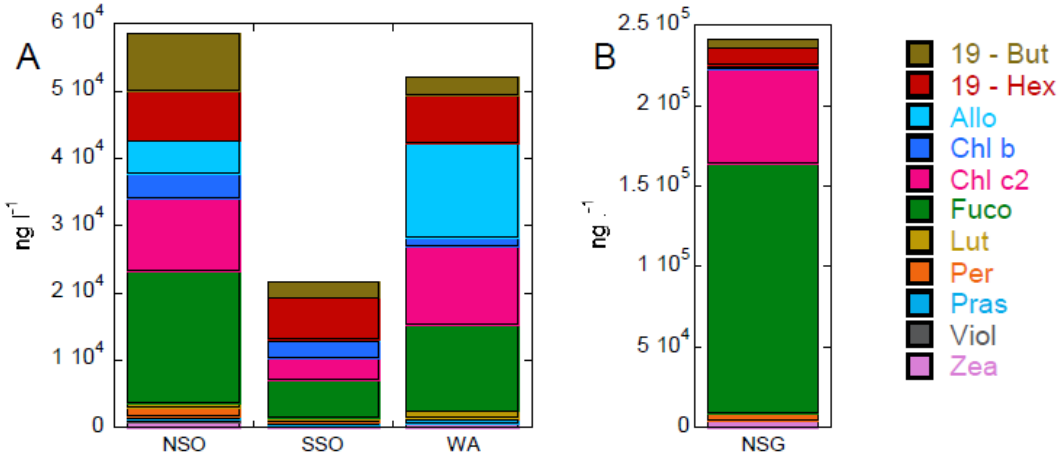

Figure S5. Mean concentration ± standard deviation (SD), for ach study region, of the ten pigments used in the CHEMTAX algorithm. NSO = North of the South Orkney Islands, SSO = South of the South Orkney Islands, NSG = Northwest of South Georgia Island, WA = West of Anvers Island.

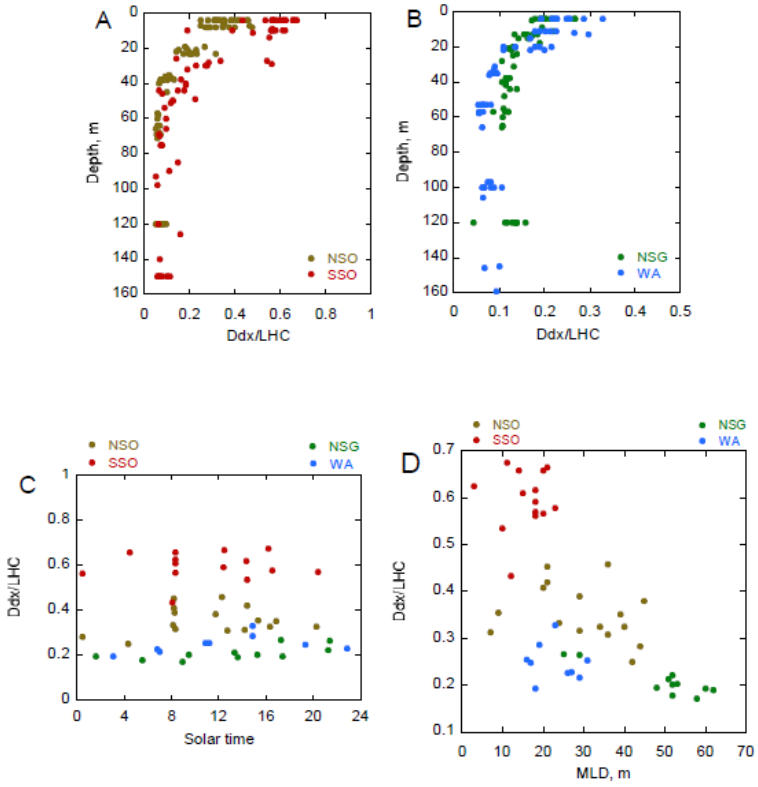

Figure S6. Vertical distribution of the ratio Phaeo/T_Chl *a* between the sum phaeophorbides + phaeophytines (Phaeo) and total chlorophyll *a* (T_Chl *a*) in (A), NSO (North of the South Orkney Islands) and SSO (South of the South Orkney Islands) regions, and (B), NSG (Northwest of South Georgia Island) and WA (West of Anvers Island) regions. An outlier os station 45, 13 m depth (NSG) has been excluded.

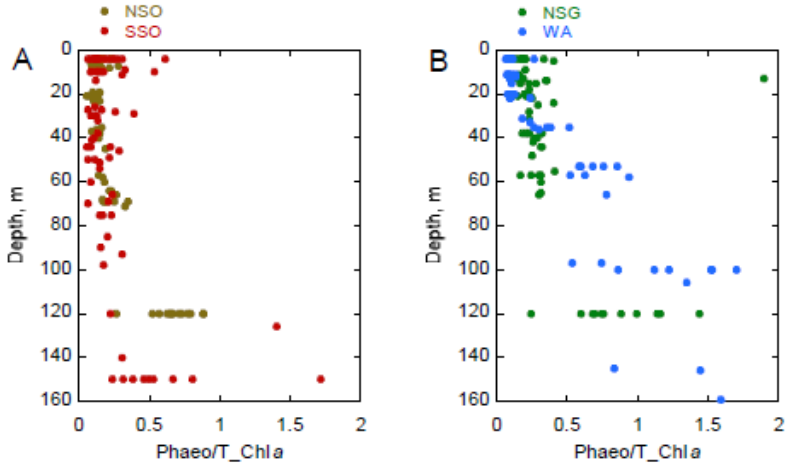

Figure S7. Variability of the ratio Ddx/LHC between diadinoxanthin (Ddx) concentration and the sum of 19-But, 19-Hex, Fuco and Per (see Table 1 for abbreviations) concentrations. (A) vertical distribution of Ddx/LHC in NSO (North of the South Orkney Islands) and SSO (South of the South Orkney Islands) regions, (B) vertical distribution of Ddx/LHC in NSG (Northwest of 45 South Georgia Island) and WA (West of Anvers Island) regions, and (C) variation of the Ddx/LHC ratio with solar time in the two upper sampling depths of the four study regions.

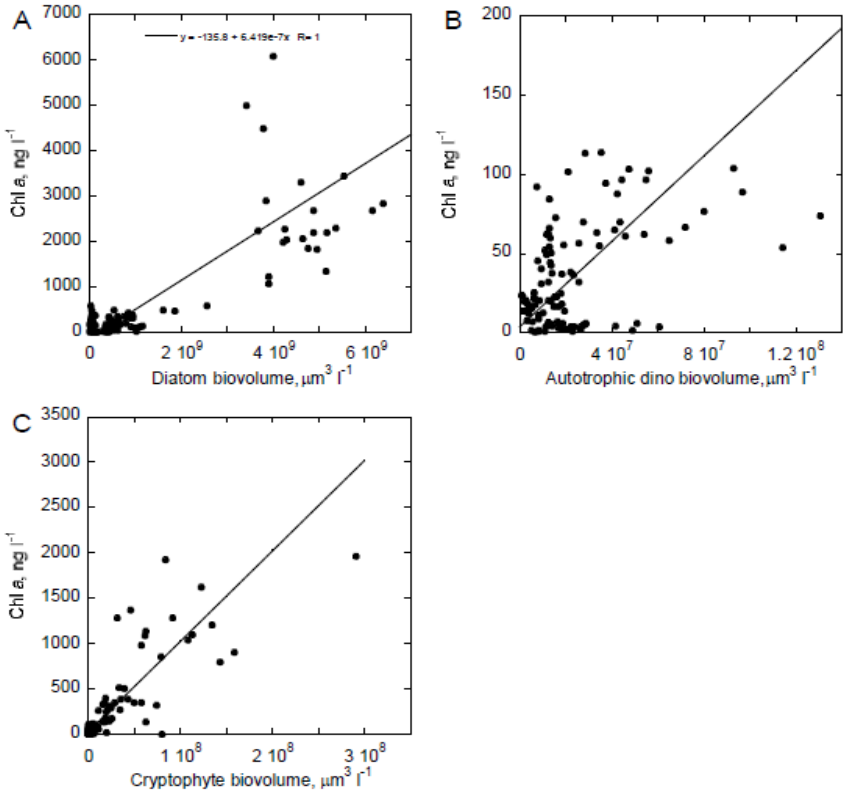

Figure S8. Relationship between biovolume calculated by microscopy and CHEMTAX-derived contribution to T_Chl *a* for (A) diatoms, (B) autotrophic dinoflagellates and (C) cryptophytes. The lines are standard major axis regression lines and their equations are: y = 6.4e-7 x – 135.8 (r_2 51 = 0.68) for diatoms, y = 1.3e-6x + 3.8 (r^2 = 0.23) for autotrophic dinoflagellates and y = 9.0e-6 x 52 + 25.9 (r^2 = 0.68) for cryptophytes; (N = 105, p < 0.0001 for all groups).

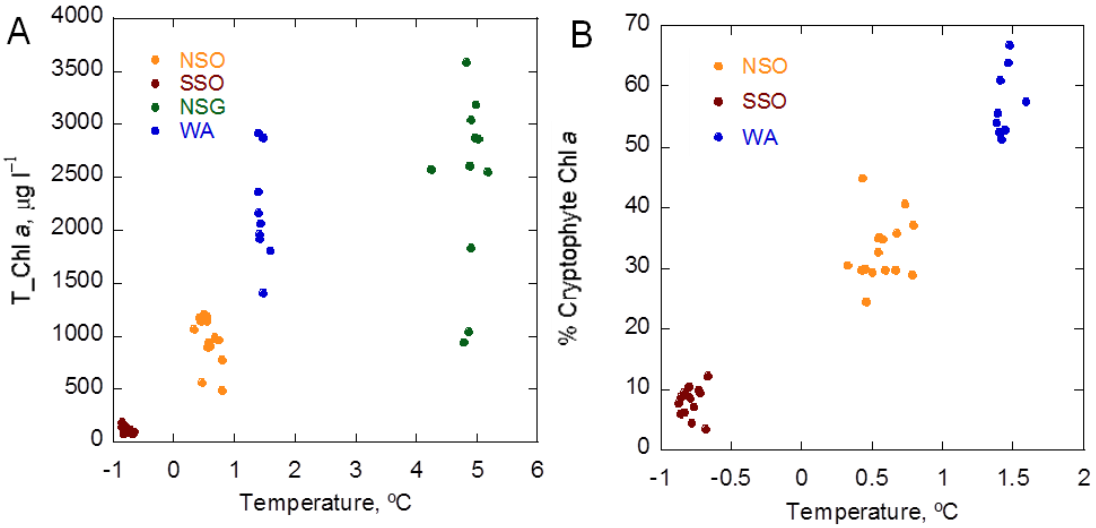

Figure S9. (A) Relationship between temperature and T_Chl *a* for the surface level (4 m depth) of the four study regions; (B) relationship between temperature and percentage contribution of cryptophytes to T_Chl *a* in NSO, SSO and WA (there were practically no cryptophytes at NSG). NSO = North of the South Orkney Islands, SSO = South of the South Orkney Islands, NSG = Northwest of South Georgia Island, WA = West of Anvers Island.

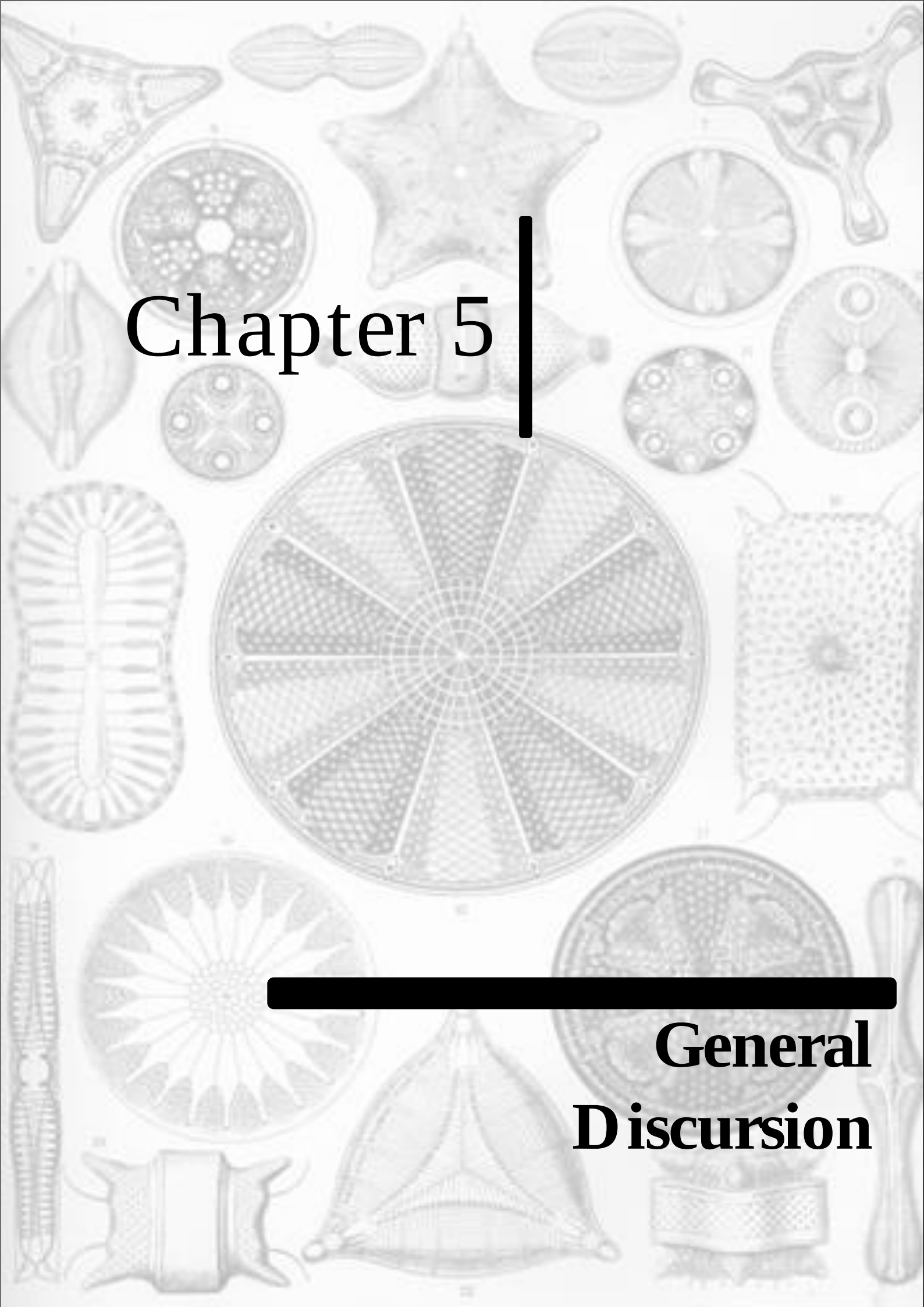

Chapter 5

General Discursion

CHAPTER 5

GENERAL DISCUSSION

5.1 METHODOLOGICAL CONSIDERATIONS ABOUT THE USE OF HPLC TO CLASSIFY PIGMENTS OF MARINE PHYTOPLANKTON

The identification of phytoplankton classes based on their pigmentary suite has largely evolved since the earliest qualitative analysis based on thin-layer chromatography (Jeffrey, 1974; Gieskes et al., 1978). Nowadays, high performance liquid chromatography (HPLC) is extensively used to assess the biomass and characteristics of phytoplankton communities as well as their physiological response (Wright 1996; Zapata et al., 2000; Le Queré et al., 2005; Mendes et al., 2007; Hirata et al., 2011; Vega-Moreno et al, 2012; Latasa, 2014; Araújo et al, 2017) and has allowed us to gain a better understanding of how the interplay between phytoplankton composition and function. This knowledge has broadened our perspective about the productivity, biogeochemical cycles and energy budgets in the ocean. In this thesis, chromatographic separation of pigments is used to provide an overview of the phytoplankton community structure in regions including the Mediterranean Sea, the Atlantic Ocean and the Southern Ocean, altogether covering several of the oceanographic provinces proposed by Longhurst (2007).

The HPLC analysis was based on the methodology developed by Latasa (2014) following the recommendations of Jeffrey et al. (1997) and Roy et al. (2011). The CHEMTAX program version 1.95 (Mackey et al., 1996) with the modifications described by Latasa (2007) was used to optimize the association between the different pigments present in each sample and to quantify the adequate contribution of the main

taxonomic groups to the total chlorophyll a. The combination of HPLC-CHEMTAX was used to study the taxonomic composition of the phytoplankton community in environments ranging from oligotrophic to eutrophic and under temporal of several years (Chapter 2) and of days-weeks (Chapter 3 and 4). The horizontal dimension (Chapter 2, 3 and 4) and the variability within the water column (Chapter 4) were also explored. The chemotaxonomic results were validated using associated microscopy data and alternative picophytoplankton quantification methods.

5. 2. THESIS OVERVIEW

Chapter 3 describes the variability of the phytoplankton community structure in Blanes Bay (northwestern Mediterranean Sea) (Fig. 1). The analyses were based on 14 years of data and focused on the seasonal and interannual changes of the quantitative and qualitative composition of the phytoplankton community and their relationship with environmental factors. HPLC pigment analysis followed by application of the CHEMTAX algorithm showed a strong seasonality, with fall-winter or winter-spring maxima of most groups (prasinophytes, diatoms, haptophytes, cryptophytes and pelagophytes) and summer minima, in association with the variability in the concentrations of major nutrients. Diatoms were the most important group in the winter-spring proliferations, while Synechococcus presented peaks in April and August. Although slight, Prochlorococcus had a fall-winter maximum, while dinoflagellates did not decrease their contribution in summer. On top of this general pattern, diatoms, prasinophytes, cryptophytes and dinoflagellates responded positively to episodic coastal fertilization associated with precipitation events. There was a decreasing multiannual trend in phytoplankton biomass that appeared to be related to a general reduction in nutrient concentration.

The size structure and the composition of the phytoplankton community in the surface waters of a transect from the Mediterranean to the Southwestern Atlantic Ocean (Fig. 1) is discussed in Chapter 3. We performed HPLC-CHEMTAX analysis to whole water and size-fractionated samples obtained by filtration through filters of 3 µm pore size (picophytoplankton or pico< 3 µm and nano- + microphytoplankton or n+m>3> 3 µm). Only in the Mediterrranean sample (taken near Gibraltar) and in those of the Soutwestern Atlantic Shelf (SWAS) was Chlorophyll a ≤ 0.5 mg m-3; in the tropical and subtropical Atlantic provinces, including the Canary Current Coastal (CNRY), chlorophyll a was < 0.25 mg m-3. The application of the Vidussi et al. (2001) - Uitz et al. (2006) and Hirata et al. (2011) expressions for estimating of the proportion of pico-, nano- and microphytoplankton indicated a high microplankton proportion in SWAS that contrasted with the relative scarcity of large cells detected by filtration and microscopic observations. The discrepancy could be explained by the presence in SWAS of picoplankton-sized diatoms and Parmales, a sister group with the diatoms that shares pigment composition with them. This finding indicates that presence of diatom pigment markers should not be authomatically considered as repesentative of microphytoplankton. The total non-water absorption in the water column was dominated by CDOM. Average phytoplankton absorption for the different provinces ranged between 19.3% in MEDI to 45.7% in SWAS and 47% in the Western Tropical Atlantic (WTRA). The chlorophyll a-specific phytoplankton absorption was lower in the high chlorophyll a provinces but was not correlated with phytoplankton size structure indicators.

Phytoplankton produces dimethylsulfoniopropionate (DMSP), a precursor of of dimethylsulfide (DMS), which is the primary source of reduced sulfur emitted from the ocean (Simó 2001). Once the DMS is released into the atmosphere, it undergoes a

sequence of oxidative reactions, giving rise to a series of products (e.g., non-sea-salt sulfate and methanesulfonate) that can act as cloud condensation nuclei (Vallina and Simó, 2007; Simó, 2011) hence potentially influencing the weather. In Chapter 4 the phytoplanktonic community, diversity, abundance and physiological characteristics are described in order to investigate the complex relationship between the phytoplankton community, the aerosol production and clouds formation in the Southern Ocean (Fig. 01). Our analysis highlighted the association of cryptophytes with stratified surface waters influenced by ice melting, the occurrence of diatom-dominated bloom in the iron-rich waters around South Georgia and the substantial contribution of less well-studied forms such as the pelagophytes to the north of the South Orkney islands. In summary, the suite of HPLC data analyses presented in this thesis evidences that the different shapes, sizes and pigments from the phytoplanktonic organisms provide relevant information regarding the functioning of the marine system. This knowledge can also help to improve ecological models and algorithms used to calibrate ocean color data.

Fig. 1. Sampling sites.

5.3. THE USE OF HPLC-CHEMTAX IN DIVERSE ECOLOGICAL PROCESSES

Phytoplankton categorization based on pigment composition can be a useful tool to in the study of aquatic ecosystems because it improves our ability to explain the dynamics of the phytoplankton community. In turn, phytoplankton organisms can be considered as a sensor of the environment because they can respond nonlinearly even to minor physical, biological and environmental perturbation (Margalef, 1978).

5.3.1 HPLC-CHEMTAX AS A MONITORING TOOL

The combined application of HPLC and CHEMTAX in a long-term study can provide valuable information for environmental management and can be very useful as a monitoring tool. The study of 14 years of data obtained from the coastal time series station of Blanes Bay, in the Northwestern Mediterranean Sea highlighted the interest of the HPLC-CHEMTAX technique to process high number of samples. The procedure was able to detect short-term proliferations of diatoms, dinoflagellates or other groups as a response to nutrient loads from precipitation events or other sources. In summary, the information obtained by HPLC and CHEMTAX can be applied as a monitoring routine to assess ocean health and can also help to take management decisions (Sebastià, 2012).

5.3.2 IN PICOPHYTOPLANCTON IDENTIFICATION

It is extensively recognized that the size distribution of phytoplankton assemblages is a key factor that governs the functioning and energy transfer through the pelagic food-webs (Legendre & Le Févre, 1985). Across different ecological domains, the functional relationship between phytoplankton size-structure and the relative contribution of each

class to the productivity and biomass of the system determine the fate of diverse processes such as new production or carbon export (Trembley & Legendre 1994, Falkowski et al. 1998).

For instance, in the Oligotrophic Atlantic Ocean, pico and nano-phytoplankton (0.2 to 2.0 µm) represent a large fraction of the total integrated carbon fixation and the autotrophic biomass (Marañon et al., 2001). When smaller phytoplankton cells dominates the autotrophic community, there is a tight coupling between primary producers, heterotrophic bacteria, and their predators. This close interaction will favour the recycling of organic carbon rather than its transfer to higher trophic levels, reducing the efficiency of the biological carbon pump (Azam 1983, Legendre & Lefevre 1995). On the other hand, when we move from low to high latitudes, the importance of larger cells increases (e.g., Marañon et al. 2001; Gibb et al., 2000; Huete-Ortega et al., 2011; Acevedo-Trejos et. al. 2018). This shift in the phytoplankton community size and composition promotes simpler trophic pathways that enhance carbon export towards the ocean's interior. Therefore, it is imperative develop adequate methods to quantify and identify simultaneously different phytoplankton size classes.

The long-term analysis of the phytoplankton community in Blanes Bay (**Chapter 2**), showed that when water column was strongly stratified, the phytoplankton community was mainly composed by primnophytes and cyanobacterias. The contribution of the cyanobacterias peaked in the summer (i.e., August), reaching up to 39 % of the total biomass (seen as Chlorophyll *a* concentration). While in the Atlantic Ocean (C**hapter 3)**, the contribution of picophytoplankton ranged between 61% in NATR, 69% in WTRA and 63% in SALT. In the Southern Ocean (South Orkney Islands; **Chapter 4**) and South West Atlantic Continental Shelf (SWAS; **Chapter 3**) the contribution of pelagophytes (on of less study groups of the picoplankton community) was highly

expressive to the total biomass, corresponded 10% and 15% to total chlorophyll *a*, respectively (Fig. 02) . This relevant finding highlights the importance of HPLC-CHEMTAX analysis as still there is a lot of uncertainties about the role and contribution of other picophytoplankton cells to the marine systems.

Among the methods to quantify and characterize the global picophytoplankton composition (e.g., by DAPI, Genomic, flow cytometry), the use of HPLC – CHEMTAX gave comparable results to results to those obtained by cell counts under microscope and flow cytometry. Moreover, the HPLC-CHEMTAX method offers the advantage of simultaneously get large amount of accurate data of pigments from HPLC (Gibb et al., 2000), functional type (**Chapter 3**; Zeng et al., 2018), classes size (**Chapter 3**; Vidussi et al., 2001; Hirata et al., 2011), physiological response (**Chapter 4**; Vega-Moreno et al., 2012; Araujo et al., 2017) and CHEMTAX results not only from the picophytoplankton groups but also nano-, microphytoplankton in the same sample, even in oligotrophic zones as the tropical and subtropical ocean, where is dominate for this smallest phytoplankton (**Chapter 3**; Gibb et al, 2000). In addition, an analysis of HPLC pigments is a quality-controlled method even when there is to date of large number of samples (Wright et al., 1996; van Heukelem and Hooker, 2011).

The used the Size-fractionated filtration (SFF) approached implemented in this thesis (**Chapter 3**) to estimate pigment concentration and the phytoplankton communities from HPLC-CHEMTAX analysis, offers an advantage over the conventional technique as it allows the user to represent the variability in each data zone and confirm the presence/absence of phytoplankton groups often not emphasized or projected such as the picoplankton Parmales and diatoms and of picoplankton-sized diatoms like *Minidiscus*, which was evidenced in the and SWAS zones. At first, in **chapter 3**, the total fraction indicated a high concentration of fucoxanthin, indicating the significant

presence of Diatoms (microphytoplankton) in the Vidussi et al. (2001) and Hirata et al. (2011) algorithms. However, microscopy samples did not confirm this result. SFF pico<3 μm allowed us verified that fucoxanthin did indeed come from picoplankton group. There are still uncertainties in relation to fitting some models. However, this SFF provides a useful possibility for knowledge of the phytoplankton size component and their distribution at large scales.

5.3.3 To Characterize Pigments and its possible use to calibrate remote models and sensors

The ability to monitor phytoplankton properties through satellite observations of ocean color at a global scale relies on previous information on the pigment composition of of phytoplankton and its bio-optical properties (see review Blondeau-Patissier et al., 2013). Climate models use data on the global distribution of major phytoplankton groups based on remote sensing information. However, the applicability of the developed algorithms may be limited by factors such as variation in phytoplankton cell size and pigment composition. Recognizing the biogeochemical roles played by the different phytoplankton groups stimulated the growth of research to identify the pigments (and consequently phytoplankton functional types – PFT) from space. **In chapter 3** we have seen that the pigment set can vary widely depending on the size distribution of phytoplankton and that some approximations developed to assess PFT contribution, such as diagnostic pigment analysis from analyzing HPLC have been used to identify and quantify the size structure of phytoplankton community (Vidussi et al., 2001; Uitz et al., 2006; Hirata et al., 2011). Similar approaches can be used in remote sensing based on statistical relationships derived from a global in-situ HPLC data set

(Kostadinov et al, 2011) and can be useful for the detection of blooms. We also contrast this kind of knowledge with bio-optical properties of phytoplankton pigments, a necessary in situ analysis to help the interpretation of remotely sensed data (Roy et al., 2011). The importance of high-quality pigments data for remotely detected ocean color models was highlighted by NASA in the last years (Hooke et al., 2009), proving that parameterization may be used to refine global and regional estimations, as carbon fixation rates or physiological parameters. Swan et al., (2016) for example, applied chemotaxonomic analysis to a global dataset of climatological HPLC pigment concentrations consolidated with satellites data from Marine Ecosystem DATa (MAREDAT) project (Buitenhuis et al., 2013). Another example is the work performed by Alvain et al. (2005; 2008), that also used the diagnostic pigment data to classify six dominant phytoplankton groups from spectral effects through remote sensing reflectance. Pigments from HPLC analysis confirmed again that can contribute to the global construction of the pigmentary knowledge of the oceans. In this sense, the pigments analysis, the monitoring of bio-optical property and their corresponding eco-physiological response will be identified from the color of the sea and integrated on remote sensing. As a caution note, we still have a lot to learn and work about the quality HPLC pigments data. However, this technique, together with microscopy and molecular development is a sophisticated analytical pigment methodology.

5.4 Phytoplankton Community structure of the Mediterranean Sea, Atlantic and Southern Oceans

The general chemotaxonomic structure derived from HPLC-CHEMTAC analyses of the phytoplankton communities of all the ecosystems studied in this thesis was illustrated as

a function of the total chlorophyll a concentration (T_Chl *a* in mg m^{-3}) and the relative contribution of the various groups (% of T_Chl *a*) as shown in the Fig. 02.

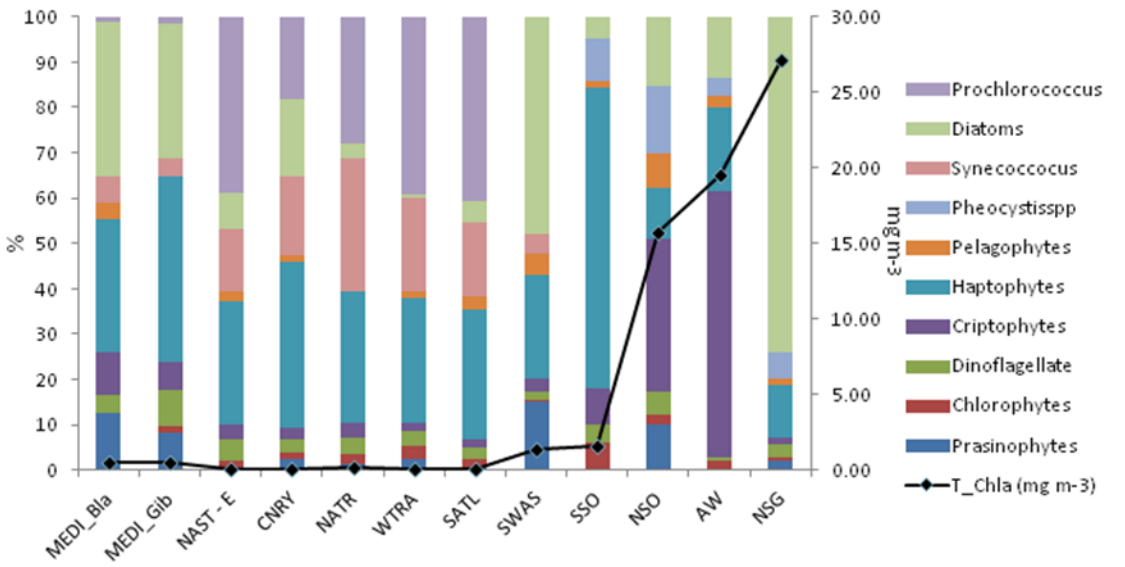

Fig. 02 Contribution of T_Chl*a* of the CHEMTAX-derived phytoplankton groups in Mediterranean Sea, Atlantic and Southern Oceans.

When viewed as a function of relative chlorophyll *a* (Fig. 2), the average community looks similar in the Mediterranean Sea (MEDI_Bla corresponds to Blanes Bay (**Chapter 2**) and MEDI_Gib to Alboran Sea (**Chapter 3**) and SWAS (**Chapter 3**), which can be considered as temperate zones, and the Subtropical and Tropical Atlantic (NAST-E, CNRY, WTRA and SALT) while in the Southern Ocean (SSO, NSO, AW and NSG; Chapter 5) the communities presented different composition, with a large contributoin of cryptophytesin some areas. Our observations suggest that this group may be associated with ice melting influence and e strong water column stratification (Scholls and Estrada, 1994: Mendes et al., 2017) and appears to follow diatoms in the seasonal succession (Garibotti et al., 2003; Moline et al., 2004; Ducklow et al., 2007; Murphy et al., 2013). The most abundant group in this thesis certainly was the haptophytes (types 6+7; see Zapata et al., 2004). Their lowest and highest contribution

to total chlorophyll *a* was in Antarctic waters (11% in NSO and NSG and 66% in SSO, respectively).

5.5 CONCLUDING REMARKS

The determination of pigment composition provides an inclusive description of the phytoplankton community, with information on functional types and size structure, and also tells about the photoacclimation status and the physiological conditions of the cells. There has been much progress in the study of phytoplankton community composition, but much is still unknown. In this thesis, we defined the phytoplankton communities through HPLC analysis followed by the CHEMTAX algorithm, which is based on the pigment ratios for the major algal groups. We obtained information on the phytoplankton functional types and size structure, physiological conditions and photoacclimation status. We carried out CHEMTAX-CHEMTAX analyses of fractions obtained by filtration (n+m>3 μm and pico<3 μm) to provide an experimental verification of the size class distributions derived from pigment composition and to improve phytoplankton identification and evaluation. In each chapter of this thesis we also tried to relate the phytoplankton findings with environmental factors. We also compared the results of the HPLC technique and the CHEMTAX analysis with other methodologies for characterizing the phytoplankton community.

The phytoplankton is a central pillar of the aquatic ecosystems and approaches that encompass analytical and molecular methods, bio-optical measurements and remote sensing are needed to understand how the marine environment works and how it could affect the esponse to future climate and other environmental changes. However, it is still difficult to ascertain ocean atmosphere interactions or how phytoplankton diversity and

productivity will respond to global change. For example, an important future challenge is to elucidate how environmental forcing will affect the occurrence of both harmful and beneficial algal blooms, which have implications for human health and welfare. In this context, we need to obtain information that can help to improve environmental mnagement and social life. For instance, it is necessary to construct reliable and multidisciplinary databases. As we have seen, the HPLC-CHEMTAX analysis may help to otain a robust identification of the tiny but mighty organisms. An accurate distinction of taxonomic groups and associated functional characteristics is necessary for ecophysiological studies and for ecosystem modeling and represents a great contribution to the knowledfge of structure and function of marine ecosystems.

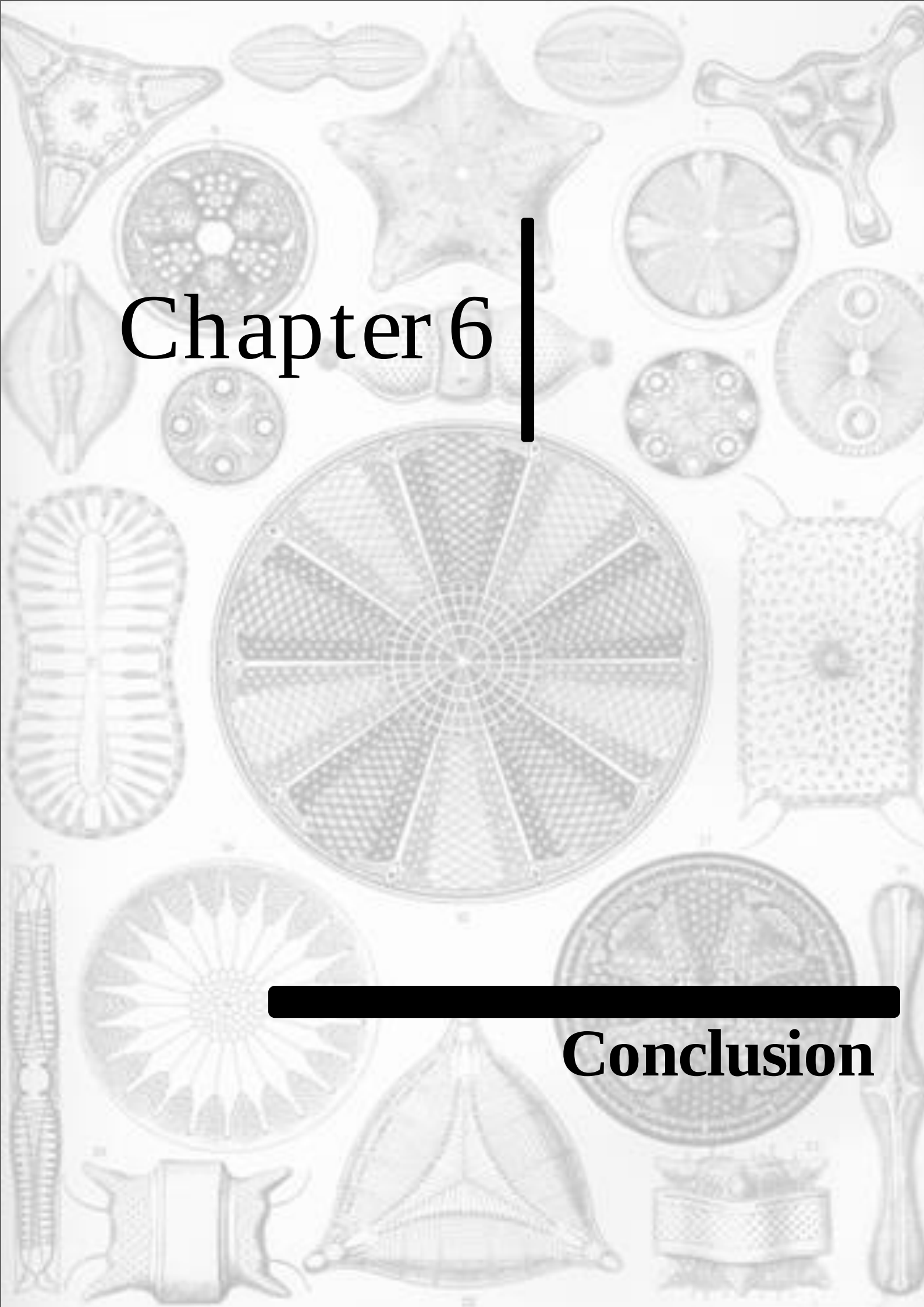

Chapter 6

Conclusion

CHAPTER 6

CONCLUSION

1. A chemotaxonomic approach based on HPLC analysis of phytoplankton pigments, followed by the CHEMTAX algorithm was applied to a set of samples taken in the Blanes Bay Observatory station between the years 2000−2014. Total chlorophyll *a* and several phytoplankton groups (prasinophytes, diatoms, haptophytes, cryptophytes and pelagophytes) presented autumn-winter or winter-spring maxima and summer minima, coinciding with similar variation in major nutrient concentrations. *Prochlorococcus* presented a fall-winter maximum and a spring-summer minimum, while *Synechococcus* peaked in April and August.

2. Episodic fertilization events in Blanes Bay caused by freshwater runoff from rain storms enhanced the growth of prasinophytes and diatoms.

3. In the Blanes Bay time series, most phytoplankton groups presented a decreasing interannual trend that could be related with a reduction in nutrient availability probably . due to the improvement of wastewater treatment in the region.

4. The structure of the phytoplankton community and the bio-optical properties of surface waters were studied during the TransPEGASO cruise, along a transect across the Atlantic Ocean that covered seven biogeographycal provinces. The composition of the phytoplankton community was characterized by means of microscopic observations and the application of HPLC - CHEMTAX pigment analyses to whole water and two filtration size fractions (> 3 and < 3 µm), and measured the absorption of particulate

matter and colored dissolved organic matter (CDOM). The provinces covered by the transect could be divided in an oligotrophic group, with Chl *a* < 0.25 mg m^{-3}, comprising the Tropical and Subtropical Atlantic and a eutrophic group (Chl *a* > 0.5 mg m^{-3}) with a Mediterranean sample (MEDI) and those from the Southwestern Atlantic Shelf (SWAS). The most important taxa in the Tropical and Subtropical Atlantic were *Prochlorococcus* spp., haptophytes and *Synecoccoccus* spp., while MEDI and SWAS were dominated by diatoms and haptophytes.

5. The Chl *a* size class distribution obtained from the fractionated filtrations was compared with with those resulting from the diagnostic pigment algorithms (VU) developed by Vidussi et al. (2001) and Uitz et al. (2006), and the total Chl *a*-based approach (HI) of Hirata et al. (2011). Both the VU and HI algorithms predicted for SWAS a high proportion of nano- and microphytoplankton, in contrast with microscopic observations and the results of the size-fractionated filtrations, which indicated dominance of the < 3 µm fraction. This discrepancy appeared to be due to the presence, confirmed by scanning electron microscopy, of picoplankton-sized forms such as cells of Parmales (a group sharing the pigment composition with the diatoms) and the diatom *Minidiscus* sp. These observations indicate that the occurrence of diatom pigment markers cannot be systematically associated with the presence of large cells.

6. The total non-water absorption in the water column was dominated by CDOM. Average phytoplankton absorption for the different provinces ranged between 19.3% in MEDI to 45.7% in SWAS and 47% in the Western Tropical Atlantic (WTRA).

7. The Chl *a*-specific phytoplankton absorption [a_{ph}*(443)] was lower in MEDI and SWAS than in the oligotrophic provinces. a_{ph}*(443) was positively related to the package index [Qa*(443)] but was not correlated with indicators of size structure. It appeared that the variability observed in aph*(443) was mainly related to differences in intracellular pigment concentration and possibly to photoacclimation processes.

8. The taxonomy and distribution of the phytoplankton in four contrasting regions (North of the South Orkney Islands = NSO, Southeast of the South Orkney Islands = SSO, Northwest of South Georgia = NSG and West of Anvers = WA) of the Atlantic sector of the Southern Ocean was studied by microscopic examination and HPLC pigment analyses followed by the CHEMTAX algorithm, during the PEGASO cruise of the BIO Hespérides (January-February 2015). A statistically significant association was found between fluorometric and HPLC determinations of chlorophyll *a*, and between chemotaxonomic and microscopy-derived estimates of the contribution of diatoms, dinoflagellates and cryptophytes, although the latter appeared to be underestimated by the microscopic observations.

9. In the PEGASO study, the highest average levels of fluorometric chlorophyll *a* (517 mg m^{-2}) were found at NSG, followed by WA (132 mg m^{-2}), NSO (120 mg m^{-2}) and SSO (34 mg m^{-2}). NSG was dominated by large diatoms like *Eucampia Antarctica* and *Thalassiosira* spp., the most abundant groups at NSO were cryptophytes and diatoms (mainly *Corethron pennatum*, small *Thalassiosira* spp. and *Fragilariopsis* spp.), followed by haptophytes types 6 + 7, *Phaeocystis* and pelagophytes, especially in the deeper levels of the euphotic zone. At SSO, the most important groups were

haptophytes types 6 + 7, followed by diatoms and *Phaeocystis*. The main chemotaxonomic groups at WA were cryptophytes (between surface and about 40 m depth), haptophytes types 6 + 7 and diatoms. Cryptophyte abundance was associated with the influence of water from melting ice.

10. These findings confirmed previous observations such as the dominance of diatoms in the iron-rich South Georgia bloom region and the association of cryptophytes with well-illuminated stratified surface waters influenced by ice melting, but also highlighted the subtantial contribution of less well-studied forms such as the pelagophytes, important components of the picoplankton.

11. The ratio between the photoprotective pigment diadinoxanthin and the sum of the light harvesting pigments of phytoplankton sharing diadinoxanthin (sum of 19'-butanoyloxyfucoxanthin, 19'-hexanoyloxyfucoxanthin, fucoxanthin and peridinin) was positively correlated with the euphotic zone depth, suggesting an enhancement due to exposure to a relatively high irradiance.

12. The current debate on climate and aquatic systems change demands robust tools to monitor the structure of phytoplankton communities and their seasonal and multiannual variability. HPLC pigment analysis followed by application of CHEMTAX has been shown to be a reliable technique for the consistent quantification of chemotaxonomic groups of phytoplankton.

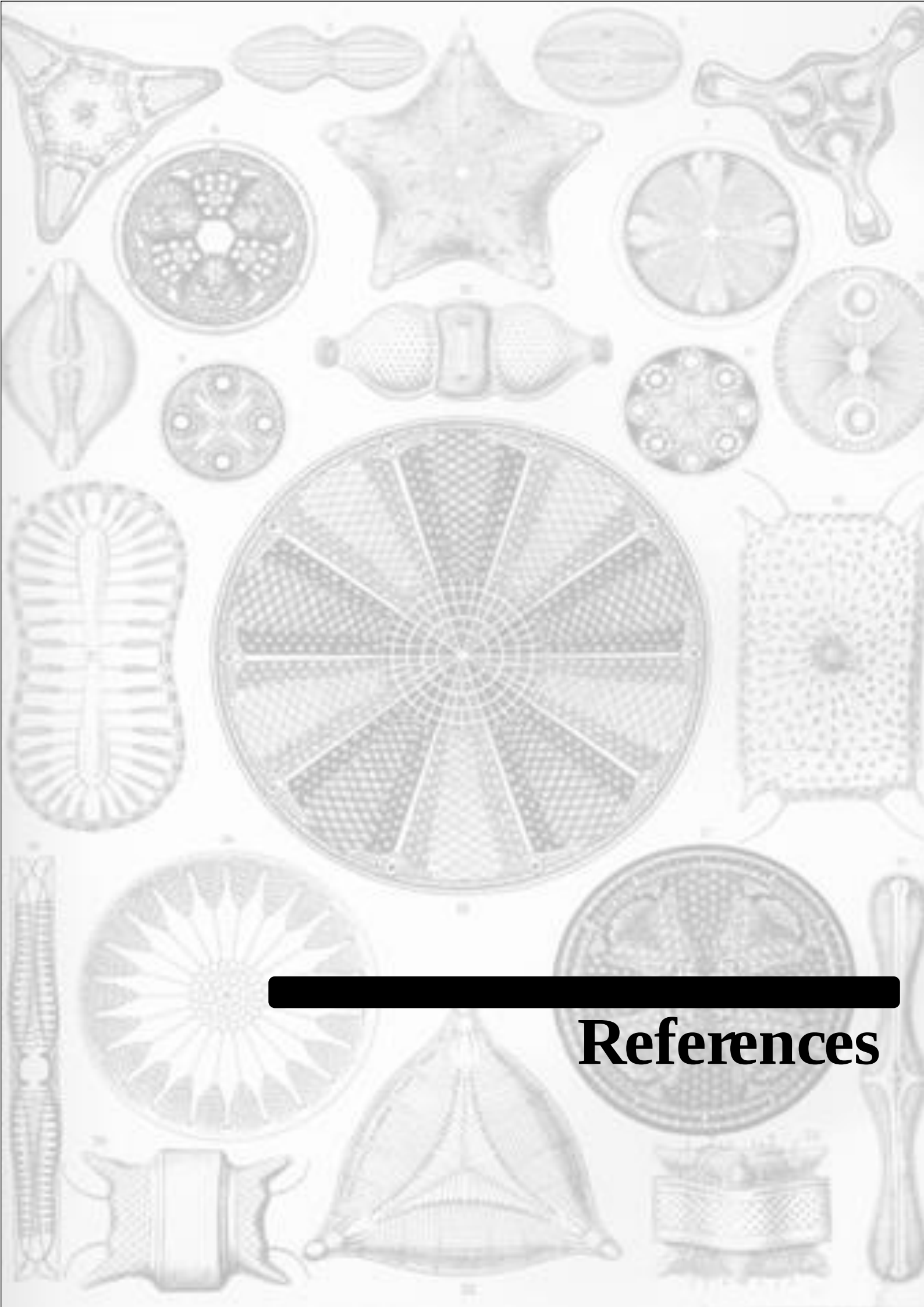

References

REFERENCES

Acevedo-Trejos, E.; Brandt, G.; Steinacher, M.; Merico, A. (2014) A glimpse into the future composition of marine phytoplankton communities. Front. Mar. Sci. 1: 15.

Acevedo-Trejos, E., Maranon, E., Merico, A. 2018. Phytoplankton size diversity and ecosystem function relationships across oceanic regions, Proc Biol Sci, 285, 10.1098/rspb.2018.0621.

Agawin, N.; Duarte, C.M.; Agustí, S (1998) Growth and abundance of Synechococcus sp. in a Mediterranean Bay: seasonality and relationship with temperature. Mar Ecol Prog Ser 15:45-53.

Alonso-Sáez, L.V.; Balagué, V.; Sà, E.L.; Sánchez, O.; González, J.M.; Pinhassi, J.; Massana, R.; Pernthaler, J; Pedrós-Alió, C.; Gasol, J.M. (2007) Seasonality in bacterial diversity in north-west Mediterranean coastal waters: assessment through clone libraries, fingerprinting and FISH. FEMS Microb Ecol 60:98-112.

Alvarez, E. S. (2014) Estructura y fisiología de la comunidad planctonica a partir de métodos de digitalización y análisis de imagen. Tesis Doctoral. Universidad de Oviedo.

Amato, A.; Kooistra, W.H.; Ghiron, J.H.; Mann, D.G.; Pröschold, T.; Montresor, M. (2007) Reproductive isolation among sympatric cryptic species in marine diatoms. Protist 158:193-207.

Aneeshkumar, N. and Sujatha C. H. (2012) Biomarker pigment signatures in Cochin back water system – A tropical estuary south west coast of India; Estuar. Coast. Shelf Sci. 99 182–190.

Araujo, M. L. V; Mendes, C. R. B., Tavano, M. T.; Garcia, C. A. E.; Baringer, M.O. (2017) Contrasting patterns of phytoplankton pigments and chemotaxonomic groups along 30°S in the subtropical South Atlantic Ocean**.** Deep Sea Research Part I: Oceanographic. Volume 120, 112-121. https://doi.org/10.1016/j.dsr.2016.12.004.

Arin, L.; Guillén, J.; Segura-Noguera, M.; Estrada, M. (2013) Open sea hydrographic forcing of nutrient and phytoplankton dynamics in a Mediterranean coastal ecosystem. Estuar Coast Shelf Sci 133:116–128.

Armbrecht, L. H.; Schaeffer, A.; Roughan, M.; Armand, L. K. (2015) Interactions between seasonality and oceanic forcing drive the phytoplankton variability in the tropical-temperate transition zone (~30°S) of Eastern Australia. Journal of Marine Systems journal (144) 2015 – 92 – 106.

Asher, E. C.; Dacey, J. W. H.; Mills, M. M.; Arrigo K. R. ; Torgell P. D. (2011) High concentrations and turnover rates of DMS, DMSP and DMSO in Antarctic sea ice. Geophysical Research Letters, Vol. 38, L23609, doi:10.1029/2011GL049712.

Atkinson, A.; Whitehouse, M. J.; Priddle, J.; Cripps, G. C.; Ward, P.; Brandon, M. A. (2001) South Georgia, Antarctica: a productive, cold water, pelagic ecosystem. Mar. Ecol. Prog. Ser. 216, 279–308.

Azam, F.; Fenchel, T.; Field, J.; Gray, J.; Meyer-Reil, L.; Thingstad, F. (1983) The ecological role of water-column microbes in the sea, Marine ecology progress series. Oldendorf, 10, 257-263.

Babin, M.; Stramski D.; Ferrari G. M.; Claustre, H.; Bricaud A.; Obolensky G.; Hoepffner, N (2003) Variations in the light absorption coefficients of phytoplankton, nonalgal particles, and dissolved organic matter in coastal waters around Europe, J. Geophys. Res., 108 (C7), 3211, doi:10.1029/2001JC000882.

BAIC = Butlletí Anual d'Indicadors Climàtics Any 2016 (2017) Equip de Canvi Climàtic, Àrea de Climatologia, Servei Meteorològic de Catalunya. Generalitat de Catalunya, Departament de Territori I Sostenibilitat, 88 pp. < http://static-m.meteo.cat/wordpressweb/wp-content/uploads/2017/05/29072030/00_BAIC-2016_TOT.pdf>, accessed 20/10/2017.

Bell, T. G.; Poulton, A. J.; Malin, G. (2010) Strong linkages between dimethylsulphoniopropionate (DMSP) and phytoplankton community physiology in a large subtropical and tropical Atlantic Ocean data set. Glob. Biogeochem. Cycles. 24, GB3009, http://doi:10.1029/2009GB003617.

Bidigare, R. R.; Ondrusek, M.; Morrow, J. H; Kiefer, D.A. (1990) In-vivo absorption properties of algal pigments. Proceedings of SPIE - The International Society for Optical Engineering 1302. DOI: 10.1117/12.21451.

Bidigare, R. R.; Buttler, F. R.; Christensen, S. J.; Barone, B.; Karl, D.M.; Wilson, S.T. (2014) Evaluation of the utility of xanthophyll cycle pigment dynamics for assessing upper ocean mixing processes at Station ALOHA. J. Plankton Res. (2014) 36(6): 1423–1433. doi:10.1093/plankt/fbu069.

Borrione, I.; Schlitzer, R. (2013) Distribution and recurrence of phytoplankton blooms around South Georgia, Southern Ocean. Biogeosciences. 10, 217-231.

Bouman, H. A.; Platt, T.; Sathyendranath, S.; Li, W. K. W.; Stu-art, V.; Fuentes-Yaco, C.; Maass, H.; Horne, E. P.W.; Ulloa, O.; Lutz, V.; Kyewalyanga, M. (2003) Temperature as indicator of optical properties and community structure of marine

phytoplankton: implications for remote sensing, Marine Ecology-Progress Series, 258, 19–30.

Boyd, P.W.; Trull, T.W. (2007) Understanding the export of biogenic particles in oceanic waters: Is there consensus? Prog. Oceanogr. 72, 276–312.

Brewin, R.J.; Lavender, S.J.; Hardman-Mountford, N.J.; Hirata, T. (2010) A spectral response approach for detecting dominant phytoplankton size class from satellite remote sensing. Acta Oceanol. Sin. 29, 14–32.

Brewin R. J. W.; Sathyendranath, S.; Lange, P.K.; Tilstone, G. (2014) Comparison of two methods to derive the size-structure of natural populations of phytoplankton. Deep- Sea Res. I 85, 72–79.

Brewin, R. J. W.; Sathyendranath, S.; Jackson, T.; Barlow, R.; Brotas, V.; Airs, R.; T. Lamont (2015) Influence of light in the mixed layer on the parameters of a three-component model of phytoplankton size structure, Remote Sens. Environ., 168, 437–450. doi: 10.1016/j.rse.2015.07.004.

Bricaud, A.; Babin, M.; Morel, A.; Claustre, H. (1995) Variability in the chlorophyll-specific absorption coefficients of natural phytoplankton: Analysis and parameterization, J. Geophys. Res. 100 (C7) 13. 321–13 332. https://doi:10.1029/95JC00463.

Bricaud, A.; Claustre, H.; Ras, J.; Oubelkheir, K. (2004) Natural variability of phytoplankton absorption in oceanic waters: influence of the size structure of algal populations. Journal of Geophysical Research 109, C11010.

Bricaud, A.; Babin, M.; Claustre, H.; Ras, J.; Tieche, F. (2010) Light absorption properties and absorption budget of Southeast Pacific waters. J. Geophys. Res. Oceans 115, 19.

Calbet, A.; Garrido, S.; Saiz, E.; Alcaraz, M.; Duarte, C. M. (2001) Annual zooplankton succession in coastal NW Mediterranean waters: the importance of the smaller size fractions. J Plankton Res 23:319-331.

Cassar, N.; DiFiore, P.J.; Barnett, B.A.; Bender, M.L.; Bowie, A.R.; Tilbrook, B.; Petrou, K.; Westwood, K.J.; Wright, S.W.; Lefevre, D. (2011) The influence of iron and light on net community production in the Subantarctic and Polar Frontal Zones, Biogeosciences. 8, 227-237.

Cassar, N.; Wright S. W.; Thomson P. G.; Trull T. W.; Westwood K. J.; de Salas M.; Davidson A.; Pearce I.; Davies D. M.; Matear R. J. (2015) The relation of mixed-

layer net community production to phytoplankton community composition in the Southern Ocean. Glob. Biogeochem. Cycles. 29, 446–462. http://doi:10.1002/2014GB004936.

Cebrián, J.; Duarte, C.M.; Marba, N.; Enriquez, S. (1996) Magnitude and fate of the production of four co-occurring western Mediterranean seagrass species. Mar Ecol Prog Ser 155:29–44.

Cefarelli, A.O.; Ferrario, M.E.; Almandoz, G.O.; Atencio, A.G.; Akselman, R.; Vernet, M. (2010) Diversity of the diatom genus *Fragilariopsis* in the Argentine Sea and Antarctic waters: morphology, distribution and abundance. Polar Biol. 33, 1463.

Cerino, F.; Zingone, A. (2006) A survey of cryptomonad diversity and seasonality at a coastal Mediterranean site. Eur J Phycol 41:363–378.

Chai C.; Jiang T.; Cen J.; Ge, W.; Lu. S. (2016) Phytoplankton pigments and functional community structure in relation to environmental factors in the Pearl River Estuary. Oceanologia. 58, 201—211 42:1353–1363.

Charles, F.; Lantoine, F.; Brugel, S.; Chrétiennot-Dinet, M-J-; Quiroga, I.; Rivière, B. (2005) Seasonal survey of the phytoplankton biomass, composition and production in a littoral NW Mediterranean site, with special emphasis on the picoplanktonic contribution. Estuar Coast Shelf Sci 65:199-212D'Ortenzio F, Ribera d'Alcalà M (2009) On the trophic regimes of the Mediterranean Sea: a satellite analysis. Biogeosciences 6:139–148.

Charlson, R. J.; Lovelock, J. E.; Andreae, M. O.; Warren, S. G. (1987) Oceanic phytoplankton, atmospheric sulphur, cloud albedo and climate. Nature. 326 (6114): 655–661. doi:10.1038/326655a0.

Cheah, W.; Soppa, M.A.; Wiegmann, S.; Ossebaar, S.; Laglera, L.M.; Strass, V.H.; Santos-Echeandía, J.; Hoppema, M.; Wolf-Gladrow, D.; Bracher, A. (2017) Importance of deep mixing and silicic acid in regulating phytoplankton biomass and community in the iron-limited Antarctic Polar Front region in summer. Deep-Sea Res. II. 138, 74-85.

Cleveland, J. S.; Weidemann A. D. (1993) Quantifying absorption by aquatic particles: A multiple scattering correction for glass-fiber filters. Limnol. Oceanogr. 38. 1321-1327.

Cros, L.; Estrada, M. (2013) Holo-heterococcolithophore life cycles: ecological implications. ;ar. Ecol. Prog. Ser. 492: 57–68. doi: 10.3354/meps10473.

Dall'Osto, M.; Ovadnevaite, J.; Paglione, M.; Beddows, D. C. S.; Ceburnis, D.; Cree, C.; Cortés, P.; Zamanillo, M.; Nunes, S.; Pérez, G.L.; Ortega-Retuerta, E.; Emelianov, M.; Vaqué, D.; Marrasé, C.; Estrada, M.; Sala, M.M.; Vidal, M.; Fitzsimons, M.F.; Beale, R.; Airs, R.; Rinaldi, M.; Decesari, S.; Facchini, M.C.; Harrison, R.M.; O'Dowd, C.; Simó, R. (2017) Antarctic sea ice region as a source of biogenic organic nitrogen in aerosols. Sci. Rep. 7(1), 6047.

Davies, C.H.; Coughlan, A.; Hallegraeff, G.; Ajani, P.; Armbrecht, L.; Atkins, N.; Bonham, P.; Brett, S.; Brinkman, R.; Burford, M.; Clementson, L.; Coad, P.; Coman, F.; Davies, D.; Dela-Cruz, J.; Devlin, M.; Edgar, S.; Eriksen, R.; Furnas, M.; Hassler, C.; Hill, D.; Holmes, M.; Ingleton, T.; Jameson, I.; Leterme, S.C.; Lønborg, C.; McLaughlin, J.; McEnnulty, F.; McKinnon, A.D.; Miller, M.; Murray, S.; Nayar, S.; Patten, R.; Pausina, R.A.; Pritchard, T.; Proctor, R.; Purcell-Meyerink, D.; Raes, E.; Rissik, D.; Ruszczyk, J.; Slotwinski, A.; Swadling, K.M.; Tattersall, K.; Thompson, P.; Thomson, P.; Tonks, M.; Trull, T.W.; Uribe-Palomino, J.; Waite, A.M.; Yauwenas, R.; Zammit, A.; Richardson, A.J. (2016) A database of marine phytoplankton abundance, biomass and species composition in Australian waters. Scientific Data. 3:160043. http:// doi:10.1038/sdata.2016.43. Updated 11 April 2017.

de Vargas, C.; Audic, S.; Henry, N.; Decelle, J.; Mahe, F.; Logares, R.; Lara, E.; Bescot, N. L.; Probert, I.; Carmichael, M.; Poulain, J.; Romac, S.; Colin, S.; Aury, J-M.; Bittner L., Chaffron, S.; Engelen, S.; Flegontova, O.; Guidi, L.; Horak, A.; Jaillon, O. (2015) Eukaryotic plankton diversity in the sunlit ocean. Science 348.

Díez, B.; Pedrós-Alió, C., Marsh, T.L.; Massana, R. (2001) Application of denaturing gradient gel electrophoresis (DGGE) to study the diversity of marine picoeukaryotic assemblages and comparison of DGGE with other molecular techniques. Appl Environ Microbiol 67:2942–2951.

Dinniman, M. S.; Klinck, J. M. (2004) A model study of circulation and cross-shelf exchange on the west Antarctic Peninsula continental shelf. Deep-Sea Res. II. 51, 2003–2022.

Doney, S. C. (2006) Plankton in a Warner World. Nature 444:695-696. DOI:10.1038/444695a.

Duarte, C. M; Agustí, S.; Kennedy, H.; Vaqué, D. (1999) The Mediterranean climate as a template for Mediterranean marine ecosystems: the example of the northeast Spanish littoral. Prog Oceanogr 44:245–270.

Ducklow, H. W.; Baker, K.; Fraser, W. R.; Martinson, D. G.; Quetin, L. B.; Ross, R. M.; Smith, R. C.; Stammerjohn, S.; Vernet, M. (2007) Marine ecosystems: the West Antarctic Peninsula. Phil. Trans. R. Soc. 362, 67–94.

Egge, J.K.; Aksnes, D.L. (1992) Silicate as a regulating nutrient in phytoplankton competition. Mar. Ecol. Prog. Ser. 83, 281– 289.

Eppley, R. W.; Peterson, B. J. (1979) Particulate organic matter flux and planktonic new production in the deep ocean. Nature 282:677-680. DOI:10.1038/282677a.

Estrada, M. (1979) Observaciones sobre heterogeneidad del fitoplancton en zona costera del mar Catalán. Inv Pesq 43:637- 666.

Estrada, M. (1999) Hidrodinàmica i fitoplàncton en el mar Català. Mem Reial Acad Ciènc Arts Barcelona. 961, vol 58(6):187-247.

Estrada, M.; Delgado, M. (1990) Summer phytoplankton distributions in the Weddell Sea. Polar Biol. 10, 441-449.

Estrada, M.; Marrasé, C.; Salat, J. (1996) *In vivo* Fluorescence/chlorophyll *a* ratio as an ecological indicator in oceanography. Scientia Marina. 60, 317-325.

Estrada, M.; Arin, L.; Blasco, D.; Blauw, A.; Camp. J.; Garcés, E.; Sampedro, N.; Vila M. (2008) A fuzzy logic model for *Alexandrium minutum* proliferations in harbours of the Catalan coast (NW Mediterranean). In: Moestrup Ø et al. (eds) Proceedings of the 12th International Conference on Harmful Algae. International Society for the Study of Harmful Algae and Intergovernmental Oceanographic Commission of UNESCO, Copenhagen, p 111-113.

Estrada, M.; Vaqué, D. (2014) Microbial components. In: Goffredo E and Dubinsky Z (eds) The Mediterranean Sea: Its history and present challenges. Springer, Dordrecht, p 87-111.

Estrada. M.; Delgado, M.; Blasco, D.; Latasa, M.; Cabello, A. M.; Benítez-Barrios, V.; Fraile-Nuez, E.; Mozetič, P.; Vidal, M. (2016) Phytoplankton across Tropical and Subtropical Regions of the Atlantic, Indian and Pacific Oceans. PLoS ONE 11(3): e0151699. DOI:10.1371/journal.pone.0151699.

Ettre, L. S. (2003) M.S. Tswett and the Invention of Chromatography. LCGC North America Volume 21 Number 5.

Falkowski P. G. (2012) Ocean Science: The power of plankton. Nature volume 483, pages S17–S20.

Falkowski, P.G.; Woodhead, A.D. (1992) Primary Productivity and Biogeochemical Cycles in the Sea (Environmental Science Research: Volume 43) Plenum Press, June 1992 ISBN 0306441926.

Falkowski, P.G.; Kolber, Z. (1995) Variations in chlorophyll fluorescence yields in phytoplankton in the world oceans. Aust. J. Plant Physiol. 22, 341-355.

Falkowski, P. G.; Raven, J. A. (1997) Aquatic Photosynthesis. Oxford, United Kingdom: Blackwell Science.

Falkowski, P. G.; Barber, R. T.; Smetacek, V. (1998) Biogeochemical Controls and Feedbacks on Ocean Primary Production. Science. Vol. 281, Issue 5374, pp. 200-206. DOI: 10.1126/science.281.5374.200.

Falkowski, P.G.; Laws, E.A.; Barber, R.T.; Murray, J.W. (2003) Phytoplankton and their role in primary, new and export production. In: Fasham, M.J.R. (Ed.) Ocean Biogeochemistry: The Role of the Ocean Carbon Cycle in Global Change. Global Change—The IGBP Series, pp. 99–119.

Falkowski P.G.; Katz M. E.; Knoll A. H.; Quigg A.: Raven J. A.; Schofield O.; Taylor F. J. R. (2004) The Evolution of Modern Eukaryotic Phytoplankton. Science. 16 Jul 2004: Vol. 305, Issue 5682, pp. 354-360. DOI: 10.1126/science.1095964.

Falster, D.S.; Warton, D.I.; Wright, I.J. (2006) SMATR: Standardised major axis tests and routines, ver 2.0. http://www.bio.mq.edu.au/ecology/SMATR/.

Farrant, G. K.; Doré, H.; Cornejo-Castillo, F. M; Partensky, F.; Ratin, M.; Ostrowski, M.; Pitt, F. D.; Wincker, P.; Scanlan, D. J.; Ludicone, D.; Acina, S. G.; Garczarek, L. (2016) Delineating ecologically significant taxonomic units from global patterns of marine picocyanobacteria. PNAS.113 (24) E3365-E3374; published ahead of print June 2, 2016. https://doi.org/10.1073/pnas.1524865113.

Ferreira, A.; Stramski, D.; Garcia, C. A. E.; Garcia, V. M. T.; Ciotti, A. M.; Mendes, C. R. B. (2013) Variability in light absorption and scattering of phytoplankton in Patagonian waters: Role of community size structure and pigment composition. Journal of Geophysic research: oceans. Vol. 118, 1-17. http://doi: 10.1002/jgrc. 20082, 2013.

Field, C.B.; Behrenfeld, M.J.; Randerson, J.T.; Falkowski, P. (1998) Primary production of the biosphere: integrating terrestrial and oceanic components. Science 281, 237-240.

Fisher, N. L.; Halsey K. H. (2016) Mechanisms that increase the growth efficience of diatoms in low light. Photosynth. Res. 129, 183–197.

Flombaum, P.; Gallegos, J.L.; Gordillo, R. A.; Rincon, J.; Zabala, L. L.; Jiao, N.; Karl, D. M.; Li, W. K. W.; Lomas, M. W.; Veneziano, D.; Vera, C. S.; Vrugt, J. A.; Martiny, A. C. (2013) Present and future global distributions of the marine Cyanobacteria *Prochlorococcus* and *Synechococcus*. Proc Natl Acad Sci 110:9824 – 9829.

Frölicher, T. L.; Sarmiento, J.L.; Paynter, D.J.; Dunne, J.P.; Krasting, J.P.; Winton, M.; (2015) Dominance of the Southern Ocean in Anthropogenic Carbon and Heat Uptake in CMIP5 Models. J. Climate. 28, 862-886.

Galí, M.; Simó, R.; Vila-Costa, M.; Ruiz-González, C.; Gasol, J. M.; Matrai, P. A. (2013) Diel patterns of oceanic dimethylsulfide (DMS) cycling: Microbial and physical drivers, Global Biogeochem. Cy., 27, 620–636.

Gallisai, R.; Peters, F.; Volpe, G.; Basart, S.; Baldasano, J. M. (2014) Saharan dust deposition may affect phytoplankton growth in the Mediterranean Sea at ecological time scales. PLoS ONE, 9 (10), e110762.

Garcia, V. M. T.; Garcia, C.A.E.; Mata, M.M.; Pollery, R. C.; Piola, A.R.; Signorini, S. R.; McClain, C. R.; Iglesias-Rodriguez, M. D. (2008) Environmental factors controlling the phytoplankton blooms at the Patagonia shelf-break in spring. Deep-Sea Research I 55, 1150–1166.

Garczarek, L.; Dufresne, A.; Rousvoal, S.; West, N. J.; Mazard, S.; Marie, D.; Claustre, H.; Raimbault, P.; Post, A. F.; Scanlan, D. J.; Partensky, F. (2007) High vertical and low horizontal diversity of Prochlorococcus ecotypes in the Mediterranean Sea in summer. FEMS MicrobEcol 60:189-206.

Garibotti, I.A.; Vernet, M.; Kozlowski, W.A.; Ferrario, M. E. (2003) Composition and biomass of phytoplankton assemblages in coastal Antarctic waters: a comparison of chemotaxonomic and microscopic analyses. Mar. Ecol. Prog. Ser. 247, 27–42.

Gasol J. M.; Giorgio P. A. (2000) Using flow cytometry for counting natural planktonic bacteria and understanding the structure of planktonic bacterial communities. Sci. Mar. 64:197–224.

Gasol, J.; Massana, R.; Simó, R.; Marrasé, C.; Acinas, S.; Pedrós-Alió, C.; Pelejero, C.; Sala, M.; Calvo, E.; Vaqué, D.; Peters, F. (2012) Blanes Bay (Site 55). ICES Cooperative Research Report No. 313, pp 136-141.

Gasol, J.; Cardelús, C.; Morán, X. A.; Balagué, V.; Forn, I.; Marrasé, C.; Massana, R.; Pedrós-Alió, C.; Sala, M.; Simó, R.; Vaqué, D.; Estrada, M. (2016) Seasonal patterns in phytoplankton photosynthetic parameters and primary production at a coastal NW Mediterranean site. Sci Mar 80S1:63-77. DOI: http://dx.DOI.org/10.3989/scimar.04480.06E.

Gibb, S. W.; Cummings D.G.; Irigoien; X.; Barlow R.G.; Mantoura R.F.C (2001) Phytoplankton pigment chemotaxonomy of the Northeastern Atlantic. Deep-Sea Res II 48:795–823.

Gieskes W.W.C., Kraay G.Y., Tijssen, S.B. (1978) Chlorophylls and their degradation products in the deep pigment maximum layer of the tropical North Atlantic. Netherlands Journal of Sea Research, 12. pp. 195-204.

Gieskes, W. W. C.; Kraay, G.W. (1986) Floristic and physiological differences between the shallow and the deep nanophytoplankton community in the euphotic zone of the open tropical Atlantic revealed by HPLC analysis of pigments. Mar Biol 91:567–576.

Gieskes, W. W.; Kraay, C.; Nontji, G.W.; Setiapermana, A. D.; Sutomo, D. (1988) Monsoonal alternation of a mixed and a layered structure in the phytoplankton of the euphotic zone of the Banda Sea (Indonesia): A mathematical analysis of algal pigment fingerprints, Netherlands J. Sea Res., 22, 123–137.

Giner, C.R. (2017) Spatial, temporal and behavioral patterns of marine protists. Tesis Doctoral. Universitat Politecnica de Catalunya.

Goericke, R; Repeta, D. J. (1993) Chlorophylls *a* and *b* and divlnyl chlorophylls *a* and *b* in the open subtropical North Atlantic Ocean. Mar. Ecol Prog. Ser. 101: 307-313.

Goericke, R.; Montoya, J.P. (1997) Estimating the contribution of microalgal taxa to chlorophyll *a* in the field-variations of pigment ratios under nutrient- and light-limited growth. Mar. Ecol. Prog. Ser. 169, 98-112.

Goffart, A.; Hecq, J. H.; Legendre, L. (2015) Drivers of the winter‐spring phytoplankton bloom in a pristine NW Mediterranean site, the Bay of Calvi (Corsica): A long-term study (1979‐2011). Prog Oceanogr 137:121-139.

Gonçalves-Araujo, R.; Rabe, B.; Peeken, I.; Bracher, A.; Wiegmann, S.; Bracher, A. (2018) High colored dissolved organic matter (CDOM) absorption in surface waters of the central-eastern Arctic Ocean: Implications for biogeochemistry and ocean color algorithm. PLOS ONE 13(1): 0190838. https://doi.org/10.1371/journal.pone.0190838

Guadayol, Ò.; Marrasé, C.; Peters, F.; Berdalet, E.; Roldán, C.; Sabata, A. (2009) Responses of coastal osmotrophic planktonic communities to simulated events of turbulence and nutrient load. J Plankton Res 31:583-600. DOI: 10.1093/plankt/fbp019.

Guillou L.; Chrétiennot-Dinet M. J.; Medlin L. K.; Claustre H., S.; Loiseaux de Goër, Vaulot D. (1999) Bolidomonas: a new genus with two species belonging to a new algal class, the Bolidophyceae (Heterokonta). Journal of Phycology 35:368-381.

Gutiérrez-Rodríguez, A.; Latasa, M.; Scharek, R.; Massana, R.; Vila, G.; Gasol, J. M. (2011), Growth and grazing rate dynamics of major phytoplankton groups in an oligotrophic coastal site, Estuar Coast Shelf Sci 95:77–87.

Hansen H.P.; Koroleff, F. (1999) Determination of nutrients, in: Grasshoff K, Kremling K, Ehrhardt M (Eds.). Methods of Seawater Analyses. Wiley-VCH, Weinheim, 161–228.

Higgins, H.W.; Wright, S.W.; Schlüter, L. (2011) Quantitative interpretation of chemotaxonomic pigment data, Phytoplankton Pigments, in: Roy S., Llewellyn C. A., Egeland E.S., Johnsen G., (Eds.), Characterization, Chemotaxonomy and Applications in Oceanography. Cambridge University Press, Cambridge, 257-313.

Hirata, T.; Hardman-Mountford, N. J.; Brewin, R. J. W.; Aiken, J.; Barlow, R.; Suzuki, K. (2011) Synoptic relationships between surface chlorophyll *a* and diagnostic pigments specific to phytoplankton functional types. Biogeosciences. 8, 311–327, doi: 10.5194/bg-8- 311-2011.

Hirata, T.; Hardman-Mountford, N. J.; Brewin, R. J. W.; Aiken, J.; Barlow, R.; Suzuki, K. (2011) Synoptic relationships between surface chlorophyll *a* and diagnostic pigments specific to phytoplankton functional types. Biogeosciences. 8, 311–327.

Hoepffner, N.; Sathyendranath, S. (1991) Effect of pigment composition on absorption properties of phytoplankton. Mar. Ecol. Prog. Ser., 73, 11–23.

Huete-Ortega, M., Calvo-Díaz, A., Graña, R., Mouriño-Carballido, B., and Marañón, E.: Effect of environmental forcing on the biomass, production and growth rate of

size-fractionated phytoplankton in the central Atlantic Ocean, Journal of Marine Systems, 88, 203-213, 2011.

Hunter-Cevera, K. R.; Neubert, M. G.; Olson, R. J.; Solow, A. R.; Shalapyonok, A.; Sosik, H. M. (2016) Physiological and ecological drivers of early spring blooms of a coastal phytoplankter. Science 354:326-329. DOI: 10.1126/scienceaaf8536.

Ichinomiya, M.; Yoshikawa, S.; Kamiya, M.; Ohki, K.; Takaichi, S.; Kuwata A. (2010) Isolation and characterization of Parmales Heterokonta / Heterokontophyta / Stramenopiles) from the Oyashio region, western north Pacific. Journal of Phycology 47:144-151.

Ichinomiya, M.; Kuwata, A. (2015) Seasonal variation in abundance and species composition of the Parmales community in the Oyashio region, western North Pacific. Aquat Microb Ecol 75: 207–223.

Ichinomiya, M.; Santo, A. L.; Gourvil, P.; Yoshikawa, S.; Kamiya, M.; Ohki, K.; Audic, S.; de Vargas C. (2016) Diversity and oceanic distribution of the Parmales (Bolidophyceae), a picoplanktonic group closely related to diatoms. The ISME Journal 10, 2419–2434. 1751-7362/16

Irigoien, X.; Huisman, J.; Harris, R.P. (2004). Global biodiversity patterns of marine phytoplankton and zooplankton. Nature 429: 863–867.

Jeffrey, S. W. (1968) Quantitative thin layer chromatography of chlorophylls and carotenoids from marine algae. Bioch. Biophys. Acta. 162:271–295.

Jeffrey, S.W. (1976) Mar. Biol. 37: 33-37.

Jeffrey, S.W. (1974) Profiles of photosynthetic pigments in the ocean using thin-layer chromatography. Mar. Biol. 26: 101-110.

Jeffrey, S. W.; Mantoura, R. F. C.; Wright, S. W. (1997) Phytoplankton Pigments in Oceanography: Guidelines to Modern Methods. Paris: UNESCO Publishing, 407–428.

Jeffrey, S.W.; Wright, S.W.; Zapata, M. (1999) Recent advances in HPLC analysis of phytoplankton. Mar Freshw Res. 50: 879–896.

Jewson, D.; Kuwata, A.; Cros, L.; Fortuño, J-M.; Estrada, M. (2016) Morphological adaptations to small size in the marine diatom Minidiscus comicus. Scientia Marina 80S1. 89-96. ISSN-L: 0214-8358. http://dx.doi.org/10.3989/scimar.04331.06C.

Jiao, N.; Herndl, G. J.; Hansell, D. A.; Benner, R.; Kattner, G.; Wilhelm, S. W.; Kirchman, D. L.; Weinbauer, M. G.; Luo, T.; Chen, F.; Azam, F. (2010) Microbial production of recalcitrant dissolved organic matter: long-term carbon storage in the global ocean. Nat. Rev. Microbiol. 8:593–599.

Jochem, F.J. (2001) Morphology and DNA content of bacterioplankton in the northern Gulf of Mexico: analysis by epifluorescence microscopy and flow cytometry. Aquat. Microb. Ecol. 25: 179-194.

Johnson, P.W.; Sieburth, J.M. (1982) In-situ morphology and occurrence of eukaryote phototrophs of bacterial size in the picoplankton of estuarine and oceanic waters. J. Phycol 18, 318–327.

Johnson, Z. I.; Zinser, E.R.; Coe, A.; McNulty, N.P.; Woodward, E.M.; Chisholm, S.W. (2006) Niche partitioning among *Prochlorococcus* ecotypes along ocean-scale environmental gradients. Science 311: 1737–1740.

Johnson, Z. I and Martiny A. C. (2015) Techniques for Quantifying Phytoplankton Biodiversity. Annu. Rev. Marine. Sci. 7:299-314. Doi 10.1146/annurev-marine-010814-015902.

Kaczsmarska, I.; Lovejoy, C.; Potvin, M.; Macgillivary, M. (2009) Morphological and molecular characteristics of selected species of *Minidiscus* (Bacillariophyta, Thalassiosiraceae), European Journal of Phycology, 44:4, 461-475, DOI: 10.1080/09670260902855873.

Kennish, M.J. (2001). Practical Handbook of Marine Science, third ed. CRC Press, Boca Raton, pp. 441- 469.

Kiørboe, T. (1993) Turbulence, phytoplankton cell size, and the structure of pelagic food webs. Advances in Marine Biolo gy, 29: 1-72.

Kirk, J. T. O. (1994) Light and Photosynthesis in Aquatic Ecosystems, Cambridge University Press, 15.

Kishino, M.; Takahashi, M.; Okami, N.; Ichimura S. (1985) Estimation of the spectral absorption coefficients of phytoplankton in the sea. Bull. Mar. Sci. 37: 634-642.

Klaas, C.; Archer, D. E. (2002)Association of sinking organic matter with various types of mineral ballast in the deep sea: Implications for the rain ratio, Global Biogeochemical cycle, 16(4).

Kopczyńska E.E. (1991) Distribution of micro flagellates and diatoms in the sea-ice zone between Elephant Island and the South Orkney Islands (December 1988 — January 1989). Pol. Polar Res. 12, 515-528.

Korb, R.E.; Whitehouse, M.J.; Gordon, M.; Ward, P.; Poulton, A.J. (2010) Summer microplankton community structure across the Scotia Sea: implications for biological carbon export. Biogeosciences. 7, 343–356. www.biogeosciences.net/7/343/2010/.

Kostadinov, T.; Siegel, D.; Maritorena, S. (2010) Global variability of phytoplankton functional types from space: assessment via the particle size distribution. Biogeosciences 7, 3239–3257.

Kozlowski, W. A.; Deutschman, D.; Garibotti, I.; Trees, C.; Vernet, M. (2011) An evaluation of the application of CHEMTAX to Antarctic coastal pigment data. Deep-Sea Res. I. 58, 350 –364.

Kumari, B. (2005) Comparison of high performance liquid chromatogra- phy and fluorometric ocean colour pigments, J. Indian Soc. Remote Sens., 33, 541–546.

Latasa, M. (2007) Improving estimations of phytoplankton class abundances using CHEMTAX. Mar Ecol Prog Ser 329:13-21

Latasa, M. (2014) A simple method to increase sensitivity for RP-HPLC phytoplankton pigment analysis Limnol. Oceanogr.: Methods 12, 2014, 46–53.

Latasa, M.; Scharek, R.; Vidal, M.; Vila-Reixach, G.; Gutiérrez-Rodríguez, A.; Emelianov, M.; Gasol, J. M. (2010) Preferences of phytoplankton groups for waters of different trophic status in the northwestern Mediterranean Sea. Mar Ecol Prog Ser 407:27–42.

Latasa, M.; Cabello, A. M.; Moraán, X. A. G.; Massana, R.; Scharek, R. (2017) Distribution of phytoplankton groups within the deep chlorophyll maximum. Limnol. Oceanogr. 62, 665-685.

Lavaysse, C.; Vrac, M.; Drobinski, P.; Lengaigne, M.; Vischel, T. (2012) Natural Hazards and Earth System Sciences. Statistical downscaling of the French Mediterranean climate: assessment for present and projection in an anthropogenic scenario. Nat Hazards Earth Syst Sci 12:651–670.

Le Quéré, C.; Harrison, S.P.; Prentice I.C.; Buitenhuis E. T. (2005) Ecosystem dynamics based on plankton functional types for global ocean biogeochemistry models. Glob Change Biol 11:2016–2040 doi:10.1111/j.1365- 2486.2005.1004.

Legendre, L.; Le Fèvre J. (1995) Microbial food webs and the export of biogenic carbon in oceans. Aquatic Microbial Ecology. Vol 9: 69-77.

Lionard, M.; Muylaert, K.; Tackx, M.; Vyverman, W. (2008) Evaluation of the performance of HPLC - CHEMTAX analysis for determining phytoplankton biomass and composition in a turbid estuary (Schelde, Belgium). Est Coast Shelf Sci 76:809-817.

Litchman, E.; Klausmeier, C. A. (2008) Trait-Based Community Ecology of phytoplankton. Annual Review of Ecology, Evolution and Systematics. Vol. 39:615-639. https: //doi.org/10.1146/annurev.ecolsys.39.110707.173549

Llabrés, M.; Agustí, S.; Alonso-Laita, P.; Gerhard, J. H. (2010) *Synechococcus* and *Prochlorococcus* cell death induced by UV radiation and the penetration of lethal UVR in the Mediterranean Sea. MEPS Vol. 399: 27– 37. DOI: 10.3354/meps08332

Lohrenz, S. E.; A. D. Weidemann; Tuel, M. (2003) Phytoplankton spectral absorption as influenced by community size structure and pigment composition, J. Plankton Res., 25(1), 35–61.

Lomas MW, Bonachela JA, Levin SA, Martiny AC (2014) Impact of ocean phytoplankton diversity on phosphate uptake. P Natl Acad Sci USA 111:17540–17545. DOI/10.1073/pnas.1420760111.

Longhurst, A. R. (2007) Ecological geography of the sea. Burlington, MA: Academic Press. 542 p

Lorenzen, C.J. (1966) A method for the continuous measurement of in vivo chlorophyll concentration. Deep-Sea Res. 13, 223-227.

Lovelock, J. E.; Maggs, J.; Rasmussen, R. A. (1972) Atmospheric dimethylsulphide and the natural sulphur cycle. Nature 1972, 237, 452.doi:10.1038/237452A0

Lucea, A.; Duarte, C. M.; Agustí, S.; Kennedy, H. (2005) Nutrient dynamics and ecosystem metabolism in the Bay of Blanes (NW Mediterranean). Biogeochemistry 73:303–323.

Macías, D.; Martin, A.P.; García Lafuente, J.; García, C. M.; Yool, A.; Bruno, M.; Vázquez, A.; Izquierdo, A.; Sein, D.; Echevarría, F. (2007) Mixing and biogeochemical effects induced by tides at on the Atlantic-Mediterranean flow in the Strait of Gibraltar. Prog. Oceanogr. 74:252–272.

Mackey, M.D.; Mackey, D.J.; Higgins, H.W.; Wright, S.W. (1996) CHEMTAX - a program for estimating class abundances from chemical markers: application to HPLC measurements of phytoplankton. Marine Ecology Progress Series 144, 265 - 283.

Marañón, E., Holligan, P. M., Barciela, R., González, N., Mouriño, B., Pazó, M. J., and Varela, M.: Patterns of phytoplankton size structure and productivity in contrasting open-ocean environments, Marine Ecology Progress Series, 216, 43-56, 2001.

Margalef, R. (1957) Fitoplancton de las costas de Blanes (Gerona) de Agosto de 1952 a Junio de 1956. Inv Pesq 8:89-95.

Margalef, R. (1964) Fitoplancton de las costas de Blanes (provincia de Gerona, Mediterráneo occidental) de julio de 1959 a junio de 1963. Inv Pesq 26:131-164.

Margalef R (1978) Life forms of phytoplankton as survival alternatives in an unstable environment. Oceanol Acta 1:493 – 509.

Marie D, Partensky F, Vaulot D, Brussaard C (2001) Enumeration of phytoplankton, bacteria, and viruses in marine samples. Curr Protoc Cytom Chapter 11: Unit 11.11Marín I, Nunes S, Sánchez-Pérez ED, Txurruka E, Antequera C, Sala MM, Marrasé C, Peters F (2017) Coastal bacterioplankton metabolism is stimulated stronger by anthropogenic aerosols than Saharan dust. Front Microbiol 8. DOI: 10.3389/fmicb.2017.02215.

Marinov, I.; Gnanadesikan, A.; Sarmiento, J. L.; Toggweiler, J. R.; Follows, M.; Mignone, B. K. (2008) Impact of oceanic circulation on biological carbon storage in the ocean and atmospheric pCO2. Glob. Biogeochem. Cycles. 22, GB3007.

Marra, J.; Trees, C. C.; O'Reilly, J. E. (2007) Phytoplankton pigment absorption: A strong predictor of primary productivity in the surface ocean. Deep Sea Research I, 54, 155−163.

Martin, J.; Fitzwater, S.; Gordon R. (1990) Iron Deficiency Limits Phytoplankton Growth in Antarctic Waters. Glob. Biogeochem. Cycles. 4, 5–12.

Martin-Vide, J. (2016) Tercer informe sobre el canvi climàtic a Catalunya. Institut d'Estudis Catalans i Generalitat de Catalunya, 624 pp.

Marty, J. C.; Chiaverini, J.; Pizay, M. D.; Avril, B. (2002) Seasonal and interannual dynamics of nutrients and phytoplankton pigments in the western Mediterranean Sea at the DYFAMED time-series station (1991-1999). Deep Sea Res Pt II 49:1965 – 1985

Masó, M.; Tintoré, J. (1991) Variability of the shelf water off the northeast Spanish coast. J Mar Sys 1: 441-460.

McClain, C.; Feldman G. C.; Hooker, S. B. (2004) An overview of the SeaWiFS project and strategies for producing a climate research quality global ocean bio-optical time series. Deep-Sea Research II 51:5-42.

Mella-Flores, D.; Mazard, S.; Humily, F.; Partensky, F.; Mahé, F.; Bariat, L.; Courties, C.; Marie, D.; Ras, J.; Mauriac, R.; Jeanthon, C.; Mahdi-Bendif, E.; Ostrowski, M.; Scanlan, D. J.; Garczarek, L. (2011) Is the distribution of *Prochlorococcus* and *Synechococcus* ecotypes in the Mediterranean Sea affected by global warming? Biogeosciences 8 2785–2804. DOI:10.5194/bg-8-2785-2011.

Mendes, C.R.; Sá, C.; Vitorino, J.; Borges, C.; Garcia, V.M.T.; Brotas, V. (2011) Spatial distribution of phytoplankton assemblages in the Nazaré submarine canyon region (Portugal): HPLC-CHEMTAX approach. J. Mar. Syst. 87, 90–101.

Mendes, C. R. B.; Silva de Souza, M.; Tavano, V. M.; Leal, M. C.; Brotas, V.; Garcia, C. A. E. (2012) Dynamics of phytoplankton communities during late summer around the tip of the Antarctic Peninsula. Deep-Sea Res. I. 65,1-14.

Mendes, C. R. B., Tavano, V.M., Leal, M.C., Silva de Souza, M., Brotas, V., Garcia, C.A.E. (2013) Polar Biol. 36, 537–547. http://10.1007/s00300-012-1282-4.

Mendes, C.R.B.; Kerr, R.; Tavano, V. M.; Cavalheiro, F. A.; Garcia, C. A. E.; Dessai, D. R. G.; Anilkumar, N. (2015) Cross-front phytoplankton pigments and chemotaxonomic groups in the Indian sector of the Southern Ocean. Deep-Sea Res. II. 118, 221–232.

Mendes C.R.B.; Odebrecht, C.; Tavano, V. M.; Abreu, P. C. (2016) Pigment-based chemotaxonomy of phytoplankton in the Patos Lagoon estuary (Brazil) and adjacent coast. Mar Biol Res. DOI: 10.1080/17451000.2016.1189082.

Mendes, C. R. B.; Tavano, V. M.; Kerr, R.; Dotto, T.S.; Maximiano, T.; Secchi, E. R.; 2017. http://doi.org/10.1016/j.dsr2.2017.12.003.

Menna, M.; Faye, S.; PoulainP-M.; Centurioni, L.; Lazar, A.; Gaye, A.; Sow, B.; Dagorne, D. (2016) Upwelling features off the coast of north-western Africa in 2009-2013. ollettino di Geofisica Teorica ed Applicata Vol. 57, n. 1, pp. 71-86; March 2016. DOI 10.4430/bgta0164.

Meredith, M.P.; Nicholls, K.W.; Renfre, I.A.; Boehme, L.; Biuw, M.; Fedak, M. (2011) Seasonal evolution of the upper-ocean adjacent to the South Orkney Islands, Southern Ocean: Results from a ‘‘lazy biological mooring’’. Deep-Sea Res. II. 58, 1569-1579.

Mignot, A.; Claustre, H.; D'Ortenzio, F.; Xing, X.; Poteau, A.; Ras., J. (2011) From the shape of the vertical profile of in vivo fluorescence to Chlorophyll-a concentration. Biogeosciences. 8, 2391–2406.

Millie, D. F.; Paerl, H. W.; Hurley, J. P. (1993) Microalgal pigment assessment using high-performance liquid chromatography: a synopsis of organismal and ecological applications. Can J Fish Aquat Sci 50:2513–2527;

Mitchell, G.; Kiefer, D. A. (1988) Chlorophyll a specific absorption and fluorescence excitation spectra for light- limited phytoplankton. Deep-Sea Res: 35: 639-663.

Mitchell, G.; Carder, K.; Cleveland, J.; Ferrari, G.; Gould, R.; Kahru, M.; Kishino, M.; Maske, H.; Moisan, T.; Moore, L.; Nelson, N.; Phimney, D.; Reynodls. R.; Sosik, H.; Stramski, D.; Tassan, S.; Trees, C.; Weideman, A.; Wieland, J.; Vodacek, A. (2000) Ocean Optics Protocols for Satellite Ocean Colour Sensor Validation, Revision 2. NASA Tech. Memo. 209966. In: Determination of Spectral Absorption Coefficients of Particles, Dissolved Material and Phytoplankton for Discrete Water Samples. NASA Goddard Space Flight Center. Greenbelt. Maryland. Ch. pp. 125e153.

Moline, M.A.; Claustre, H.; Frazer, T.K.; Schofield, O.; Vernet, M. (2004) Alteration of the food web along the Antarctic Peninsula in response to a regional warming trend. Glob. Change Biol. 10, 1973–1980.

Monterey, G.; Levitus, S. (1997) Seasonal Variability of Mixed Layer Depth for the World Ocean. NOAA Atlas NESDIS 14, U.S. Gov. Printing Office, Washimgton D.C. 96 pp. 87 figs.

Moore, C. M.; Mills M. M.; Arrigo K. R.; Berman-Frank I.; Bopp L.; Boyd P.; Galbraith W., E. D.; Geider R. J.; Guieu C.; Jaccard S. L.; Jickells T. D.; La Roche J.; Lenton T. M.; Mahowald N. M.; Marañón E.; Marinov I.; Moore J. K.; Nakatsuka T.; Oschlies A.; Saito M. A.; Thingstad T. F.; Tsuda A.; Ulloa O. (2013) Processes and patterns of oceanic nutrient limitation. Nat. Geosci. 6, 701-710.

Morel, A. (1991) Light and marine photosynthesis: A spectral model with geochemical and climotoligical implications. Progr. Oceanogr. 26: 263-306

Morel, A.; A. Bricaud (1981) Theoretical results concerning light absorption in a discrete medium, and application to specific absorption of phytoplankton, Deep Sea Res., 28, 1375–1393.

Morel, A.; Gentili, B.; Claustre, H.; Babin, M.; Bricaud, A.; Ras, J.; Tieche F. (2007). Optical properties of the "clearest" natural waters, Limnol. Oceanogr., 52, 1, 217–229.

Moutin, T.; Thingstad, T. F.; Van Wambeke, F.; Marie, D.; Slawyk, G.; Raimbault, P.; Claustre, H. (2002) Does competition for nanomolar phosphate supply explain the predominance of the cyanobacterium *Synechococcus*? Limnol Oceanogr 47:1562–1567.

Mozetič, P.; Francé, J.; Kogovšek, P.; Talaber, I.; Alenka Malej, A. (2012) Plankton trends and community changes in a coastal sea (northern Adriatic): Bottom-up vs. top-down control in relation to environmental drivers. Estuar Coast Shelf Sci 115:138-148.

Mura, M. P.; Agustí, S.; Cebrián, J.; Satta, M. P. (1996) Seasonal Variability of Phyto-plankton Biomass and Community Composition in Blanes Bay: a Paradigm of the NW Mediterranean Litoral. Publicaciones Especiales Instituto Español de Oceanografía. 22:23 – 29.

Murphy, E.J.; Hofmann, E.E.; Watkins, J.L.; Johnston, N.M.; Piñones, A.; Ballerini, T.; Hill, S.L.; Trathan, P.N.; Tarling, G.A.; Cavanagh, R.A.; Young, E.F.; Thorpe, S.E.; Fretwell, P. (2013) Comparison of the structure and function of Southern Ocean regional ecosystems: The Antarctic Peninsula and South Georgia. J. Mar. Sys. 109–110, 22–42 .

NASA - https://modis.gsfc.nasa.gov/ / Access en 20.08.2018

Nelson, N. B.; Siegel, D. A.; Michaels, A. F. (1998) Seasonal dynamics of colored dissolved material in the Sargasso Sea, Deep Sea Res., Part I, 45, 931-957.

Nielsdóttir, M.C; Bibby, T.S.; Moore, C.M.; Hinz, D.J.; Sanders, R.; Whitehouse, M.; Korb, R.; Achterberg, E.P. (2012) Seasonal and spatial dynamics of iron availability in the Scotia Sea. Mar. Chem. 130–131, 62–72.

Not, F.; del Campo, J.; Balague, V.; de Vargas, C.; Massana, R. (2009). New insights into the diversity of marine picoeukaryotes. PloS one, 4, 7143.

Nunes, S.; Perez, G.L, Latasa, M.; Zamanillo, M. Delgado, M.; Ortega-Retuerta, E.; Marrasé, C.; Simó, R.; Estrada, M. (2018a). Size fractionation, chemotaxonomic groups and bio-optical properties of phytoplankton along a transect across the Atlantic Ocean. Scientia Marina. *Aceptado*

Nunes, S.; Latasa, M.; Gasol, J. M.; Estrada, M. (2018b) Seasonal and interannual variability of phytoplankton community structure in a Mediterranean coastal site. Mar Ecol Prog Se. Vol. 592: 57–75, 2018 https://doi.org/10.3354/meps12493.

Nunes-Neto N. F.; Carmo R. S.; El-Hani1 C. N. (2009) Uma conexão entre algas e nuvens: fundamentos teóricos da hipótese CLAW e suas implicações para as mudanças climáticas. Oecologia brasiliensis. 13(4): 596-608. doi:10.4257/oeco.2009.1304.04.

Orsi, A. H.; Whitworth III, T. W.; Nowlin Jr, W. D. (1995) On the meridional extent and fronts of the Antarctic Circumpolar Current. Deep-Sea Res. Part I. 42, 641 – 673.

Partensky, F.; Blanchot, J.; Vaulot, D. (1999) Differential distribution and ecology of *Prochlorococcus* and *Synechococcus* in oceanic waters: A review. In: Charpy L, Larkum AWD (eds.) Marine Cyanobacteria. Bull Inst Oceanogr Monaco. Special issue 19:457 – 475.

Partensky, F.; Hess, W.R.; Vaulot, D. (1999) Prochlorococcus, a marine photosynthetic prokaryote of global significance. Microbiol Mol Biol Rev. 63(1):106-27.

Pérez, G. L.; Galí, M.; Royer, S-J.; Sarmento, H.; Gasol, J. M.; Marrasé, C.; Simó, R. (2016) Bio-optical characterization of offshore NW Mediterranean waters: CDOM contribution to the absorption budget and diffuse attenuation of downwelling irradiance. Deep-Sea Research I 114: 111–127.

Peters, R. H. (1983) The Ecological Implications of Body Size, Cambridge Univ. Press, Cambridge, U. K.

Porra, R.J.; PfuK del, E.E.; Engel, N. (1997). Metabolism and function of photosynthetic pigments. In: Jeffrey, S.W., Mantoura, R.F.C., Wright, S.W. (Eds.), Phytoplankton Pigments in Oceanography: Guidelines to Modern Methods. UNESCO, Paris, pp. 429 - 445.

Porter, K. G.; Feig, Y. S. (1980) The use of DAPI for identification and enumeration of bacteria and blue-green algae. Limnol Oceanogr 25:943–948.

Ptacnik, R.; Solimini, A. G.; Andersen, T.; Tamminen, T. (2008) Diversity predicts stability and resource use efficiency in natural phytoplankton communities. Proc Natl Acad Sci USA 105:5134-5138

Quinn, P. K; Bates, T. S. (2011) The case against climate regulation via oceanic phytoplankton sulphur emissions. Nature. 480, 51-56.

Ribera d'Alcalà, M.; Conversano, F.; Corato, F.; Licandro, P.; Mangoni, O.; Marino, D.; Mazzocchi, M. G.; Modigh, M.; Montresor, M.; Nardella, M.; Saggiomo, V.; Sarno, D.; Zingone, A. (2004). Seasonal patterns in plankton communities in a pluriannual time series at a coastal Mediterranean site (Gulf of Naples): an attempt to discer recurrences and trends. Sci Mar 68 (Suppl. 1):65-83.

Richards, F. A.; Thompson, T. G. (1952) The estimation and characterization of plankton populations by pigment analysis; A spectrophotometric method for the estimation of plankton pigments. J. Mar. Res., 11, 156-172.

Rodríguez, F. (2001) Aplicación del análisis de pigmentos por cromatografía líquida de alta eficacia (HPLC) al estudio de la composición y distribución del fitoplancton marino. Tesis Doctoral. Vigo, Universidad de Vigo.

Rodríguez, F.; Varela, M.; Zapata, M. (2002) Phytoplankton assemblages in the Gerlache and Bransfield Straits (Antarctic Peninsula) determined by light microscopy and CHEMTAX analysis of HPLC pigment data. Deep-Sea Res. II. 49, 723–747.

Romera-Castillo, C.; Nieto, M.; Castro, C. C. G.; Marrasé, C.; Largier, J.; Barton, E. D.; Álvarez-Salgado, X. A. (2011) Fluorescence: Absorption coefficient ratio — Tracing photochemical and microbial degradation processes affecting coloured dissolved organic matter in a coastal system. Marine Chemistry 125(1-4): 26-38. https://doi.org/10.1016/j.marchem.2011.02.001

Roy, S.; Llewellyn C.A.; Egeland E.S.; Johnsen G. (2011) Phytoplankton Pigments: Characterization, Chemotaxonomy and Applications in Oceanography. Cambridge University Press, Cambridge.

Rygaard, M.; Albrechtsen, H. J.; Binning, P. J. (2009) Alternative water management and self-sufficient water supplies. IWA Publishing, London, UK, 136 pp.

Ryther, J. H. (1969) Photosynthesis and fish production in the sea. Science 166: 72–76

Sabine CL, Feely RA (2007) The oceanic sink for carbon dioxide. In: Reay D, Hewitt, N, Grace J, Smith K (Eds.), Greenhouse Gas Sinks. CABI Publishing, Oxfordshire, UK, pp 31 – 49.

Sackmann, B. S.; Perry M. J.; M. J., Eriksen, C. C. (2008) Seaglider observations of variability in daytime fluorescence quenching of chlorophyll-a in Northeastern Pacific coastal waters. Biogeosci. Discuss. 5, 2839–2865.

Šantić, D.; Krstulović, N.; Šolić, M.; Kušpilić, G. (2011) Distribution of *Synechococcus* and *Prochlorococcus* in the central Adriatic Sea. Acta Adriat 52:101 – 114.

Sathyendranath, S.; Platt, T. (1988) The spectral irradiance field at the surface and in the interior of the ocean: a model for applications in oceanography and remote sensing. J. Geophys. Res. 93: 9270-9280.

Sathyendranath, S.; Stuart, V.; Cota, G.: Maas, H.: Platt, T. (2001) Remote sensing of phytoplankton pigments: a comparison of empirical and theoretical approaches. International Journal of Remote Sensing 22, 249–273.

Schauer, M.; Balagué, V.; Pedrós-Alió, C.; Massana, R. (2003) Seasonal changes in the taxonomic composition of bacterioplankton in a coastal oligotrophic system. Aquat Microb Ecol 31:163 – 174.

Schlitzer, R. (2016) Ocean Data View, http://odv.awi.de

Schloss, I.; Estrada, M. (1994) Phytoplankton composition in the Weddell-Scotia confluence area during austral spring in relation to hydrography. Polar Biol. 14, 77-90.

Schlüter, L.; Møhlenberg, F.; Havskum, H.; Larsen, S. (2000) The use of phytoplankton pigments for identifying and quantifying phytoplankton groups in coastal areas: testing the influence of light and nutrients on pigment/chlorophyll a ratios. Mar Ecol Prog Ser 192:49-63.

Segura-Noguera, M.; Cruzado, A.; Blasco, D. (2011) Nutrient preservation, analysis precision and quality control of an oceanographic database (inorganic nutrients, dissolved oxygen and chlorophyll *a*) from the NW Mediterranean Sea. Sci Mar 75:321-339;

Sieburth J. M.; Smetacek, V.; Lenz, J. (1978) Pelagic ecosystem structure - heterotrophic compartments of plankton and their relationship to plankton size fractions. Limnol Oceanogr 23, 1256–1263.

Sieracki, C. K.; Sieracki, M. E.; Yentsch, C. M. (1998) An imaging-in-flow in-flow system for automated analysis for marine microplankton. Mar. Ecol. Prog. Ser. 168:285–96.

Simó, R. (2001) Production of atmospheric sulfur by oceanic plankton: biogeochemical, ecological and evolutionary links, Trends in Ecology & Evolution, 16(6), 287–294.

Simon, N.; Cras, A-L.; Foulon, E.; Lemée, R.; Falkowski, P. G. (2004) The evolution of modern eukaryotic phytoplankton. Science. 305:354–360.

Siokou-Frangou, I.; Christaki, U.; Mazzocchi, M. G.; Montresor, M.; Ribera d'Alcalà, M.; Vaqué, D.; Zingone, A. (2010) Plankton in the open Mediterranean Sea: A review. Biogeosciences 7:1543–1586.

Sommaruga, R.; Höfer, J.; Alonso-Saez, L.; Gasol, J. M. (2005) Differential sensitivity to sunlight of picophytoplankton from surface Mediterranean coastal waters. Appl Environ Microbiol 71:2154-2157.

Sournia, A.; Chrétiennot-Dinet, M. J. and Ricard, M. (1991) Marine phytoplankton: how many species in the world ocean? Journal of Plankton Research 13, 1093-1099.

Souza, M. S.; Mendes, C. R. B; Garcia, V. M. T.; Pollery, R.; Brotas, V. (2012) Phytoplankton community during a coccolithophorid bloom in the Patagonian Shelf: microscopic and high-performance liquid chromatography pigment analyses. Journal of the Marine Biological Association of the United Kingdom. Volume 92, Issue 1. pp. 13-27. https://doi.org/10.1017/S0025315411000439.

Stramski, D.; Reynolds, R. A. (1993) Diel variations in the optical properties of a marine diatom. Limnol. Oceanogr., 38, 1347–1364.

Stull, R. B. (1988) An introduction to boundary layer meteorology. Atmospheric sciences library. Vol. 13. Kluwer Academic Publishers. Dordrecht, The Netherlands, 670 pp.

Taylor, B. B.; Torrecila, E.; Bernhardt, A.; Taylor, M. H.; Peeken, I.; Roettgers, R.; Bracher, A. (2011) Bio-optical provinces in the eastern Atlantic Ocean and their biogeographical relevance. Biogeosciences, 8, 3609–3629. https://doi: 10.5194/bgd-8-7165-2011.

Ternon, E.; Guieu, C.; Loye-Pilot, M. D.; Leblond, N.; Bosc, E.; Gasser, B.; Martin, J.; Miquel, J. C. (2010) The impact of Saharan dust on the particulate export in the water column of the North Western Mediterranean Sea. Biogeosciences 7:809‑826.

Tintoré, J.; Gomis, D.; Alonso, S.; Parrilla, G. (1991) Mesoscale dynamics and vertical motion in the Alboran Sea. J. Phys. Oceanogr. 21, No. 6, 811-823.

Tremblay J.E.; Legendre L. (1994) A model for the size-fractionated biomass and production of marine phytoplankton. Limnol Oceanogr 39:2004–2014.

Uitz, J.; Claustre, H.; Morel, A.; Hooker S. B. (2006) Vertical distribution of phytoplankton communities in Open Ocean: An assessment based on surface chlorophyll. J. Geophys. Res., 111, 1–23. Doi: 10.1029/2005JC003207.

UNEP-MAP-RAC/SPA (2010) Impact of climate change on marine and coastal biodiversity in the Mediterranean Sea: Current state of knowledge. By S. Ben Haj and A. Limam, RAC/SPA Edit., Tunis, Tunisia, 1-28.

Unrein, F.; Gasol, J. M.; Not, F.; Forn, I.; Massana, R. (2014) Mixotrophic haptophytes are key bacterial grazers in oligotrophic coastal waters. ISME J 8:164-176.

Utermöhl, H. (1958) Zur Vervollkommung der quantitativen Phytoplankton- Methodik. Mitteilungen. Internationale Vereiningung fuer Theoretische und Angewandte Limnologie. 9, 1-38.

Uusitalo, L.; Fleming-Lehtinen V.; Hallfors H.; Jaanus A.; Hallfors, Seija.; London, L. (2013) A novel approach for estimating phytoplankton biodiversity. Journal of Marine Science. 70(2), 408–417. doi:10.1093/icesjms/fss198.

Vallina, S.M., Simó, R., 2007. Strong relationship between DMS and the solar radiation dose over the global surface ocean. Science 315, 506 - 508.

van de Poll, W. H.; Boute, P. G.; Rozema, P. D.; Buma, A. G. J.; Kulk G, Rijkenberg MJA (2015) Sea surface temperature control of taxon specific phytoplankton production along an oligotrophic gradient in the Mediterranean Sea. Mar Chem 177:536-544.

Van Lenning, K.; Vila, M.; Masó, M.; Garcès, E.; Anglès, S.; Sampedro, N.; Morales-Blake, A.; Camp, J. (2007) Short-term variations in development of a recurrent toxic Alexandrium minutum - Dominated dinoflagellate bloom induced by meteorological conditions. J Phycol 43:892-907.

Vanilla, S.M., Simó, R., Gassó, S., Boyer-Montegut, C., Rio, E. Jurado, E., Dachs, J. 2007b. Analysis of a potential “solar radiation dose–dimethylsulfide–cloud condensation nuclei” link from globally mapped seasonal correlations. Global Biogeochemical Cycles, vol. 21, Gb2004, doi:10.1029/2006GB002787.

Vaulot, D.; Partensky, F.; Neveux, J.; Mantoura, R. F. C.; Llewellyn, C. A. (1990) Winter presence of prochlorophytes in surface waters of the northwestern Mediterranean Sea. Limnol Oceanogr 35:1156–1164.

Vaulot, D.; Eikrem, W.; Viprey, M.; Moreau, H. (2008) The diversity of small eukaryotic phytoplankton (≤ 3 μm) in marine ecosystems. FEMS Microbiology Reviews 32:795-820.

Vega-Moreno, D.; Marrero, J. P; Morales, J.; Garcia L.; Villagarcia-Úbedac, M.G. (2012) Phytoplankton functional community structure in Argentinian continental shelf determined by HPLC pigment signatures. Estuarine, Coastal and Shelf Science 100 72 – 81.

Venables, H.; Moore, C. M. (2010) Phytoplankton and light limitation in the Southern Ocean: Learning from high-nutrient, high-chlorophyll areas. J. Geophys. Res. 115, C02015.

Vernet, M.; Martinson, D.; Iannuzzi, R.; Stammerjohn, S.; Kozlowski, W.; Sines, K.; Smith, R.; Garibotti, I. (2008) Primary production within the sea-ice zone west of the Antarctic Peninsula: I — Sea ice, summer mixed layer, and irradiance. Deep-Sea Res. II. 5, 2068–2085.

Vidussi, F.; Claustre, H.; Manca, B. B.; Luchetta, A.; Marty, J. C. (2001) Phytoplankton pigment distribution in relation to upper thermocline circulation in the eastern Mediterranean Sea during winter, J. Geophys. Res., 106(C9), 19,939–19,956, doi: 10.1029/1999JC000308.

Wang, C.; Granskog, M.A.; Gerland, S.; Hudson, S.R.; Perovich, D.K.; Nicolaus, M.; Bratrein, M. (2014) Autonomous observations of solar energy partitioning in first-year sea-ice in the Arctic Basin. J. Geophys. Res. Oceans 119 (3), 2066–2080. http://dx.doi.org/ 10.1002/2013JC009459.

Whitehouse, M.J.; Korb, R.E.; Atkinson, A.; Thorpe, S.E.; Gordon, M. (2008) Formation, transport and decay of an intense phytoplankton bloom within the High-Nutrient Low-Chlorophyll belt of the Southern Ocean. J. Mar. Sys. 70, 150–167.

Wright, S.W.; Shearer, J.D. (1984) Rapid extraction and High-performance Liquid Chromatography of chlorophylls and carotenoids from marine phytoplankton. Journal of Chromatography 294, 281—295.

Wright, S.W.; Thomas, D.P.; Marchant, H.J.; Higgins, H.W.; Mackey, M.D.; Mackey, D.J. (1996) Analysis of phytoplankton in the Australian sector of the Southern Ocean: comparisons of microscopy and size frequency data with interpretations of pigment HPLC data using the 'CHEMTAX' matrix factorization program. Marine Ecology Progress Series 144, 85—298.

Wright, S. W.; Jeffrey, S. W. (1997) High- resolution HPLC system for chlorophylls and carotenoids of marine phytoplankton. En: Jeffrey, S.W., Mantoura, R.F.C. & Wright, S.W. (eds) Phytoplankton pigments in oceanography: guidelines to modern methods. UNESCO, Paris, pp 327-360.

Wright, S.W.; Jeffrey, S.W. (2006). Pigment markers for phytoplankton production, in: Marine Organic Matter: Biomarkers, Isotopes and DNA, edited by J.K. Volkman. The Handbook of Environmental Chemistry vol. 2, Part N. Springer, Berlin, pp. 71 – 104.

Yentsch, C. M.; Horan, P. K.; Muirhead, K.; Dortch, Q.; Haugen, E.; Legendre, L.; Murphy, L. S.; Perry, M. J.; Phinney, D. A.; Pomponi, S.; Spinrad, R. W.; Wood, M.; Yentsch, C. S.; Zahuranec, B. J. (1983) Flow cytometry and cell sorting: A technique for analysis and sorting of aquatic particles, Limnol. Oceanogr., 28, 1275-1280, 1983.

Yentsch, C.; Menzel D. W. (1963) A method for the determination of phytoplankton chlorophyll and phaeophytin by fluorescence Woods Hole Oceanographic Institution. Deep-Sea Research, Voi. 10, pp. 221 to 231. Pergamon Press Ltd. Printed in Great Britain.

Yentsch, C.S.; Phinney, D.A. (1985) Spectral fluorescence: a taxonomic tool for studying the structure of phytoplankton populations. J. Plankton Res. 7 (5), 15.

Zamanillo, M.; Ortega-Retuerta, E.; Nunes, S.; Rodríguez-Ros, P.; Estrada, M.; Sala, M. M.; Simó, R. (2018) Main drivers of transparent exopolymer particle distribution across the surface Atlantic Ocean. Biogeosciences Discussions.

Zapata, M.; Rodriguez, F.; Garrido, J. L. (2000) Separation of chlorophylls and carotenoids from marine phytoplankton: a new HPLC method using a reversed phase C-8 column and pyridine-containing mobile phases. Mar Ecol Prog Ser 195:29 – 45.

Zapata M, Jeffrey SW, Wright SW, Rodríguez F, Garrido JL, Clementson L (2004) Photosynthetic pigments in 37 species (65 strains) of Haptophyta: implications for oceanography and chemotaxonomy. Mar Ecol Prog Ser 270:83–10.

Zeng, C.; Rosengarda, S. Z.; Burta, W.; Peñac, A.; Nemcekc, N.; Zeng T.; Kevin R. A.; Tortell P. (2018) Optically-derived estimates of phytoplankton size class and taxonomic group biomass in the Eastern Subarctic Pacific Ocean. https://doi.org/10.1016/j.dsr.2018.04.001.

Zubkov, M.V.; Fuchs, B.M.; Tarran, G.A.; Burkill, P.H.; Amann, R. (2003) High rate of uptake of organic nitrogen compounds by Prochlorococcus cyanobacteria as a key to their dominance in oligotrophic oceanic waters. Appl Environ Microbiol 69: 1299–1304.

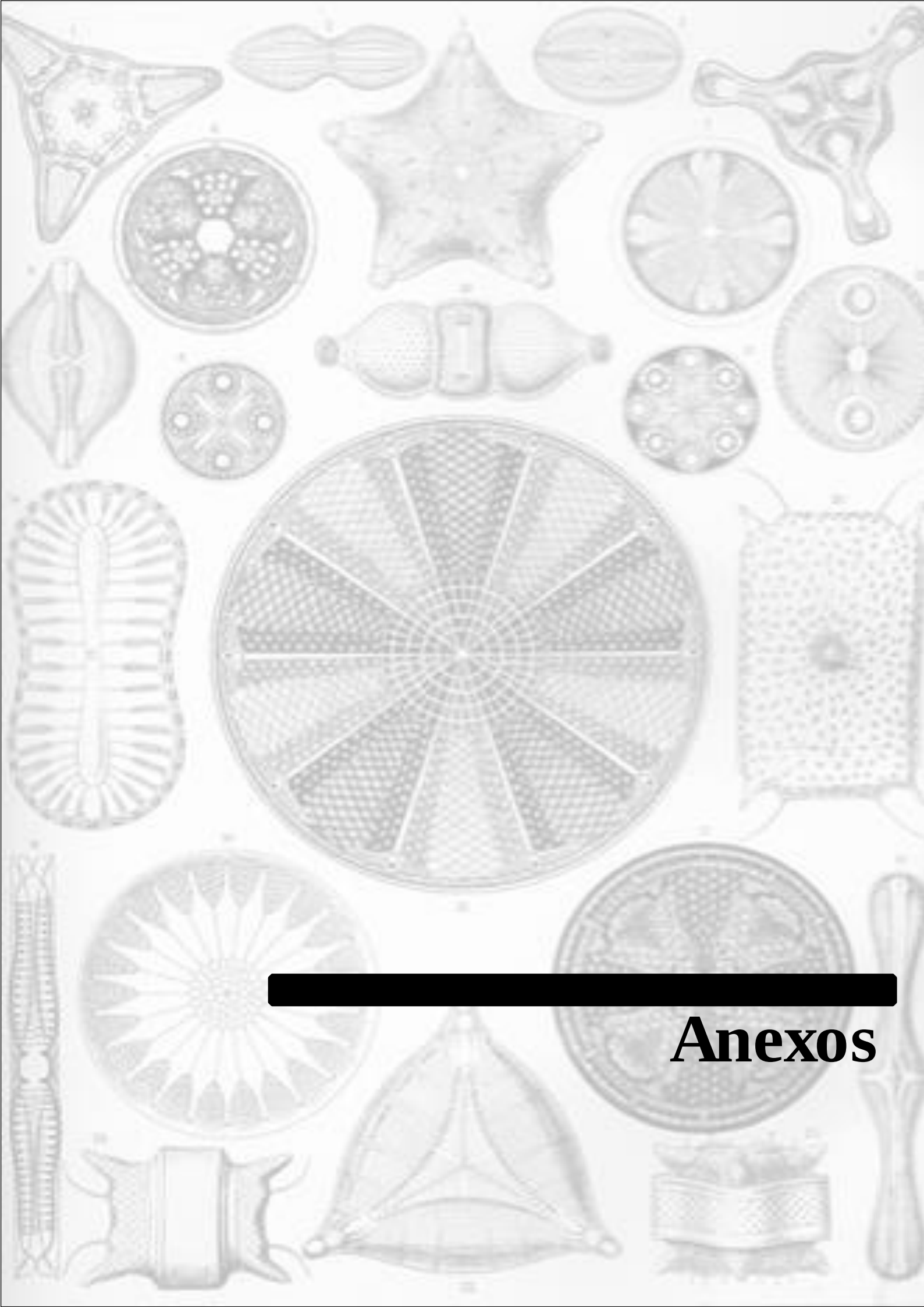

Anexos

Vol. 592: 57–75, 2018
https://doi.org/10.3354/meps12493

MARINE ECOLOGY PROGRESS SERIES
Mar Ecol Prog Ser

Published March 29

Seasonal and interannual variability of phytoplankton community structure in a Mediterranean coastal site

Sdena Nunes[1], Mikel Latasa[2], Josep M. Gasol[1], Marta Estrada[1,*]

[1]Institut de Ciències del Mar, CSIC, Passeig Marítim de la Barceloneta 37–49, 08003 Barcelona, Catalunya, Spain
[2]Centro Oceanográfico de Gijón/Xixón (IEO), Avda. Príncipe de Asturias 70bis, 33212 Gijón/Xixón, Asturias, Spain

ABSTRACT: We studied phytoplankton community structure in surface waters of the fixed coastal station of the Blanes Bay Microbial Observatory (NW Mediterranean Sea). A chemotaxonomic approach based on HPLC analysis of phytoplankton pigments, followed by CHEMTAX algorithm implementation, was applied to a set of monthly samples taken during a 14 yr period (2000–2014). Additional samples were taken for nutrient analyses, flow cytometric measurements and during part of the period for phytoplankton cell counts by optical microscopy. Overall, the most abundant groups in terms of chlorophyll *a* (chl *a*) were haptophytes, diatoms and prasinophytes. In general, diatoms were the most important components of the total chl *a* maxima (T_Chl *a*). We observed a marked seasonality of T_Chl *a* and several phytoplankton groups (prasinophytes, diatoms, haptophytes, cryptophytes and pelagophytes) with autumn-winter or winter-spring maxima and summer minima, coinciding with similar variation in major nutrient concentrations. *Prochlorococcus* presented a fall-winter maximum and a spring-summer minimum, while *Synechococcus* peaked in April and August, and dinoflagellates were relatively important in summer. Superimposed to this general pattern, prasinophytes and diatoms responded positively to episodic fertilization events associated with freshwater runoff caused by rain storms. Most phytoplankton groups presented a decreasing linear interannual trend that could be associated with a reduction in nutrient availability. A possible driver for this oligotrophication is the improvement of wastewater treatment in the region.

KEY WORDS: Mediterranean · Blanes Bay · Phytoplankton · Community structure · HPLC · Pigments · Time series

INTRODUCTION

Phytoplankton organisms constitute a crucial link in marine ecosystem dynamics. They contribute about half of the world's total primary production, are the main base of the food web of ocean communities and represent a key component of nutrient cycling and particle fluxes from surface to deep waters (Ryther 1969, Eppley & Peterson 1979). Furthermore, phytoplankton plays a key role in climate processes, contributing to the biological carbon pump and helping to remove the anthropogenic carbon liberated to the atmosphere (Sabine & Feely 2007).

Phytoplankton distributions are strongly influenced by abiotic factors, such as turbulence, temperature, irradiance and nutrient availability (Margalef 1978), and by interactions with other biological components of the food web. Classically, most studies on the composition of phytoplankton have been conducted by means of microscopic examination, which is time-consuming, requires a high level of taxonomic skill and is only adequate for the larger forms (>10 µm). For groups in the picoplankton (<2 µm)

*Corresponding author: marta@icm.csic.es

SCIENTIA MARINA

INTERNATIONAL JOURNAL ON MARINE SCIENCES
http://www.icm.csic.es/scimar
published by

Institut de Ciències del Mar (ICM)
Consejo Superior de Investigaciones Científicas (CSIC)
Passeig Marítim de la Barceloneta, 37-49
08003 Barcelona - Spain
Tel. +34 93 230 95 00 - Fax +34 93 230 95 55
E-mail: scimar@icm.csic.es

Barcelona, 25th September 2018

Dear Dr. Nunes,

Ref. Scientia Marina manuscript SM 4866

I am glad to inform you that your manuscript "Size fractionation, chemotaxonomic groups and bio-optical properties of phytoplankton along a transect across the Atlantic Ocean" by Sdena Nunes, Gonzalo Luís Perez, Mikel Latasa, Marina Zamanillo, Maximino Delgado, Eva Ortega-Retuerta, Celia Marrasé, Rafel Simó, Marta Estrada has now been accepted for publication in *Scientia Marina*.

The manuscript will now undergo the regular English revision. If the changes are few we will introduce them in the text. If there are too many, we will send them to you for inclusion in the final version.
You will receive galley proofs a few weeks after we receive the file with the revised version of your manuscript.

Thank you for considering *Scientia Marina* as an outlet for your work.

Yours sincerely,

Dr. Dolors Vaqué.
Editor-in-chief *Scientia Marina*

25/09/18 - SDENA OLIVEIRA NUNES

Redactar

Entrada
Borradores
Enviados
Papelera
Spam

Acc. de carpeta

Carp Virtuales

Buscar (Mensaje completo)

Actualizar Responder Otro Filtro

Reenviar Eliminar

de	asu…	Fecha	Tamaño
Deep-Sea Research Part I	Your…	29/05/18	14 KB

Your co-authored submission de Deep-Sea Rese: 29/05/18 (19:38:33 CEST)

Texto (2 KB)

Dear Miss. Nunes,

You have been listed as a Co-Author of the following submission:

Journal: Deep-Sea Research Part I

Title: Phytoplankton community structure in contrasting ecosystems of the Southern Ocean: South Georgia, South Orkneys and Western Antarctic Peninsula

Corresponding Author: Sdena Nunes

Co-Authors: Marta Estrada, Mikel Latasa, Maximino Delgado, Mikhail Emelianov, Rafel Simó

Sdena Nunes submitted this manuscript via Elsevier's online submission system, EVISE®. If you are not already registered in EVISE®, please take a moment to set up an author account by navigating to http://www.evise.com/evise/faces/pages/navigation/NavController.jspx?JRNL_ACR=DSR1

If you already have an ORCID, we invite you to link it to this submission. If the submission is accepted, your ORCID will be

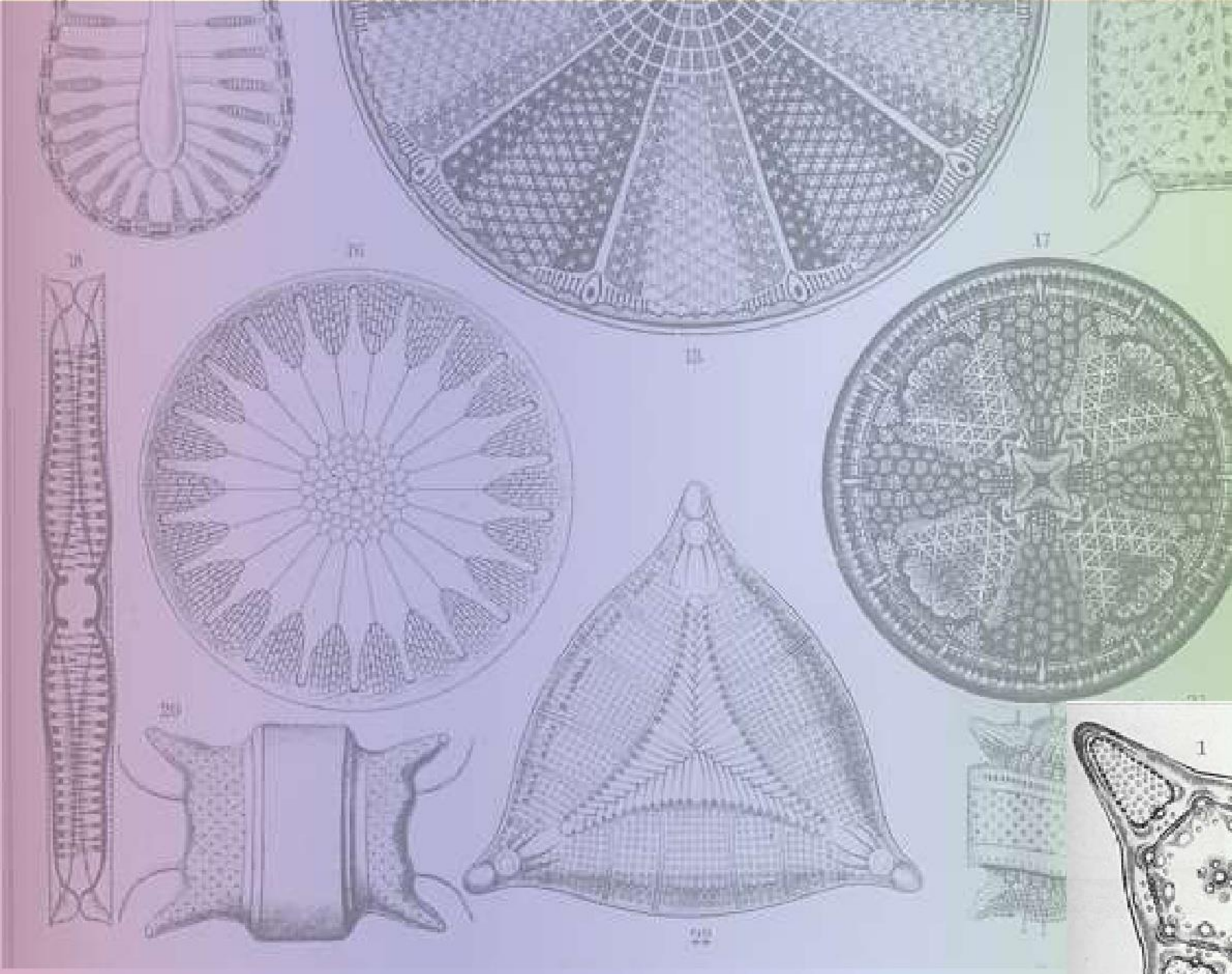

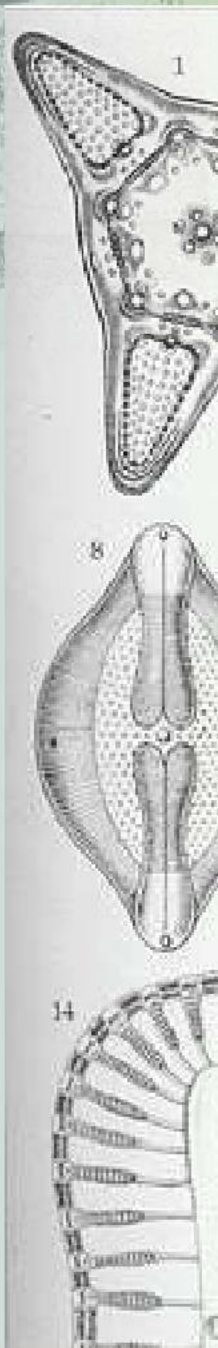

ICM Institut de Ciències del Mar
INSTITUTO ESPAÑOL DE OCEANOGRAFÍA
CSIC
CNPq Conselho Nacional de Desenvolvimento Científico e Tecnológico
UNIVERSITAT DE BARCELONA